UNIVERSITE SAAD DAHLAB DE BLIDA 1

Technology Faculty

Mechanical Engineering Department

Doctorate Thesis

In Mechanical Engineering

Experimental study and analytical modeling of turning process operations for improving the machinability of stainless steels

By:

TOUGGUI Youssef

In front of the jury composed of:

M. Ouali	Professor, USD of Blida 1	President
A. Allali	Professor, USD of Blida 1	Examiner
M. Gaceb	Professor, U of Boumerdes	Examiner
M. Temmar	Professor, USD of Blida 1	Advisor
S. Belhadi	MCA, U of Guelma	Co- Advisor

BLIDA 2021

Dedication

To my beloved parents; Mrs. Irzagh Aicha & Mr. Touggui Abdelkader

An attempt to pay off a debt that cannot be repaid.

Acknowledgments

I could not have completed this work without the help, encouragement, and contributions of several significant people in my life, and I am deeply grateful that I acknowledge their guidance, support, and efforts.

First and foremost, I would like to express my sincere gratitude to my supervisor and co-supervisor, Prof. Temmar Mustapha and Dr. Belhadi Salim for all of their invaluable guidance, support, and encouragement in achieving the goals that I set out to achieve during my Ph.D. studies at Blida 1 University.

I would also like to thank Prof. Mohammed Yallese for guiding me and supporting me throughout this study. It was a great privilege to join his research group and work with him at the Mechanics and Structures Research laboratory at Guelma University.

I would also like to thank Dr. Alper Uysal, who has been a constant source of motivation for me during my stay in Turkey, helping me complete the Ph.D. studies required at his Machining laboratory at Yildiz technical University, Istanbul.

I would like to thank the co-authors and collaborators of this research project: Dr. Salah Mechraoui, Prof. Tarek Mabrouki and Mr. Uğur Emiroglu. Without their kind help, it would have been difficult to make this study go as smoothly as it did.

I would also like to thank my committee members, Prof. Ouali Mohammed and Prof. Allali Abderrazak, for their willingness to evaluate my Ph.D. dissertation. I would also like to express my gratitude to Prof. Mohammed Gaceb for participating as my Ph.D.'s external examiner.

I convey special acknowledgment to the Algerian Ministry of Higher Education and Scientific Research for their financial scholarship.

Finally, but most importantly, I would want to convey my heartfelt appreciation and gratitude to my parents, who always pray for me, as well as my brothers and sisters for their constant encouragement and unending assistance.

Abstract

Application of environmentally friendly strategies instead of conventional flood in machining of hard to cut materials such as stainless steels has become more favorable. Proceeding from that, it seems important to carry out experimentation helping to study the effects of different cutting process parameters on measured responses under sustainable alternatives. Hence, the research in this thesis consists of three main stages. In the first stage, the comparison of cutting tools performance, namely cermet (GC1525) and coated cemented carbide (GC1125) in dry turning of AISI 316L was the rationality of this stage. The cutting tools performance was evaluated in terms of surface roughness (*Ra*), cutting force (*Fz*) and tool lifespan. Afterwards, regression models for *Ra* and *Fz* outputs criteria were developed based on surface response methodology (RSM). Furthermore, Simulated annealing (SA) and simple genetic algorithm (SGA) were used for single objective optimization purpose then Genetic Algorithm (GA) was used for multi-objective optimization. At the end of this stage, the surface topographies (3D) were also compared.

In the second stage, Taguchi and Technique for Order Preference by Similarity to Ideal Solution (TOPSIS) approaches were applied to determine an optimal combination of cutting parameters during dry turning of AISI 316L austenitic stainless steel (ASS) using cermet insert. Cutting speed (Vc), feed (f), cutting depth (ap) and cutting time (tc) were selected as four input parameters. Flank wear (VB), tangential cutting force (Fz), surface roughness (Ra) and material removal rate (MRR) were considered as the major process responses.

In the third stage, an experimental study was conducted from the perspective of performance analysis of machining characteristics in turning of AISI 304 ASS under dry, minimum quantity lubrication (MQL) and nanofluids and hybrid nanofluids assisted MQL cooling/lubricating conditions with consideration of surface roughness (Ra), main cutting forces (Fc), cutting temperature (T) and tool wear (VB).

Keywords: Austenitic stainless steel, Machinability; Cermet insert; Coated carbide insert; Optimization; Modelling; Minimum Quantity Lubrication (MQL); Turning.

ملخص

أصبح تطبيق الاستراتيجيات الصديقة للبيئة بدلاً من الغمر التقليدي في تصنيع المواد التي يصعب قطعها أكثر ملاءمة. انطلاقا من ذلك، يبدو من المهم إجراء تجارب تساعد في دراسة آثار شروط عملية القطع المختلفة على الاستجابات المقاسة في ظل البدائل المستدامة. ومن ثم، فإن البحث في هذه الأطروحة يتكون من ثلاث مراحل رئيسية.

في المرحلة الأولى، كانت المقارنة بين أداء أدوات القطع ، وبالتحديد لقم cermet (GC1525) و لقم من الكربيد المعدني (GC1125) في الخراطة الجافة لـ AISI 316L هي محور هذه المرحلة. تم تقييم أداء أدوات القطع من حيث خشونة السطح وقوة القطع وعمر الأداة. بعد ذلك، تم تطوير نماذج رياضية للمخرجات Ra و Fz بناءً على منهجية استجابة السطح (RSM) . علاوة على ذلك ، تم استخدام التلدين المحاكي (SA) والخوارزمية الجينية البسيطة (SGA) لغرض تحسين الهدف الفردي ، ثم تم استخدام الخوارزمية الجينية (GA) للتحسين متعدد الأهداف. في نهاية هذه المرحلة، تمت أيضًا مقارنة التحليل الطوبوغرافي الثلاثي الأبعاد للسطوح المشغلة.

في المرحلة الثانية، تم تطبيق نهج Taguchi و TOPSIS لتحديد التركيبة المثلى ل شروط القطع أثناء الخراطة الجافة لـ AISI 316L باستخدام لقم السيرمي. تم اختيار سرعة القطع ،سرعة التغذية، عمق التمريرة وزمن القطع كأربعة شروط إدخال. في حين تم اعتبار تآكل القطع، وقوة القطع، وخشونة السطح ومعدل إزالة المواد كإ ستجابات مقاسة للعملية .

تتعلق المرحلة الثالثة من هذه الأطروحة بتلبية متطلبات عملية التصنيع المستدامة. لتحقيق هذا الغرض، أجريت دراسة تجريبية من منظور تحليل الأداء لخصائص المعالجة الآلية في تحويل الفولاذ الأوستنيتي المقاوم للصدأ AISI 304 تحت شروط التصنيع الجاف، تزييت بكمية أدنى (MQL)، والسوائل النانوية والسوائل النانوية الهجينة المرتكزة على التزييت بكمية أدنى مع مراعاة خشونة السطح وقوى القطع الرئيسية ودرجة حرارة القطع وتآكل الأداة.

من المتوقع أن تساعد هذه الأطروحة المهندسين والعاملين في صناعات قطع المعادن، حيث أنه يساهم في تقييم أداء شروط القطع ، وتحسين معايير القطع للتحكم بشكل أفضل في المعايير التكنولوجية للتصنيع وتوفير تقييم لأداء MQL أثناء عملية تصنيع الفولاذ الأوستنيتي المقاوم للصدأ AISI 316L و AISI 304.

الكلمات الرئيسية: الفولاذ المقاوم للصدأ الأوستنيتي، قابلية التحسين، لقم السيرمي. لقم من الكربيد المعدني؛ النمدجة؛ تزييت بكمية أدنى.

Résumé

L'application de stratégies respectueuses de l'environnement au lieu de l'inondation conventionnelle dans l'usinage de matériaux difficiles à couper est devenue plus favorable. Partant de là, il semble important d'effectuer des expérimentations permettant d'étudier les effets des différents paramètres du processus de coupe sur les réponses mesurées dans le cadre des alternatives durables. Par conséquent, la recherche dans cette thèse se compose de trois étapes principales. Dans la première étape, la comparaison des performances des outils de coupe, à savoir le cermet (GC1525) et le carbure cémenté revêtu (GC1125) dans le tournage à sec de l'AISI 316L était la rationalité de cette étape. Les performances des outils de coupe ont été évaluées en termes de rugosité de surface (Ra), de force de coupe (Fz) et de durée de vie de l'outil. Ensuite, des modèles de régression pour les critères de sortie Ra et Fz ont été développés sur la base de la méthodologie de réponse de surface (RSM). En outre, le recuit simulé (SA) et l'algorithme génétique (GA) ont été utilisées pour l'optimisation mono-objectif puis l'algorithme génétique (GA) a été utilisées pour l'optimisation multi-objectif. A la fin de cette étape, les topographies de surface (3D) ont également été comparées.Dans la deuxième étape, les approches Taguchi et TOPSIS ont été appliquées pour déterminer une combinaison optimale de paramètres de coupe pendant le tournage à sec de l'AISI 316L (ASS) en utilisant une plaquette en cermet. La vitesse de coupe (Vc), l'avance (f), la profondeur de coupe (ap) et le temps d'usinage (tc) ont été sélectionnés comme quatre paramètres d'entrée. L'usure de dépouille (VB), la force de coupe tangentielle (Fz), la rugosité de surface (Ra) et le taux d'enlèvement de matière (MRR) ont été considérés comme les principales réponses du processus. Dans le troisième étape, une étude expérimentale a été menée du point de vue de l'analyse des performances des caractéristiques d'usinage lors du tournage de l'acier AISI 304 (ASS) dans des conditions de l'usinage à sec, de lubrification par quantité minimale (MQL) et de refroidissement-lubrification par nanofluides et par nanofluides hybrides assistés par MQL en tenant compte de la rugosité de surface (Ra), des forces de coupe principales (Fc), de la température de coupe (T) et de l'usure de l'outil (VB).

Mots clés : Acier inoxydable austénitique ; Usinabilité ; Cermet ; Carbure revêtu ; Optimisation ; Modélisation ; Lubrification par Quantité Minimale (MQL) ; Tournage.

Table of Contents

General Introduction 1
1.1. Goal and objectives 2
1.2. Thesis structure 3
1.3. Note to the reader 4
Chapter 1. Literature review 5
1.1 Stainless steels 5
1.1.1 Introduction to Austenitic stainless steels (ASS) 7
1.1.2. Application fields of austenitic stainless steel 7
1.2. Introduction to Turning 8
1.2.1. Material removal rate 9
1.3. Cutting tools 10
1.3.1 Cutting tool geometry 10
1.3.2. Cutting tools' materials 14
1.3.3. Coating tool materials 15
1.4. Coating Methods 18
1.5. Cutting fluids in cutting process 20
1.5.1 Types of cutting fluids 21
1.5.2 Functions of cutting fluids 22
1.6. Machinability 23
1.6.1. General aspects of machinability of stainless steel 27
1.6.1.1. Cutting forces 28
1.6.1.2. Cutting temperature 30
1.6.1.3 Tool wear rates 36
1.6.1.5. Surface roughness 40
1.6.1.6. Chip morphologies 41
1.7. Summary 43
Chapter 2: A comparative study on performance of cermet and coated carbide inserts in straight turning AISI 316L austenitic stainless steel 45
2.1. Introduction 45
2.2. Methodology 47
2.2.1. Turning conditions and materials 47
2.2.2. Response Surface Methodology 51

2.2.3. Simulated Annealing....51
2.2.3.1. Theory of simulated annealing....51
2.2.3.2. Implementation of simulated annealing algorithm....53
2.2.4 Genetic Algorithm....54
2.2.4.1. Overall concepts of genetic algorithms....54
2.2.4.2. Standard GA operations....56
2.2.4.3. Overview of basic GA search method....60
2.2.4.4. Using GA in optimization problem....61
2.3. Results and discussion....62
2.3.1. Analysis of Variance (ANOVA) results....62
2.3.2. Development of predictive models....65
2.3.2.1. Models formulated using RSM....65
2.3.2.2. 3D response surfaces of *Ra* and *Fz*....65
2.3.2.3. RSM models performance assessment....66
2.3.2.4. Validation of RSM models....69
2.3.3. Single- and Multi-objective optimizations of cutting parameters....71
2.3.3.1. Single-objective optimization using SA....71
2.3.3.2. Single-objective optimization using GA....73
2.3.3.3. SA and GA optimization results assessment....73
2.3.3.4. Multi-objective optimization using GA....77
2.3.4. Flank wear estimation under machining time....80
2.3.5. 3D surface topography....81
2.4. Conclusion....84
Chapter 3: Dry turning optimization of austenitic stainless steel 316L based on Taguchi and TOPSIS approaches....86
3.1. Introduction....86
3.2. Experimental materials and turning conditions....88
3.2.1. Workpiece material, cutting tool and turning machine....88
3.2.2. Dry cutting process....90
3.2.3 Response Measurements....91
3.2.3.1. Cutting forces....91
3.2.3.2. Surface roughness....92
3.2.3.3. Tool wear....92

3.2.4 Design of experiments (DOE) 93
3.2.4.1 Taguchi design approach 96
3.2.4.2. Analysis of Variance (ANOVA) 98
3.2.4.3. Full factorial design 99
3.3. Results and discussion 100
3.3.1 Analysis of variances (ANOVA) results 100
3.3.2 Effect of process parameters on VB 102
3.3.3 Effect of process parameters on Fz 103
3.3.4 Effect of process parameters on Ra 104
3.3.5 Effect of process parameters on MRR 104
3.3.6. Single-objective Optimization of cutting parameters based on Taguchi approach 105
3.3.7. Multi-objective Optimization of cutting parameters based on TOPSIS approach 107
3.4. Conclusion 111
Chapter 4: Evaluation of MQL Performances using Various Nanofluids in Turning of AISI 304 Stainless Steel 112
4.1. Introduction 112
4.2. Experimentation and Methodology 115
4.2.1. Minimum Quantity Lubrication (MQL) 115
4.2.1.1. MQL strategy 115
4.2.1.2. Advantage of MQL method 116
4.2.1.3. Nanofluid based MQL 116
4.2.1.4. Summary of Nanofluid-MQL's Mechanism 118
4.2.2. Preparation nanofluids 119
4.2.3. Workpiece material, cutting tool and CNC machine tool 122
4.2.4. Cutting parameters and conditions 124
4.2.5. Measurements of turning characteristics 124
4.3. Results and Discussion 127
4.3.1. Surface roughness 128
4.3.2. Cutting force 130
4.3.3. Cutting temperature 132
4.3.4. Comparison of performance outputs 134

4.3.5. Flank wear 135
4.3.6. Statistical analysis 137
4.3.7. Composite Desirability Approach 141
4.4. Conclusion 146
General Conclusion 148
References 151

List of Figures

Figure 1. 1. Classification of stainless steels [1.4] 6
Figure 1. 2. Example of straight turning operation. 9
Figure 1. 3. Effect of different cutting tool geometries (a) on the tool temperature profile on rake surface (b) during dry machining of 4340 steel with uncoated carbide tools (Vc = 200 m/min, f = 0.1 mm/rev), [1.13]. 10
Figure 1. 4. Influence of different edge geometries (a) on cutting force components (b) [1.14].....11
Figure 1. 5. Maximum flank wear width achieved by different edge geometries after a cutting time of 16 min [1.14]. 11
Figure 1. 6. Characterization of cutting tool micro-geometry (a) and the effects of edge radius (r_n) (b) on surface roughness at f =0.08 mm/rev and ap =0.1mm, under dry turning of AISI 52100 steel [1.16].....12
Figure 1. 7. Inserts' chip breaker geometries and their effects on cutting force (f = 0.08, 0.14, 0.20, 0.26 mm/rev, ap =2.5 mm and tool edge radius 0.03 mm), [1.17]. 13
Figure 1. 8. Various chip breakers and their influence on the formation of chips during turning operation (Vc =150 m/min, f = 0.26 mm/rev) [1.17].....13
Figure 1. 9. Coating of a cutting insert [1.29]. 15
Figure 1. 10. Cutting force data vs. cutting speed for turning (a) AISI 304 and (b) AISI 316 austenitic stainless steels using TiC/TiCN/TiN and TiCN/TiC/Al2O3 coated carbide tools at a feed rate of 0.16 mm/rev and depth of cut of 1.6 mm [1.30]. 16
Figure 1. 11. Surface roughness data vs. cutting speed for straight turning of AISI 316L using TiCN+Al2O3 and (Ti, Al)N coated cutting tools [1.31]. 17
Figure 1. 12. Main effect plots for surface roughness and flank wear [1.32].....18
Figure 1. 13. Box plot of average surface roughness values obtained by two cutting inserts [1.33]. 19
Figure 1. 14. Flank wear of cutting tools versus machining time at Vc = 280 m/min, f = 0.08 mm/rev and ap = 0.2 mm [1.35]. 20
Figure 1. 15. Distribution of manufacturing costs in the European automotive industry [1.37].....21
Figure 1. 16. a) Feed rats vs. surface roughness, b) Cutting speed vs. tool wear at ap = 0.5 mm and feed rate (f) = 0.2, 0.25 and 0.28 mm/rev at three points a, b and c, respectively. (1) Coconut oil, (2) soluble oil and (3) straight cutting oil [1.8]. 22
Figure 1. 17. Factors affecting machinability [1.26].....24
Figure 1. 18. Causes for poor or difficult machinability [1.45]. 25
Figure 1. 19. Input parameters, output variables and machinability criteria. 27
Figure 1. 20. Resultant force and its components in cutting process [1.10]. 29
Figure 1. 21. Representation of the different heat flows and energy sources [1.51]. 30
Figure 1. 22. Temperature distribution in workpiece and chip during orthogonal cutting (obtained from infrared photograph) for free-cutting mild steel where the cutting speed is 0.38 m/s, width of cut is 6.35 mm, the working normal rake is 30 degrees and the workpiece temperature is 611C°.....32

Figure 1. 23. Cutting temperature of (a) simulated results and (b) experimental results obtained by infrared image during tuning operation [1.58]. 33
Figure 1. 24. Temperature profiles at the tool-chip interface during machining of hardened steel, α =0^°, (a) Effect of cutting speed and (b) Effect of feed rate [1.13]. 34
Figure 1. 25. Tool maximum temperature obtained simulation dependent on rake angle for TiAlN and cBN/diamond-coated Si3N4 cutting tools with the constant clearance angle of 5° and the constant Vc of 270 m/min [1.58]. 35
Figure 1. 26. Tool temperature in drilling with different cutting conditions [1.61]. 35
Figure 1. 27. Flank wear and crater wear [1.4]. 37
Figure 1. 28. Typical stages in flank wear [1.4]. 38
Figure 1. 29. Graphical view of worn cutting tool, showing the principal locations and kinds of wear that occur [1.67]. 38
Figure 1. 30. Causes of wear in cutting processes [1.10]. 39
Figure 1. 31. Deviation from nominal surface used in the definition of surface roughness [1.1]. 40
Figure 1. 32. Three basic chip forms a) Side-curling, b) Up-curling and c) Straight chip [1.75]. 42
Figure 1. 33. Chip morphologies according to ISO 3685-1977, [1.75] 42
Figure 1. 34. Classification of chip types (A) discontinuous, (B) elemental, (C) segmented, (D) continuous [1.76]. 43

Figure 2. 1. Schematic illustration of experimental setup in the present work. 50
Figure 2. 2. Framework of simulated annealing algorithm. 54
Figure 2. 3. Crossover operator under bit coding. Case A shows one splice point; Case B shows two splice points. 58
Figure 2. 4. Mutation operator affecting one bit in a binary coding. 59
Figure 2. 5. Framework of genetic algorithms. 61
Figure 2. 6. 3D surface response for Ra (a) and Fz (b) for cermet (GC 1525) and coated carbide (GC 1125). 66
Figure 2. 7. Comparison of the predictive models with experimental results of Ra and Fz for Cermet (GC1525) and Coated carbide (GC1125) cutting inserts. 70
Figure 2. 8. Fitness function plots of SA for cermet (a-b) and coated carbide (c-d) cutting inserts. 72
Figure 2. 9. Fitness function plots of GA for cermet (a-b) and coated carbide (c-d) cutting inserts. 75
Figure 2. 10. Pareto front plots for (Left) cermet and (Right) coated carbide cutting insert. 78
Figure 2. 11. Evolution of VB with respect to machining time for cermet (GC 1525) and coated carbide (GC1125) cutting inserts at Vc = 340 m/min, f = 0.8 mm/rev and ap = 0.2 mm. 81
Figure 2. 12. 3D Topography for Cermet (GC1525) and Coated carbide (GC1125) inserts. 83

Figure 3. 1. Workpiece material AISI 316L. 88
Figure 3. 2. Cutting insert and its holder. 89
Figure 3. 3. Lathe TOS TRENCIN 89
Figure 3. 4. Advantage of dry machining [3.33] 91
Figure 3. 5. Cutting forces data assessment system: a) Kistler Dynamometer (type 9257B), b) Kistler charge amplifier....92
Figure 3. 6. Roughness meter. 92
Figure 3. 7. Microscope Visual Gage 250. 93
Figure 3. 8. Schematic design of the present work. 93
Figure 3. 9. Process parameters and responses in machining [3.37]. 95
Figure 3. 10. Process parameters and responses in machining [3.37]. 102
Figure 3. 11. Main effects plot for VB....103
Figure 3. 12. Main effects plot for Fz. 103
Figure 3. 13. Main effects plot for Ra. 104
Figure 3. 14. Main effects plot for MRR. 105
Figure 3. 15. Main effects plot for the S/N ratios of the VB, Fz, Ra and MRR. 106
Figure 3. 16. Main effect plot of Closeness coefficient....109
Figure 3. 17. Chip morphologies produced during cutting tests 2,5 and 8. 110

Figure 4. 1. The MQL-nanofluid mechanism schematic [4.20]. 116
Figure 4. 2. Heat dissipation mechanism through a) base liquid b) MWCNTs based nanofluid [4.22]. 117
Figure 4. 3. Functions on nanoparticles between contacting surfaces a) mending effect b) protective film effect c) third body effect d) rolling/ sliding effect e) polishing effect [4.22]....118
Figure 4. 4. A double-step method for nanofluids preparing. 121
Figure 4. 5. Illustration of CNC machine, workpiece and insert used in this work. 123
Figure 4. 6. Cutting insert and its holder geometries. 123
Figure 4. 7. Experimental set-up. 125
Figure 4. 8. Variation of Ra under different cutting conditions. 130
Figure 4. 9.Variation of Fc under different cutting conditions and parameters. 132
Figure 4. 10.Variation of T under different cutting conditions and parameters. 133
Figure 4. 11.Effect of nano graphene reinforced nanofluid assisted MQL on performance outputs against other lubricating conditions. 135
Figure 4. 12.Evolution of VB with respect of machining time under different cutting conditions and parameters. 136
Figure 4. 13.Percentage contributions of the process parameters on measured outputs. 139
Figure 4. 14.Residuals plots for normal probability of a) Ra, b) Fc and c) T 140
Figure 4. 15.Contour plots for a) Ra, b) Fc, c) T and d) overall desirability. 144
Figure 4. 16.Desirability bar-graph for the optimization. 145

List of Tables

Table 1. 1.Relative machinability ratings [1.46]. 26
Table 1. 2.Typical machinability ratings for selected work materials [1.44]. 28

Table 2. 1.Chemical composition of the AISI 316L. 48
Table 2. 2.Machining conditions. 48
Table 2. 3.Experimental design using the L27 orthogonal array and experimental results. 49
Table 2. 4.ANOVA for Ra. 63
Table 2. 5.ANOVA for Fz. 64
Table 2. 6.RSM prediction results for cermet (GC 1525) and coated carbide (GC 1125) inserts. 68
Table 2. 7.Summary of RSM developed models performance. 69
Table 2. 8.Optimal cutting parameters for single-objective optimization of Ra and Fz by SA. 71
Table 2. 9.Optimal cutting parameters for single-objective optimization of Ra and Fz by GA. 73
Table 2. 10.Validation of SA-based optimization Ra model. 75
Table 2. 11.Validation of SA-based optimization Fz model. 76
Table 2. 12.Validation of GA-based optimization Ra model. 76
Table 2. 13.Validation of GA-based optimization Fz model. 76
Table 2. 14.SA and GA iteration. 77
Table 2. 15.Results of Pareto-optimal solutions. 79
Table 2. 16.Comparison of optimal solutions derived by GA with confirmation run. 80

Table 3. 1.Chemical composition of the AISI 316L. 89
Table 3. 2.Common DOE methods used in industrial application [3.40]. 96
Table 3. 3.Assignment of levels to the cutting process parameters. 100
Table 3. 4.Experimental results 100
Table 3. 5.ANOVA for VB, Fz, Ra and MRR. 101
Table 3. 6.Response of S/N ratios for VB, Fz, Ra and MRR. 106
Table 3. 7.Optimum parameters setting. 107
Table 3. 8.TOPSIS outcomes. 109
Table 3. 9.ANOVA for TOPSIS. 110

Table 4. 1Technical properties and specifications of nano particles.. 120
Table 4. 2.Chemical composition and mechanical properties of AISI 304. 122
Table 4. 3.Turning parameters and cutting conditions. 126
Table 4. 4.Experimental results of measured outputs. 127
Table 4. 5.ANOVA for a) Ra, b) Fc and c) T 138

Table 4. 6.Conditions and goals for optimization of cutting parameters and responses. 142
Table 4. 7.Optimum findings derived by composite desirability approach (CDA) for multi-criteria Ra, Fc and T 143
Table 4. 8.Comparison between optimal solutions delivered by DF and experimental run 145

Nomenclature

Vc: cutting speed (m/min)

f: feed rate (mm/rev)

ap: cutting depth (mm)

tc: cutting time (min)

VB: flank wear (mm)

Fz: tangential cutting force (N)

Ra: arithmetic mean roughness (µm)

MRR: Material Removal Rate (cm^3/min)

RSM: Response Surface Methodology

BUE: Built-Up-Edge

ANOVA: Analysis of Variance

DF: Degree of Freedom

SS: Sum of Squares

MS: Mean of Squares

F: Fisher value

P: P-value

Pc: Percentage Contribution

R^2: coefficient of determination

DoE: Design of Experiment

TOPSIS**:** Technique for Order Preference by Similarity to Ideal Solution

AHP: Analytical Hierarchy Process

PCA: Principal Component Analysis

GRA: Gray Relational Analysis

ASS: Austenitic Stainless Steel

PVD : Physical Vapor Deposition

CVD : Chemical Vapor Deposition

AISI: American Iron and Steel Institute

S/N: Signal-to-Noise

MCDM: Multi–Criteria Decision Making Method

T: Cutting temperature (°C)

MQL: Minimum quantity lubrication

MoS_2 : Molybdenum disulfide

MWCNT: Multi-walled carbon nanotube

LC: Lubricating Conditions

MoS_2-MQL**:** Nano MoS_2 reinforced nanofluid assisted MQL

MWCNT-MQL: MWCNT reinforced nanofluid assisted MQL

Graphene-MQL**:** Nano graphene reinforced nanofluid assisted MQL

Hybrid-1-MQL: MWCNT/MoS_2 reinforced hybrid nanofluid assisted MQL

Hybrid-2-MQL: Graphene/MoS_2 reinforced hybrid nanofluid assisted MQL

CDA: Composite Desirability Approach

SDS : Sodium Dodecyl Sulfate

1. General Introduction

Cutting austenitic stainless steels is well-known to be more challenging than other engineering materials such carbon steel. Austenitic stainless steel materials are preferred in variety industries, including food, medical, aerospace and automotive, due to their high ductility, high creep rupture strength, high operating temperature and exceedingly excellent corrosion resistance properties. The properties that give the alloys their required qualities, however, also make them notoriously difficult-to-machine due to their low thermal conductivity, work hardening tendency and high built up edge (BUE) formation. For instance, low thermal conductivity (i.e., 16.2 W/m. k for AISI 304 and AISI 316L at 100 °C) allows heat to accumulate at the apex of the cutting tool, resulting in poor surface quality and geometrical precision, as well as high tooling costs.

The use of conventional flood coolant is a common cooling strategy in the manufacturing industry to dissipate the high heat generated during machining operation. However, the extravagant use of harmful conventional cutting fluids such as synthetic, semi-synthetic and petroleum/mineral oil-based fluids not only has raised environmental and health concerns but also they are expensive (up to 17.9% of the total manufacturing costs) due to strict disposal regulations, necessitating other desired alternatives.

One of these alternatives is dry machining, which has been implemented to eliminate the usage of cutting fluids. Elevated temperatures are experienced during this process. To address this problem, researchers attempted to use an acceptable coating layer on tool substrate materials. As a result, the range of cutting speeds that can be employed in dry cutting can be increased. However, it has its own limitations such as excessive tool wear, heat dissipation and poor surface integrity, especially in the case of hard-to-cut materials. These drawbacks led the researchers to explore another conscious strategy known as Minimum Quantity Lubrication (MQL).

MQL was developed as a bridging technology to address the issue of fluid consumption associated with traditional flood cooling. Although the fact that MQL has technical benefits such as limited harmful effects on the environment caused by the abundant use of the conventional cutting fluid, less production cost, increased workers' safety. Nevertheless, it has its own restrictions related to inefficient cooling role because of the incapability of the lesser oil flow rate to fully limit heat generation at both primary and secondary

machining regions, especially at high cutting speeds. Therefore, the necessity has arisen to improve the MQL performance. In this vein, nanofluids assisted MQL and hybrid nanofluids assisted MQL have recently emerged as important research trends in order to enhance MQL efficiency as they provide substantial improvements in the tribological and heat transfer characteristics.

1.1. Goal and objectives

The main goal of this research is to evaluate the machinability of austenitic stainless steels, including AISI 316L and AISI 304 during sustainable turning process. The following basic objectives must be met to achieve this goal:

- To carry out a comprehensive literature review, particularly on machining of stainless steels. This provides a foundation for understanding the need for cermet inserts in stainless steels turning, as well as eliminating or reducing the extravagant use of cutting fluid.
- To optimize the key process parameters (cutting speed, feed rate, depth of cut and cutting time) using single and multi-objective optimization methods.
- To study the influence of cutting parameters, including cutting speed, feed rate and depth of cut on machining performance (surface roughness and cutting force) during dry turning of AISI 316L austenitic stainless steel using cermet and coated carbide cutting inserts.
- To investigate and determine the effect and role of dispersed nanofluids, namely multi-walled carbon nano-tubes (MWCNT), Molybdenum disulfide (MoS_2) and graphene and their hybrids into vegetable oil base cutting fluid by implementing the MQL strategy during turning AISI 304 austenitic stainless steel.
- To analyze the machining characteristics such as surface roughness, cutting force, cutting temperature and tool flank wear in turning of AISI 304 austenitic stainless steel (ASS) under dry, MQL and nanofluids and hybrid nanofluids assisted MQL lubricating/cooling conditions.

1.2. Thesis structure

This thesis is structured around four chapters.

Chapter 1. Literature review

The first chapter provides a comprehensive literature review related to the work carried out. Stainless steels are briefly described in terms of their composition and current applications. It then describes the machining process with the emphasis on turning, which is the procedure used for the work performed, and it also presents the cutting tools in terms of their geometries, materials and coating materials. Then, coating methods in machining are briefly reviewed. In addition, cutting fluid and their types and functions in the cutting process are briefly documented. The last part of this chapter is devoted to explaining the machinability of the materials as well as to describing the machinability aspects of a machined material such as cutting forces, cutting temperature, tool wear, surface roughness and chip morphology. A summary with a critical assessment of the literature, indicating the gap in the research, is also given at the end of the chapter.

Chapter 2. A comparative study on performance of cermet and coated carbide inserts in straight turning AISI 316L austenitic stainless steel.

This chapter focuses on the machinability of austenitic stainless steel AISI 316L. In order to achieve this objective, the influence of cutting parameters (cutting speed, feed rate and depth of cut) on surface roughness (Ra) and cutting forces (Fz) was determined. The machining is carried out under dry cutting using two cutting tools, namely cemented coated carbide (GC 1125) with PVD coating and cermet (GC 1525) with PVD coating. Then, from the experimental results, the mathematical prediction models based on response surface methodology (RSM) were developed. These models were used to accomplish the optimization task by embracing the simulated annealing (SA) and genetic algorithm (GA) in order to obtain optimum cutting parameter sets. The results of the evolution of tool wear as a function of machining time as well as the surface topography (3D) were also presented. The results obtained make it possible to define the performance of the cutting tools used and the appropriate cutting conditions to optimize the cutting process for the considered steel.

Chapter 3. Dry turning optimization of austenitic stainless steel 316L

The second chapter includes the application of two types of optimization: single-objective optimization, using the Taguchi method, and multi-objective optimization, using TOPSIS. Thus, the optimal values of the cutting parameters with respect to the optimization objectives were calculated for each of the machining technology parameters (surface roughness, cutting force, flank wear and material removal rate).

Chapter 4. Evaluation of MQL Performances using Various Nanofluids in Turning of AISI 304 Stainless Steel.

In this chapter, the description of MQL strategy and the preparation of nanofluids were presented. A comparative performance of nanofluids and their hybrids in terms of machining characteristics quality was then presented. In addition, ANOVA and RSM multiple regression were employed in order to determine the significant process parameters on measured outputs and to establish the empirical models for optimization task. Then, desirability function approach was utilized to determine the key process parameters that contribute to the optimal condition of turning process.

Finally, this thesis ends with a general conclusion that summarizes the work carried out and presents some perspectives that can be undertaken based on the key findings revealed by this research.

1.3. Note to the reader

Since this thesis is organized around four important chapters, the first of which is devoted to a bibliographic synthesis and the other chapters are a series of journal articles (3 scientific papers), some material might be repeated during reading process. In particular, there is some overlap in the introduction sections of some chapters. In addition, the sections describing experimental instruments and measurement methodology in some of the chapters contain significant repetition because the same facilities were used for all experiments.

Chapter 1. Literature review

This chapter gives background information about the main themes related to the works carried out during this thesis. Doing so, allows us to explore and understand the fundamental subjects and experiments of the current thesis, as well as to determine the gap in the subject area. The literature review chapter consists of the following sections:

- The first section sheds the light on stainless steels and an introduction to austenitic stainless steels. It includes a brief history of the stainless steels and their classifications, as well as application and properties of austenitic stainless steels.
- A brief introduction on the turning process is outlined in section 2. The key parameters of the turning process are mentioned. The material removal process is also described.
- In the third section, a presentation of the cutting tools in machining is made, including their geometries, materials and coating.
- The coatings methods are briefly reviewed in section 4.
- An overview of the cutting fluids, including their types and functions, is provided in section 5.
- The sixth section presents the description concerning machinability and its general aspects such as cutting forces, cutting temperature, tool wear, surface roughness and chip morphology.

The chapter then concludes with a summary with a critical assessment of the literature, indicating the gap in the research.

1.1 Stainless steels

Stainless steels were introduced at the beginning of the twentieth century as a result of pioneering work in England and Germany. Over the next half century, manufacturers have developed a large family of stainless steels that have proven to be extremely useful in chemical, energy, food and other industries.

Stainless steels contain chromium with a content of 12-25% Cr, which is responsible for corrosion resistance [1.1]. They are called stainless because, in the presence of oxygen (air), they develop a thin, hard, adherent film of chromium oxide that protects the metal

from corrosion [1.2]. This protective film builds up again in the event that the surface is scratched [1.2]. In addition to chromium, several alloying elements in stainless steels typically are nickel (Ni), molybdenum (Mo), copper (Cu), titanium (Ti), silicon (Si), manganese (Mn), aluminum (al) and sulfur (S).

Stainless steels are available in a wide variety of shapes such as coil sheets, plates, bars, wire, and tubing. Their typical applications in cookware, cutlery, Kitchen equipment, health care and surgical instruments, petroleum industries, automotive and aerospace structural alloy, and constructional materials in large buildings [1.3]. They are usually divided into five categories (Figure 1.1), may depend on their primary constituent of the matrix such as ferritic, martensitic, austenitic, and duplex (combined ferritic-austenitic), or may depend on their heat treatment utilized rather than microstructure like precipitation hardenable (PH) alloy. The category of austenitic stainless steels is the type being investigated in this thesis.

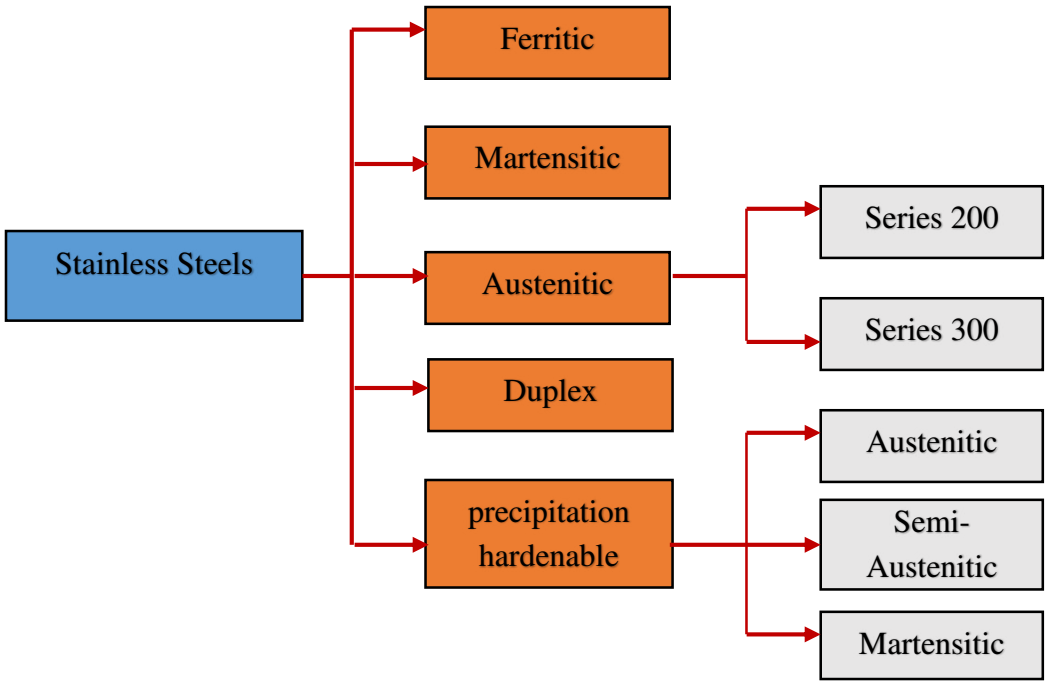

Figure 1.1. Classification of stainless steels [1.4]

1.1.1 Introduction to Austenitic stainless steels (ASS)

The austenitic stainless steels represent the largest group of stainless steels in use, making up 65-70% of the total for the past several years [1.1]. This kind of steels generally composed of nitrogen, nickel or manganese in addition to chromium. The most commonly used types of this kind of stainless steel are based on 17-18% chromium and 8-11% nickel (304) and with the addition of molybdenum (type 316). Likewise, they are characterized by a Face Centre Cubic (FCC) microstructure phase that becomes a ductile phase at high temperature [1.5] and also enables them to provide good impact strength at low temperatures [1.6]. As a result, they have excellent corrosion resistance, good formability, weldability, ductility and toughness. They are also recognized as non-magnetic in the solution annealed condition owing to their austenitic structure. This kind of grade is further classified by numbers in the 200 and 300 series [1.2]. The most common grade of the AISI 300 series of austenitic stainless steels with a basic level of corrosion resistance is the type 18/8 type (AISI 304) with 18% Cr and 8% Ni.

The 300 series also have the letter L (as in 304L or 316L), which is used to indicate the low-carbon content (around 0.03%). This allows them to prevent intergranular corrosion when they are employed in the welding process. In addition, this series is commercially available in various grades such as 301, 302, 303, 304, 308, 309, 316, 304L, 316L, 317, 321, 347 [1.7].

Another category is also called the Chrome-Manganese (Cr-Mn) group (200series). This latter was developed in the early 1930s. Its usage increased during the 1950s due to the rise in nickel prices [1.7]. This series is characterized by its lower nickel content than the 300 series. However, the small amount of chromium makes the 200 series have lower corrosion resistance in comparison with 300 series grades [1.7]. The 200 series is commercially available in grades such as 201, 202, 205 [1.7]

1.1.2 Application fields of austenitic stainless steel

Due to its excellent resistance to corrosion and heat, austenitic stainless steel is used in a wide range of industries. Indeed**,** Xavior et al. [1.8] reported in their study that AISI 304 steels find their applications in air craft fittings, aerospace components such as bushings, shafts, valves, special screws, cryogenic vessels and components for severe chemical

environments. They are also being used for welded construction in aerospace structural components. Similarly, Abbas et al. [1.9] have mentioned that 316 stainless steel materials are ubiquitously utilized in the chemical and petrochemical industry, in food processing, medical devices, pharmaceutical equipment, in potable water, wastewater treatment, in marine applications, and architectural applications near the seashore or in urban areas [1.9].

Austenitic stainless steels can be manufactured by various processes. Indeed, the family of manufacturing processes concerned in this thesis is machining. Machining is one of the most commonly used manufacturing processes in the automotive, aerospace and biomedical industries for producing complex 3D parts with a high level of surface finish and accuracy. It involves mechanically separating layers of material from a workpiece in the form of chips by using a cutting tool [1.10]. There are conventional and nonconventional machining processes. Conventional machining is referred to turning, milling, drilling …etc., where the parts are created using a cutting tool, whereas unconventional machining such as electro discharge machining, electrochemical machining and laser machining, have no direct contact between the tool and the workpiece. Turning (straight turning) is the machining process studied in this thesis, which produces revolution parts.

The following sections describe the turning process and its parameters such as tool geometry and material removal rate, as well as other parameters that must be considered when machining austenitic stainless steels, such as cutting tools and their coating and the use of cutting fluids.

1.2 Introduction to Turning

Turning is a popular machining process used to create cylindrical shaped parts in a variety of materials including stainless steels, hardened steels, nickel super alloys, and titanium alloys. During this process, the cylindrical workpiece is rotated when being machined by removing a layer of material, known as chips that slides on the tool's rake face. The cutting tool is mounted on the tool holder whereas the workpiece is clamped and fixed by the chuck jaws of the machine. However, the basic parameters in turning that play a vital role in defining the characteristic of manufactured parts are cutting speed, which is defined by

the workpiece rotation speed, the feed rate, which is defined by the cutting tool travel in a direction parallel to the longitudinal axis of the workpiece and depth of cut is also specified by cutting tool travel in the transversal axis, which allows to determine the amount of material to be removed from the workpiece, as illustrated in Figure 1.2. In the turning process, various operations such as facing, drilling, threading and so on can be performed. In the experimental work of this thesis, straight turning has been made.

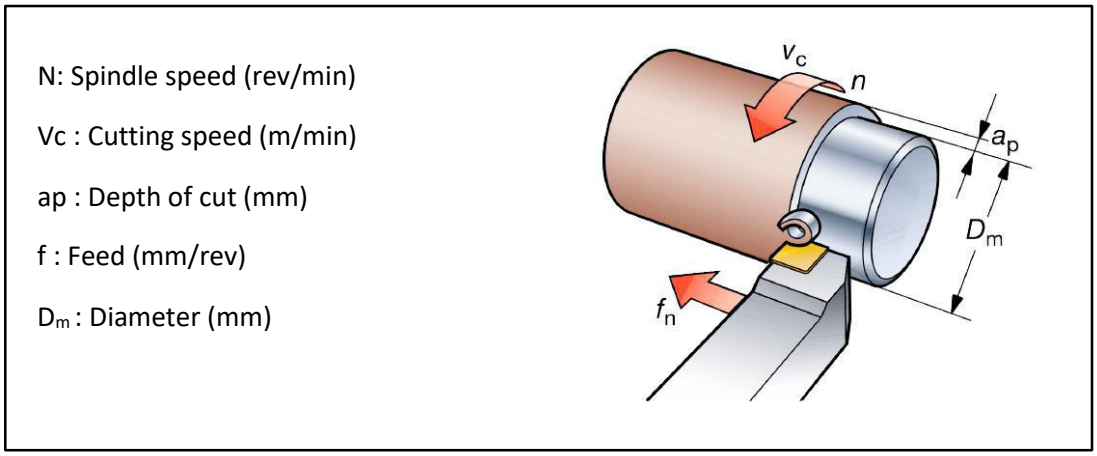

Figure 1.2: Example of straight turning operation.

1.2.1 Material removal rate

The material removal rate (MRR) is the volume of material removed per unite time, with the unite of mm^3/min [1.5]. MRR is a function of both uncut chip cross-section and cutting speed as the specific characteristics of the cutting process, as well as the workpiece material properties [1.1, 1.11].

MRR can be expressed as:

$$MRR = 1000 * Vc*f*ap* \frac{(D-ap)}{D} \quad (1.1)$$

where $D_m = D - ap$, in case, D (diameter) >>> ap, so, Eq. (1.1) also can be written as

$$MRR= 1000*Vc*f*ap\ [mm^3/min] \text{ or } MRR= Vc*f*ap\ [cm^3/min]. \quad (1.2)$$

1.3 Cutting tools

The machining process, the geometry and the material of the machined component are all factors to consider when selecting a cutting tool [1.12]. Cutting tools and their coatings in machining are discussed in this section.

1.3.1 Cutting tool geometry

There have been numerous studies of the effects of cutting tool geometry on machining process, such as that of M'Saoubi et Chandrasekaran [1.13]. They studied the effects of different cutting tool geometries on the temperature during dry machining of AISI 4340 Steel, Figure 1.3.

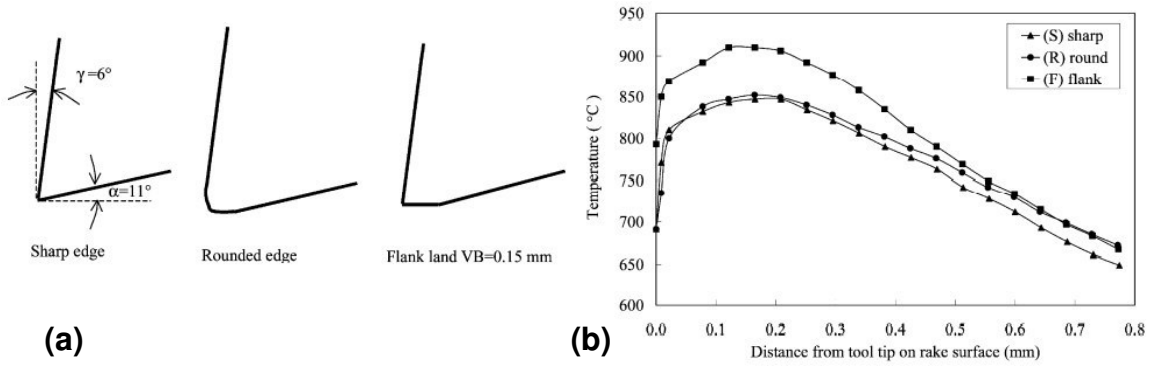

Figure 1.3. Effect of different cutting tool geometries (a) on the tool temperature profile on rake surface (b) during dry machining of 4340 steel with uncoated carbide tools (Vc = 200 m/min, f = 0.1 mm/rev), [1.13].

The results of M'Saoubi and Chandrasekaran [1.13] presented in Figure 1.3 show that the geometry of the cutting tool significantly affects the temperature along its surface. We observed that the maximum temperature point on the rake was located at a distance of ~ 0.155. However, the case simulated with a tool with a flank land stands out from the others with higher temperatures of approx. 60 °C. Further studies have been carried out on the influence of cutting tool geometry [1.14, 1.15], during the cutting process. For instance, Ventura et al. [1.14] have studied the influence of tool edge geometry on cutting forces and tool wear performance. The researchers noticed that the cutting forces increase proportional to the bluntness of the edge geometry (Figure 1.4).

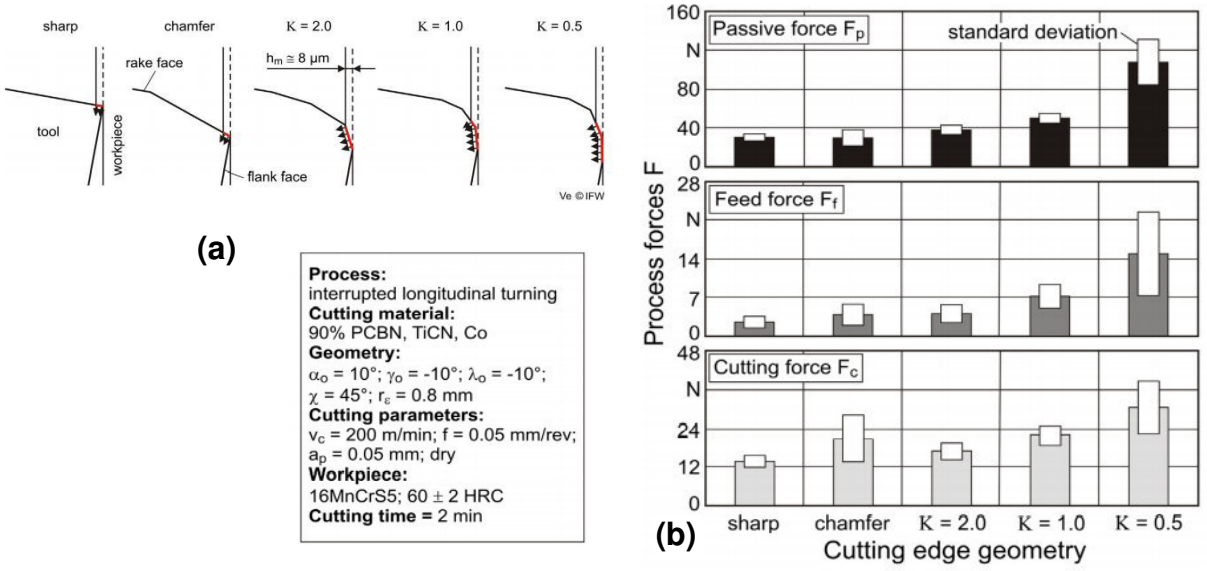

Figure 1.4. Influence of different edge geometries (a) on cutting force components (b) [1.14].

In addition, the results reported in the study of Ventura et al. [1.14] illustrated in Figure 1.5 revealed that a single chamfered cutting edge is the most appropriate. We can see that the flank wear width increases from the chamfered edge to the edge rounding with K = 0.5 for a fixed cutting time.

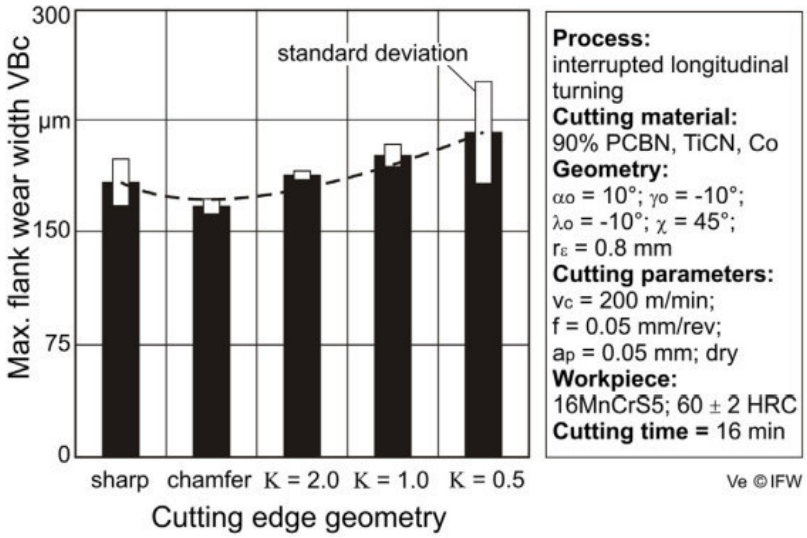

Figure 1.5. Maximum flank wear width achieved by different edge geometries after a cutting time of 16 min [1.14].

We are now interested in the work of Zhao et al. [1.16] who studied the effect of the nose radius of cutting tools during dry turning of a common steel with CBN cutting tools, Figure 1.6.

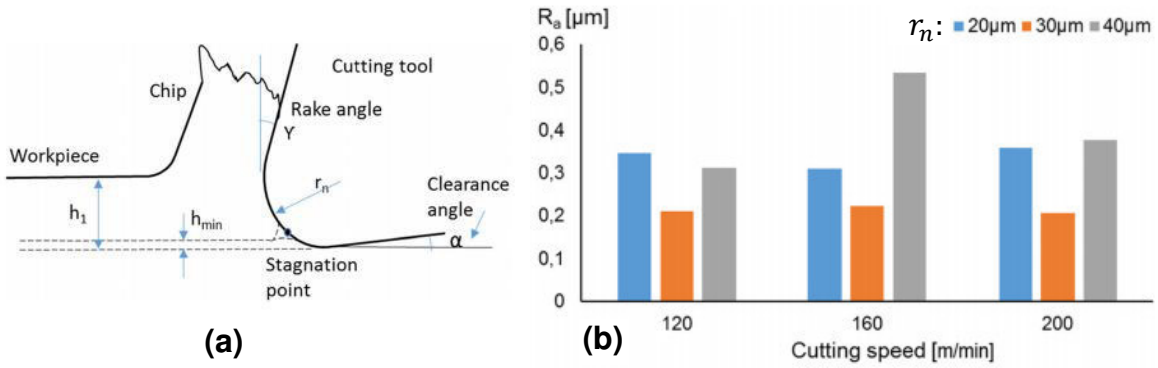

Figure 1.6. Characterization of cutting tool micro-geometry (a) and the effects of edge radius (r_n) (b) on surface roughness at f =0.08 mm/rev and ap =0.1mm, under dry turning of AISI 52100 steel [1.16].

With respect to Figure 1.6, we can note that the increase in the edge radius leads to an increase in the surface roughness. However, according to the authors' opinion, the lowest roughness of the machined surface achieved with an edge radius of 30 µm could be attributed to the stability of the cutting process [1.16].

The chip breaker is another feature of cutting tool geometry that has a major impact. Some examples of that are presented by Lotfi et al. [1.17]. Figure 1.7 presents the effects of chip breaker geometries on the cutting force and the chips obtained in turning test of AISI 1045 steel using tungsten carbide inserts. We notice that the lowest cutting forces are recorded for "CG" geometry and the highest one for "W" type. In addition, the chips obtained by Lotfi et al [1.17] have been classified into three categories: favorable, useable and disadvantage. This classification was made on the basis of morphologies produced according to CIRP classification [1.18]. We can also see that chip breaker geometries of "CG", "CM" and "PM" have produced favorable chip morphologies and useable ones have been obtained by using "DM" geometry, while "W" geometry has formed disadvantage types, as shown in Figure 1.8.

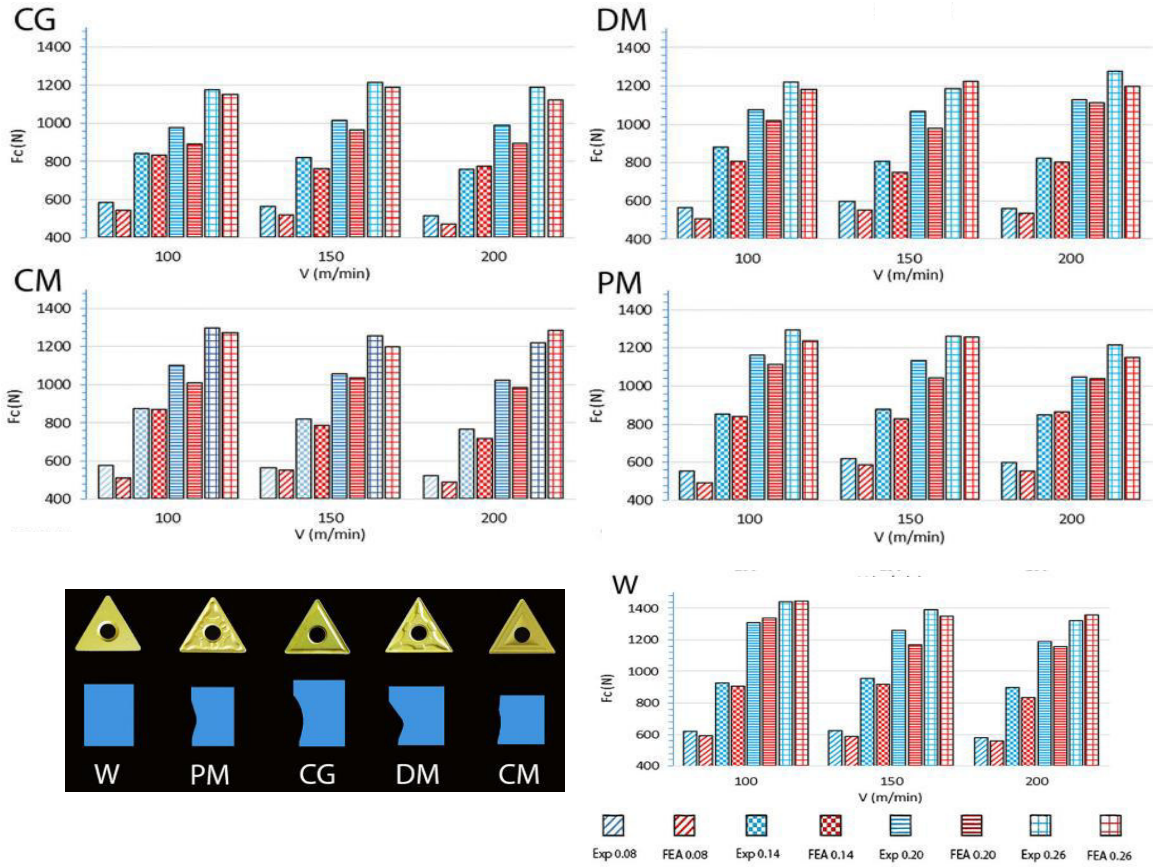

Figure 1.7. Inserts' chip breaker geometries and their effects on cutting force (f = 0.08, 0.14, 0.20, 0.26 mm/rev, ap =2.5 mm and tool edge radius 0.03 mm), [1.17].

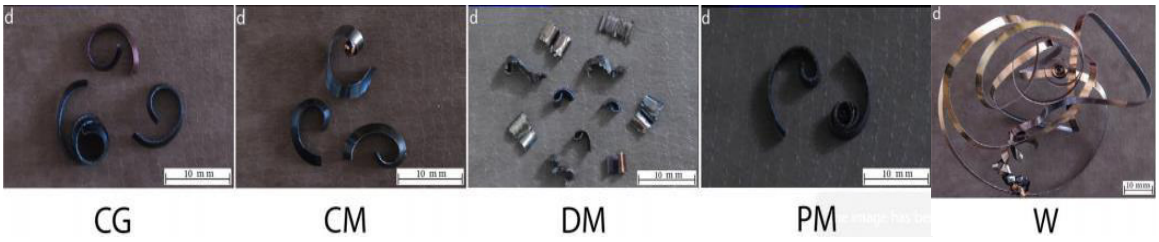

Figure 1.8. Various chip breakers and their influence on the formation of chips during turning operation (Vc =150 m/min, f = 0.26 mm/rev) [1.17].

Aside from the geometry of the cutting tools, the materials used to make them play an important role and their selection is based on the material being machined and the cutting conditions, among other factors.

1.3.2 Cutting tools' materials

Tool materials generally in use are classified into various categories: High-speed steels (HSS), Carbides, Cermets, Ceramics and ultra-hard materials (Cubic boron nitride (CBN), diamond), ...etc. Among these types, the family of carbides is the most widely used for the machining of stainless steels [1.19, 1.20].
To make right choices in this situation, a thorough understanding of the characteristics and application ranges of specific tool materials is needed.
Cutting tool materials made of carbides (also known as cemented or sintered carbides) can be classified into two categories [1.21]:

- Simple carbides consisted of tungsten-carbide (WC) particles bonded together in a cobalt (Co) matrix. The amount of Co present varies between 2 and 15%. Among these carbides there are (*K* et *E* being respectively thermal conductivity and Young's modulus):
  - ✓ 85% WC+ 15% Co (k=100 $Wm^{-1}K^{-1}$, E= 530 GPa),
  - ✓ 98% WC + 2% Co (k = 79 $Wm^{-1}K^{-1}$, E= 630 GPa),
- Mixed carbides which possess, in addition to WC, titanium carbide (TiC), tantalum (TaC), vanadium (VC) and niobium (NbC). Within this category there are:
  - ✓ 84%WC + 9%Co + 5% TiC+ 2%TaC (k=110 $Wm^{-1}K^{-1}$, E= 530 GPa),
  - ✓ 55.5% WC + 9.5 Co + 19.7% TiC (k=50 $Wm^{-1}K^{-1}$, E= 550-600 GPa).

The following basic grades of coated carbides are recommended for machining austenitic stainless steels [1.1]: PVD-TiCN/TiN coated carbide for finishing operations, CVD-TiCN/Al_2O_3/TiN coated carbide for finishing and semi-finishing operations and PVD-TiAlN/TiN-coated for medium and roughing operations.

Besides, Cermet tools have recently received research attention to support the usage of coated cemented carbide for increasing productivity in stainless steels turning [1.22]. However, there are few studies on cermet tools for machined stainless steel because the performance of cermet tools is not yet proven [1.23]. Proceeding from that, the intention of investigating the performance of carbide and cermet cutting tools is one of the rationalities of this thesis.

Cermets exist on the nexus of ceramics and metals. They contain titanium nitride (TiC), titanium carbide (TiC) or titanium carbo-nitride (TiCN). Their physical characteristics and implantation range fall amid those of WC and plain ceramics. Cermets provide better dimensional accuracy in work pieces and good resistance to chipping [1.24, 1.25] and they also are less susceptible to diffusion wear than WC. However, they possess a lower strength and toughness and a higher thermal expansion coefficient compared to WC [1.26].

Cutting tools may be coated with one or more layers of coating to enhance their pertinent properties, thereby improving the cutting operation. The materials used in coatings are discussed in the following section.

1.3.3 Coating tool materials

In terms of coating materials, there are commonly used materials for single-layer coating such as titanium nitride (TiN), titanium carbide (TiC), titanium carbo-nitride (TiCN), titanium aluminum nitride (TiAlN), aluminum oxide (Al_2O_3) and WC/C (amorphous diamond-like carbon hard lubricant) [1.26-1.28]. These materials can also be combined to form multilayer coatings, such as: Al_2O_3 on TiC or TiCN, TiN on TiC, TiN/ TiC/ TiN, TiN/ TiCN/ TiN, TiN/ TiC/ TiCN, Ti(C)N/ Al_2O_3/TiN, Al_2O_3/TiC, TiN/TiC/Al_2O_3/TiN, and TiAlN + WC/C [1.26-1.28].

Among this variety of coating materials, Titanium carbonitride (TiCN) and titanium-aluminum nitride (TiAlN) are effective in cutting stainless steels [1.5]. Figure 1.9 shows coating layers of coated insert.

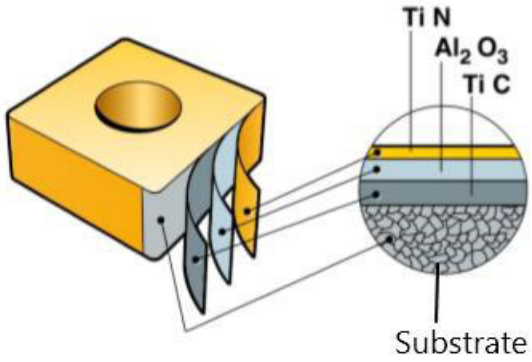

Figure 1.9. Coating of a cutting insert [1.29].

Ciftci [1.30] performed dry turning experiments on AISI 304 and AISI 316 austenitic stainless steels using two different grades of cemented carbide cutting tools having top layer coating, namely TiC/TiCN/TiN and TiCN/TiC/Al_2O_3. From Figure 1.10, Ciftci [1.30] concluded that TiC/TiCN/TiN coated cutting tools gave lower cutting forces than TiCN/TiC/AL_2O_3 coated tools, due to the lower coefficient of friction of the TiN top coating layer [1.30].

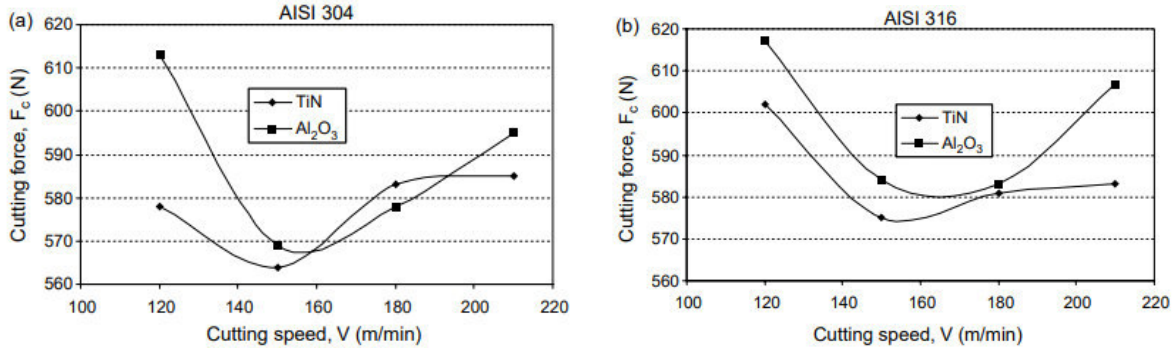

Figure 1.10. Cutting force data vs. cutting speed for turning (a) AISI 304 and (b) AISI 316 austenitic stainless steels using TiC/TiCN/TiN and TiCN/TiC/Al_2O_3 coated carbide tools at a feed rate of 0.16 mm/rev and depth of cut of 1.6 mm [1.30].

Likewise, Marimuthu et al. [1.31] have conducted turning tests during straight turning of AISI 316L using multi-layered (TiCN+Al2O3) and single layered (Ti, Al)N coated cutting tools. Based on their results, we can highlight that the single layer coated (Ti, Al) N insert gave better performance than the multi-layer coated (TiCN+Al_2O_3) insert, as depicted in Figure 1.11.

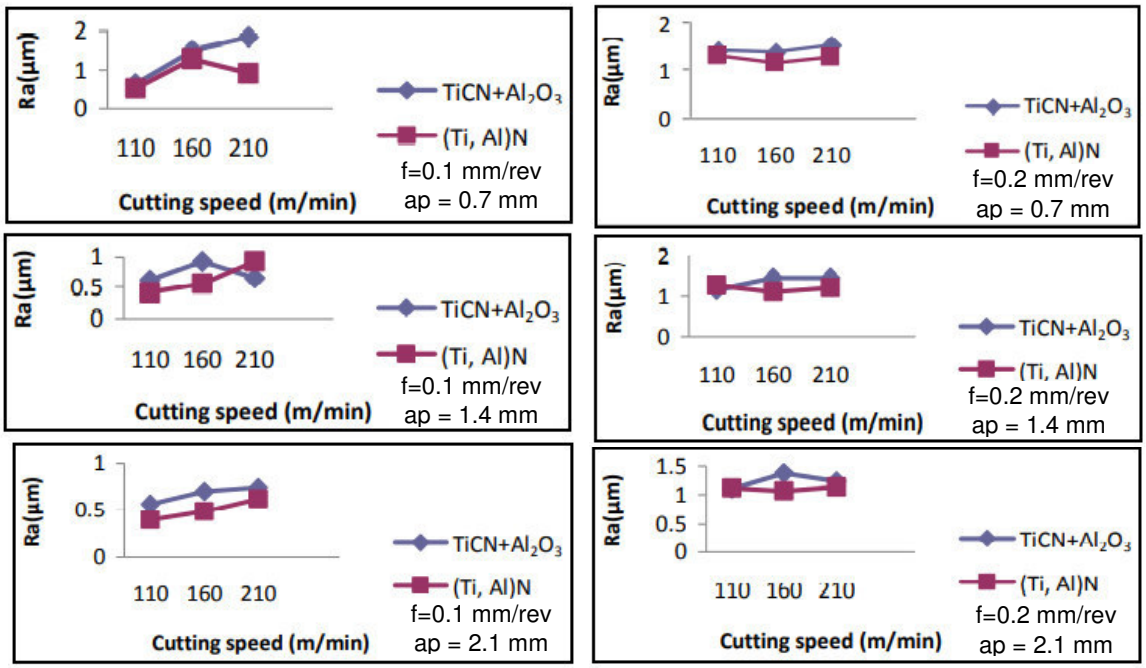

Figure 1.11. Surface roughness data vs. cutting speed for straight turning of AISI 316L using TiCN+Al_2O_3 and (Ti, Al)N coated cutting tools [1.31].

Kaladhar [1.32] carried out machining experiments on AISI 304 austenitic stainless steel using five different coated tools, namely (TiCN-Al2O3-TiN) cemented carbide coded GC2015, (TiAiN-TiN) cemented carbide coded GC1025, (TiCN-TiN) Cermet coded GC 1525, (TiN-Al_2O_3-TiCN-TiN) cemented carbide coded KC 9225 and CVD (Ti (C, N)-Al_2O_3) cemented carbide coded TP 2500, and evaluated their performance on surface roughness and flank wear. From Figure 1.12, the results indicated that the TiAlN-TiN (Titanium Aluminum-Nitride/Titanium Nitride) coated cemented carbide insert (GC 1025) showed better surface quality and reduced flank wear rate followed by TiCN-TiN (Titanium Carbo-Nitride/Titanium Nitride) coated cermet insert (GC1525).

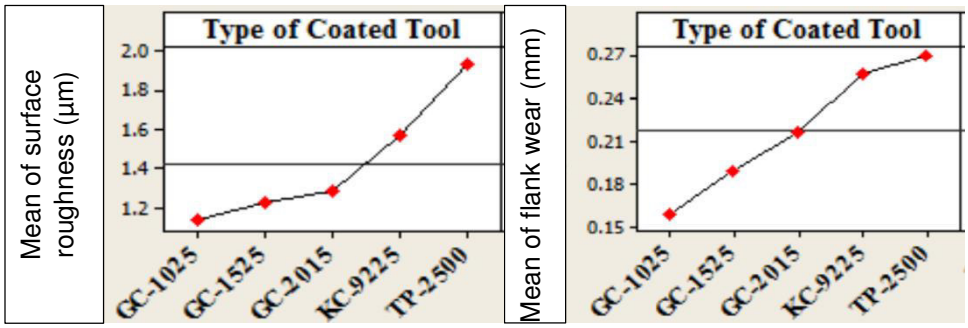

Figure 1.12. Main effect plots for surface roughness and flank wear [1.32]

These coating materials are applied on cutting tools by the following two methods.

1.4 Coating Methods

Coatings can be done using two different processes, either by Chemical Vapor Deposition (CVD), or Physical Vapor Deposition (PVD). These coating processes are generally applied to both single and multilayer coatings.

CVD process is achieved by heating and subjecting the substrate (workpiece surface) to a gas stream of appropriate chemistry pumped inside a reactor, which reacts with the substrate and deposited on its surface, forming a thin, hard coating layer. This process is carried out at high temperatures, reaching temperatures of up to 900°C. However, deposited coating at high temperatures may cause the embrittlement of the cutting edge [1.33].

In a PVD process, the coating material is vaporized and deposited by vacuum deposition or sputtering. This process runs in a high vacuum at lower substrate temperatures in the range of 200° to 500°C. In PVD, the particles to be deposited are transferred physically to the workpiece, rather than being transferred by chemical reactions as in a CVD process. However, CVD-deposited coatings are typically harder than PVD-deposited coatings due to the metallurgical bond formed between a coating and substrate produced by CVD rather than the mechanical bond formed by PVD, resulting in longer tool lives when properly applied. Nonetheless, the PVD process, when compared to the CVD process, takes a less typical cycle, and is more environmentally safe due to the type of the gases used in the CVD process, which are toxic [1.34].

In the context of comparison between the two types of coating, Kaladhar et al. [1.33] have evaluated the performance of coating materials including PVD coated insert-1025 and CVD coated insert-2015 in terms of surface roughness during turning of AISI 304 austenitic stainless steel (Figure 1.13). Figure (1.13) shows that the values of average surface roughness found by PVD and CVD coated inserts are 1.13 µm and 1.28 µm, respectively. The findings obtained when turning with a PVD coated tool have shown better performance, resulting in a 13.27% improvement of Ra, than the findings obtained with a CVD coated tool [1.33].

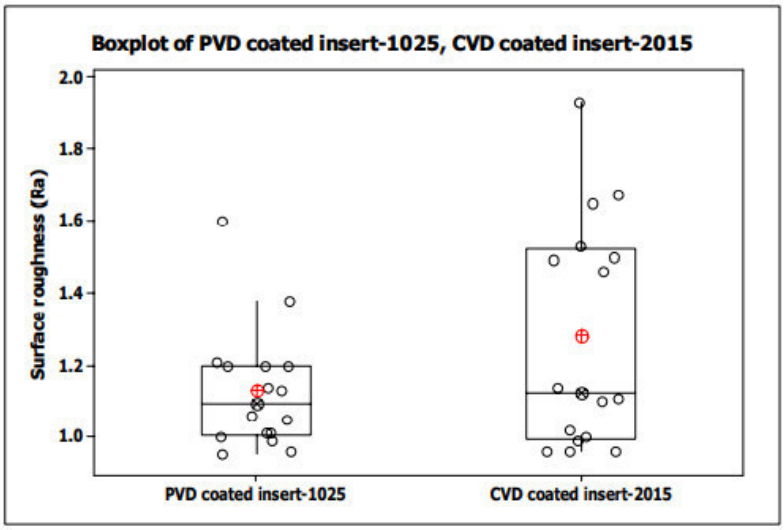

Figure 1.13. Box plot of average surface roughness values obtained by two cutting inserts [1.33].

Similarly, the investigation carried out by Bouzid et al. [1.35] has highlighted the crucial role for different types of coating (CVD and PVD) when dry machining of AISI 304 stainless steel. The authors have tested the performance of the cutting tools in terms of flank wear (Figure 1.14).

Figure 1.14 illustrates the tool life of each cutting tool. The tool life of CVD coated carbide coded as GC 2015 and PVD coated carbide coded as GC 1015 are respectively found to be 65 min and 13 min [1.35].

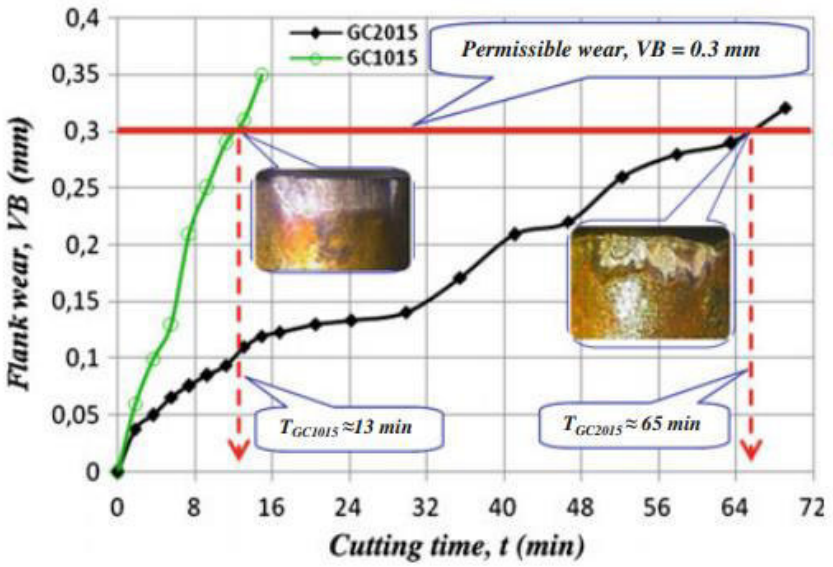

Figure 1.14. Flank wear of cutting tools versus machining time at Vc = 280 m/min, f = 0.08 mm/rev and ap = 0.2 mm [1.35].

1.5 Cutting fluids in cutting process

The cutting process (alternatively known as chip removal) is a shearing mechanism that generates heat as a result of friction and deformation at the tool-chip-workpiece interfaces to transform a workpiece to an end shape and size. During this fundamental mechanism, higher temperature occurs in a very small area between the tool-workpiece. Subsequently, it has an effect on a number of quality indicators.

For efficient and cost-effective machining, a slight reduction in the machining zone's temperature is needed. Some factors such as feed rate, depth of cut and cutting speed are optimized to lower the temperature at the cutting area. One of the most effective ways to reduce the temperature at the cutting area is to employ cutting fluids while machining. The cutting fluids have been employed extensively in the machining processes to achieve the following purposes [1.5]:

- Reduce friction and wear, thus improving tool life and the surface finish of the workpiece.
- Cool the cutting zone, thus improving tool life and reducing the temperature and thermal distortion of the workpiece.
- Reduce forces and energy consumption.

- Flush away the chips from the cutting zone, thus preventing the chips from interfering (i.e., scratching the machined surface) with the cutting process.
- Protect the machined surface from environmental corrosion.
- Prevent a welding effect on the rake face, which could promote tool failure.

Due to their advantages, cutting fluids can contribute significantly towards machining costs [1.36]. For instance, it was estimated the costs relevant to cutting fluids represent up to 17.9% of total manufacturing costs in the European automotive industry, which compares to tooling costs of about 7.5%, as shown in Figure.1.15 [1.37].

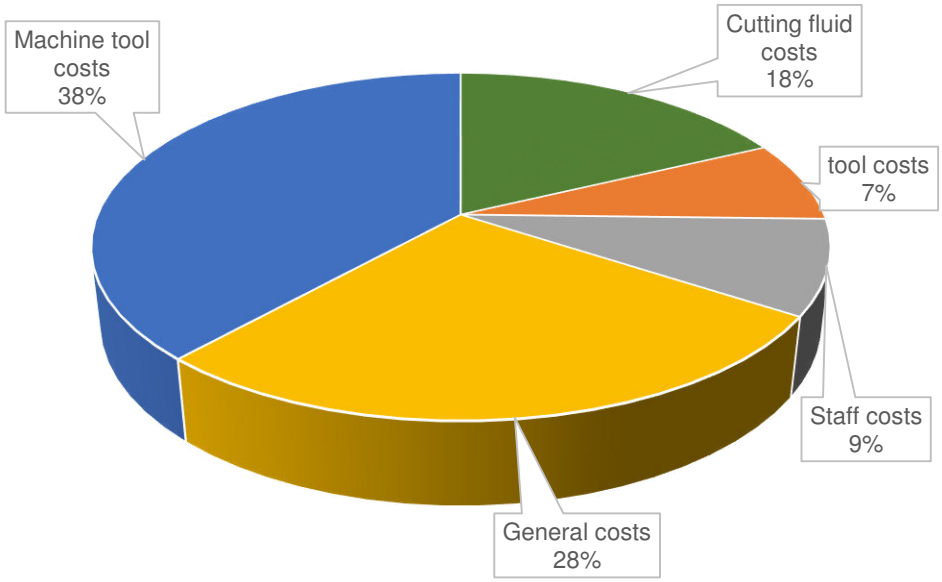

Figure 1.15. Distribution of manufacturing costs in the European automotive industry [1.37].

1.5.1 Types of cutting fluids

It is interesting to note that in the beginning of twenty centuries (1907), F. Taylor stated that the cutting speed could be raised by up to 40% without decreasing tool life by supplying sufficient quantities of water to the cutting area [1.38]. Despite its excellent coolant and availability, water is regarded as ineffective as a lubricant, resulting in serious corrosion issues i.e., oxidation of machine tool components and machined parts. Since then, new formulations of cutting fluids have been developed to cover most workpiece

materials and metal cutting processes [1.36, 1.39]. Neat cutting oils (petroleum oil-based, vegetable or animal base oils), water-soluble fluids (soluble oils, semi-syntactic (semi-chemical), and syntactic (chemical) fluids, and Gas-based fluids (air, liquid nitrogen (LN_2), carbon dioxide, argon) are widely used on machining shop floors in order to increase the productivity and the quality of manufacturing processes by cooling and lubricating during metal cutting [1.36]. The classification of cutting fluids used in metalworking operations is described in greater detail in literature [1.40, 1.41]. To determine the influence of the type of cutting fluids on machining characteristics, Anthony Xavior and Adithan [1.8], have used three types of cutting fluids, including vegetable (Coconut oil), soluble oil and straight or neat cutting oil during machining of AISI 304, as shown in Figure 1.16. The researchers found that the cutting fluids has some considerable effect on both surface roughness and tool wear. Also, they observed that vegetable based oil (Coconut) was found to be a better cutting fluid than conventional mineral oils in reducing the surface roughness and tool wear [1.8].

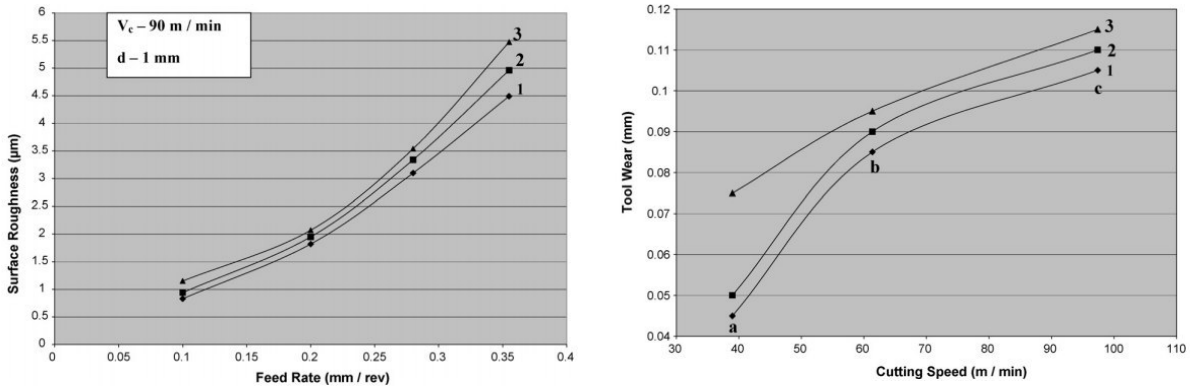

(a) (b)

Figure 1.16. a) Feed rats vs. surface roughness, b) Cutting speed vs. tool wear at ap = 0.5 mm and feed rate (f) = 0.2, 0.25 and 0.28 mm/rev at three points a, b and c, respectively. (1) Coconut oil, (2) soluble oil and (3) straight cutting oil [1.8].

1.5.2 Functions of cutting fluids

Depending on the type of machining operation, the cutting fluid role provided may be a coolant, a lubricant, or both to the cutting zone. Coolant at relatively higher cutting speeds (to increase heat dissipation from the machining zone) and lubricating at relatively low cutting speeds (to reduce the heat generated by friction) [1.40]. To accomplish such

functions, the fluids should illustrate a number of tribological and thermal properties [1.42]. As a coolant, the cutting fluid can reduce the distortion of the workpiece material, particularly at high cutting speeds and temperature [1.36]. The ability of a cutting fluid to keep the temperature below the thermal softening temperature of the tool material significantly extends its tool life [1.36]. As a lubricant, it minimizes friction and wear in the working zone, and thus the heat generated by frictional force and wear is also reduced [1.36].

Cutting fluids' well-known function in any cutting operation has rendered them unavoidable in terms of providing sufficient cooling and lubrication. However, the extravagant use of these fluids (conventional flooding cooling) augments their disposal and maintenance costs (about up to 59% of total fluid costs) [1.37], particularly when non-biodegradable conventional fluids are used. Furthermore, as stated by Sarikaya et al [1.43] in their review, the use of millions of liters of coolant in machining operations every year not only harms millions of operators exposed to them but also has an unfavorable effect on the environment. As a result, it has become essential to balance the use of cutting fluids, which is generally done by flooding cooling, in order to achieve clean and highly efficient production processes in machining operations. Dry cutting, minimum quantity lubrication (MQL) and nanofluid based MQL have been introduced to achieve this goal. In the following chapters, we will go through these alternative approaches.

1.6 Machinability

The machinability term was suggested for the first time by Taylor in the 1920s [1.3] in order to describe the machining behavior of workpiece materials. Since that time, it has frequently employed, but rarely fully explained. The term of machinability refers to either how easily or difficulty with which a given material can be cut, meaning how easy or demanding it is to shape the workpiece with a selected cutting tool [1.1]. The machinability of any work material is affected by many factors, as shown in Figure 1.17.

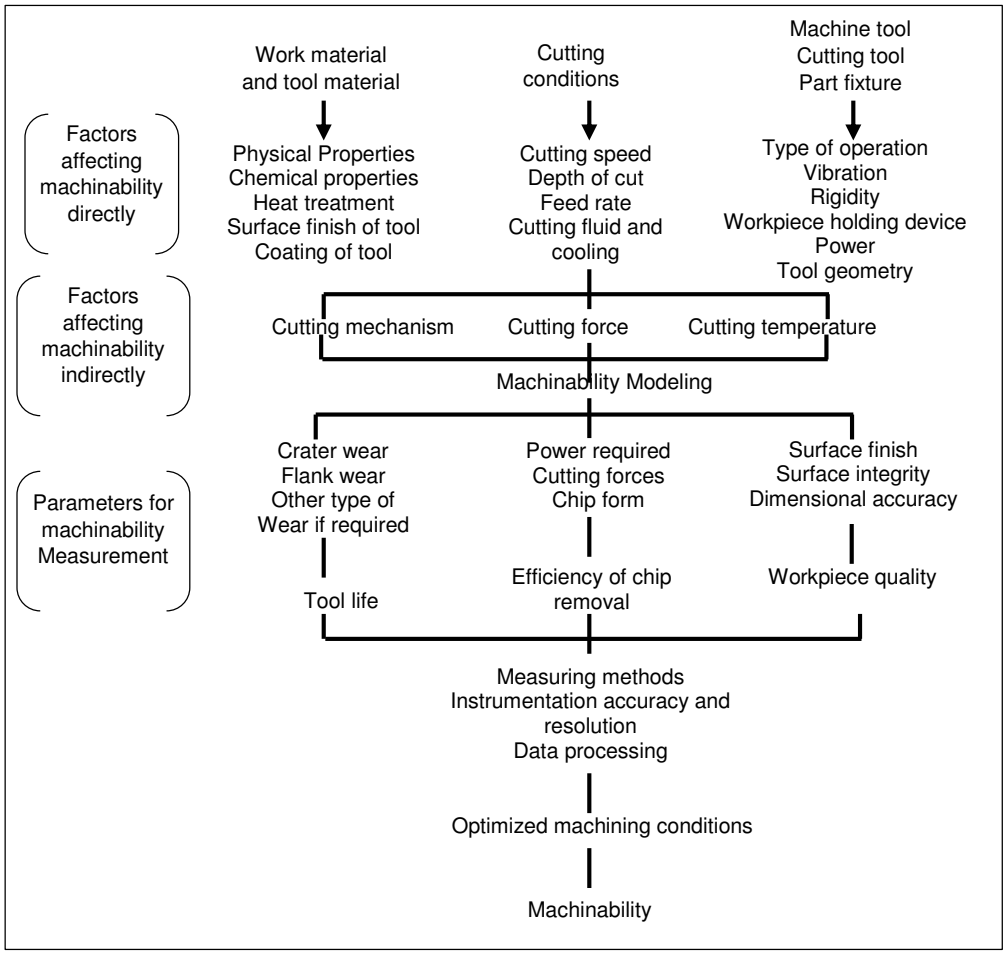

Figure 1.17. Factors affecting machinability [1.26].

Some frequently appearing causes of difficulties in conducting the machining process in an efficient/optimal manner are seen in Figure 1.18. In general, the sources of machining problems are very complex and concern all elements of the machining system [1.1].

Machinability may not be uniquely described in quantitative terms and can have different definitions in different contexts. A material may have good machinability by one criterion, but poor by another one. Also, relative machinability may change when different machining operations are conducted, i.e., turning versus milling, or when the cutting tool material is changed [1.44]. In such cases, the term machinability is often used for comparison of cutting performance or ranking purposes [1.1].

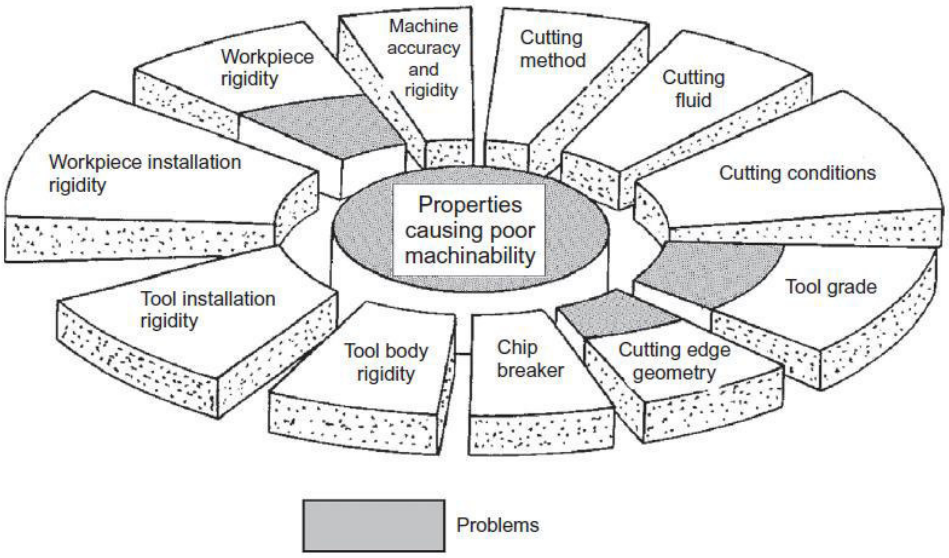

Figure 1.18. Causes for poor or difficult machinability [1.45].

In addition, it is noteworthy that, since there is no unit of machinability, it is usually judged by comparing one material against another which is taken as reference [1.3]. For example, according to the American Iron and Steel Institute (AISI), the machinability of a material can be estimated in percentage by comparing it to the machinability rating of a material with which they have more experience, such as AISI-B1112 material (resulfurized plain carbon free machining steel of 160 BHN), which has an assigned machinability rating of 100% [1.3]. The machinability data is generally collected from production experience and, therefore, it can be determined by measuring surface quality and tool life for each material under common operating conditions. In that case, the higher the value of the machinability rating material than 100%, the easier to manufacture it becomes than B1112 and one with a value lower than 100% will be more difficult to manufacture [1.46]. Table 1-1 presents the relative machinability of some common alloys. Note that the problem associated here is that if different tool materials are used to assess relative machinability, different ratings may occur. Thus, tables and data supplied should only be used as guidelines.

Table 1.1. Relative machinability ratings [1.46]

Machinability ratings	Materials
Excellent rating (200%- 400%)	Al-alloys, Mg-alloys
Good rating (150%- 250%)	Gray cast iron, brass, free cutting steel
Fair rating (~100%)	Law carbon steel, low alloy steel
Poor rating (50%-60%)	Free cutting 18-8 stainless steel
Very poor rating (20%-40%)	18-8 stainless steel, super alloys, Ti alloys

In general, machinability is often assessed by: 1) the magnitude of cutting forces; 2) surface finish of the machined part; 3) tool wear/tool life; 4) the cutting temperature; and 5) chip morphology [1.47]. In machining practice, tool life and surface roughness are generally considered to be the most important criteria [1.5]. Our thesis is limited to studying the effects of some factors (Input) on some criteria (Outputs), as shown in Figure 1.19. These machinability criteria (outputs) are presented in the following sections.

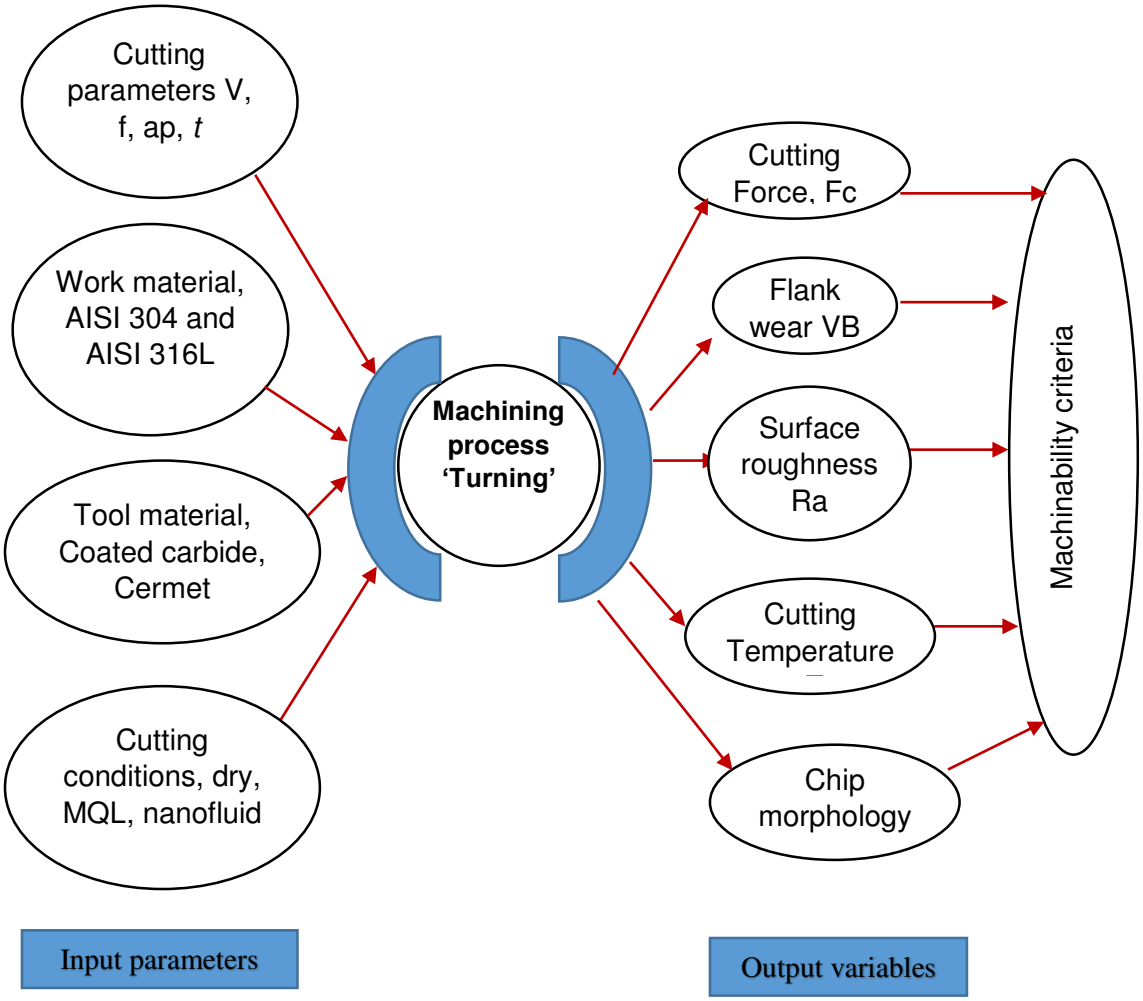

Figure 1.19. Input parameters, output variables and machinability criteria.

1.6.1 General aspects of machinability of stainless steel

Table 1.2 provides the machinability ratings of some types of stainless steels. The rating test typically involves a comparison between work materials. With respect to Table 1.2, stainless steels can be considered as more difficult to machine materials due to their high tensile strength, high ductility, high work hardening, low thermal conductivity and abrasive character [1.26]. The combination of these properties often results in high cutting forces, rise in temperatures, and tool wear rates, as well as a susceptibility to notch wear, difficulties with chip breakability, built up edge (BUE) formation, and poor machined surface finish [1.46,1.48,1.49]. Therefore, by analyzing the cutting forces, cutting

temperature, tool wear, surface roughness and chip morphologies, properties related to difficult-to-machine stainless steels can be extracted.

Table 1.2. Typical machinability ratings for selected work materials [1.44].

Work material	Machinability rating
Base steel: B1112	1.00
Stainless steels	
301, 302	0.50
304	0.40
316, 317	0.35
403	0.55
416	0.90

1.6.1.1 Cutting forces

When the cutting process begins, the cutting tool makes contact with the workpiece, causing extensive stress, deformation, separation and friction processes at the cutting area. The high compressive and frictional contact stresses on the tool face result in a substantial cutting fore F, which is the force needed to finish the machining operation to cut the workpiece and deform the materials to produce the chips [1.50].

Knowledge of the cutting forces involved in the cutting process is critical for the following reasons [1.5]:

- Proper cutting tools design to minimize distortion of the machine components and maintain the desired dimensional accuracy of the machined parts.
- Proper design of the fixtures used to hold the workpiece in order to be capable of withstanding these forces without excessive distortion.
- Finding the required power to cut the alloy, which in turn assists in selecting a machine tool with adequate electric power.

The cutting forces can be precisely measured by means of special device called tool force dynamometer mounted on the tool holder.

There are three kinds of forces can be extracted and evaluated form the cutting process, as illustrated in Figure 1.20.

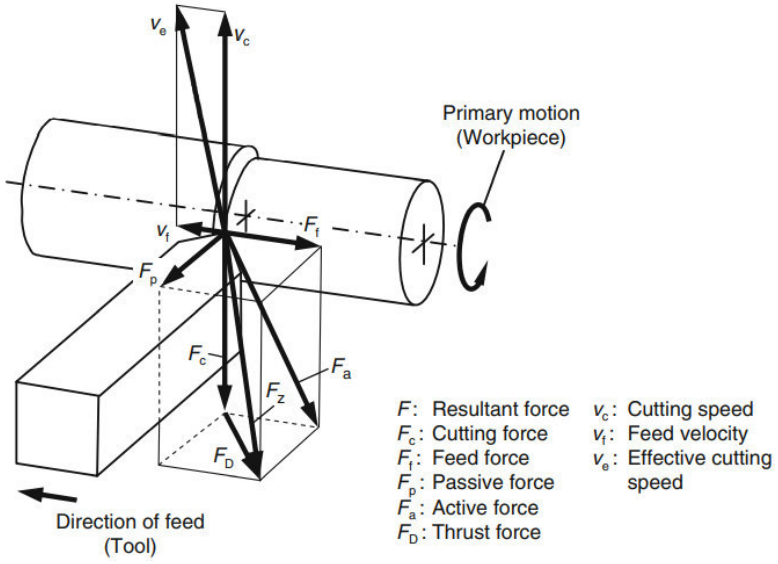

Figure 1.20. Resultant force and its components in cutting process [1.10].

- **Tangential cutting force (Fz)**

Fz or Fc acts along the y-axis. It is normally the greatest component responsible for the chip separation of the workpiece during the cutting process and supplies the energy required for it.

- **Radial cutting force (Fy)**

Fy is also known as a thrust force, and it acts along the x-axis, which is the radial direction of the workpiece.

- **Axial cutting force (Fx)**

Fx is also known as a feed force, and it acts in a direction parallel to the feed motion, which is the z-direction.

Moreover, the forces required to machine a material are directly related to the consumed power. Since the greatest component acts in the cutting velocity direction is tangential force. Therefore, the cutting power (Pc) is the product of force and cutting speed. Thus, Pc is normally calculated as:

$$Pc\ (W) = Fz * Vc \quad (1.3)$$

where Fz is tangential cutting force (N), Vc is cutting speed (m/min).

1.6.1.2 Cutting temperature

As in all machining processes where plastic deformation takes place, the energy dissipated in cutting is transferred into heat that, in turn, increases the temperature in the deformation zones and surrounding areas of the chip, tool and workpiece. According to Trent and Wright [1.44], 99 per cent of the work done is converted into heat. There are three main sources of produced heat during the process of cutting metal with a machine tool (Figure 1.21) [1.51]:

- The work done in shearing in the primary shear zone as the workpiece is subjected to large irreversible plastic deformation.
- Heat generated by friction and shear on the tool rake face, or secondary shear zone. The ship material is further deformed and some adheres to the tool face.
- Heat generated as the tool rubs against the machined surface, especially for worn tools.

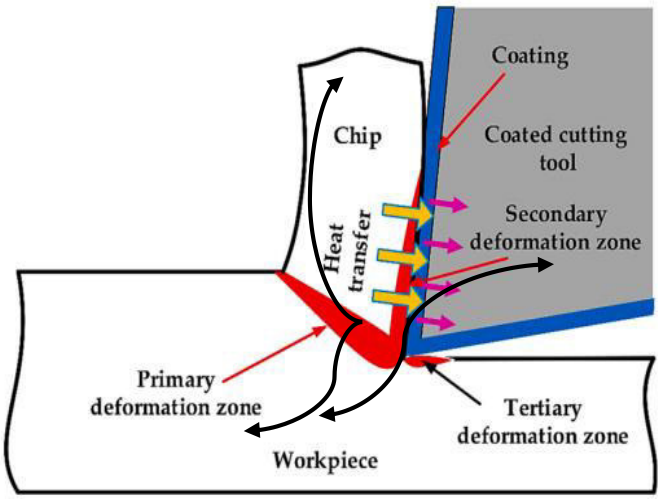

Figure 1.21. Representation of the different heat flows and energy sources [1.51]

The induced heat is distributed to the different parts of the tool, the workpiece and the chip (Figure 1.21). The heat transfers in the chip and workpiece are primarily carried out by conduction, whereas heat transfers in the tool are carried out by diffusion. The flow distribution depends on the cutting conditions and the properties of the materials. Only a

small percentage of the heat generated is transmitted to the tool and the workpiece, the majority of it is evacuated through the chip [1.51, 1.52].

1.6.1.2.1 Measuring temperature

There are many methods of measuring temperature rise in machining, including thermocouples, metallurgical changes, infrared thermometer, infrared cameras… etc. The details of these techniques are documented in literature [1.53]. Some methods are more practical than others. All the techniques, without exception, have their individual limitations [1.54].

Applied to machining, the thermocouple technique is used in two different ways [1.55]:

(1) with small thermocouples inserted into the cutting tool.

(2) using the natural thermocouple formed by the workpiece and tool itself.

Although fairly simple to use, thermocouple techniques are still imprecise and only provide a temperature and can only provide an average temperature at the tool-chip interface. In order to have a complete information on the temperature distribution other techniques must be considered.

Infrared thermography techniques are also used to measure the temperature fields in the cutting areas. As early as 1961, the photographic device proposed by Boothroyd [1.56] made it possible to obtain the complete temperature field on the tool, the chip and the workpiece (Figure 1.22). Infrared cameras are increasingly used to measure temperature and its distribution.

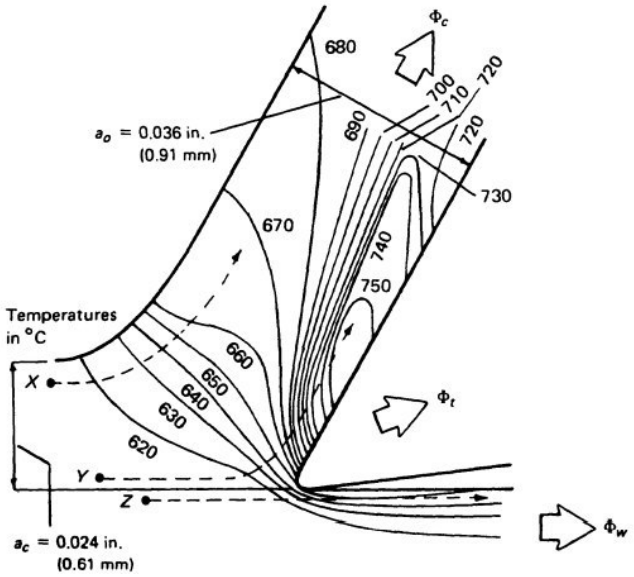

Figure 1.22. Temperature distribution in workpiece and chip during orthogonal cutting (obtained from infrared photograph) for free-cutting mild steel where the cutting speed is 0.38 m/s, width of cut is 6.35 mm, the working normal rake is 30 degrees and the workpiece temperature is 611°C [1.56].

However, these techniques require sophisticated equipment that must be rigorously calibrated and the various methods used are not yet capable of ensuring spatial and temporal resolution.

In parallel to the experimental techniques, analytical and numerical methods have been developed to analyze the temperature distribution during cutting process [1.57]. Among the latter, finite element method is the most widely used (Figure 1.23).

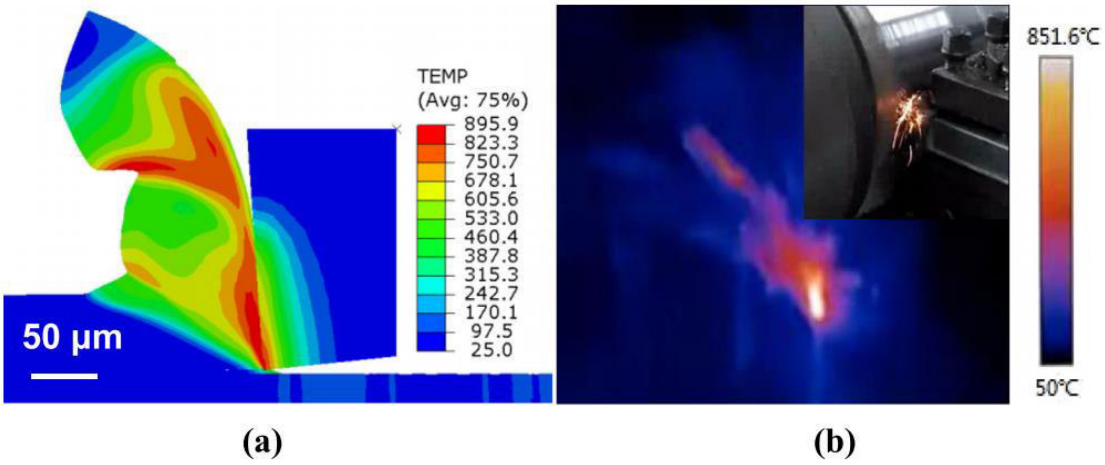

Figure 1.23. Cutting temperature of (a) simulated results and (b) experimental results obtained by infrared image during tuning operation [1.58].

In this dissertation's experimental work, an Infrared thermometer or pyrometer technique was used to measure the tool cutting temperature. This technique has been used by researchers to estimate cutting temperature more than any other method. However, since this technique only indicates surface temperature, the precision of the results is dependent on the emissivity of the surfaces, which is difficult to determine accurately.

1.6.1.2.2. Temperature at the tool-chip interface

The temperature on the cutting face is the main parameter that influences tool wear through phenomena such as abrasion, adhesion and diffusion. It plays a determining role in the nature of the friction at the interface and significantly changes the physical and mechanical properties of the materials making up the tool.

The shape of the temperature profile can be different depending on the cutting parameters process and the nature of the materials considered, but the different measurement methods agree that the maximum temperature is only reached at a certain distance from the tool tip.

Recently M'Saoubi and Chandrasekaran have studied the temperature profile at the tool-metal interface using an infrared camera, [1.13]. Examples of the profiles are shown in Figure 1.24. They logically show that the temperature increases with cutting speed and feed rate and that these parameters have an opposite effect on the position of the

maximum temperature. The latter approaches the tool tip as the cutting speed increases (Figure 1. 24(a)) and away from the tool tip as the feed rate increases (Figure 1.24(b)).

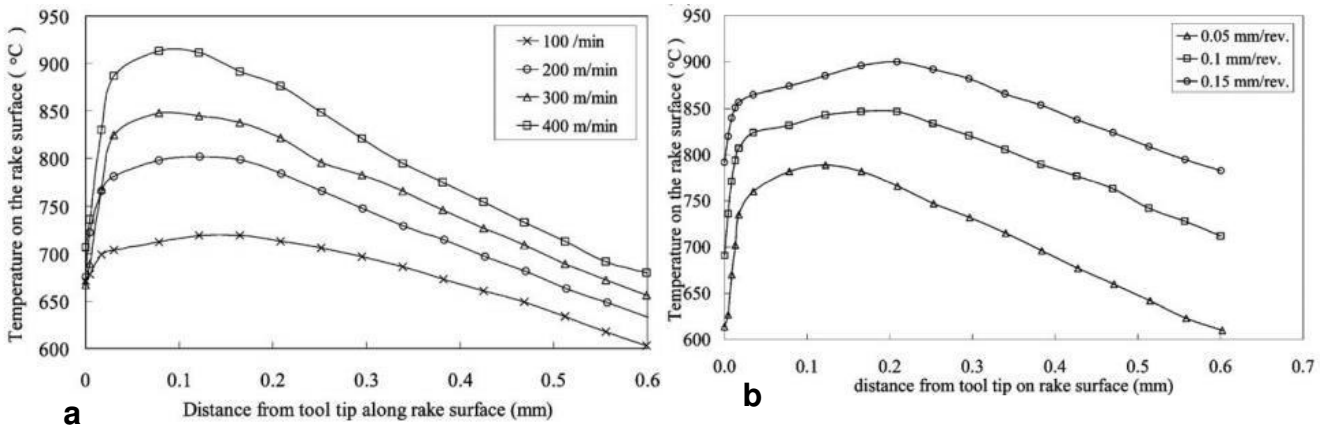

Figure 1.24. Temperature profiles at the tool-chip interface during machining of hardened steel, α =0°, (a) Effect of cutting speed and (b) Effect of feed rate [1.13].

Cutting temperature is often influenced by other parameters such as the tool geometry and cutting conditions.

Tool geometry has a noticeable impact on the cutting temperature during turning operation. Generally, the negative rake angle (γ_0) and positive clearance angle (a_0) are recommended for machining difficult-to-cut materials such as stainless steels, Ti-alloys and Inconel alloys [1.59]. In this context, Tu et al. [1.58] have observed that the temperature decreases with the increase of rake angle, indicating the proper increase of tool rake can reduce the tool temperature as shown in Figure 1.25. Similarly, Hu et al. [1.60] have demonstrated that relatively large rake angle not only can improve friction state of tool surface but also can reduce chip deformation during turning process, thus leading to less heat generation.

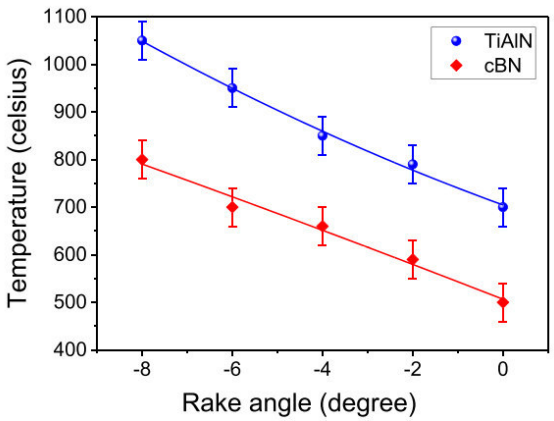

Figure 1.25. Tool maximum temperature obtained simulation dependent on rake angle for TiAlN and cBN/diamond-coated Si_3N_4 cutting tools with the constant clearance angle of 5° and the constant Vc of 270 m/min [1.58].

Cutting conditions also strongly influence cutting temperature. The comparison of cutting temperature is made between dry, wet and MQL drilling of AISI 1045 steel at f = 0.2 mm/rev in a study reported by Weinert et al [1.61]. From Figure 1.26, temperature changes as a function of cutting speed are the same for all three cutting conditions. However, we can note a deviation of about 200°C between wet and dry cutting. This difference is large enough to cause faster wear when no lubricant is used. On the other hand, the gap is roughly 50°C between dry and MQL condition.

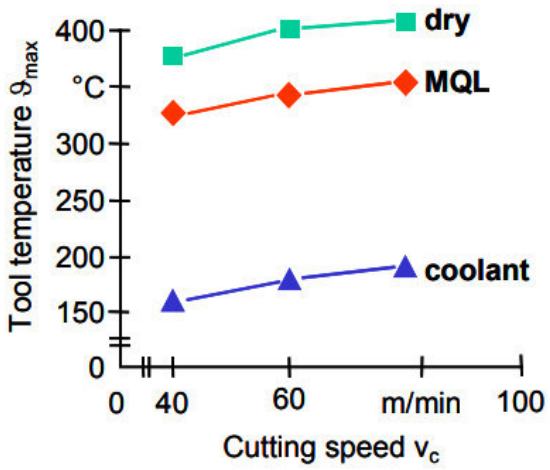

Figure 1.26. Tool temperature in drilling with different cutting conditions [1.61].

Similarly, Hadad et al. [1.62] have also claimed the influence of lubricating conditions on the cutting temperature when the turning experiments of AISI 4140 have been carried out under dry, wet and MQL at Vc = 50.2-141.4 m/min, f = 0.09-0.22 mm/rev and ap = 0.5-1.5 mm with HSS tools. They found that the tool temperature in MQL condition is about 350°C lower than dry turning. Additionally, the tool-chip interface temperature in wet turning is about 300°C lower than in dry cutting. The main reason of that difference in cutting temperature under the three cases is nearly attributed to the difference in cutting forces. The higher the cutting forces, especially in dry case due to the absence of the lubrication, the more heat and higher temperature are produced.

1.6.1.2.3. Major adverse effects of cutting temperature

Cutting temperature rise is a vital parameter in machining to consider due to its major negative effects, including the following [1.63]:

- Elevated cutting temperature lowers the strength, hardness, stiffness, and wear resistance of the cutting tool.
- Cutting tools also may soften and undergo plastic deformation, thus tool shape is altered.
- Raised heat causes uneven dimensional changes in the part being machined, making it difficult to control its dimensional accuracy and tolerances.
- An excessive cutting temperature rise can induce thermal damage, that causes tool wear and unfavorable residual stress, and metallurgical changes in the machined surface, adversely affecting its properties.

When the above simulated results are combined, it is found that the highest temperature is located at rake face. The rake face is subjected to extreme temperature as well as intense friction from chips, resulting in severe tool wear [1.58].

1.6.1.3 Tool wear rates

Based on the preceding discussion, the cutting tool are subjected to extremely complex loads. These complex loads induce tool wear, which is a major parameter for characterizing the machinability of a material. Tool wear adversely influences tool life, as well as the quality of the produced surface and its dimensional accuracy and functionality and, consequently, the manufacturing costs.

The rate of tool wear depends on different machining conditions such as tool, workpiece materials, tool geometry, process parameters, cutting environments, and the characteristics of the machine tool. Changing in these conditions, the dominant tool wear mechanism and tool wear rate may change as well. Tool wear is generally classified into various types of wear that can be seen after machining operation, including flank wear (VB), crater wear, notching, chipping, plastic deformation of the tool tip and gross fracture [1.64]. Most of these kinds occur primarily due to abrasion and adhesion wear mechanisms. Rough particles or formed bonds are present as intermediate material on the surface of the contact zone, leading to growing most of the mentioned wear kinds [1.47].

Among different kinds of tool wear, flank wear and crater wear are the most commonly encountered during machining austenitic stainless steel, both of which are associated with BUE formation. These two main types of wear are basically localized in two regions of the cutting tool: the flank wear occurs on the flank face and the crater wear is produced on the rake face [1.65], as displayed in Figure 1.27.

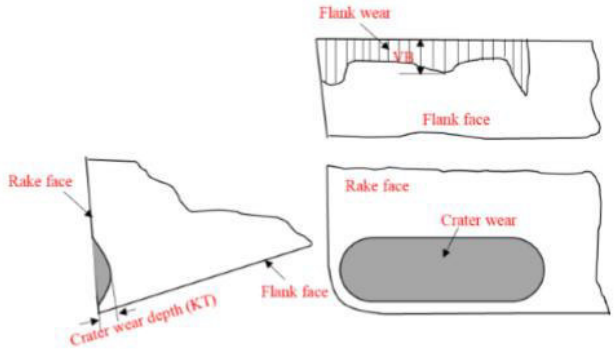

Figure 1.27. Flank wear and crater wear [1.4]

Flank wear (VB) generally results from rubbing between the newly generated work surface and the flank face adjacent to the cutting edge [1.66]. When this type of wear occurs during a turning operation, it affects both the surface finish and the dimensional accuracy [1.67]. The flank wear (VB) is often chosen as a practical tool life criterion, which has an admissible value of 0.3 mm for turning operation according to IS0 3685: 1993 standard. Figure 1.28 presents the characteristic tool wear curve.

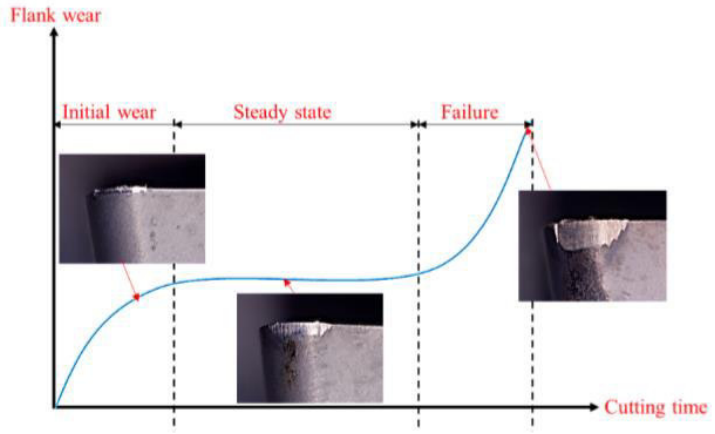

Figure 1.28. Typical stages in flank wear [1.4].

A **Crater** consists of a cavity in the rake face of the tool that forms and grows from the action of the hardened chip flowing on the surface. The presence of stresses and high temperatures at the tool-chip contact interface during the cutting process, contributes to the wearing action. As a result, decreasing the strength of the cutting edge, increases the likelihood of tool breakage [1.4]. The crater can be measured by its depth or area, as pictured in Figure 1.29.

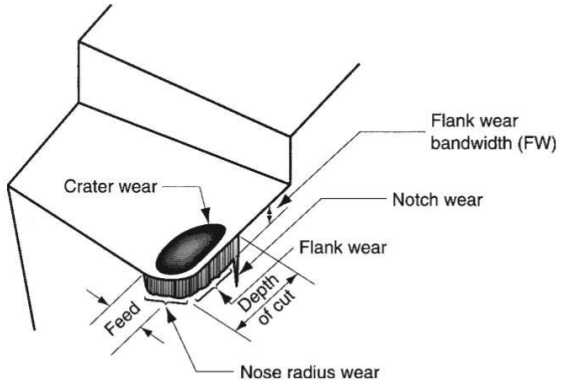

Figure 1.29. Graphical view of worn cutting tool, showing the principal locations and kinds of wear that occur [1.67].

When machining ductile materials such as stainless steel, which has low thermal conductivity and high ductility, friction between tool and chip causes workpart fragments to weld on the rake face of the tool near the cutting edge to form the BUE [1.66, 1.68].
Built Up Edge (BUE) is an unstable layer that transfers from the material to be machined to the cutting tool [1.10]. This BUE produces and grows until breaking off. When it detaches, it takes small parts of the tool rake face with it, resulting in chipping wear on the rake face of cutting tool [1.19]. Consequently, as chipping wear aggrandizes and increases through the cutting edge of the cutting tool as the machining process progresses, notch wear can occur [1.69] potentially contributing to cutting tool failure [1.70].
Broadly, tool wear may result from different principal mechanisms, including abrasion, adhesion, diffusion and oxidation, as shown in Figure 1.30.

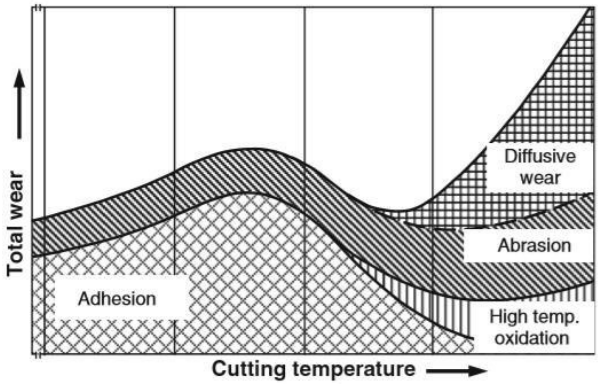

Figure 1.30. Causes of wear in cutting processes [1.10].

Abrasion occurs when hard particles in the workpiece gouging and removing small portions of the tool. The area of the tool worn by abrasion generally shows scratches in the same as cutting direction. Abrasion contributes mainly to the formation of flank wear.
Adhesion is defined as bonds formed between the chip and the rake face of the tool, which are forced into contact under high pressure and temperature. As the chip slides across the tool, small molecules of the tool are sheared off from the surface, resulting in attrition of the surface of the tool. Adhesion is a significant cause of BUE formation.
Diffusion includes the change of position of individual atoms from one substance to another, which takes place at the chip-tool-workpiece interfaces. This involves a

temperature dependent physicochemical affinity between the materials of the workpiece and the tool in that region. Diffusion is believed to be a main mechanism of crater wear [1.69].

Oxidation happens when the hot part of the tool in and around the tool-chip contact zone is exposed to the atmosphere [1.26]. It is often found on the tool during the depth of cut notch forming region [1.71].

1.6.1.5 Surface roughness

Surface roughness is a measurable characteristic based on the roughness deviations. Surface finish is a more subjective term denoting smoothness and general quality of a surface. In popular usage, surface finish is often used as a synonym for surface roughness.

Surface roughness is the most commonly used indicator of surface texture. With respect to Figure 1.31, **Surface roughness** can be defined as the average of the vertical deviations from the nominal surface over a specified surface length.

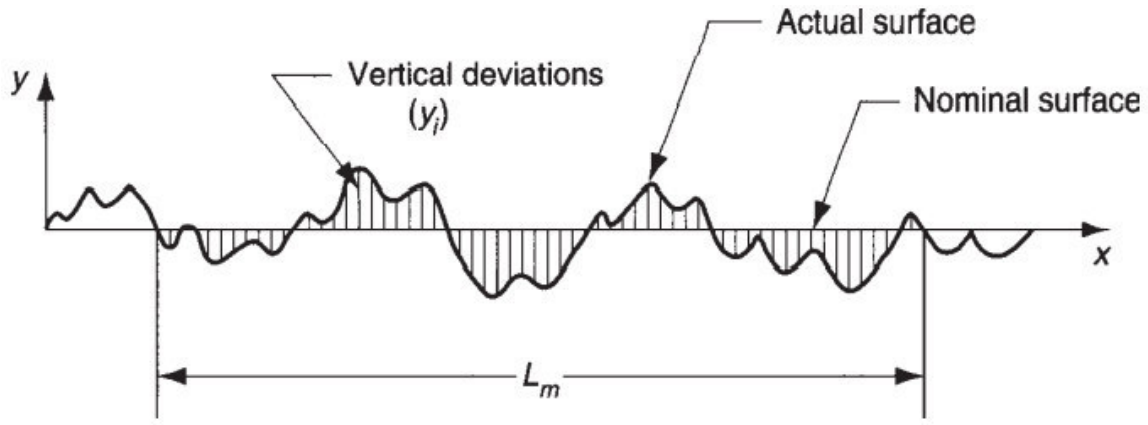

Figure 1.31. Deviation from nominal surface used in the definition of surface roughness [1.1].

Based on the absolute values of the deviations, an arithmetic average is generally used, and this roughness value is referred to as average roughness. In equation form [1.1]

$$Ra = \int_0^{L_m} \frac{|y|}{L_m} dx \quad (1.5)$$

where: Ra: arithmetic mean value of roughness, (µm); y: the vertical deviation from nominal surface (converted to absolute value); L_m: is the total path length which the surface deviations are measured.

The parameter Ra has a significant effect on the functionality of the machined components, during their life span, as this parameter determines the friction values amid the touching surfaces [1.30, 1.72].

The surface roughness depends on many factors that can be grouped as follows: (1) geometric factors, (2) work material and (3) vibration and machine tool [1.10].

1.6.1.6 Chip morphologies

Chip morphology is utilized to examine the behavior of a material during machining. The color and geometry of the chips demonstrate the behavior of materials during the cutting process. Varying cutting parameters during the cutting process influences the magnitude and type of tool wear and the surface roughness of machined parts, resulting in multiple shapes of produced chips [1.73,1.74]. Researchers have investigated the morphology of chips while processing of different kinds of materials.

According to Grzesik [1.1], there are different possibilities for classification of chip morphologies, and three cases are presented as follows:

The first classification concerns machining with a flat-face cutting tool, for which there are three basic cases according to Jawahir et al. [1.75]. These three cases are shown in Figure 1.32.

- A circular form on the rake face of the tool, called side-curling (Figure 1.32.a).
- A circular form perpendicular to the rake face of the tool, called up-curling (Figure 1.32. b).
- A straight line form on the rake face of the tool, but at an angle with the cutting edge: this angle indicates the chip flow direction (Figure 1.32.c).

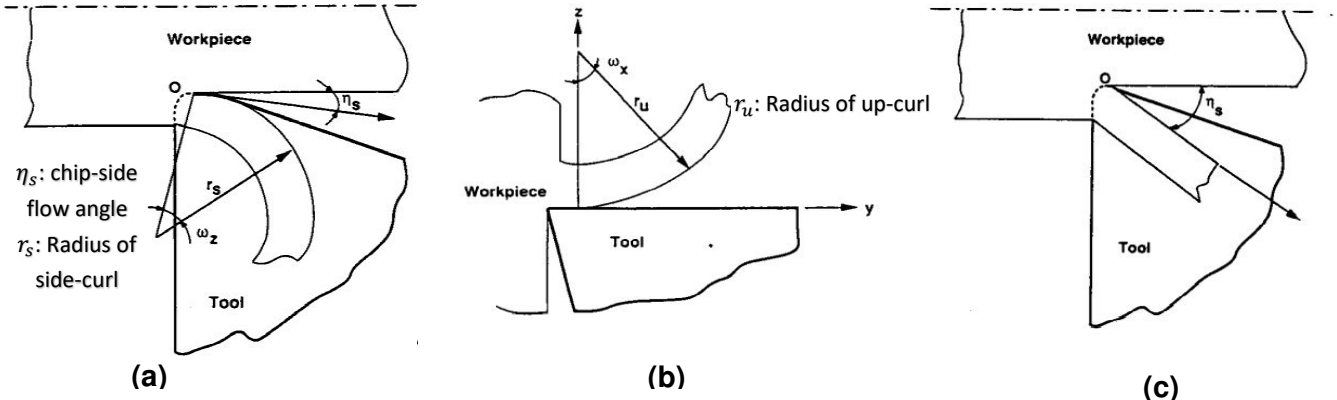

Figure 1.32. Three basic chip forms a) Side-curling, b) Up-curling and c) Straight chip [1.75].

Another classification of different chip morphologies is proposed by the ISO standard 3685-1977, the latter gives a comprehensive classification based on their sizes and shapes. This classification form, depicted in Figure 1.33, consists of eight descriptive shape groups, with each of these groups divided into sub-groups based on the size of the chips (short, long…) and links between the chips (snarled, connected, separated…).

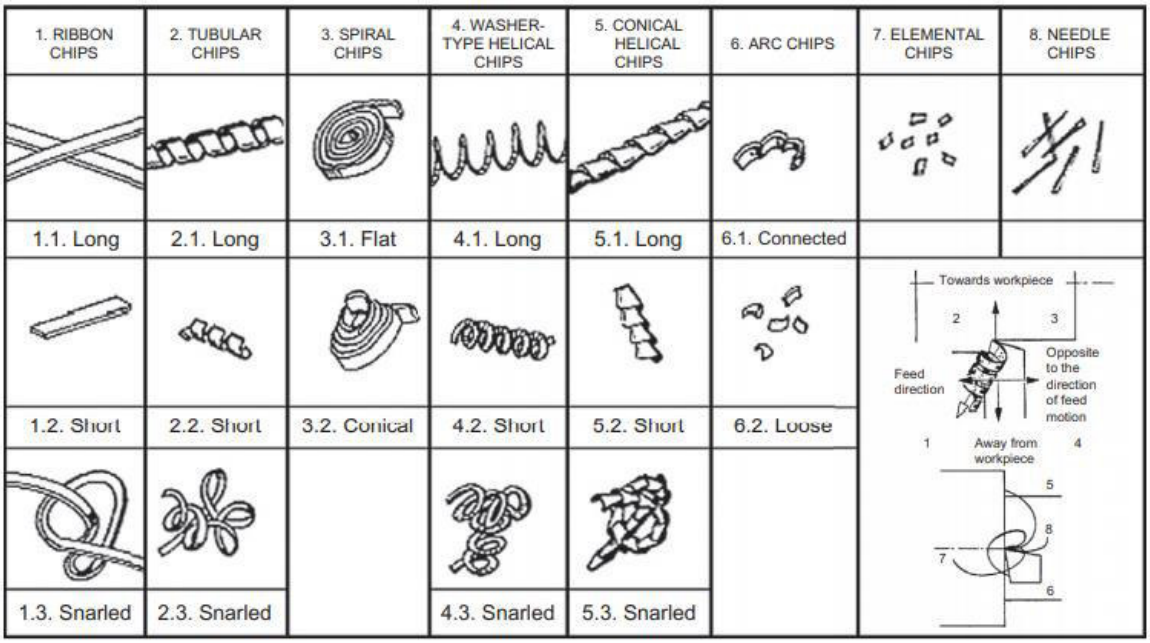

Figure 1.33. Chip morphologies according to ISO 3685-1977, [1.75]

The third possible classification of chips depicted in Figure 1.33 is based on deformation mechanisms and damage resulting from the properties of the material being machined and the cutting conditions, [1.76], (Figure 1.34).

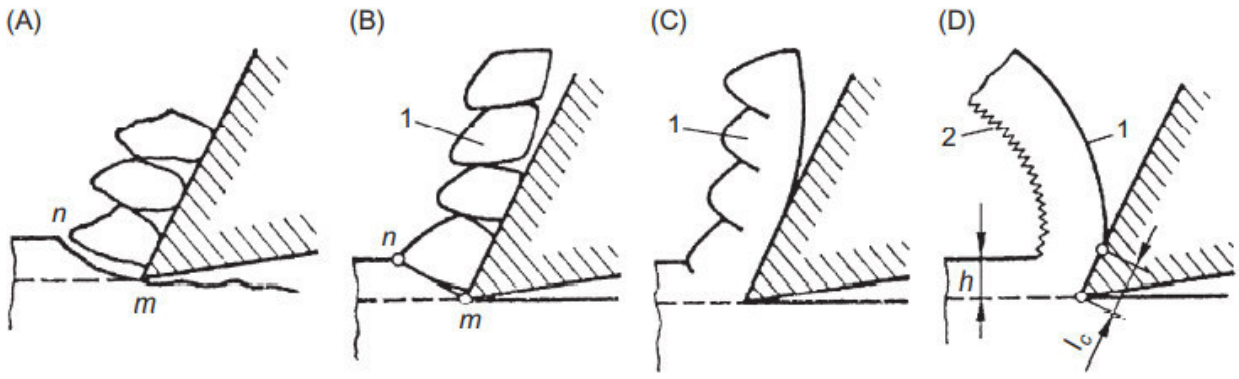

Figure 1.34. Classification of chip types (A) discontinuous, (B) elemental, (C) segmented, (D) continuous [1.76].

Boothroyed et al. [1.76] present the morphologies in two categories: the first one leading to discontinuous chips is due to tearing of the machined material (Figure 1.34, A), whereas the second category is the shearing of the machined material in the area of the primary shear (Figure 1.21). This second category is subdivided into three sub-groups: elementary shearing (Figure 1.34.b), segmented (Figure 1.34.c), continuous (Figure 1.34.d).

1.7. Summary

This first chapter on the literature review offered an overview of the key points upon which the work in this thesis was established. The machined materials used in this dissertation (AISI 316L and AISI 304) are members of the large family of stainless steels known as “austenitic”. The machinability of these steels, which is difficult due to their low thermal conductivity and their tendency to BUE formation, was prioritized. Much efforts have been made by researchers and scientist in the manufacturing engineering sector in order to improve the machinability of stainless steels. However, evaluating the literature of AISI 316L and AISI 304 machining data did not yield satisfactory results in terms of improving the machinability of these materials. For instance, there is a gap in the literature regarding

assessing the machinability of AISI 316L and AISI 304 using Cermet cutting tool in order to support the widely usage of coated carbide while machining stainless steels, optimizing cutting parameters by using recent decision making optimization technique and improving the MQL performance in order to meet the requirements of an eco-friendly machining process.

The following chapters provide a contribution to filling this gap and thereby improving the machinability of austenitic stainless steels.

Chapter 2: A comparative study on performance of cermet and coated carbide inserts in straight turning AISI 316L austenitic stainless steel

2.1. Introduction

Stainless steel materials have been preferred in various fields such as food, medical, aerospace, automotive industries due to their high ductility, high creep rupture strength, high temperature etc. properties [2.1]. However, they are classified as difficult-to-machine owing to the low thermal conductivity, work hardening tendency and high built up edge (BUE) formation [2.2].

In literature, some investigations have been conducted with relation to machining of these materials. Kaladhar [2.3] carried out machining experiments on AISI 304 austenitic stainless steel using five different coated tools and evaluated the evolution of the hard coated cutting tools' performance on surface roughness and flank wear. The results indicated that the TiAlN-TiN (Titanium Aluminum-Nitride/Titanium Nitride) coated cemented carbide insert showed better surface quality followed by TiCN-TiN (Titanium Carbo-Nitride/Titanium Nitride) coated cermet insert. Recently, Patel et al. [2.4] reported an investigation on performance of TiCN-TiN coated cermet inserts under dry finish turning of AISI 304 austenitic stainless steel.

For high quality characteristic assessments, effective controls of cutting parameters are needed in order to achieve desired surface roughness, cutting force etc. To achieve this, a good predictive mathematical models help for understanding the relationship between input factors and output responses.

Several alternative modeling techniques both conventional (i.e., RSM) and non-conventional (i.e., ANN) have been proved to be effective for the prediction. The studies of RSM and ANN have been vastly published. For instance, Nouioua et al. [2.5] studied surface roughness and tangential cutting force predictions using RSM approach in dry and other turning conditions of X210Cr12 steel. The inputs of the RSM models included cutting speed, feed rate, depth of cut and nose radius. Finally, experimental results illustrated that the models were suitable for prediction of surface roughness and tangential cutting force with satisfactory goodness of fit. Laouissi et al. [2.6] presented a comparative study between RSM and ANN methods. Mean absolute deviation (MAD), mean absolute error in percent (MAPE), mean square error (RMSE), and coefficient of determination (R^2) comparisons were performed. Tebassi et al. [2.7] used RSM approach for prediction of surface roughness and tangential cutting force.

Experimental results showed that the coefficients of determination for *Ra* and *Fz* were determined as 0.93 and 0.98, respectively. Gupta [2.8] specified a statistical model for surface roughness in turning process of metal matrix composite. Error estimation of RSM-based model was done as well. However, a superiority of RSM predicted models of surface finish and forces were found out than those derived by ANN in a research carried out by Mia el al [2.9].

Likewise, finding the optimum cutting parameters have been considered as a necessity in the field of machining process to prevent poor quality characteristics. Therefore, various alternative computational methods such as Simulated Annealing (SA), Genetic Algorithm (GA) and Desirability Function (DF) have been applied successfully for the optimization of process parameters. Thence, single and multi-objective optimizations have been performed by many researchers in turning [2.10-2.12], drilling [2.13, 2.14] and milling [2.15, 2.16]. Indeed, Zain et al. [2.17] applied GA and SA for optimization of cutting parameters leading to minimize surface roughness. Both techniques have delivered satisfied optimum results. Mia et al. [2.18] optimized surface roughness by using SA method and recommended to use 149 m/min cutting speed, 0.10 mm/rev feed and 43 hardness for minimum Ra. In another study conducted by Mia et al. [2.19], feed of 0.10 mm/rev, material hardness of 43 HRC and cutting speed of 161 m/min corroborated the minimum surface roughness when separate DF and GA optimization methods were employed. Besides, Bagaber et al. [2.20] reported a multi-objective optimization study using DF in order to achieve minimum *Ra* and other responses in turning of AISI 316. Researchers presented that the appropriate selection of machining parameters reduced surface roughness by 4.71%. By using DF in optimization of cutting factors for AISI 304 turning, Berkani et al. [2.21] obtained depth of cut of 0.295 mm, cutting speed of 104.54 m/min and feed of 0.08 mm/rev as optimum cutting parameters for minimum cutting force and surface roughness, simultaneously. Moreover, in investigation reported by Laouissi et al. [2.6] the multi-response optimization was established using GA. Researchers' results revealed that the cutting regimes were attained to be in ranges of 0.08 - 0.121 mm/rev of feed, 299.525 - 512.571 m/min of cutting speed and 0.251 - 0.586 mm of depth of cut in order to minimize *Ra* and *Fz*.

According to literature, no such comparative study has been made to predict and optimize the surface roughness and cutting force for a range of values of cutting speed,

feed and depth of cut in dry straight turning of AISI 316L using two different cutting inserts as cermet (GC 1525) and coated carbide (GC 1125) inserts. The main goal of the present comparative study is to experimentally investigate the effects of cutting parameters including cutting speed, feed and depth of cut on responses as surface roughness and cutting force. Then the experimental results were used to formulate mathematical prediction models based on RSM. Thus, the predictive of their capabilities was done in terms of coefficient of determination (R^2), absolute mean percentage error (MAPE) and mean square error (RMSE). After that, the optimization models were developed by embracing the simulated annealing (SA) and genetic algorithm (GA), in order to obtain optimum cutting parameter sets. These models are expected to help the engineers and operators in metal cutting industries for better control of surface roughness and cutting force while turning of AISI 316L. In addition, the evolution of flank wear with respect of machining time and the surface topography (3D) were also presented.

2.2. Methodology

2.2.1. Turning conditions and materials

The cylindrical dry turning experiments of AISI 316L having an axial length of 400 mm and diameter of 80 mm were carried out on a universal lathe (TOS TRENCIN- SN 40C) having spindle power of 6.6 kW. The chemical compositions of AISI 316L were presented in Table 2.1. In this study, two different cutting inserts were used as cermet and coated carbide inserts which are designated as ISO specification, namely CNMG 120408-PF 1525 and CNMG 120408-MF 1125, respectively, supplied by Sandvik. The details for cutting inserts and tool holder and cutting parameters were given in Table 2.2. Twenty-seven experiments were conducted according to the Taguchi L_{27} orthogonal array. Measurements of cutting force, surface roughness, tool wear and 3D surface topography were carried out by means of Kistler piezoelectric dynamometer (type 9257B), Mitutoyo Surftest-210 roughness meter, microscope Visual Gage 250 and AltiSurf®500 optical metrology device, respectively. Figure 2.1 shows the schematic illustration of experimental setup in the present work. Table 2.3 lists the twenty-seven data sets representing the considered combination of cutting parameters. Thence, the gathered data are used for the development of mathematical models applied in the optimization phase.

Table 2.1. Chemical composition of the AISI 316L.

Composition	Wt. %	Composition	Wt. %
C	0.013	Al	0.0028
Si	0.50	Cu	0.373
Mn	1.79	Co	0.163
S	0.031	V	0.074
Cr	16.57	Ca	0.0022
Ni	9.79	Fe	68.3
Mo	2.00		

Table 2.2. Machining conditions

Machining conditions	Descriptions
Workpiece	AISI 316L austenitic stainless steel
Cutting speed	125 – 170 – 260 m/min
Feed	0.08 – 0.12 – 0.16 mm/rev
Depth of cut	0.1 – 0.2 – 0.3 mm
Cutting condition	Dry
Coating insert	PVD (TiCN-TiN) Cermet, PVD (TiALN-TiN) Coated carbide
Tool insert geometric form	ISO- CNMG 120408
Tool insert manufacturer and code	Sandvik GC1525, GC 1125
Tool holder	PSBNR2525 M12
Responses	Surface roughness and Cutting force

Table 2.3. Experimental design using the L27 orthogonal array and experimental results.

Input parameters				Output parameters			
				Cermet		Coated carbide	
No.	*Vc*(m/min)	*f* (mm/rev)	*ap* (mm)	*Ra* (µm)	*Fz* (N)	*Ra* (µm)	*Fz* (N)
1	125	0.08	0.1	0.88	23.84	0.47	21.79
2	125	0.08	0.2	0.43	56.27	0.64	54.87
3	125	0.08	0.3	0.81	77	0.58	75.11
4	125	0.12	0.1	1.19	46.8	0.68	35.15
5	125	0.12	0.2	0.68	80.1	0.90	64.67
6	125	0.12	0.3	1.19	110	0.72	87.85
7	125	0.16	0.1	1.41	55.65	1.24	45.6
8	125	0.16	0.2	1.42	98.99	1.15	78.3
9	125	0.16	0.3	1.48	128.6	1.10	116.93
10	170	0.08	0.1	0.51	26	0.61	32.17
11	170	0.08	0.2	0.51	55.9	0.64	54.12
12	170	0.08	0.3	0.56	81.48	0.63	79.84
13	170	0.12	0.1	0.74	52.6	0.68	49.58
14	170	0.12	0.2	0.89	80.77	0.67	74.47
15	170	0.12	0.3	0.77	109.4	0.71	107.79
16	170	0.16	0.1	1.28	60.06	1.01	59.5
17	170	0.16	0.2	1.33	99.91	1.01	94.47
18	170	0.16	0.3	1.17	132.8	1.04	139.46
19	260	0.08	0.1	0.49	26.78	0.62	15.31
20	260	0.08	0.2	0.47	49.58	0.64	50.53
21	260	0.08	0.3	0.47	74.83	0.67	81.1
22	260	0.12	0.1	0.74	52.97	0.69	41.45
23	260	0.12	0.2	0.79	84.78	0.64	80.12
24	260	0.12	0.3	0.79	105.69	0.70	104.71
25	260	0.16	0.1	1.18	68.05	0.97	65.9
26	260	0.16	0.2	1.23	100.63	1.00	97.65
27	260	0.16	0.3	1.27	135.72	0.99	141.53
Mean				0.91	76.66	0.79	72.22

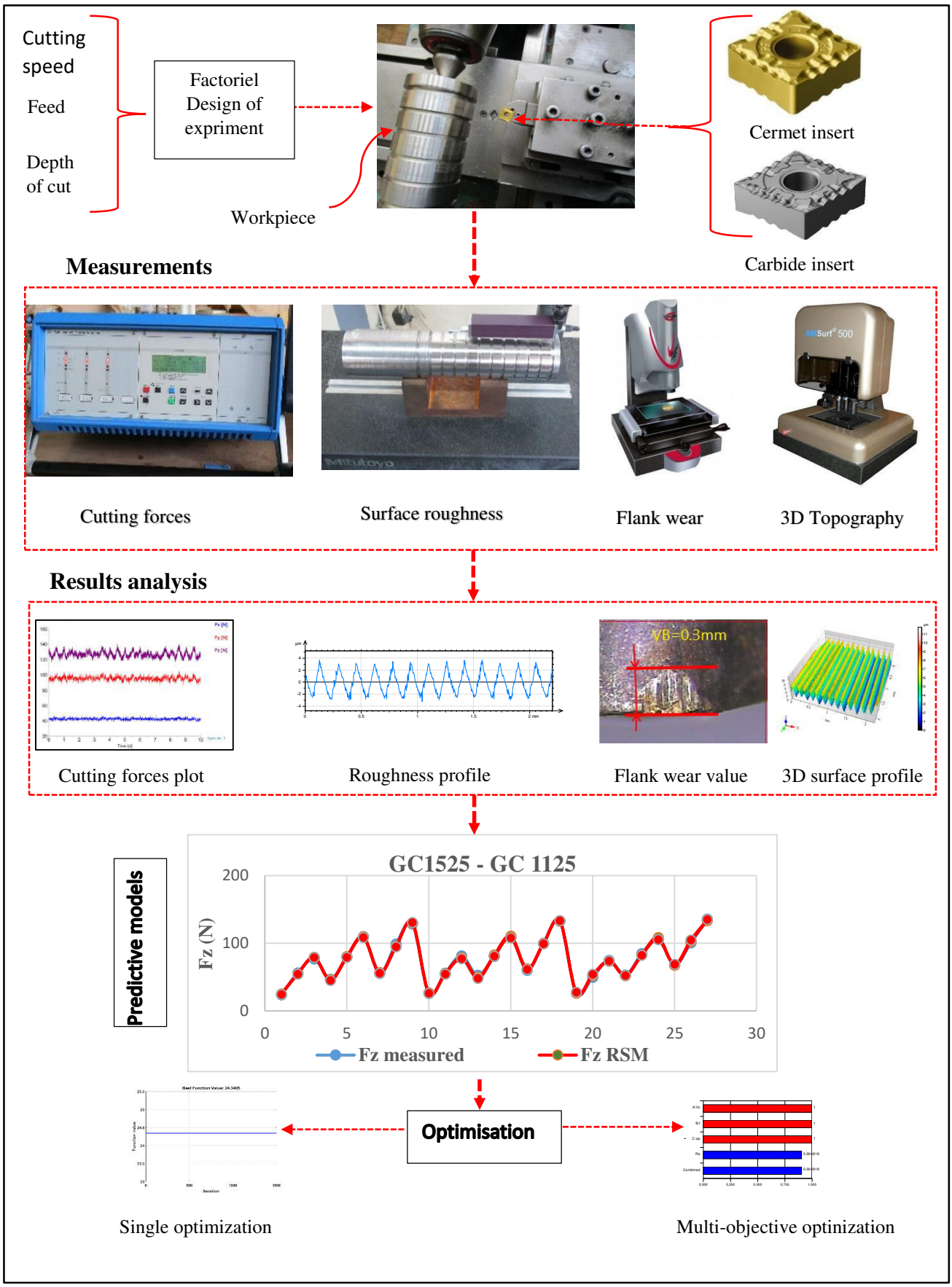

Figure 2.1. Schematic illustration of experimental setup in the present work.

2.2.2. Response Surface Methodology

Response surface methodology (RSM) is an empirical modeling method that works as statistical tool used to construct a relationship between different output parameters (herein, the *Ra* and *Fz*) and input parameters (herein, *Vc, f* and *ap*) [2.18]. Likewise, RSM is a sequential experimentation strategy that helps to develop the empirical model and define an optimum solution for machining process.

In RSM, an empirical model can be established using a second order quadratic- model that is normally utilized when the response function is not known or nonlinear such as in machining process [2.18]. This model is expressed by equation (2.1) [2.22]:

$$\varphi = a_0 + \sum_{i=1}^{k} a_i X_i + \sum_{\substack{i=1 \\ i \neq j}}^{k} a_{ij} X_i X_j + \sum_{i=1}^{k} a_{ii} X_i^2 + \varepsilon \quad (2.1)$$

where a_0, $a_{i,}$ a_{ii} and a_{ij} are the constant terms, the coefficients of the linear terms, quadratic and interactive terms, respectively. X_i and X_j indicate the independent variables (Vc, f and ap). ε corresponds statistical experimental error. K denotes number of variables (in this case, K=3). Finally, φ is the desired machining responses (*Ra* and *Fz*). Note that the empirical models were generated by Design-Expert 10 software.

2.2.3. Simulated Annealing

2.2.3.1. Theory of simulated annealing

Simulated annealing is an emerging- stochastic- method, that has major advantage over other methods such as hill climbing or random walk, to avoid getting stuck in local, non-global minima, when searching for global minima. This is achieved based on the fitness function when the probability function gives the process a unique capability to accept the generated solutions. Thus, it can be applied to solve both constrained and bound-constrained combinatorial optimization problems [2.17].

SA originates from the analogy between the physical annealing process, where the term annealing comes from analogies to the cooling of a liquid or solid, and the problem of finding (near) minimal solutions for discrete minimization problems.

As it is well-known that a central issue in statistical mechanics is analyzing the behavior of substances as they cool. At high temperature, molecules have a lot of mobility, but as the temperature drops, this mobility goes down, and the molecules may tend to align themselves in a crystalline structure. This aligned structure is known as the minimum

energy state for the system. The principle behind annealing in physical systems is the gradual cooling of substances to achieve the minimum energy state.

In optimization, the analogy to a minimum energy state for a system is a minimizing value of the loss function. The SA technique attempts to mathematically capture the process of controlled cooling associated with physical processes with the aim of achieving the lowest value of the loss function in the face of possible local minima. As in the physical cooling process, SA also allows for temporary increases in the loss function as the learning process captures the information necessary to reach the global minimum.

A key distinction between SA and the majority of other optimizations approaches is the willingness to give up the fast gain of a rapid decrease in the loss function. SA derives this property from the Boltzmann-Gibbs probability distribution of statistical mechanics, which describes the probability of a system possessing a given discrete energy state:

$$p(E = k) = \frac{1}{Z(T)} exp\left(-\frac{k}{k_b T}\right) \tag{2.2}$$

where Z(*T*) is a normalizing constant, k_b is known as the Boltzmann constant, and *T* is the temperature of the system.

As far back as 1953, Metropolis et al. [2.23] introduced the Boltzmann-Gibbs distribution-based concept into numerical analysis through developing a method for simulating a system at some fixed temperature. In fact, if a system is in some current energy state E_{curr}, and some system features are modified to make the system potentially achieve a new energy state E_{new}, the Metropolis simulation always causes the system go to the new state $E_{new} < E_{curr}$. On the other hand, if $E_{new} \geq E_{curr,}$ the the probability of the system going to the new state is

$$\exp(-\frac{E_{new}-E_{curr}}{c_b T}). \tag{2.3}$$

The Metropolis algorithm is only concerned with a single constant temperature. Kirkpatrick et al. [2.24], generalized it by introducing an annealing schedule that defines how the temperature is lowered. Beginning with a high initial temperature T_0, the Metropolis algorithm is pursued until equilibrium is reached. The temperature is then reduced in accordance with the annealing schedule, and the Metropolis equation is applied at this new temperature until a new equilibrium is attained and the temperature

is decreased again. This process is repeated until the system freezes. If the annealing schedule is sufficiently slow, then the system will freeze in a state of minimum energy, corresponding to the global minimum of our objective function [2.25].

2.2.3.2. Implementation of simulated annealing algorithm

The following steps can be used to introduce a general simulated annealing algorithm.

Step 1: starting at an initial temperature T_0, we choose an initial set of parameter values with function value *E.*

Step 2: randomly choose another point in the parameter space that is close of the original, and measure the corresponding function value.

Steps 3: using the Metropolis criterion, compare the two points in terms of their function value. Let $\Delta = E_{new} - E_{current}$, and move the system to the new point if and only if a random variable *U*, distributed uniformly over (0,1), satisfies $U \leq \exp\left(-\frac{\Delta}{T}\right)$

when *T* is the current temperature, or equivalently $E_{new} \leq E_{current} - T \log U$.

Thus E_{new} - E_{curr} is compared with an exponential random variable with mean of *T.* It is worth noting that we always switch to the new point if its corresponding function value is lower than that of the old point, and that at every temperature, the system has a chance of moving upwards.

Step 4: repeat steps 2-3 whether the system has moved or not. At each stage, compare the function value of new points with function value of the current point until the sequence of accepted points is judged, by some criterion, to have reached a state of equilibrium.

Step 5: once an equilibrium state has been reached for a given temperature, the temperature is reduced to a new temperature determined by the annealing schedule. The procedure then restarts again from step 2, with an initial state at the point after the last iteration of the algorithm, until some stopping criterion is met, and the system is assumed to be frozen.

The framework of the proposed SA algorithm is depicted in the Figure 2.2.

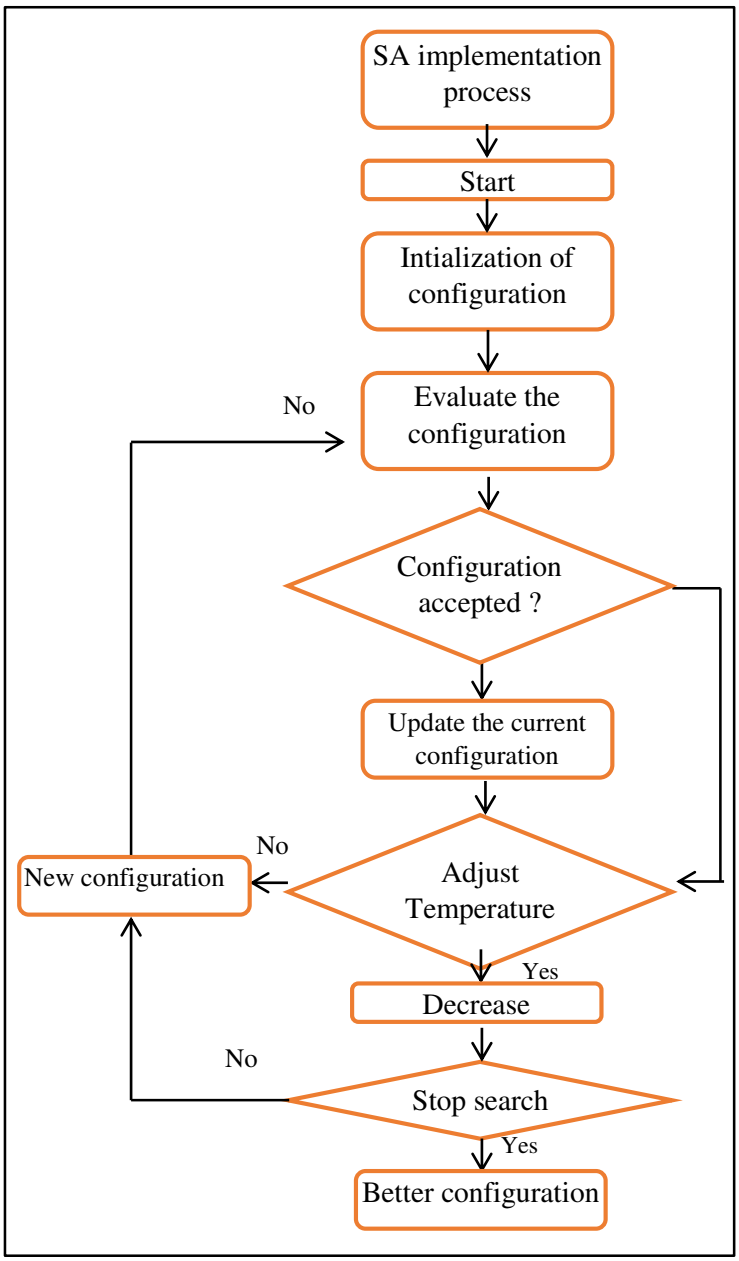

Figure.2.2. Framework of simulated annealing algorithm.

2.2.4 Genetic Algorithm

2.2.4.1. Overall concepts of genetic algorithms

The limitations of classical optimization techniques restrict their use and the therefore favors the implementation of more recently developed global searching algorithms. Genetic Algorithm (GA) is a non-traditional search and optimization method, which has become very popular in various engineering fields due to their easy implementation, capability and efficiency to solve the multi-dimensional problems. Unlike, the annealing algorithms, which are based on analogies to the physical cooling of substances, the

GA is based loosely on principles of natural evolution and survival of the fittest. It is considered as stochastic optimization method inspired from Darwin's principle of biological natural selection processes [2.26] and principles of genetics. It was first developed by Johan Holland in 1975 [2.27], and since then it has been increasingly introduced in diverse areas such as music generation, genetic synthesis, machine learning, manufacturing [2.28]. Likewise, while the dominant use of GA has been in optimization, it is worth mentioning at least some of the related applications. One is automatic programming (genetic programming), where the algorithm automatically adapts software to perform certain tasks. Another application involves the use of GA to study human social systems, where one might be interested in investigating the evolution of societies, including the impact of government policies, resources shortages, and human interaction with the environment [2.29].

GA consists of many main operators to influence the optimization response, namely population, fitness scaling, selection strategies, crossover, mutation, termination strategies and selection of the GA parameters [2.19, 2.30]. the cycle of GA process can be summarized as follows: it starts with creating a population of random adopted initial implicit solutions which known as chromosomes of individuals. Each one of those is formed by the variable of the problem, which simulates a sequence of genes. Then, the objective function is mapped by fitness function to evaluate the performance of each chromosome. Next, the algorithm uses a roulette wheel to designate a higher probability of individuals proportional to their higher fitness value and select them to move and survive into the next generation. After the selection of individuals, the chromosomes that referred to as implicit solutions called parents are randomly combined. The algorithm employs the selection, crossover and mutation operators, to produce new generation called children. Crossover and mutation are applied randomly with a probability of p_c and p_m. After that, the new generation is evaluated. This cycle is iterated for a number of generations until a promising solution is achieved.

2.2.4.2. Standard GA operations

2.2.4.2.1. Representation

Any GA needs a chromosome representation. This representation specifies how the problem is constructed as well as genetic operators and parameters that are employed. Each chromosome is represented by a sequence of genes in a specific alphabet. This alphabet can be represented as binary digits (0 and 1), in expression (2.4), or real-numbers, as in expression (2.5) [2.31].

$$\underbrace{1011111}_{x_1}\ \underbrace{10000}_{x_2}\ \underbrace{1000011}_{x_3}\ \ldots\ \underbrace{100001}_{x_n} \tag{2.4}$$

$$\underbrace{9.5}_{x_1}\ \underbrace{1.6}_{x_2}\ \underbrace{6.7}_{x_3}\ \ldots\ \underbrace{3.3}_{x_n} \tag{2.5}$$

2.2.4.2.2. Fitness function

The fitness function converts the objective function values into fitness values. A fitness value is an indicator of the chromosome performance. A GA always optimizes the fitness. Thus, in a maximization problem, the fitness values are equal to the objective function values. On the other hand, in a minimization problem, the fitness function determines the fitness values as a suitable number subtracted by the objective function values.

To maintain uniformity and to avoid premature convergence caused by a dominant chromosome. The algorithm can apply fitness scaling methods, some of these methods are:

Linear scaling: in this method the fitness is scaled as

$$F_{i'} = a.F_i + b \tag{2.6}$$

where $F_{i'}$ and F_i are the scaled and initial fitness values, respectively, of chromosome i, a and b are constants chosen to keep the fitness in a predefined range.

Sigma truncation: this method is an improvement of the linear scaling,

$$F_{i'} = F_i + (\bar{F} - c.\sigma) \tag{2.7}$$

where $\bar{F}$and σ are the population's mean fitness value and standard deviation respectively, c is a small integer (usually in the range (1-5)).

Power law scaling: in this method the initial fitness is scaled to some specific power,

$$F_{i'} = F_i^k \tag{2.8}$$

The value of the parameter k depends on the problem**.**

2.2.4.2.3. Selection strategies

GAs rely heavily on the selection of individuals to produce successive generations. Overall, selection strategies prefer the selection of better individuals depending on the selection pressure. The greater the selection pressure, the greater the likelihood of selecting the best individuals. The selection pressure defines the convergence speed of a GA. Thus, if the selection pressure is too low, the GA will take an excessively long period. On the opposite, if the selection pressure is too high, the GA will converge prematurely to a suboptimal solution. The selection strategy and its parameters determine the selection pressure. Selection schemes are classified as: proportional selection (roulette wheel), ranking selection and tournament selection. Roulette wheel [2.32] normalized geometric [2.33] and tournament selection [2.34] are the most representative methods of each selection scheme.

Roulette wheel: roulette wheel was the first selection method. The probability p_i of selecting an individual i is proportional to his fitness value.

$$p_i = \frac{F_i}{\sum_j F_i} \tag{2.9}$$

where F_i is the fitness of individual i. In general, the roulette wheel selection scheme is inherently slow [2.32]. To counteract this, the algorithm can adopt an elitist strategy. An elitist strategy copes the best or a few of the best chromosomes into the succeeding generation, which speeds up the searching process. Even though, this elitist strategy may increase the speed of domination of a population by a super chromosome, it appears to improve the performance [2.35].

Tournament selection: Tournament selection, chooses randomly n individuals from the population, and inserts the best individual of the n into the new population. The number of individuals, n, is called the tournament size. An increment/ reduction of the tournament size increases/ reduces the tournament selection pressure [2.31].

2.2.4.2.4. Crossover

Crossover is the most effective GA operator. The core research subject of GAs is the development of successful crossover operators. Consequently, several kinds of crossover have been suggested in the literature [2.36] including, one-point crossover, two-point crossover, uniform crossover, flat crossover, arithmetic crossover and heuristic crossover**, …**etc**.,**

Crossover operation creates offspring (children) of the pairs of parent from the selection step. It is applied with a probability p_c to determine if the offspring will represent a blend of the chromosomes of the parent [2.29]. If no crossover takes place, the two children are exact copies of their respective parents. If crossover does take place, then the two offspring are produced according to an interchange of parts of the chromosome structure of the two parents.

As an example, Figure 2.3. shows for the case of a nine-bit representation of the chromosomes. Case 1 illustrates one-point crossover, where the bits appearing after one randomly chosen dividing point in the chromosome are interchanged. Case B illustrates two-point crossover, where only the middle selection is interchanged.

	Parents		Children
A	**101|100101** **001|011010**	→	**101|011010** **001|100101**
	Parents		**Children**
B	**1|01100|101** **0|01011|010**	→	**1|01011|101** **0|01100|010**

Figure 2.3. Crossover operator under bit coding. Case A shows one splice point; Case B shows two splice points.

2.2.4.2.5. Mutation

In order to avoid losing the useful information that is may not rich enough to find the solution through crossover operator alone, the GA also uses a mutation operator. The mutation operation changes a gene in a chromosome with one randomly chosen from the solution space. That might be happen with small probability P_m to preserve the good chromosomes produced by crossover. In the case of a binary-coded genetic algorithm, the mutation is usually performed bit-by bit, with selected bit being moved from 0 to 1, or vice versa. Figure 2.4 shows a mutation in the third bit for the first child chromosome appearing in Figure 2.3.

Figure 2.4. Mutation operator affecting one bit in a binary coding.

For real-coded algorithm (RCGA), several mutations have been developed, here two are considered, uniform and boundary mutation.

Let us consider that $x = \{x_1, x_2, \dots, x_n\}$ $(x_i \in [a_i, b_i])$ is the chromosome selected for application of the mutation operator.

Uniform mutation: uniform mutation randomly selects one variable, x_j, and sets it equal to a uniform random number in the interval $[a_i, b_i]$ [2.37]:

$$x_i' = \begin{cases} \cup\,(a_i, b_i), & if\ i = j \\ x_i, & if\ i \neq j \end{cases} \tag{2.9}$$

Boundary mutation: Boundary mutation selects one variable, x_j, and sets it equal to either its lower or upper bound [2.37]:

$$x_i' = \begin{cases} a_i\,, if\ i = j, r < 0.5 \\ b_i, if\ i = j, r \geq 0.5 \\ x_i, if \quad i \neq j \end{cases} \tag{2.10}$$

where r is a uniformly distributed number between 0 and 1.

Other mutation operators that have been recommended for RCGAs are as follows: non-uniform mutation [2.37], time variant mutation [2.38], power mutation [2.39] and many more [2.40].

2.2.4.2.6. Termination strategies

In general, the GA will stop once a convergence criterion is met. Some stopping criteria are [2.31]:

- The “target” fitness value is attained.
- The maximum number of generations is attained.
- The deviation of the population is lower than some considered threshold, i.e. the entire population has converged to the same solution.
- The feasible solution has not changed after a predefined number of generations.
- A combination of the above.

2.2.4.3. Overview of basic GA search method

Genetic algorithms are iterative algorithms that follow the classical pattern of evolutionary algorithms. The basically steps to govern the implementation of GA are schematized in Figure 2.5, which are as follows:

(1) During the algorithm’s initialization, an initial population of N individuals is randomly generated. It is usually distributed uniformly over the search space. The objective function of the optimization problem is then used to evaluate each individual. This assessment allows for determination of each individual’s adaptation (or fitness).

(2) (Selection) For generation k, portion of the population is replicated based on each individual’s adaptation: the higher the adaptation (relative to other individuals) of an individual, the more often that individual is selected in the new population.

(3) (Crossover) A pair of parent individuals found in the previous step is selected at random from this new population and then the recombination operator is applied to them with a certain probability p_c. The children then replace the parents in the population of generation k+1.

(4) (Mutation) The mutation operator is then used to mutate each individual with probability P_m that is typically chosen to be an order of magnitude smaller than P_c. A mutation causes a local change in an individual. The mutants then replace their parents in the new generation k+1.

(5) Individuals that have not crossed or mutated are copied into the new population.

(6) These operations are repeated from the 2nd step until a certain stopping criterion is met. Different stopping criteria of the genetic algorithm can be chosen: fixed number of generations (constant time), convergence of the population, population no longer evolving sufficiently, etc.

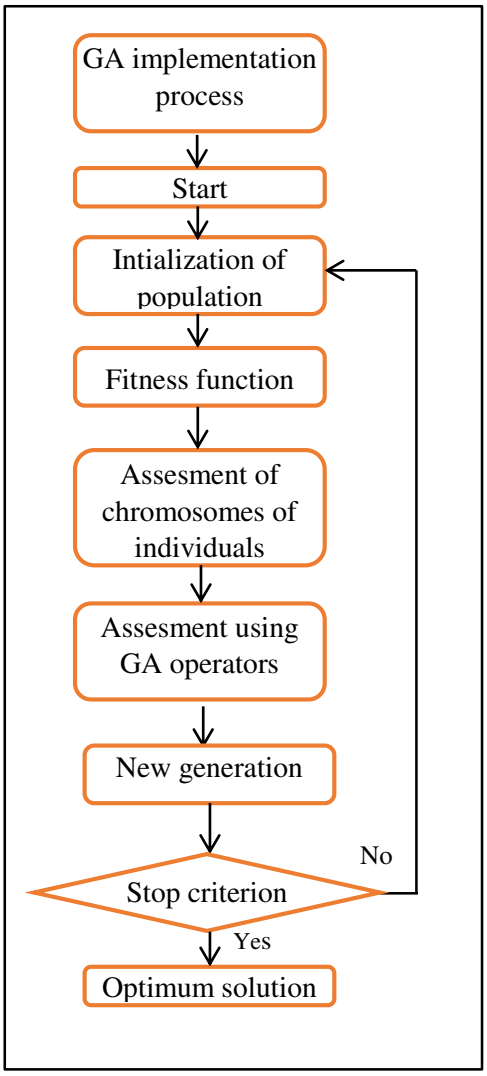

Figure 2.5. Framework of genetic algorithms.

2.2.4.4. Using GA in optimization problem

The simple genetic algorithm (SGA), also called single objective, is suitable for optimization problems with a single objective function. In this case of study, it is a question of finding the best model, which usually corresponds to the global minimum. Most real problems involve at the same time multi-objective optimization of several functions. These problems from a design point of view are different from those optimizing a single objective function. In the case of multi-objective function

optimization, there is no one solution that is the best (global optimum) with respect to all objectives. Instead, there may be a set of optimal solutions that are all equally good. These solutions are known as Pareto (non-dominated) optimal solutions. A Pareto set, for example, for a two-objective function problem, is described by a set of points such that by moving from one point to another, one objective function improves, while the other deteriorates. The choice of one solution among the others requires more knowledge of the problem, which is often intuitive and not quantifiable. However, the Pareto front is very useful as it narrows down the choices and helps the decision maker in selecting a desired operating point (called the preferred solution) from the (limited) set of Pareto optimal points.

2.3. Results and discussion

2.3.1. Analysis of Variance (ANOVA) results

Tables 2.4 and 2.5 show the ANOVA's outcomes for *Ra* and *Fz,* respectively. Table 2.4 represents ANOVA's outcomes for *Ra* for AISI 316L obtained by cermet and coated carbide inserts (GC 1525 and GC 1125). Based on the *P* value, it may be noticed that the cutting speed, feed and square term (Vc^2) are statistically significant for cermet insert and cutting speed, feed, square term (f^2) and interaction (Vc*f) are statistically significant for coated carbide insert. Furthermore, the highest contribution is provided by feed of 79.61% for cermet insert and 74.11% for coated carbide insert. This result is compatible with the literature [2.3, 2.41, 2.42].

Table 2.5 exhibits ANOVA's findings for *Fz* for AISI 316L obtained by cermet (GC 1525) and coated carbide (GC 1125) inserts. It can be asserted that most parameters were obtained statistically significant except the square term (Vc^2) for GC 1525 and the cutting speed, feed, depth of cut, square term (Vc^2) and interaction terms (Vc*f and f*ap) were found statistically significant for GC 1125, according to their *P* value. Moreover, the greatest impact in term of contribution was accredited by depth of cut of 62.12% for GC 1525 and 64.88% for GC 1125, respectively. Then, it was immediately followed by the feed with a contribution of 35.23% and 29.42%, respectively. Similar to literature [2.21], depth of cut was the main parameter that mainly acted on the cutting force.

Table 2.4: ANOVA for *Ra*

Source	SS	DF	MS	F- value	*P*- value	PC (%)	Remark
a) Cermet							
Model	2.80141	9	0.31127	18.6	0	90.78	
Vc	0.19339	1	0.88484	14.04	0.002	6.27	Significant
f	2.45681	1	0.23499	144.55	0	79.61	Significant
ap	0.00042	1	2.41889	0.04	0.848	0.01	Insignificant
Vc *Vc	0.07842	1	0.00063	4.69	0.045	2.54	Signficant
f *f	0.03276	1	0.04951	1.96	0.18	1.06	Insignificant
ap *ap	0.03734	1	0.07842	2.23	0.154	1.21	Insignificant
Vc *f	0.00016	1	0.03276	0.01	0.924	0.01	Insignificant
Vc *ap	0.0014	1	0.03734	0.08	0.776	0.05	Insignificant
f *ap	0.00073	1	0.00076	0.04	0.837	0.02	Insignificant
Error	0.28448	17	0.00016			9.22	
Total	3.0859	26					
b) Coated carbide							
Model	1.06	9	0.12	31.57	0	94.64	
Vc	0.018	1	0.018	4.78	0.04	1.61	Significant
f	0.83	1	0.83	221.29	0.0001	74.11	Significant
ap	1.72E-003	1	1.72E-003	0.46	0.50	0.15	Insignificant
Vc *Vc	6.33E-003	1	6.33E-003	1.70	0.21	0.57	Insignificant
f *f	0.095	1	0.095	25.47	0.0001	8.48	Significant
ap *ap	3.97E-003	1	3.97E-003	1.06	0.31	0.35	Insignificant
Vc *f	0.041	1	0.041	11.06	0.004	3.66	Significant
Vc *ap	1.75E-003	1	1.75E-003	0.047	0.83	0.16	Insignificant
f *ap	6.22E-003	1	6.22E-003	1.67	0.21	0.56	Insignificant
Error	0.063	17	3.73E-003			11.08	
Total	1.12	26					

Table 2.5: ANOVA for *Fz*

Source	SS	DoF	MS	F- value	*P*- value	PC (%)	Remark
a) Cermet							
Model	26261.9	9	2918	596.58	0	99.68	
Vc	20.1	1	26.4	5.39	0.033	0.08	Significant
f	9281.1	1	9330.1	1907.51	0	35.23	Significant
ap	16366.6	1	15868.5	3244.26	0	62.12	Significant
Vc *Vc	14.8	1	14.8	3.03	0.1	0.06	Insignificant
f *f	164.1	1	164.1	33.55	0	0.62	Significant
ap *ap	38.5	1	38.5	7.87	0.012	0.15	Significant
Vc *f	69.3	1	69.3	14.17	0.002	0.26	Significant
Vc *ap	39.7	1	39.7	8.12	0.011	0.15	Significant
f *ap	267.6	1	267.6	54.72	0	1.02	Significant
Error	83.2	17	4.9	596.58	0	0.32	
Total	26345.1	26					
b) Coated carbide							
Model	27270.73	9	3030.08	174.10	0	98.93	
Vc	533.88	1	533.88	30.68	0.0001	1.94	Significant
f	8110.02	1	8110.02	465.99	0.0001	29.42	Significant
ap	17885.93	1	17885.93	1027.70	0.0001	64.88	Significant
Vc *Vc	439.64	1	349.64	25.26	0.0001	1.59	Significant
f *f	2.94	1	2.94	0.17	0.686	0.01	Insignificant
ap *ap	0.10	1	0.10	5.97E-003	0.939	0.00	Insignificant
Vc *f	374.39	1	374.39	21.51	0.0002	1.36	Significant
Vc *ap	65.18	1	65.18	3.75	0.069	0.24	Insignificant
f *ap	301.40	1	301.40	17.32	0.0007	1.09	Significant
Error	295.87	17	17.40			1.07	
Total	27566.60	26					

2.3.2. Development of predictive models

2.3.2.1 Models formulated using RSM

According to the selected cutting parameters, the empirical models of *Ra* and *Fz* were formulated by using RSM for the two selected inserts as given in Eqs. 2.11-2.14. Their coefficients of determination (R^2) were also described. Bagaber et al. [2.20] also found almost similar value of R^2 (93.5%) when researchers constructed response surface model of *Ra*. In another study [2.21], very close values of R^2 for *Ra* and *Fz* models were also obtained as 96.84 % and 99.61%, respectively.

$$Ra_{GC1525} = +2.09586 - 0.013232 * \mathrm{Vc} - 2.48082 * \mathrm{f} - 3.63113 * \mathrm{ap} + 1.32275\mathrm{E} - 003 * \mathrm{Vc} * \mathrm{f} + 1.65966\mathrm{E} - 003 * \mathrm{Vc} * \mathrm{ap} + 1.94444 * \mathrm{f} * \mathrm{ap} + 2.87456\mathrm{E} - 005 * \mathrm{Vc}^2 + 46.18056 * \mathrm{f}^2 + 7.88889 * \mathrm{ap}^2 \quad (R^2 = 90.78\%) \quad (2.11)$$

$$\mathrm{Fz}_{GC1525} = -83.3 + 0.1182 * \mathrm{Vc} + 954 * \mathrm{f} + 310.1 * \mathrm{ap} + 0.874 * \mathrm{Vc} * \mathrm{f} - 0.2647 * \mathrm{Vc} * \mathrm{ap} + 1181 * \mathrm{f} * \mathrm{ap} - 0.000395 * \mathrm{Vc}^2 - 3268 * \mathrm{f}^2 - 253.3 * \mathrm{ap}^2 \quad (R^2 = 99.68\%) \quad (2.12)$$

$$\mathrm{Ra}_{GC1125} = +0.84196 - 1.16191\mathrm{E} - 003 * \mathrm{Vc} - 8.23721 * \mathrm{f} + 1.70463 * \mathrm{ap} - 0.021340 * \mathrm{Vc} * \mathrm{f} + 5.55556\mathrm{E} - 004 * \mathrm{Vc} * \mathrm{ap} - 5.69444 * \mathrm{f} * \mathrm{ap} + 8.16949\mathrm{E} - 006 * \mathrm{Vc}^2 + 78.70370 * \mathrm{f}^2 - 2.57407 * \mathrm{ap}^2 \quad (R^2 = 94.64\%) \quad (2.13)$$

$$\mathrm{Fz}_{GC\ 1125} = -47.09 + 0.59775 * \mathrm{Vc} - 211.27 * \mathrm{f} + 97.14 * \mathrm{ap} + 2.03 * \mathrm{Vc} * \mathrm{f} + 0.33905 * \mathrm{Vc} * \mathrm{ap} + 1252.92 * \mathrm{f} * \mathrm{ap} - 2.15\mathrm{E} - 003 * \mathrm{Vc}^2 + 437.50 * \mathrm{f}^2 + 13.17 * \mathrm{ap}^2 \quad (R^2 = 98.93\%) \quad (2.14)$$

2.3.2.2. 3D response surfaces of *Ra* and *Fz*

The 3D response surface plot is an adequate graphical tool that allows understanding and visualizing the variation of a response as a function of two variables at a time [2.43]. Figure 2.6 a-b shows the 3D surface response plots of the investigated response, i.e. *Ra* and *Fz* with respect of *Vc*, *f* and *ap* for both inserts. According to Figure 2.6-a, *Ra* values increased as feed increased as well from 0.08 mm/rev to 0.16 mm/rev for both GC 1525 and GC 1125 inserts. It is discernable that this increment in *Ra* values can be explained by the generation of helical grooves yielded by the relative motion between workpiece and tool. As soon as these grooves were deeper and wider, the feed assumed higher values [2.8, 2.44]. In turning, consequently, this leads to

augment sliding and straining of materials as chips formation [2.45]. Moreover, *Fz* values increased as *ap* and *f* increased from 0.1 mm to 0.3 mm and from 0.08 mm/rev to 0.16 mm/rev, respectively for both inserts (Figure. 2.6-b). This steady increment in *Fz* values was attributed to the soft ferrite phase which in machining of ductile material such as AISI 316L caused a long tool-chip contact area on the rake face. Therefore, the enlargement in tool-chip contact area associated with increased in *ap* and *f* which impact higher material straining for chips, generated higher temperature and increased the shear stress [2.19, 2.46, 2.47]. In the cutting zone, the increment in temperature and the excess of shear stress increased the plastic deformation of the material, which led to an increment in the volume of chips removed [2.47].

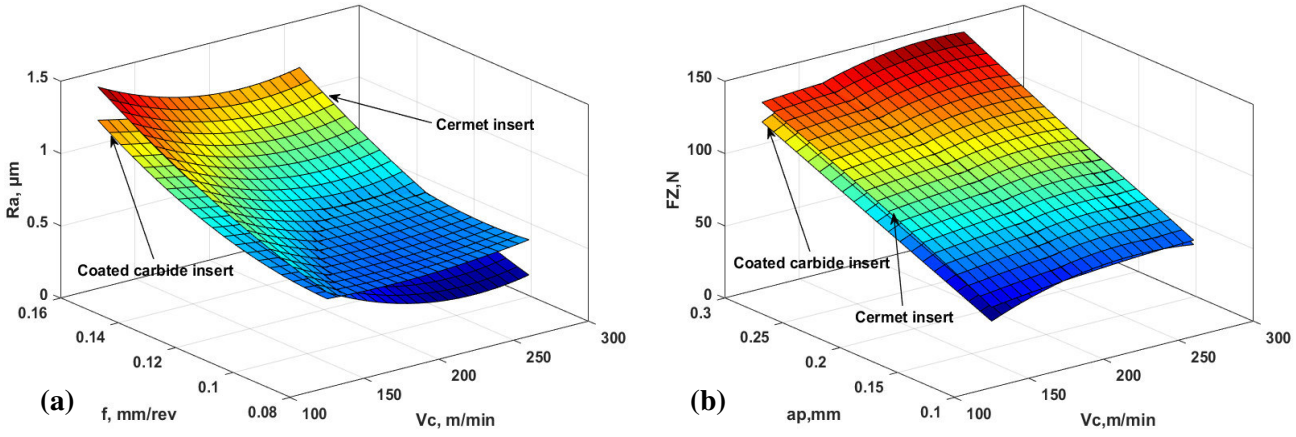

Figure 2.6: 3D surface response for *Ra* (a) and *Fz* (b) for cermet (GC 1525) and coated carbide (GC 1125)

2.3.2.3. RSM models performance assessment

Herein, RSM models were checked in terms of R^2, MAPE and RMSE values, when *Ra* and *Fz* were taken into consideration. The R^2, MAPE and RMSE were derived in Eqs. 2.15-2.17. Firstly, it was discernable that the R^2 of all models of *Ra* and *Fz* for the two selected inserts formulated by RSM were higher, which were closer to unity. In addition, the absolute percentage errors (APE) were calculated for each experimental and predicted responses. The APE values were listed in Table 2.6. It can be seen that the MAPE for *Ra* and *Fz* concerning the GC 1525 insert were 10.07% and 2.28%. Also, it can be observed that the MAPE for *Ra* and *Fz* regarding to the GC 1125 insert were

4.98% and 4.83%, respectively. In literature, Laouissi et al. [2.6] assessed the predictive capabilities of models established by RSM for *Ra* and *Fz*. Their results showed that the MAPE values of *Ra* and *Fz* were found to be vary between (1.95 % to 9.30%). Furthermore, Mia et al. [2.9] developed predictive models for surface roughness and cutting force using RSM. The obtained results revealed that the MAPE of *Ra* and *Fz* were obtained as 9.06% and 1.73%, respectively for RSM models. Besides, it can be indicated that the RSM based *Ra* and *Fz* prediction models suggested RMSE varied between 0.04 and 2.71. The Table 7 outlined the R^2, MAPE and RMSE values. Based on predictive capabilities, the RSM models showed satisfactory results for predicting *Ra* and *Fz*. This was also underlined by Laouissi et al. [2.6].

$$R^2 = \frac{\sum_{n=1}^{N}(Res_M - \overline{Res}_M)(Res_P - \overline{Res}_P)}{\sqrt{\sum_{i=1}^{N}(Res_M - \overline{Res}_M)}\sqrt{\sum_{i=1}^{N}(Res_P - \overline{Res}_P)}} \quad (2.15)$$

$$MAPE = \frac{1}{N}\sum_{i=1}^{N}\left(\frac{Res_M - Res_P}{Res_M}\right)X100 \quad (2.16)$$

$$RMSE = \sqrt{\frac{\sum_{i=1}^{n}(Res_M - Res_P)^2}{n}} \quad (2.17)$$

where Res_M and Res_P are the measured and the predicted response values, respectively. $\overline{Res}_M$ and $\overline{Res}_P$ are the mean of the measured and the predicted response values, respectively.

Table 2.6: RSM prediction results for cermet (GC 1525) and coated carbide (GC 1125) inserts.

No.	Predicted *Ra*		APE-*Ra*		Predicted *Fz*		APE- *Fz*	
	GC 1525	GC1125	GC 1525	GC1125	GC 1525	GC1125	GC 1525	GC1125
1	0.75	0.56	14.45	19.15	25.04	24.32	5.03	11.61
2	0.66	0.62	52.31	3.13	54.64	48.69	2.90	11.26
3	0.73	0.62	9.50	6.90	79.18	73.32	2.83	2.38
4	1.04	0.73	12.85	7.35	46.09	34.54	1.52	1.74
5	0.95	0.76	39.02	15.56	80.42	63.92	0.40	1.16
6	1.03	0.74	13.45	2.78	109.68	93.57	0.29	6.51
7	1.47	1.15	4.26	7.26	56.70	46.16	1.89	1.23
8	1.39	1.16	2.11	0.87	95.74	80.55	3.28	2.87
9	1.48	1.12	0.22	1.82	129.73	115.21	0.88	1.47
10	0.55	0.54	7.84	11.48	27.02	31.48	3.92	2.14
11	0.47	0.6	7.24	6.25	55.29	57.38	1.09	6.02
12	0.54	0.61	2.99	3.17	78.48	83.54	3.68	4.63
13	0.84	0.68	14.03	0.00	49.85	45.36	5.23	8.51
14	0.76	0.71	14.93	5.97	82.83	76.27	2.55	2.42
15	0.84	0.69	8.62	2.82	110.75	107.44	1.23	0.32
16	1.27	1.06	1.04	4.95	62.21	60.63	3.58	1.90
17	1.2	1.07	9.77	5.94	99.92	96.55	0.01	2.20
18	1.29	1.03	9.94	0.96	132.56	132.74	0.18	4.82
19	0.5	0.61	1.35	1.61	26.33	19.66	1.68	28.41
20	0.43	0.67	9.15	4.69	52.36	48.61	5.61	3.80
21	0.51	0.68	7.75	1.49	73.32	77.82	2.02	4.04
22	0.79	0.66	6.28	4.35	52.09	40.85	1.66	1.45
23	0.72	0.7	8.47	9.37	82.84	74.81	2.29	6.63
24	0.82	0.69	3.80	1.43	108.53	109.04	2.69	4.14
25	1.23	0.97	4.24	0.00	67.40	63.44	0.96	3.73
26	1.17	0.99	5.14	1.00	102.87	102.41	2.23	4.87
27	1.28	0.95	1.05	4.04	133.28	141.65	1.80	0.08
MAPE			10.07	4.98			2.28	4.83

Table 2.7: Summary of RSM developed models performance.

	Cermet		Coated carbide	
	Ra	*Fz*	*Ra*	*Fz*
R^2*(%)*	97.76	97.13	90.78	94.64
MAPE(%)	10.07	2.28	4.98	4.83
RMSE	0.08	1.51	0.04	2.71

2.3.2.4. Validation of RSM models

The comparisons between the predicted and experimental values were described in Figure. 2.7. Obviously, there was a good approximation between them. Overall, it can be inferred that the proposed models were reliable. Henceforth, this research work could be useful for metal cutting industries for the selection of cutting parameters in turning of AISI 316L using GC 1525 and GC 1125 inserts, and it would be helpful for engineers and operators for better control surface roughness and cutting force of the investigated material.

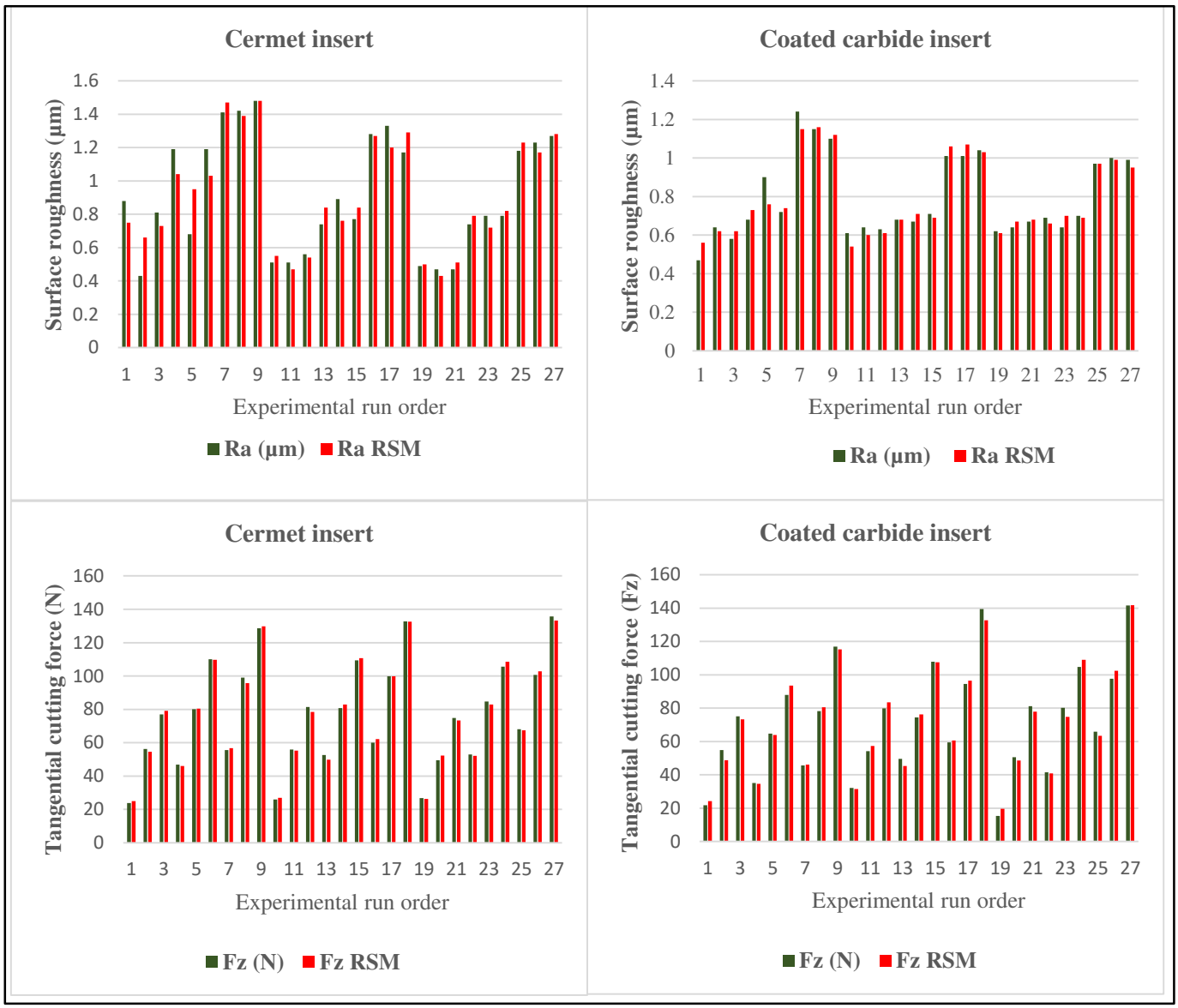

Figure 2.7. Comparison of the predictive models with experimental results of *Ra* and *Fz* for Cermet (GC1525) and Coated carbide (GC1125) cutting inserts.

2.3.3. Single- and Multi-objective optimizations of cutting parameters

In the current study, the purpose of the optimization studies is to obtain the optimal values for turning parameters to separately and simultaneously minimize the *Ra* and *Fz* values for both inserts (GC1525 and GC1125). In this section, single and multi-objective optimization were interested and the SA and GA methods were employed by using RSM models, which were taken to be the objective function.

2.3.3.1. Single-objective optimization using SA

To accomplish our target, some criteria of SA parameters such as annealing function, initial temperature and temperature update function were tested using MATLAB Optimization tool box 7.6. Table 2.8 presents the SA optimization results for *Ra* and *Fz* for both inserts. The optimal sets of cutting parameters for minimum *Ra* values delivered by SA were determined as the cutting speed of 214.293 m/min, feed of 0.08 mm/rev and depth of cut of 0.198 mm for GC 1525 insert and as the cutting speed of 177.588 m/min, feed of 0.08 mm/rev and depth of cut of 0.1 mm for GC 1125 insert. The optimal cutting parameters for minimum *Fz* values were calculated as the cutting speed of 125 m/min, feed of 0.08 mm/rev and depth of cut of 0.1 mm for both inserts. The best results for the minimum *Ra* and *Fz* were obtained as 0.3988 µm and 26.2491 N, respectively for GC 1525 insert and as 0.5440 µm and 24.0642 N, respectively for GC 1125 insert. The best fitness function plots of SA were shown in Figure 2.8.

Table 2.8: Optimal cutting parameters for single-objective optimization of *Ra* and *Fz* by SA.

Responses	Cutting inserts	*Vc* (m/min)	*f* (mm/rev)	*ap* (mm)	Minimum value
Ra (µm)	Cermet	214.293	0.08	0.198	0.3988
	Coated carbide	177.588	0.08	0.1	0.5440
Fz (N)	Cermet	125	0.08	0.1	24.0642
	Coated carbide	125	0.08	0.1	24.3405

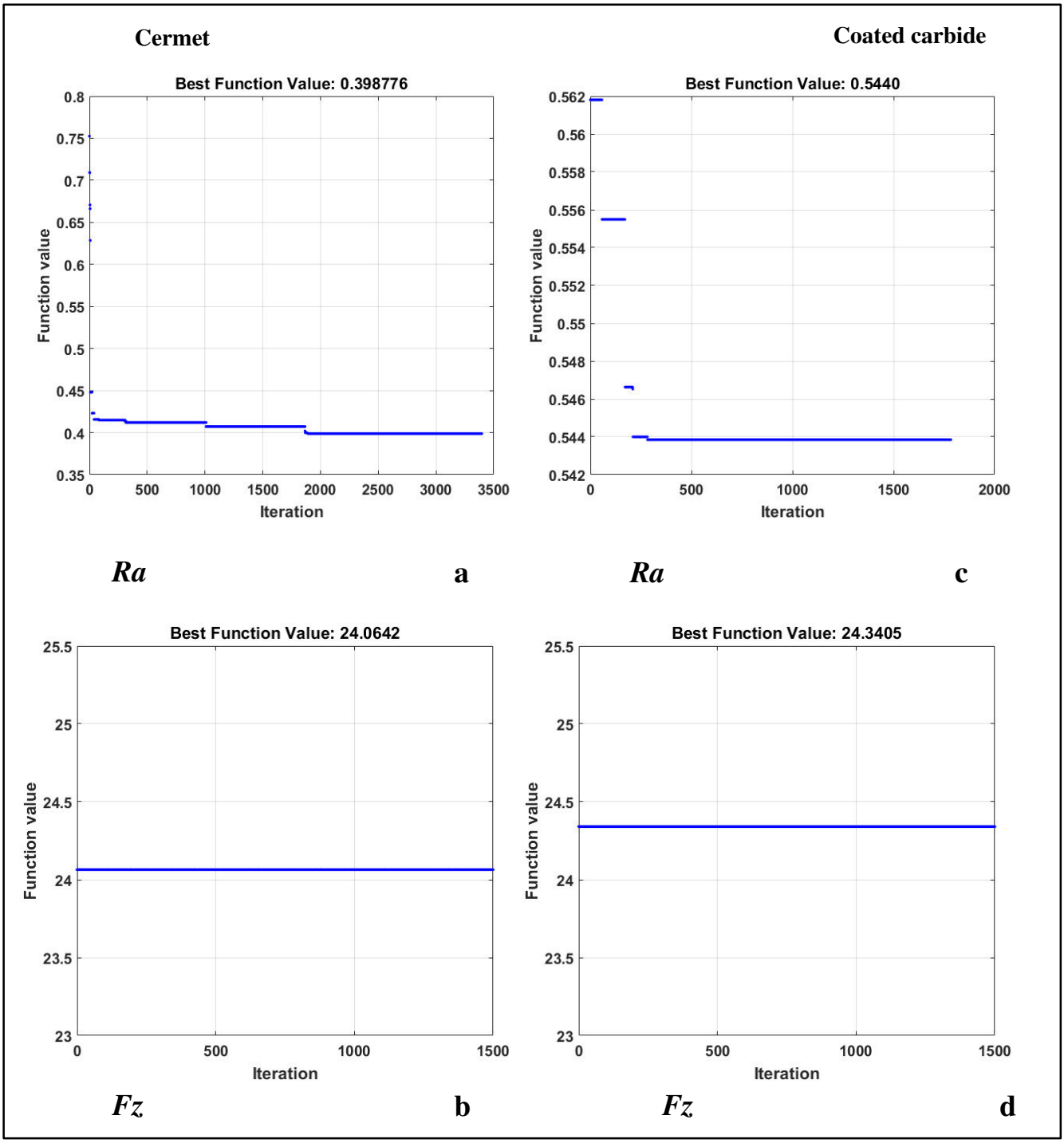

Figure 2.8. Fitness function plots of SA for cermet (a-b) and coated carbide (c-d) cutting inserts.

Even though SA provides good results, for better performance, another algorithm named GA is employed which is discussed in the next section.

2.3.3.2. Single-objective optimization using GA

To fulfill our objective, MATLAB Optimization toolbox 7.6 was also employed with some combinations of GA parameters such as population size, crossover rate and elite count to obtain the most accurate results. Table 2.9 lists the GA optimization results for *Ra* and *Fz* for both inserts. The optimal sets of cutting parameters that led to minimize *Ra* values were determined as the cutting speed of 216.1 m/min, feed of 0.08 mm/rev and depth of cut of 0.198 mm for GC 1525 insert and as the cutting speed of 172.199 m/min, feed of 0.08 mm/rev and depth of cut of 0.198 mm for GC 1125 insert, whereas the cutting speed of 125 m/min - 260 m/min, feed of 0.08 mm/rev and depth of cut of 0.1 mm were adopted cutting regimes that led to minimize *Fz* values for both inserts. The accurate results for the minimum *Ra* and *Fz* values were determined to be 0.3987 µm and 24.0642 N, respectively for GC1525 insert and to be 0.5436 µm and 19.7918 N, respectively for GC1125 insert. The best fitness function plots of GA were displayed in Figure 2.9.

Table 2.9: Optimal cutting parameters for single-objective optimization of *Ra* and *Fz* by GA.

Responses	Cutting inserts	*Vc* (m/min)	*f* (mm/rev)	*ap* (mm)	Minimum value
Ra (µm)	Cermet	216.1	0.08	0.198	0.3987
	Coated carbide	172.199	0.08	0.1	0.5436
Fz (N)	Cermet	125	0.08	0.1	24.0642
	Coated carbide	260	0.08	0.1	19.7918

2.3.3.3. SA and GA optimization results assessment

In order to extrapolate the relative benefit of optimum set of cutting regime over any other regime, the optimum results proposed by SA and GA were compared with three random experimental runs. For *Ra*, experiments of 9, 10 and 19 (Table 2.3) and experiments of 5, 18 and 19 (Table 2.3) were selected for GC 1525 and GC 1125, respectively. For *Fz*, experiments of 4, 9 and 11 (Table 2.3) and experiments of 16, 21 and 27 (Table 2.3) were chosen for GC 1525 and GC 1125, respectively. These

comparisons were presented in Tables 2.10, 2.11, 2.12 and 2.13. As shown in Tables 2.10 and 2.12, it was found that the SA and GA improved the *Ra* at almost similar values 73% and 47% for GC1525 and GC1125 inserts, respectively. Furthermore, as listed in Tables 2.11 and 2.13, it was obtained that the SA and GA improved the *Fz* values at about 81% for GC 1525 insert and at about 82% and 86%, respectively for GC1125 inserts. Moreover, as reported in Table 2.14, it was clearly seen that the GA generated lower number of iteration that conduct to minimum *Ra* and *Fz* for both inserts compared to that given by SA. Therefore, referring to the differences between the optimum values determined by SA and GA, improvement rate and the number of iteration of *Ra* and *Fz* for both inserts, it can be concluded that the GA-based optimization models exhibited superior performance than the SA. This is because of the capability of GA to achieve optimum solution faster and to perform complex optimization problem efficiently as stated by Bouacha et al. [2.48]. This study showed similar results with a study conducted by Zain et al [2.17] for superior performance of GA than SA. Hence, it was recommended for multi-objective optimization of *Ra* and *Fz* while turning of AISI 316L using both inserts.

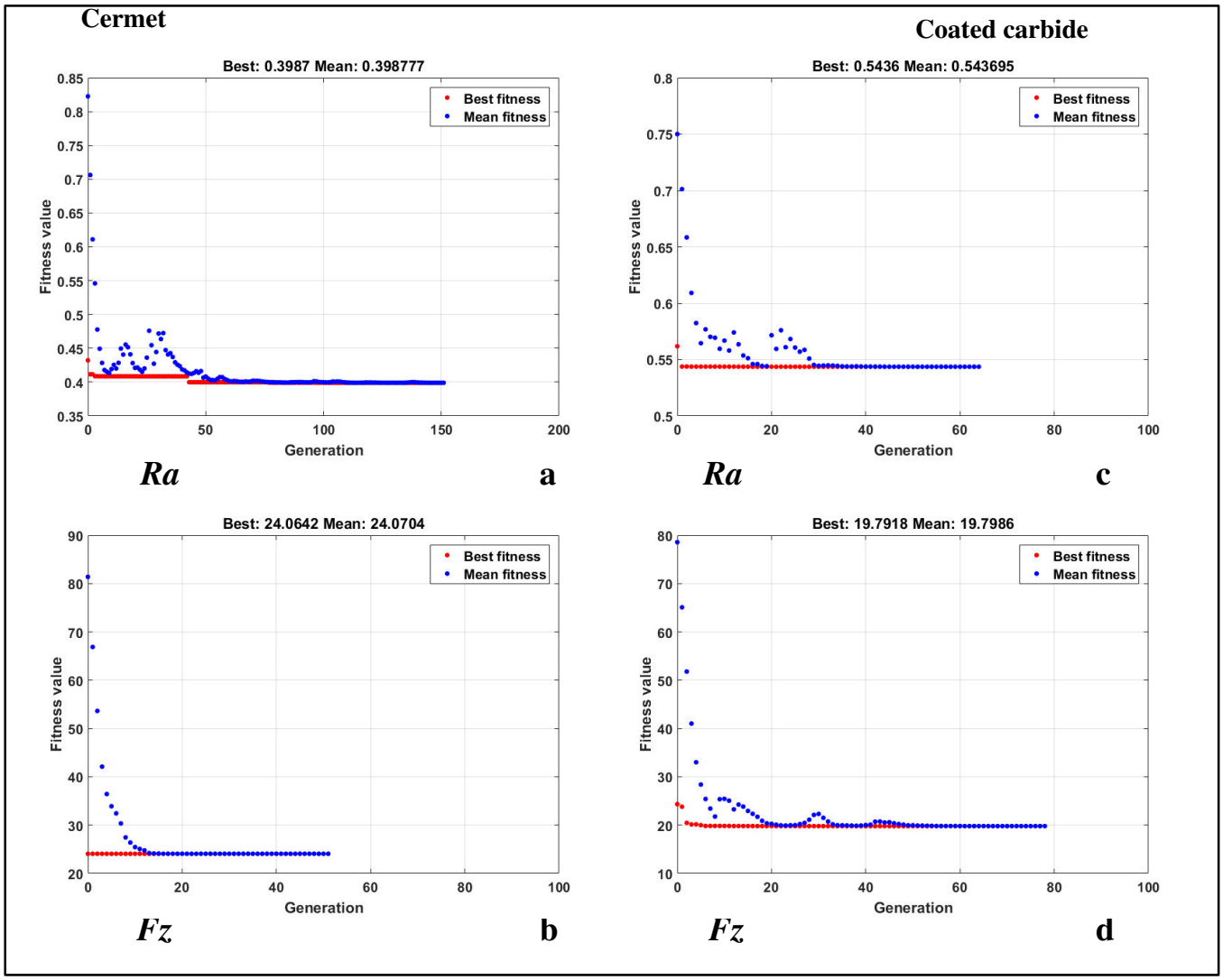

Figure 2.9. Fitness function plots of GA for cermet (a-b) and coated carbide (c-d) cutting inserts.

Table 2.10: Validation of SA-based optimization *Ra* model.

Inserts	Model/Run	*Vc* (m/min)	*f* (mm/rev)	*ap* (mm)	*Ra* (µm)	% Improvement
Cermet	**Optimum run**	**214.29**	**0.08**	**0.198**	**0.3988**	-
	Random run1	125	0.16	0.3	1.48	73.05
	Random run 2	170	0.08	0.1	0.51	21.80
	Random run 3	260	0.08	0.1	0.49	18.61
Coated carbide	**Optimum run**	**177.588**	**0.08**	**0.1**	**0.5440**	-
	Random run1	125	0.12	0.2	0.90	39.55
	Random run 2	170	0.16	0.3	1.04	47.69
	Random run 3	260	0.08	0.1	0.62	12.26

Table 2.11: Validation of SA-based optimization *Fz* model.

Cutting inserts	Model/Run	*Vc* (m/min)	*f* (mm/rev)	*ap* (mm)	*Fz (N)*	% Improvement
Cermet	**Optimum run**	**125**	**0.08**	**0.1**	**24.0642**	**-**
	Random run1	125	0.12	0.1	46.8	48.58
	Random run 2	125	0.16	0.3	128.6	81.29
	Random run 3	170	0.08	0.2	55.9	56.95
Coated carbide	**Optimum run**	**125**	**0.08**	**0.1**	**24.3405**	**-**
	Random run1	170	0.16	0.1	59.5	59.09
	Random run 2	260	0.08	0.3	81.1	70
	Random run 3	260	0.16	0.3	141.53	82.80

Table 2.12: Validation of GA-based optimization Ra model.

Cutting inserts	Model/Run	*Vc* (m/min)	*f* (mm/rev)	*ap* (mm)	*Ra* (µm)	% Improvement
Cermet	**Optimum run**	**216.1**	**0.08**	**0.198**	**0.3987**	-
	Random run1	125	0.16	0.3	1.48	73.06
	Random run 2	170	0.08	0.1	0.51	21.82
	Random run 3	260	0.08	0.1	0.49	18.36
Coated carbide	**Optimum run**	**172.199**	**0.08**	**0.1**	**0.5436**	-
	Random run1	125	0.12	0.2	0.90	39.61
	Random run 2	170	0.16	0.3	1.04	47.73
	Random run 3	260	0.08	0.1	0.62	12.32

Table 2.13: Validation of GA-based optimization *Fz* model.

Cutting inserts	Model/Run	*Vc* (m/min)	*f* (mm/rev)	*ap* (mm)	*Fz*(N)	% Improvement
Cermet	**Optimum run**	**125**	**0.08**	**0.1**	**24.0642**	**-**
	Random run1	125	0.12	0.1	46.8	48.58
	Random run 2	125	0.16	0.3	128.6	81.29
	Random run 3	170	0.08	0.2	55.9	56.95
Coated carbide	**Optimum run**	**260**	**0.08**	**0.1**	**19.7918**	**-**
	Random run1	170	0.16	0.1	59.5	66.73
	Random run 2	260	0.08	0.3	81.1	75.60
	Random run 3	260	0.16	0.3	141.53	86.01

Table 2.14: SA and GA iteration.

Cutting inserts	Responses	SA iteration	GA iteration
Cermet	*Ra* (µm)	3396	151
	Fz (N)	1500	51
Coated carbide	*Ra* (µm)	1783	64
	Fz (N)	1500	78

2.3.3.4. Multi-objective optimization using GA

Another goal of this research is to determine the most promised cutting regime sets leading to minimize *Ra* and *Fz* values simultaneously for both inserts. Therefore, genetic algorithm was utilized. To perform such multi-objective optimizations, several combinations of genetic criteria were implemented using MATLAB optimization tool box 7.6 for the purpose of attaining the optimal possible solutions. In this context, the Pareto-optimal front that aids the user compromise between the various objectives functions (Two, in this case) was illustrated in Figure 2.10. Therefore, by using the GA for both objective functions (*Ra* and *Fz*), 17 optimal solutions (Purple stars) were found within the range considered as depicted in Figure 2.10.

The choice of the best solution depends on the constraints being included or specific requirements [2.49]. Table 2.15 presents the non-dominated Pareto-optimal solutions for *Ra* and *Fz* for both inserts. It was indicated that the cutting regimes supported to obtain a compromise among the selected parameters. The input parameter sets were identified as the cutting speed of 125 m/min - 212.596 m/min, feed of 0.08 mm/rev and depth of cut of 0.1 mm - 0.193 mm for both inserts.

According to the results obtained in single optimization case, the best optimum solutions could be selected as the experiments of 4 and 1 in Table 2.15 for cermet and coated carbide inserts, respectively.

In addition, to verify the optimal solutions found in the multi-objective optimization phase, a confirmation runs were planned and carried out on the basis of the suggested optimum levels of cutting parameters derived by GA as shown in Table 2.16. The percentage deviations between estimated and experimental measured values of *Ra* and *Fz* were also given in Table 2.16. It could be seen that the obtained deviations are

within a reasonable range, i.e. within ± 10 %, which validating the suitability of the optimal results achieved in this study.

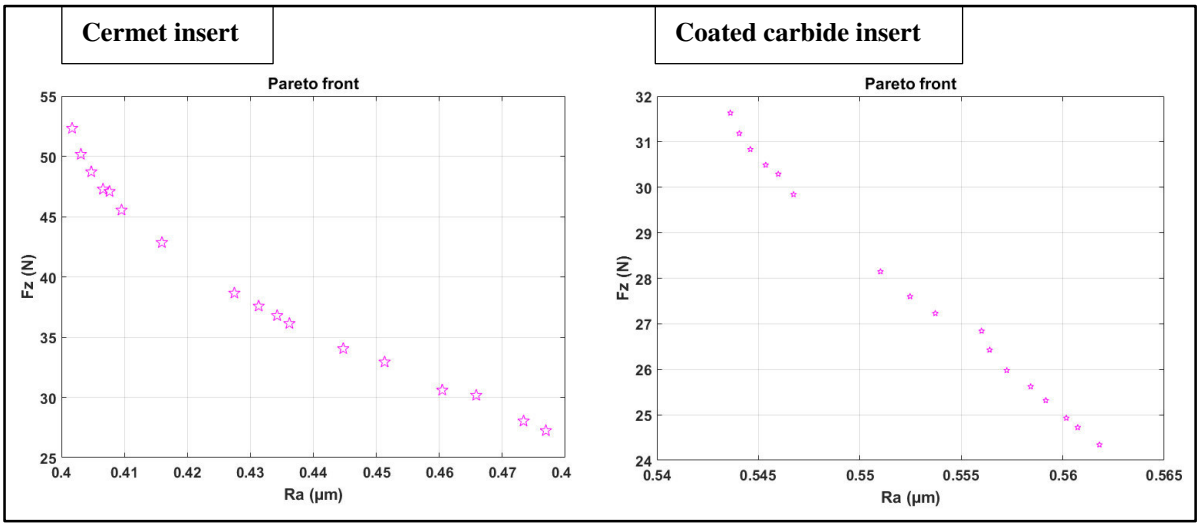

Figure 2.10. Pareto front plots for (Left) cermet and (Right) coated carbide cutting inserts

Table 2.15: Results of Pareto-optimal solutions.

Solutions	*Vc* (m/min)	*f* (mm/rev)	*ap* (mm)	*Ra* (µm)	*Fz* (N)
Cermet insert					
1	212.596	0.08	0.193	0.402	52.32
2	210.858	0.081	0.11	0.466	30.167
3	211.531	0.08	0.125	0.445	34.037
4	***209.714***	***0.08***	***0.101***	***0.477***	***27.236***
5	212.107	0.08	0.141	0.427	38.646
6	212.469	0.081	0.172	0.408	47.076
7	212.596	0.08	0.193	0.402	52.32
8	211.863	0.08	0.178	0.405	48.708
9	212.258	0.08	0.166	0.41	45.534
10	212.059	0.08	0.137	0.431	37.568
11	210.931	0.081	0.12	0.451	32.932
12	212.358	0.08	0.132	0.436	36.126
13	210.919	0.08	0.156	0.416	42.842
14	212.262	0.08	0.173	0.407	47.268
15	209.96	0.08	0.113	0.46	30.597
16	212.439	0.08	0.184	0.403	50.158
17	211.512	0.081	0.104	0.473	28.036
Coated carbide insert					
1	***125***	***0.08***	***0.1***	***0.562***	***24.341***
2	171.642	0.081	0.1	0.544	31.633
3	157.84	0.08	0.1	0.545	30.489
4	152.82	0.08	0.1	0.547	29.942
5	129.942	0.08	0.1	0.558	25.621
6	125	0.08	0.1	0.562	24.341
7	127.265	0.08	0.1	0.56	24.928
8	139.361	0.08	0.1	0.552	27.599
9	164.977	0.08	0.1	0.544	31.183
10	133.243	0.08	0.1	0.556	26.425
11	134.56	0.081	0.101	0.556	26.843
12	142.228	0.08	0.1	0.551	28.147
13	126.463	0.08	0.1	0.561	24.721
14	161.263	0.08	0.1	0.545	30.832
15	137.324	0.08	0.1	0.554	27.229
16	155.745	0.08	0.1	0.546	30.29
17	128.759	0.08	0.1	0.559	25.315

Bold (Italic) refers to the best optimum solutions have been chosen.

Table 2.16. Comparison of optimal solutions derived by GA with confirmation run

Cutting Inserts	Run	Cutting parameters			Responses	
		Vc, m/min	f, mm/rev	ap, mm	*Ra*, µm	*Fz*, N
Cermet	GA	209.714	0.08	0.101	0.477	27.236
	Experimental run	210	0.08	0.1	0.54	30.25
	% Deviation with respect to experimental run				*11.66*	*9.96*
Carbide	GA	125	0.08	0.1	0.562	24.341
	Experimental run	125	0.08	0.1	0.61	26.94
	% Deviation with respect to experimental run				*7.87*	*9.65*

2.3.4. Flank wear estimation under machining time

Tool wear largely depends upon coating and type of cutting insert. Thus, to compare the performance of GC1525 and GC1125 inserts, it is imperative to quantify the tool flank wear (*VB*) which has an admissible value of 0.3 mm for turning operation according to IS0 3685 standard. Beyond this value, wear accelerates sharply which induce losing cutting performances of the cutting tool. As a result, this case affects negatively both the surface finish and dimensional accuracy [2.50]. The flank wear was measured in respect to machining time under cutting speed of 340 m/min, feed of 0.08 mm/rev, and depth of cut of 0.2 mm for GC1525 and GC1125 inserts as shown in Figure 2.11. The results showed that the admissible *VB* values were reached after 30 min and 24 min of machining time for GC1525 and GC 1125 inserts, respectively. The flank wear images in Figure 2.11 clearly indicated that the *VB* increased rapidly as increasing the machining time. Yallese et al. [2.51] highlighted similar observation. As the cutting insert continuously works, the temperature at the cutting zone increases due to the large tool-chip contact area and relative tool-workpiece sliding associated with the absence of any lubrication, and consequently leads to occur adherence and welding chips to the rake face of the cutting insert. As a result, there are an acceleration of abrasion and diffusion wear mechanisms [2.52, 2.53]. The tool lives were determined as 30 min and 24 min for cermet (GC 1525) and coated carbide (GC 1125) inserts, respectively as displayed in Figure 2.11. Based on the results and the ratio of the tool life of GC 1525 to the tool life of GC 1125 (which was calculated as 1.25) it can

be revealed that GC 1525 insert showed superior performance in reference to the tool life. This could be attributed to the lower diffusion wear and thermal expansion coefficients in cermet (GC1525) insert [2.54].

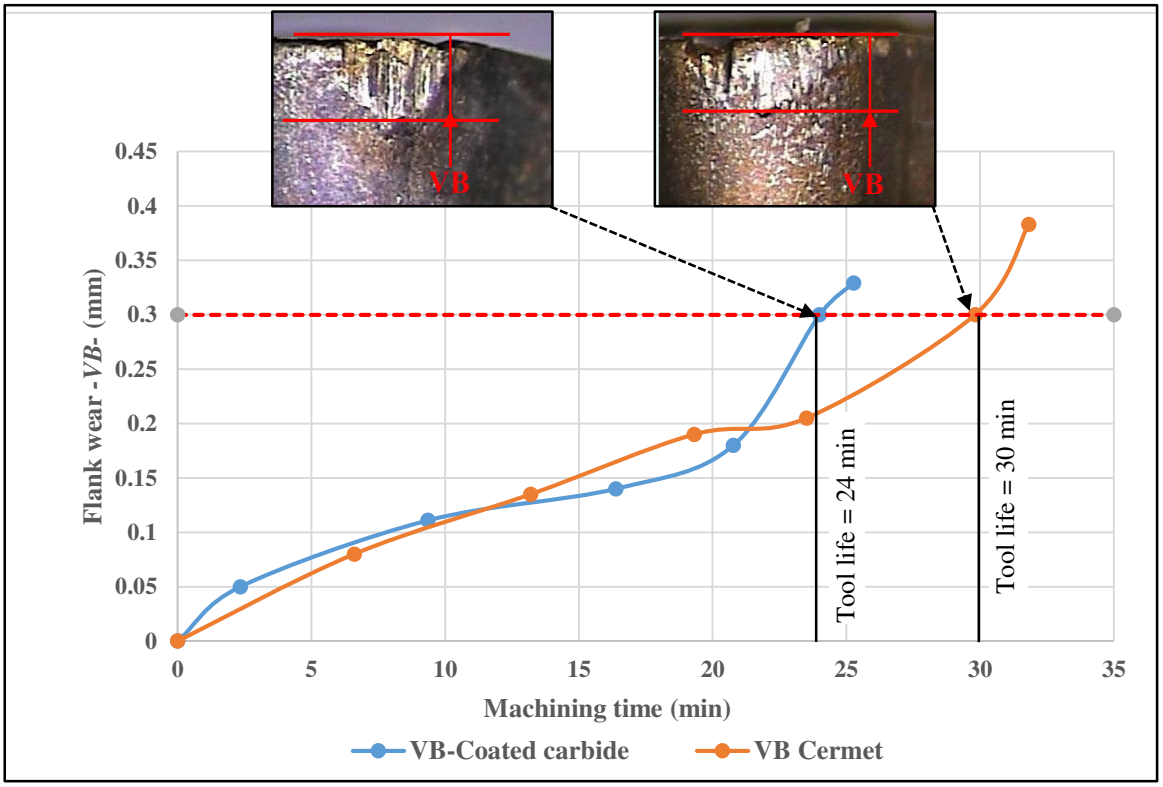

Figure 2.11. Evolution of VB with respect to machining time for cermet (GC 1525) and coated carbide (GC1125) cutting inserts at *Vc* = 340 m/min, *f* = 0.8 mm/rev and *ap* = 0.2 mm.

2.3.5. 3D surface topography

In Figure 2.12, AISI 316L austenitic stainless steel surface topographies were shown after dry turning at constant cutting speed and depth of cut (Vc = 170 m/min and ap = 0.2 mm) and two feed values (f = 0.08 mm/rev and 0.16 mm/rev). In case of GC 1525 insert (Fig. 2.12- Above) at low feed (f =0.08 mm/rev), the machined surface was marked with quite uniform summits that were much higher than depth of single cavities. Also, a single peak was noticed when looking at the subjected part of the surface. Raising feed value from 0.08 mm/rev to 0.16 mm/rev increased the average values of roughness as depicted on a legend bar. As a result, crests, valley and sharp summits quit typical for turning were also observed on the analyzed surfaces. In a sense form that a cavity deeper than the once for lower feeds was also found out. As impact of that

higher value of surface roughness were obtained. In case of GC 1125 (Fig. 2.12-Below), a better visualization of the machined surface indicated that the surface had also quite uniform peaks that were considerably higher than the depth of single pits. Increasing feed value from 0.08 mm/rev to 0.16 mm/rev generated an increment in surface roughness indicated on a legend bar. Additionally, deeper pits at high feed were observed than those at lower feed. Furthermore, an increment in feed caused sharp peaks, dales and ridges on the generated surfaces. As effect of that, the metal was torn off due to its ductility at high feeds leading to deterioration of machined surface [2.55]. This observation result complies with findings extracted by Krolczyk [2.56], they noticed that the more increasing feed, the more grooves, dales and peaks appear to be evidence on the investigated material surface. When the machined surface topographies were compared for both inserts, it was noted that the surface roughness values were measured as Ra_{GC1525}= 0.718 µm and Ra_{GC1125}= 0.437 µm at low feed (f =0.08 mm/rev) and as Ra_{GC1525}= 1.52 µm and Ra_{GC1125}= 1.17 µm at high feed (f =0.16 mm/rev). Hence, it can be said that the GC1125 insert showed lower roughness criterion than that of the GC1525 insert. This notability was mainly due to the coating type of GC1125 insert (PVD, TiAlN-TiN) [2.3].

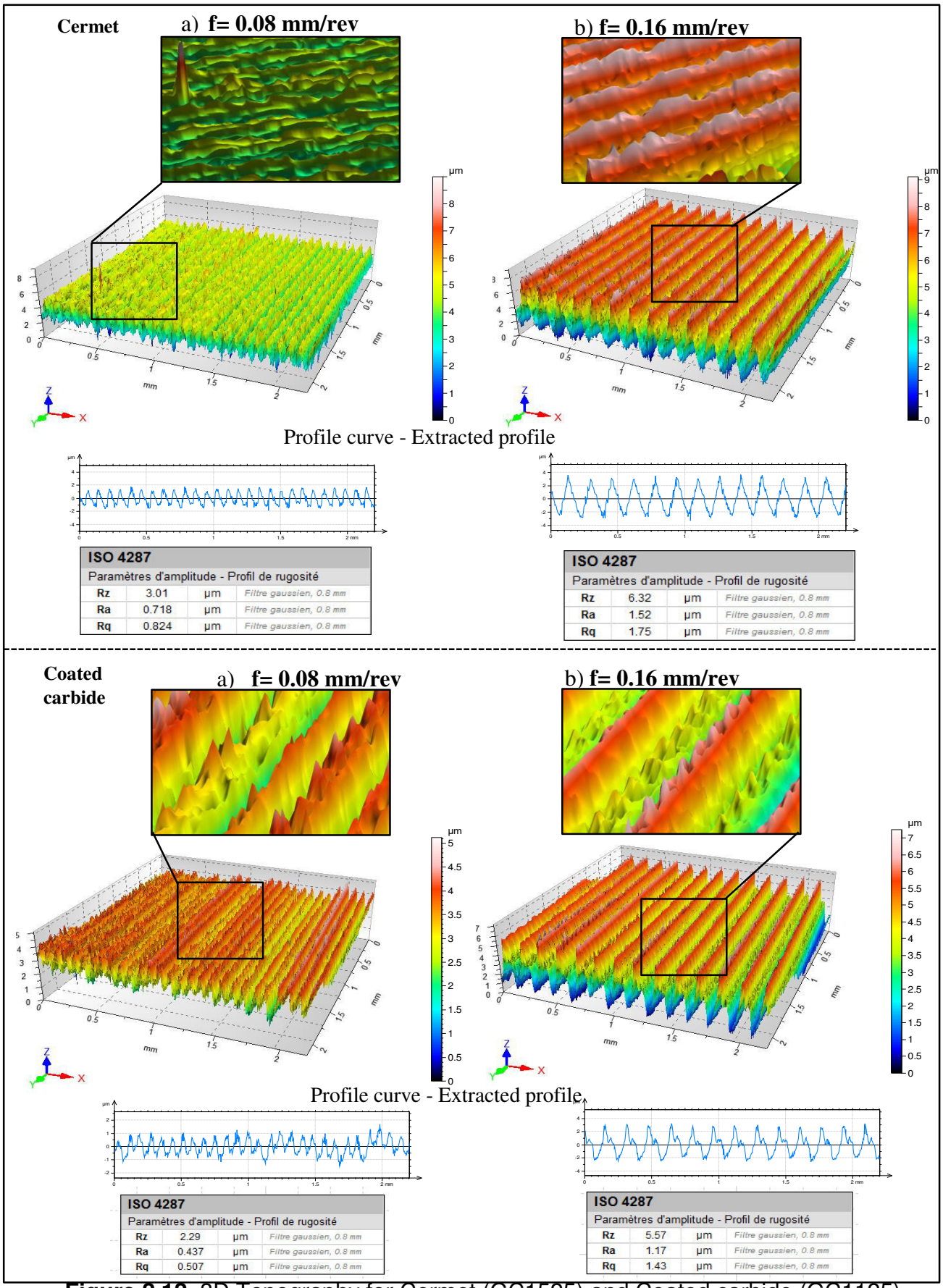

Figure 2.12. 3D Topography for Cermet (GC1525) and Coated carbide (GC1125) inserts.

2.4. Conclusion

In this study, an effort was performed to experimentally explore the effects of cutting parameters during dry turning of AISI 316L using cermet (GC1525) and coated carbide (GC1125) inserts. Furthermore, RSM predictive models of *Ra* and *Fz* were developed. Afterwards, the optimizations of the investigated responses were also presented by using Simulated annealing (SA) and Genetic Algorithm (GA). Later, the wear tests and surface topography (3D) analysis were carried out. From the practical tests, data gathering, models development assessment and results analysis, the following worthy outcomes can be drawn:

1) ANOVA results demonstrated that the feed had higher impact in determining the *Ra* value with contribution of 79.71% for GC 1525 and 74.11% for GC 1125. Thus, the effect of the depth of cut was recognized as the most significant factor on the *Fz* with contribution of 62.12% and 64.88% for GC1525 and GC1125 inserts, respectively followed by feed with contribution ratios of 35.23% and 29.42%.
2) All predictive models established by RSM produced very promising overall performance. This was documented by higher R^2, lower MAPE and RMSE, which are varying between (90.78 and 99.88), (1.67 and 10.07) and (0.03 and 2.71), respectively.
3) Validities of the RSM models have been checked by means of a comparison between the estimated and observed values. Obviously, there was a good closeness between the estimated values and the observed one. Hence, the yielded models could be useful for metal cutting industries for prediction *Ra* and *Fz* in dry turning of AISI 316L using GC1525 and GC1125 inserts.
4) The Simulated Annealing (SA) and Genetic Algorithm (GA) used in this study appeared to be encouraging computational approaches for single optimization of *Ra* and *Fz* for both inserts. However, referring to the improvement rate and the number of iteration, it can be concluded that the GA-based optimization models exhibited superior performance than the SA.
5) According to multi-objective optimization by Genetic Algorithm (GA), the cutting parameter sets that led to obtain minimum values of *Ra* and *Fz* simultaneously were recommended in range as follows: (Vc = 125 – 212.596 m/min, f= 0.08 mm/rev and ap = 0.1 – 0.193 mm).

6) The flank wears of the cermet (GC1525) and coated carbide (GC1125) inserts were reached its admissible value (VB= 0.3 mm) after 30 min and 24 min of machining time, respectively at the same cutting parameters. Apart from this and according to the tool life ratio (tool life$_{GC1525}$/ tool life$_{GC1125}$) which found to equal 1.25, it can be revealed that the GC1525 insert showed superior performance in reference to tool life.

Chapter 3: Dry turning optimization of austenitic stainless steel 316L based on Taguchi and TOPSIS approaches

3.1. Introduction

Nowadays, one of the important challenges in manufacturing industry is to provide workpieces having desired quality characteristics in the required quantity and in the fastest and most cost-effective way possible. Therefore, the improvement on the machining of hard-to-cut materials such as stainless steels, titanium alloy, nickel alloys etc… becomes an absolute necessity in the manufacturing processes (turning, milling, drilling etc.). Among hard-to-cut materials, stainless steels are widely used in many fields such as food, medical, chemical, petrochemical, aviation, defense etc. industries due to their high mechanical properties and excellent corrosion resistance. Many researchers have tried to improve their machinability in response to the diversity of their applications.

Bouzid et al. [3.1] have employed the ANOVA and RSM statistical analysis to investigate the effect of machining control factors (cutting speed, feed and cutting time) on the evolutions of flank wear, surface roughness criteria and tool life when turning AISI 304 stainless steel with a CVD coated carbide insert. The results have shown that tool flank wear is mainly influenced by cutting time followed by cutting speed. In addition, it was noticed that cutting time is the dominant factor affecting workpiece surface roughness followed by feed while tool life evolution principally depends on cutting speed. Nur et al. [3.2] have conducted a study dealing with the machining of AISI 316L, under dry condition, with coated carbide insert. Based on RSM method, these authors have discussed the effects of machining parameters on surface roughness, cutting forces and tool life. Their results denoted that feed has significant influence on surface roughness and cutting forces, while it has insignificant effect on tool life. Kaladhar et al. [3.3] have conducted experimental study dealing with the machining of AISI 304L with a PVD coated Cermet tool. The authors have highlighted that machined generated surface is affected predominantly by feed followed by insert nose radius. The cutting depth is the main factor influencing the material removal rate (MRR) followed by the feed. Marimuthu et al. [3.4] have studied the effect of cutting conditions on surface roughness during the straight turning of AISI 316 using ANOVA and Taguchi method. The authors have noted that single layer coated insert (Ti, Al) N perform better performance in term of minimization of surface roughness than the

multi-layer coated insert TiCN+Al_2O_3. Mohanad et al. [3.5] have studied the machinability assessment of super austenitic stainless steel AL-6XN alloy during wet milling environment. Their investigation has interested to examine tool wear evolution and phenomena accompanying tool-workpiece interaction. As a result, built-up-edge, insert crater wear, tool chipping and insert flank wear were investigated. Optimum cutting tool life was attained at cutting speed of 100 m/min, feed of 0.1 mm/tooth and cutting depth of 3 mm. Seid-Ahmed et al. [3.6] have performed drilling experiments on AISI 304 and AISI 2205 austenitic stainless steels. The results have showed that AISI 304 has better machinability compared to AISI 2205. Nomani et al. [3.7] have carried out drilling tests on AISI 2507, AISI 2205 and AISI 316L. Results prove that the latter material exhibit better machinability when compared to the others in terms of tool wear, cutting forces and surface finish.

To find out optimum cutting conditions, using different empirical optimization methods, several parametric studies were conducted [3.8-3.11]. Indeed, Bouzid et al. [3.12] have used the Taguchi method and GRA technique for multi-criteria response optimization of turning process while machining of AISI 420. The feed, cutting speed and cutting depth were considered as input factors and Ra and MRR as the responses. Zerti et al. [3.13] used the Taguchi method to minimize some response parameters in dry turning of AISI D3. The effects of main cutting edge angle, nose radius, cutting speed, feed and depth of cut on surface roughness were analyzed and the results showed that both feed and cutting insert nose radius were the most significant parameters influencing the surface roughness.

Nowadays, the use of statistical techniques is becoming essential to study forming processes by and without material removal. For examples, Sudhagar et al. [3.14] have applied TOPSIS and GRA techniques to optimize friction stir welding parameters. In order to optimize the machining of CP-Ti grade II, Khan et al. [3.15] have used a Fuzzy –TOPSIS combination approach. Results have shown that optimum machining parameters are 35 m/min cutting speed, 0.05 mm/rev feed and 0.1 mm cutting depth leading to minimize Fz, Ra and VB. These authors pointed out that the proposed method is efficient in obtaining optimal process parameters within a predefined range of machining conditions. Anand Babu at al. [3.16] have utilized the combining analytic hierarchy process (AHP) and the technique of Deng's similarity index investigate optimal parameters in the case of wire electrical discharge machining process of Al/SiCp composite material. In a recent investigation reported by Shankar et al. [3.17]

an integrating design of experiment (DoE) and TOPSIS method for non-traditional method process was established to determine optimal process parameters during machining of Inconel 718 alloy.

Based on previous state of art, it appears that the machinability of Austenitic stainless steel remains a current subject that deserves to be investigated specially with TiCN-TiN PVD cermet tool. In the present contribution, the machinability assessment focuses particularly on evolutions of tool wear, cutting forces, surface roughness criterion and material removal rate during the turning of AISI 316L. Furthermore, process optimization using Taguchi and TOPSIS approaches is undertaken. The objective is to obtain optimal combination of process parameters yielding to minimum responses in terms of flank wear (VB), tangential cutting force (Fz) and surface roughness (Ra) and maximum material removal rate (MRR) when machining of the considered material.

3.2. Experimental materials and turning conditions

3.2.1. Workpiece material, cutting tool and turning machine

The workpiece material investigated in this study is an austenitic stainless steel (AISI 316L). The standard for the specimen is a cylindrical rod with an axial length of 400 mm and a diameter of 80 mm with an average hardness of 197 HV (Figure 3.1). Table 3.1 presents the chemical composition of the workpiece material.

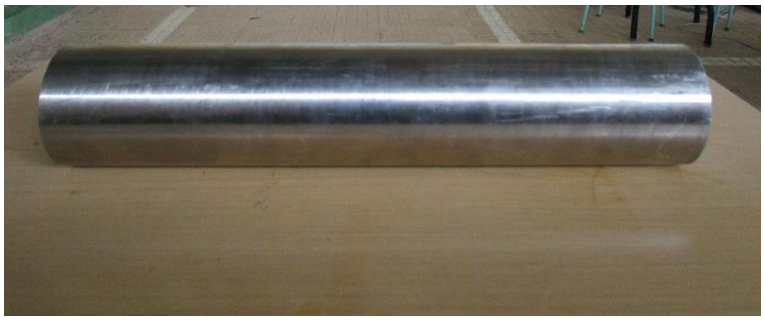

Figure 3.1. Workpiece material AISI 316L.

Table 3.1. Chemical composition of the AISI 316L.

Composition	Wt. %	Composition	Wt. %
C	0.013	Al	0.0028
Si	0.50	Cu	0.373
Mn	1.79	Co	0.163
S	0.031	V	0.074
Cr	16.57	Ca	0.0022
Ni	9.79	Fe	68.3
Mo	2.00		

The cutting insert used in this investigation, PVD Cermet, was designated as ISO CNMG 120408, supplied by Sandvik (GC 1525) clamped on the tool holder named PSBNR2525 M12 (Figure 3.2). The turning process was carried out on a lathe TOS TRENCIN- SN 40C model with spindle power of 6.6 kW (Figure 3.3).

Figure 3.2 Cutting insert and its holder.

Figure 3.3. Lathe TOS TRENCIN

The use of cutting fluids to lower temperature elevation during cutting operation is thought to improve machining performance. However, the excessive use of cutting fluid has become a major source of concern for practitioners in the machining industry, both in terms of environmental safety and economic issues, as storage, supply, maintenance, and disposal can cost roughly from 7 to 17% of the total machining cost [3.18,3.19]. Furthermore, as stated in litterateur [3.20, 3.21, 3.22], long exposure to cutting fluid can cause health problems to the operators.

The previously mentioned negative effects of using cutting fluid make it not feasible to attain the criterion of sustainable machining [3.22], particularly in industrialized countries with strict environmental regulations.

Therefore, beginning with the mid-1990s, there has been a major trend toward dry machining process [3.23]. This process is presented in the following section.

3.2.2. Dry cutting process

Dry cutting is a strategy associated with machining processes that avoids the use of cutting fluids. In this strategy, the generated temperature is reduced by lowering the friction at interfacial faces (i.e., tool-workpiece/ tool-chip interfaces) with the use of an appropriate coating layer on tool substrate materials. Recently, there has been a noticeable uphill trend in the search for a suitable material for coating, with many studies aimed at discovering an ideal coating material that can be used to enhance the efficiency of the dry machining process [3.24-3.27]. As a result, the range of cutting speeds that can be employed in dry cutting can be extended.

In addition, dry cutting reduces the machining costs, environmental hazards and worker health concerns arising from the use of coolant [3.28, 3.29]. Dry cutting, as illustrated in Figure 3.4, not only reduces production costs by eliminating the need for cutting fluid and its associated processes (supply, use, and disposal, for example.), but it also protects worker and the environment by preventing harmful chemicals from coming into contact with humans and environment [3.30]. However, higher temperature is expected in dry cutting because it is well-known that it is cutting speed dependent. When the cutting speed increases, so does the cutting temperature, increasing the heat produced at the contact area. The heat generated will dissipate through the solid body involved in removal of material, including workpiece material, which will encounter microstructure changes. Consequently, it can lead to weak workpiece material structural integrity [3.31]. Furthermore, dry cutting is not completely free of release of toxic components, which results in a number of unpleasant conditions

such as cutting tool wear and surface roughness. Consequently, dry machining reduces the coolant/lubrication cost and leads to an increase in some costs, most notably the cost of the cutting tool [3.30].

It is possible to achieve effective application of dry cutting for a wide range of machining conditions, including workpiece material, if the superior friction properties of cutting tools can be improved to the point that the role of cutting fluid can be fully altered. Moreover, it must be capable of outperforming the product quality and machining time that can be obtained by using cutting fluid [3.31, 3.32].

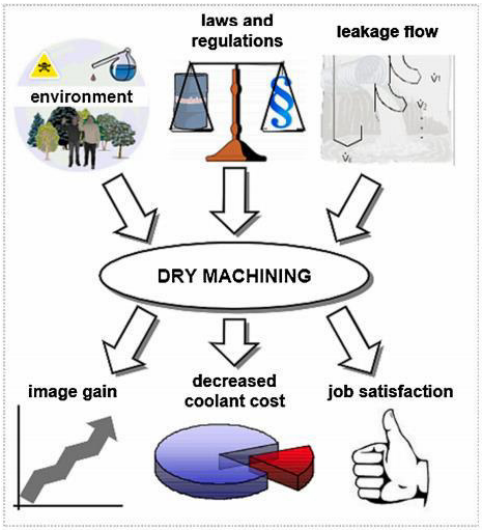

Figure 3.4. Advantage of dry machining [3.33]

3.2.3 Response Measurements

This section outlines the devices that were used to obtain detailed measurements of the process responses.

3.2.3.1. Cutting forces

The cutting forces were recorded by means of a Kistler piezoelectric dynamometer (type 9257B) with a range [-5 to 5] KN of measurements. During the cutting process, the reactions that occur are converted into electrical charges, which are then amplified by a Kistler 5070 charge amplifier (Figure 3.5). On the computer, the Dynoware software package was employed to analyze, process and convert these charges into signals, expressing the forces generated during the turning operation in three components Fx, Fy and Fz.

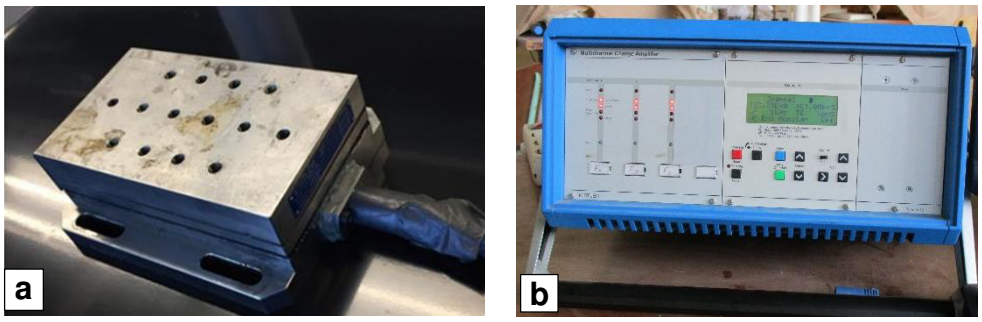

Figure 3.5. Cutting forces data assessment system: a) Kistler Dynamometer (type 9257B), b) Kistler charge amplifier.

3.2.3.2. Surface roughness

Surface roughness (Ra) was obtained by means of Mitutoyo Surftest SJ-210 roughness meter (Figure 3.6), which was coupled with a diamond point (feeler) with a radius nose of 5 µm moving linearly along the machined surface. To prevent rework errors, roughness measurements were made on the workpiece three times.

Figure 3.6. Roughness meter.

3.2.3.3. Tool wear

The rubbing between the tool's flank face and the machined surface causes the flank wear on the cutting tool. In this study, a microscope Visual Gage 250 was used to determine and quantify the amount of tool flank wear, as seen in Figure 3.7.

Figure 3.7. Microscope Visual Gage 250.

Figure 3.8 illustrates the experimental set-up and instruments used for the obtained results in the current work.

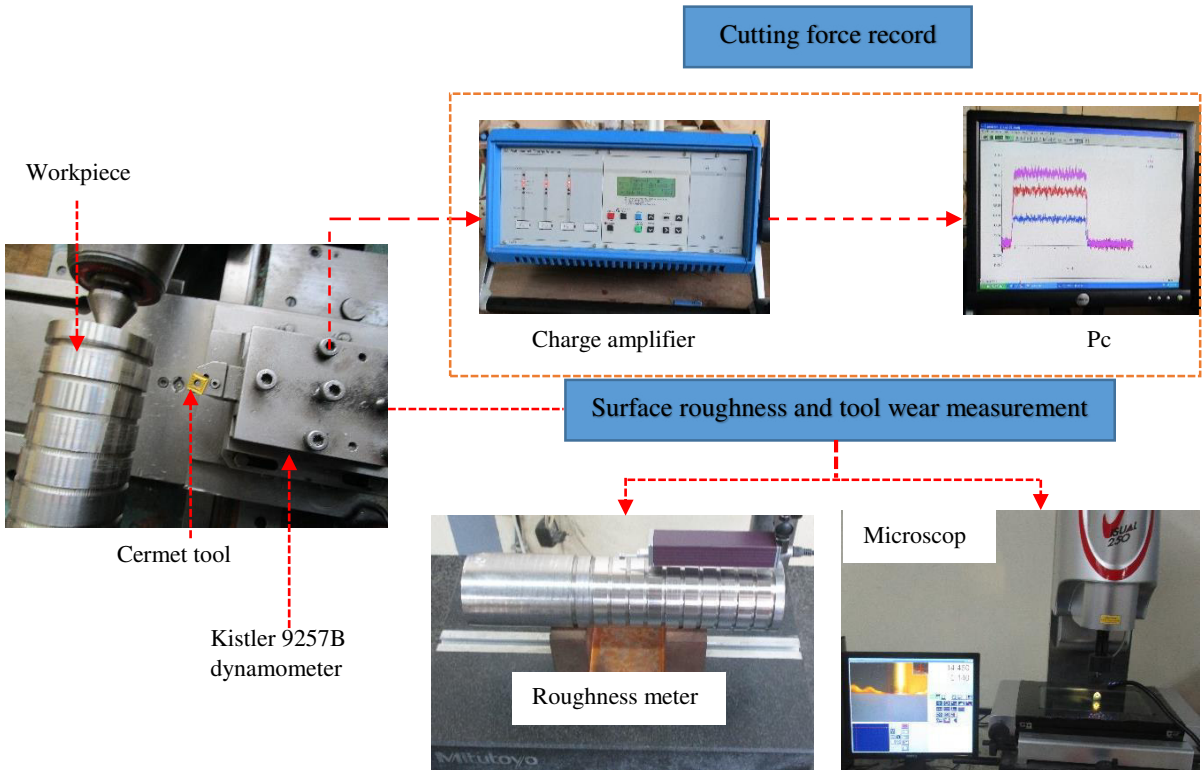

Figure 3.8. Schematic design of the present work.

3.2.4 Design of experiments (DOE)

In multi-parametric experimental studies such as machining, the number of variables can be elevated. The strategies commonly used to perform these experiments are

often costly, and they can lead, over time, to a number of results that are difficult to exploit because of the increasing complexity in the metal cutting process. In order to determine the optimal cutting conditions using appropriate organization of experiments and to exploit the results efficiently, methods such as design of experiments may be useful. The general principle of the design of experiments is to study only certain points of an experimental field, while understanding the physical phenomenon being studied over the considered field. The design of experiments (DOE) can be defined as “a systematic method to determine the relationship between factors affecting a process and the output of that process” [3.34]. However, an important difficulty of the methodology then lies in how to choose the optimal study points. On the one hand, the use of this method helps to improve the quality of products and processes, and on the other hand, it helps to reduce development time and costs [3.35].

The design of experiments provides predictive knowledge of a complex, multi-variable process with few practical tests.

In summary, the most recognized advantages of design of experiment are [3.35]:

- Economic: only the necessary experiments are carried out, thereby decreasing the time and the cost of operation.
- Accuracy: for a given experimental effort, the greatest possible accuracy will be achieved, hence minimizing the operation fluctuation to obtain high quality of product,
- The interactions between the different parameters studied are identified and better understood.

Generally speaking, the goal of the design of experiments is to provide a clear understanding of the relationship between two types of process parameters:

- The factor/input parameter: a variable, which acts on the process under study, like cutting speed, feed rate, depth of cut, cooling conditions.
- The response/output measure: a measured quantity, in order to know the effects of the input factors on the process outcome such as cutting force, cutting temperature, tool wear, surface roughness and chip formation.

Also, the most typically utilized terms in DOE methodology are controllable, uncontrollable input parameters and outputs [3.36], as seen in Figure 3.9. controllable

input parameters are those inputs that can be accurately set at the beginning of an experiment or process, such as cutting speed, feed rate and depth of cut. Uncontrollable input parameters are those factors that cannot be changed, for instance, vibration of machine tool and ambient temperature.

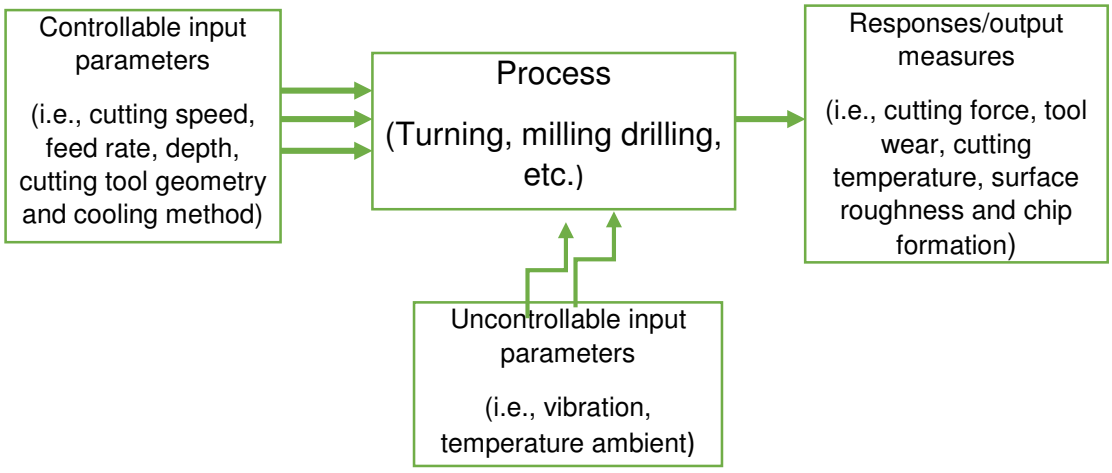

Figure 3.9. Process parameters and responses in machining [3.37]

In DOE, there are several statistical techniques such as full and factional factorial, Taguchi robust design, Box Behnken, central composite, Plackett-Burman design, Latin square, randomized complete and D-optimal that have been introduced to carry out experiments efficiently. Depending on the objective of the experimentation and the problem to be investigated, the suitable choice of one among these DOE's aforementioned techniques could be made. As example, Cavazzuti [3.38], reported that if a rough estimate of the main effects is sufficient, a Plackett-Burman design would be preferable. If a more precise computation of the main and interaction effects must be accounted for, a fractional or full factorial method is better. If the aim is to focus on a primary factor, a Latin square or randomized complete block design would be suitable. If noise variables could influence the problem, the Taguchi method is recommended. For RSM purposes, a Box-Behnken, a full factorial and a central composite has to be chosen [3.39]. However, amid these methods, the Taguchi robust design along with an ANOVA statistical tool are now prevalent in industrial optimization methods to achieve the maximum level of profit and the best quality of manufactured products [3.35, 3.39]. Table 3.2 outlines common statistical experimental design methods used in industrial applications and their main features.

Table 3.2. Common DOE methods used in industrial application [3.40]

DOE technique	Main features/Suitability
Full factorial	Calculates the main and interaction effects, and builds response surface
Taguchi robust design	Addresses the effect of discrete noise variables
Fractional factorial	Requires less effort and fewer tests
Randomized complete block design (RCBD)	Concentrates on a primary factor using blocking techniques
Box Behnken design (BBD)	Builds quadratic response surfaces
Random	Builds response surfaces
Latin squares	Focuses mainly on a primary factor
Plackett-Burman design (PBD)	Estimates the main effects
Central Composite design	Builds response surfaces
D-optimal design	Builds response surfaces

In this thesis, Taguchi and full factorial designs were employed. Hence, they are discussed in detail in the next sections.

3.2.4.1 Taguchi design approach

The Taguchi approach is a statistical method developed by Genichi Taguchi in Japan to enhance the total quality of goods that are manufactured. It is described as satisfactory and effective for achieving the optimal parameters setting (controllable parameters) for the machining process, which makes a process less sensitive to changes in uncontrollable parameters. Taguchi designs are based on orthogonal arrays that aim to study the entire parameter space with a lesser number of experiments to be performed. In this approach, as a main idea, a loss function (Signal to Noise (S/N) ratio) was applied to compute the deviations between the quality characteristics and the desired values [3.12]. Generic terms signal and noise indicate the desirable and undesirable values for the output response, respectively. A higher S/N ratio corresponds to the optimal level of the parameter's setting [3.41]. In this S/N

ratio, there are three categories available, in accordance with the type of output response [3.42];

1. The smaller-the better (SB), the experimenter is interested in minimizing the response.

$$\frac{S}{N_{SB}}(y) = -10\log\left[\frac{1}{n}\sum_{i=1}^{n} y_i^2\right] \quad (3.1)$$

2. the larger-the better (LB), the experimenter is interested in maximizing the response.

$$\frac{S}{N_{LB}}(y) = -10\log\left[\frac{1}{n}\sum_{i=1}^{n} \frac{1}{y_i^2}\right] \quad (3.2)$$

3. the nominal-the better (NB) or Specific target, the experimenter wishes for the response to attain a certain target value.

$$\frac{S}{N_{NB}}(y) = -10\log\left[\frac{y'}{S^2}\right] \quad (3.3)$$

where y is the measured experimental value, n is the number of measurements, y' is the average of the measured experimental value and S^2 is the variance of y.

The Taguchi method involves several steps which are recommended to be followed for attaining the best value of final results as follows [3.43, 3.44]:

a. Identify the main function and its side effects.
b. Identify the noise factors, testing condition and quality characteristics.
c. Identify the objective function to be optimized.
d. Identify the control factors and their levels.
e. Select a suitable Orthogonal array and construct the matrix.
f. Conduct the matrix experiment.
g. Examine the data, predict the optimum control factor levels and its performance. There are two complementary methods: the graphic analysis developed by Taguchi and the analysis of statistical variance (AVOVA).
h. Conclude from the synthesis of the results obtained, select the optimal levels of the process parameters and decide on the actions to be taken.

3.2.4.2. Analysis of Variance (ANOVA)

ANOVA is a statistical method widely used to examine the influence of cutting parameters on machinability issues in terms of signification parameters [3.9]. For that, many statistical indicators can be exploited. For example, the F-ratio is a statistical factor used to evaluate the signification contribution of each parameter. Also, the statistical significance of the fitted quadratic models is evaluated by the P-values of ANOVA. The analysis was undertaken at a level of significance of 5%, i.e. for a level of confidence of 95% [3.45]. Consequently, P-value is the probability that the results found in a study could have occurred by chance.

- If P-Value > 0.05, the parameter is insignificant.
- If P-Value < 0.05, the parameter is significant.

There are other factors which need to be calculated to complete the analysis of variance procedures. These factors include degree of freedom (DF), sum of squares (SS), mean of square (MS), percentage contribution (PC) and determination coefficient (R^2), which can be computed based on the Minitab 18 software. For instance, to estimate the contribution of parameters design and their interactions, the total sum of squared deviations (SS_f) is given by equation (3.4).

$$SS_f = \frac{N}{Nnf}\sum_{i=1}^{Nnf}(\bar{y}_i - \bar{y})^2 \tag{3.4}$$

where $\bar{y} = \frac{1}{N}\sum_{i=1}^{N} y_i$, *i* is the average of the responses, y_i is the average response observed during experiments where the factor f takes its i^{th} level of each factor. *Nnf* is the level of each factor.

The total degree of freedom (DF) was counted by considering the main effect of factors and their interactions from the data analysis which is expressed by Eq (3.5).

*DF= (number of levels – 1) * (number of factor*) (3.5)

The mean square (MS) is the ratio of factor spared deviation $\mathrm{SS_f}$ of $\mathrm{DOF_i}$. it is mentioned by Eq (3.6)

$$\mathrm{MS_i} = \frac{\mathrm{SS_i}}{\mathrm{DF_i}} \tag{3.6}$$

The $\mathrm{F_i}$ index is employed with the basis that calculated F_i values will be higher than those acquired by $\mathrm{F_i}$ in ANOVA table (Eq (3.7)).

$$F_i = \frac{MS_i}{MS_e} \tag{3.7}$$

with $\mathrm{MS_i}$ is the average square of regression model and $\mathrm{MS_e}$ indicates the mean square errors.

The percentage contribution exhibit in the AVOVA table is written by the following equation (3.8).

$$\mathrm{Pc}\ (\%) = \frac{\mathrm{SS_f}}{\mathrm{SS_t}} * 100 \tag{3.8}$$

The coefficient of determination (R^2) is an important criterion, which is defined as the ratio of the explained variation to the total variation. The latter is a measure of the goodness of fit. In addition, the more R^2 'approaches unity, the response model adapts better to the real data.

3.2.4.3. Full factorial design

The study of a full factorial design consists of studying all possible combinations of the factors (variables) taken into consideration in the experiment. This design is denoted by X^k, which means that the experiment concerns a system with k factors at X levels. The main disadvantage of such a method is when k or levels of k become large. This will require a large number of experiments, which tends to increase the running time and costs [3.36]. However, its great advantage is that no factor introduces bias (or systematic error according to ISO/DIS 3534-2 Standard-ISO 3534-3 [3.46]) in the calculation of the effects of other factors (independent effects) [3.47].

To study a response y as a function of k factors, experiments corresponding to all possible combinations of factors are carried out. If each factor A_i has Nn_i levels, then the number of trials N to be performed is given by Eq (3.9):

$$N = \prod_{i=1}^{K} Nn_i \tag{3.9}$$

For example, for three factors with three levels, the number of possible combinations results in $3^3 = 27$ configurations. In the case of a design with factors at different levels, the calculation of the number of experiments in the complete design is done in a similar way. For example, for a complete design with 3 factors at 2 levels and 2 factors at 4 levels, $2^3 \times 4^2 = 128$ experiments are needed.

In the current research, nine cutting tests were conducted according to the Taguchi's L9 orthogonal array by varying the cutting parameters (cutting speed (Vc), feed rate (f), cutting depth (ap) and cutting time (t_c)) in order to measure the investigated responses of the process. Table 3.3 lists the cutting process parameters and their considered levels.

Table 3.3. Assignment of levels to the cutting process parameters.

Process parameters	Level 1	Level 2	Level 3
Cutting speed (m/min)	250	320	390
Feed rate (mm/rev)	0.08	0.12	0.16
Cutting depth (mm)	0.1	0.2	0.3
Cutting time (min)	5	10	15

3.3. Results and discussion

The experimental results are provided in Table 3.4.

Table 3.4. Experimental results

Cutting speed (m/min)	Feed rate (mm/rev)	Cutting depth (mm)	Cutting time (min)	Ra (µm)	Fz (N)	VB (mm)	MRR (cm^3/min)
250	0.08	0.1	5	0.522	38.47	0.047	2.00
250	0.12	0.2	10	0.699	77.00	0.069	6.00
250	0.16	0.3	15	2.574	143.75	0.154	12.00
320	0.08	0.2	15	1.881	140.54	0.086	5.12
320	0.12	0.3	5	0.673	103.12	0.064	11.52
320	0.16	0.1	10	1.126	60.12	0.080	5.12
390	0.08	0.3	10	0.755	86.81	0.100	9.36
390	0.12	0.1	15	3.128	56.34	0.162	4.68
390	0.16	0.2	5	1.455	93.28	0.098	12.48

3.3.1 Analysis of variances (ANOVA) results

The outcomes of the ANOVA for VB, Fz, Ra and MRR were calculated, as described in Table 3.5, respectively. As far as the VB is concerned (Table 3.5 - a), it can be underlined that the cutting time is the most effective parameter affecting VB with 50.69%, followed by feed and cutting speed with 13.34% and 11.02%, respectively. The cutting depth has an ineffective effect on VB with 1.14%. Regarding Fz in Table 3.5 - b, it can be concluded that cutting depth is the most important factor affecting Fz with 50.84 %, followed by cutting time with 17.80%. Meanwhile, the feed and cutting speed have less signification effect on Fz with 1.56% and 0.80%, respectively.

Concerning Ra in Table 3.5 - c, it was found that the cutting time is the meaningfully factor affecting the Ra evolution with 58.97%, followed by feed and cutting speed with 9.61% and 5.75%, respectively. As expected, cutting depth does seem to have an insignificant effect on Ra variations with 1.44%. Further, the percentage contributions with respect to the cutting depth, feed, cutting speed and cutting time for MRR (Table 3.5 - d) were found to be: 93.64%, 24.65%, 6.09% and 2.53%, respectively.

Table 3.5. ANOVA for VB, Fz, Ra and MRR.

Source	DF	SS	MS	F	Cont. (%)
a) VB					
Cutting speed (m/min)	1	0.001350	0.001350	1.85	11.02
Feed (mm/rev)	1	0.001633	0.001633	2.24	13.34
Cutting depth (mm)	1	0.000140	0.000140	0.19	1.14
Cutting time (min)	1	0.006208	0.006208	8.81	50.69
Error	4	0.002916	0.000729		23.81
total	8	0.012248			100
b) Fz					
Cutting speed (m/min)	1	86.56	86.56	0.11	0.83
Feed (mm/rev)	1	163.59	163.59	0.22	1.56
Cutting depth (mm)	1	5325.26	5325.26	7.02	50.84
Cutting time (min)	1	1864.20	1864.20	2.46	17.80
Error	4	3034.54	758.64		28.97
total	8	10474.2			100
c) Ra					
Cutting speed (m/min)	1	0.39527	0.395277	0.95	5.75
Feed (mm/rev)	1	0.66002	0.66002	1.59	9.61
Cutting depth (mm)	1	0.09882	0.09882	0.24	1.44
Cutting time (min)	1	4.05082	4.05082	9.74	58.97
Error	4	1.66437	0.41609		24.23
total	8	6.86929			100
d) MRR					
Cutting speed (m/min)	1	7.085	7.0851	7.85	6.09
Feed (mm/rev)	1	28.689	28.6891	31.80	24.65
Cutting depth (mm)	1	74.061	74.0611	82.09	63.63
Cutting time (min)	1	2.940	2.9400	3.26	2.53
Error	4	3.609	0.90022		3.10
total	8	116.384			100

3.3.2 Effect of process parameters on VB

After each cutting test, the cermet insert was removed, and its primary flank wear was measured. Accordingly, the flank wear appears as a brightening band striated on the cutting insert edges during all cutting tests as observed in Fig.3.10. It can be clearly mentioned that, this appearance was observed for all used process parameters. Results outlined in Figure 3.11, clarify that as cutting time and cutting speed increases as well from 5 min to 15 min for 250 m/min to 390 m/min, respectively, the correspondingly VB values increases. This increase in VB values can be explained by the expansion of tool-workpiece contact zone and by the effect of the relative sliding speed between cutting tool and cut material causing an increase in the tool/material interface temperature. The effects of vibration can also yield to an increase in VB, especially at cutting speeds above 390 m/min, where the maximum value of VB is reached (test number 8). Same explanation was also stated by Nicolodi et al [3.48]. Low VB value was observed in test 4. Probably, this can be attributed to the presence of BUE on the tool edge at cutting speed 320 m/min. As an impact of that, the BUE can have beneficial effect in term of protecting the tool edge. Indeed, this can reduce flank wear progression as it was outlined by Seid Ahmed et al [3.49].

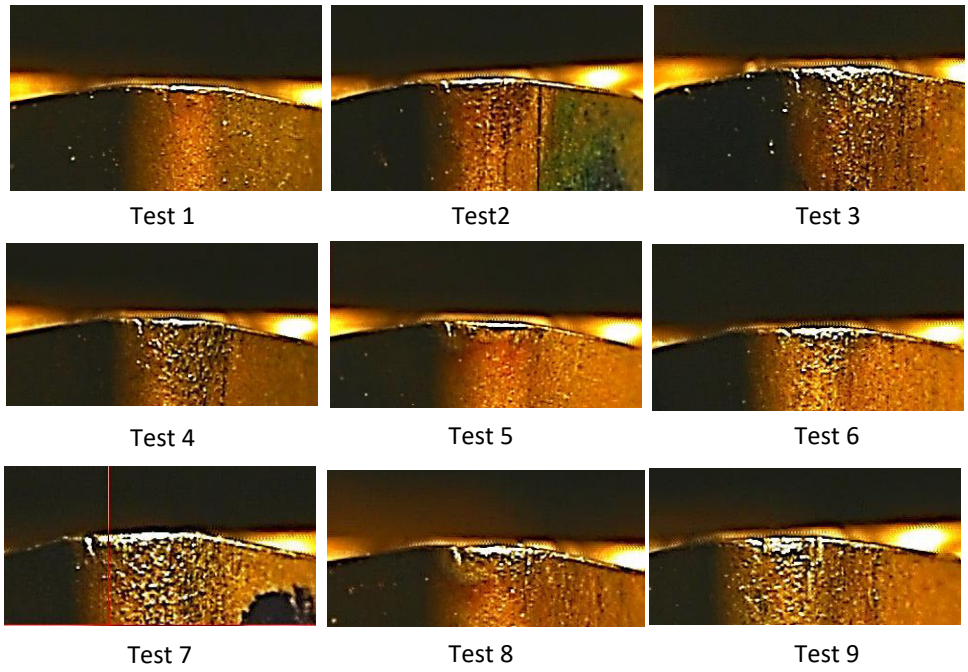

Figure 3.10. Visualization of the flank wear on the cutting edges at the end of machining.

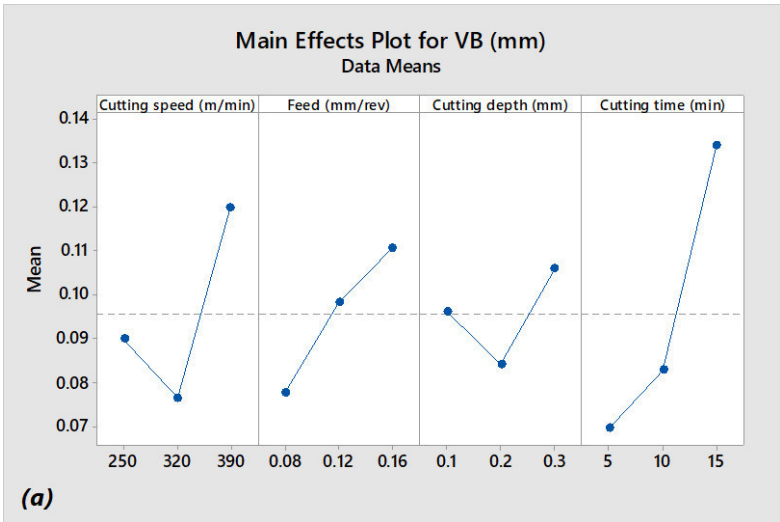

Figure 3.11. Main effects plot for VB

3.3.3 Effect of process parameters on Fz

The effect of the variation of the cutting parameters (Vc, f, ap and tc) on the Fz evolution is displayed in Fig. 3.12. In the latter, it can be seen that the Fz values increase correspondingly as cutting depth increases as well for the nine cutting tests. In addition, the Fz was achieved with highest values (about 144 N and 140 N) at cutting tests 3 and 4, respectively, when holding third and fourth parameters at ap = 0.2 mm, ap = 0.3 mm and tc= 15 min. These parameters are the most predominant ones affecting Fz variations. This can be caused by the presence of soft ferrite phase during the machining of AISI 316L inducing a long zone at the tool-chip contact on the rake face. Consequently, the friction forces increase [3.50]. Here also, stick-slip behavior can occur at tool-workpiece interface [3.51]. The band width at the flank surface increases causing a rising of the tangential cutting force (Fz) [3.50, 3.2].

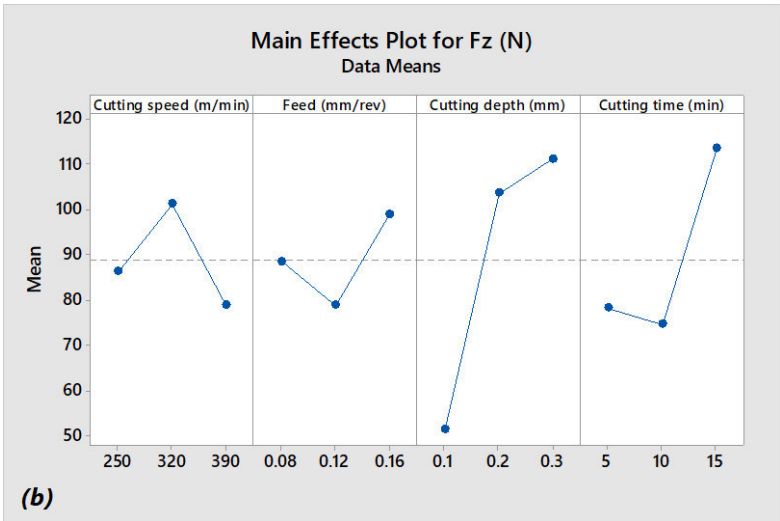

Figure 3.12. Main effects plot for Fz.

3.3.4 Effect of process parameters on Ra

Figure 3.13 indicates the evolution of average surface roughness values (Ra) as a function of cutting parameters (Vc, f, ap and tc). As observed in Table 3.4 , the Ra is obtained with highest values (3.12 µm and 2.57 µm) at cutting tests 8 and 3, respectively. It can be observed from Fig 3.13 that higher cutting time (tc = 15 min) is the most significant parameter affecting the Ra variations. Moreover, it can be underlined that the higher are cutting time and feed, the higher is tool vibration. Consequently, the arithmetic roughness value Ra of the generated surface by cutting increases. Also, for the same cutting tests 8 and 3, width of band (VB) at flank surface increases and is about 0.162 mm and 0.154 mm, respectively. This increase causes deterioration of generated surface finish of the workpiece. This interpretation was also reported by Ciftci [3.52].

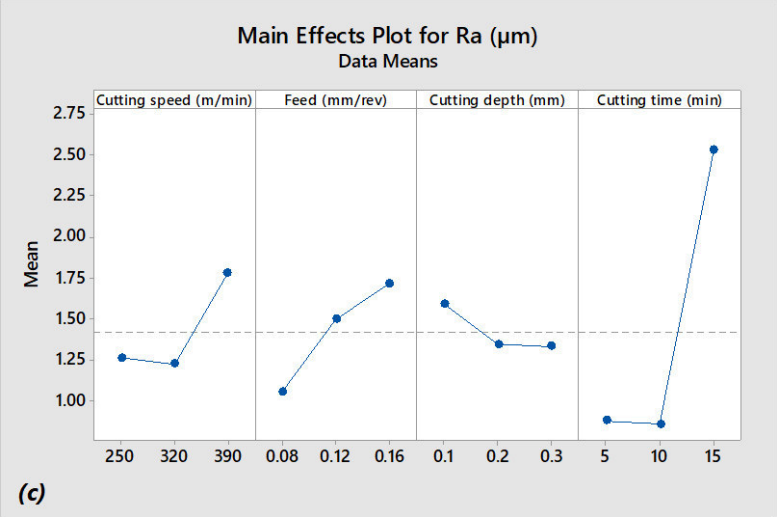

Figure 3.13. Main effects plot for Ra.

3.3.5 Effect of process parameters on MRR

Figure 3.14 illustrates the impact of the cutting parameters (Vc, f, ap and tc) on the material removal rate (MRR). As shown in this figure, the MRR is obtained with highest values (12.48 cm^3/min and 12 cm^3/min), especially at cutting tests 9 and 3, respectively. It can be underlined that higher cutting depth and feed values (ap = 0.3 mm and f = 0.16 mm/rev.)) are the most significant parameters inducing higher MRR. This is due to the fact that tool deeper penetration in the workpiece, induces increase in chip section, which induce an increase in the removed chip volume (equation (3.10)).

$$MRR = Vc * f * ap \tag{3.10}$$

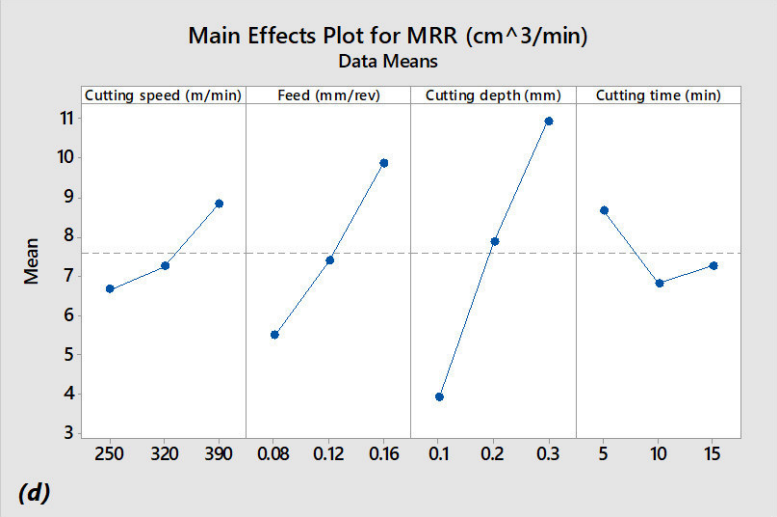

Figure 3.14. Main effects plot for MRR.

3.3.6. Single-objective Optimization of cutting parameters based on Taguchi approach

In the present study, since low VB, Fz and Ra and high MRR were desirable, the equation (3.1) and equation (3.2) was preferred, respectively. The mean of S/N ratios of the VB, Fz, Ra and MMR for the nine cutting tests are given in table 3.6 and the main effect plots for S/N ratios of the VB, Fz, Ra and MMR are displayed in Figure 3.15. The achieved optimum parameter settings for VB, Fz, Ra and MRR are provided in Table 3.7.

Table 3.6. Response of S/N ratios for VB, Fz, Ra and MRR.

Output responses	Cutting parameters	S/N ratios (dB)		
		Level 1	Level 2	Level 3
VB	Vc (m/min)	22.01	**22.37**	18.66
	f (mm/rev)	**22.62**	20.97	19.45
	ap (mm)	21.44	**21.57**	20.04
	tc (min)	**23.54**	21.72	17.79
Fz	Vc (m/min)	**-37.53**	-39.60	-37.73
	f (mm/rev)	-37.81	**-37.67**	-39.38
	ap (mm)	**-34.10**	-40.03	-40.73
	tc (min)	**-37.12**	-37.36	-40.37
Ra	Vc (m/min)	**0.2348**	-0.9963	-3.5372
	f (mm/rev)	**0.8985**	-1.0605	-4.1368
	ap (mm)	-1.7292	-1.8292	**-0.7405**
	tc (min)	**1.9770**	1.5791	-7.8550
MRR	Vc (m/min)	14.39	16.53	**18.25**
	f (mm/rev)	13.21	16.73	**19.23**
	ap (mm)	11.20	17.22	**20.75**
	tc (min)	**16.39**	16.39	16.39

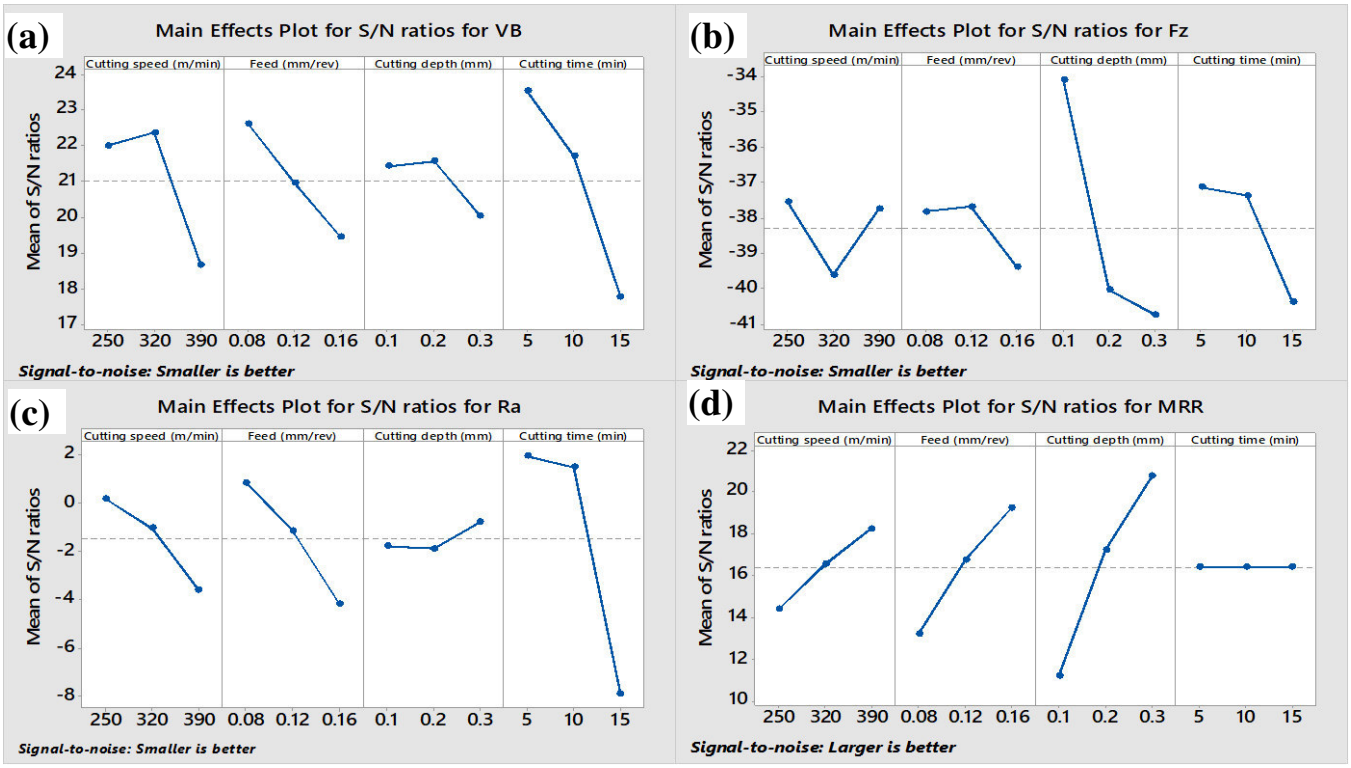

Figure 3.15. Main effects plot for the S/N ratios of the VB, Fz, Ra and MRR.

Table 3.7. Optimum parameters setting

Output responses	Optimum parameters setting
VB	Vc= 320 m/min, f= 0.08 mm/rev, ap = 0.2 mm and tc = 5 min
Fz	Vc= 250 m/min, f= 0.12 mm/rev, ap = 0.1 mm and tc = 5 min
Ra	Vc= 250 m/min, f= 0.08 mm/rev, ap = 0.3 mm and tc = 5 min
MRR	Vc= 390 m/min, f= 0.16 mm/rev, ap = 0.3 mm and tc = 5 min

3.3.7. Multi-objective Optimization of cutting parameters based on TOPSIS approach

It is underlined here that, the main aim is to identify optimal cutting parameters yielding to minimizing VB, Fz and Ra and maximizing MRR. To attain this objective, TOPSIS approach has been chosen for converting multi-attribute problems into a single-attribute. The TOPSIS approach is considered as a suitable multi–criteria decision making (MCDM) method for selecting optimal parameters in machining processes. This approach has gained popularity thanks to its ease to be implemented and executed during simple computational steps [3.17, 3.53]. According to Yurdakul et al [3.54], the included steps in TOPSIS approach are described as follows:

Step 1: Constructed a decision matrix using all experimental data representing m alternative solutions and n criteria. In this case, the cutting tests are the alternative solutions and the output responses are the criteria.

$$Z_m = \begin{bmatrix} x_{11} & x_{12} \dots & x_{1n} \\ \vdots & \vdots & \vdots \\ x_{m1} & x_{m2} & x_{mn} \end{bmatrix} \tag{3.11}$$

where x_{ij} is the measure performance of j^{th}attribute to the i^{th}alternative.

Step 2: Obtaining a normalized design matrix through following formula

$$Q_{ij} = \frac{x_{ij}}{\sqrt{\sum_{i=1}^{m} x_i^2}} \quad , i = 1, 2\dots\dots, m, j= 1,2, \dots\dots, n \tag{3.12}$$

where Q_{ij} is the normalized value of x_{ij}.

Step 3: Once a normalized design matrix is established, the weights of the normalized decision matrix (B_{ij} ; i = 1, 2……, m, j= 1,2, ……., n) are computed through equation (3.13).

$$B_{ij} = w_j \text{ X } Q_{ij}, \tag{3.13}$$

where w_j is denotes the weight of the measure performance, $\sum_{j=1}^{n} w_j = 1$

In this study, the weighted normalized values were taken to equals 0.25 for the fourth output responses (VB, Fz, Ra and MRR).

Step 4: Calculate the positive ideal solution and the negative ideal solution using the following equations (3.14) and (3.15):

$$B^+ = \{B_1^+, B_2^+, \ldots\ldots\ldots, B_n^+\} = \left\{(max B_{ij} | j \in K_1), (\min B_{ij} | j \in K_2, i = 1,2, \ldots n)\right\} \tag{3.14}$$

$$B^- = \{B_1^-, B_2^-, \ldots\ldots\ldots, B_n^-\} = \left\{(min\ B_{ij} | j \in K_1), (max\ B_{ij} | j \in K_2, i = 1,2, \ldots n)\right\} \tag{3.15}$$

where $B^+$and B^- are defined as the positive ideal solution and negative ideal solution, respectively, and $K_1$and K_2 are indices set for positive response and negative response, respectively.

Step 5: Calculate the distance of every alternative from positive and negative ideal solutions using Eqs. (3.16) and (3.17)

$$S_i^+ = \sqrt{\sum_{j=1}^{n} (B_{ij} - B^+)^2} \quad , \quad i= 1, 2, \ldots\ldots\ldots m \tag{3.16}$$

$$S_i^- = \sqrt{\sum_{j=1}^{n} (B_{ij} - B^-)^2} \quad , i= 1, 2, \ldots\ldots\ldots m \tag{3.17}$$

where $S_i^+$and S_i^- are denote as the positive and the negative ideal solutions, respectively.

Step 6: Compute the relative closeness coefficient for individual ideal solution using Eq. (3.18)

$$C_i = \frac{S_i^-}{S_i^+ + S_i^-}, \quad 0 \leq C_i \leq 1 \tag{3.18}$$

Step 7: Arrange a set of every alternatives from the higher to the lowest, according to the decreasing values of C_i. A higher value of C_i corresponds the most preferred.

The Table 3.8 listed the TOPSIS outcomes including weighted normalized values, the distances, closeness coefficient and arrange for each alternative are calculated through Eqs 3.11-3.18. It is found that the cutting test number 5 has highest C_i of 0.7489. Consequently, it is considered as the best alternative.

Table 3.8. TOPSIS outcomes.

Exp. No	Weighted normalized values				S_i^+	S_i^-	C_i	Arrange
	B_{VB}	B_{Fz}	B_{Ra}	B_{MRR}				
1	0.15295	0.13476	0.10415	0.07940	0.104	1.1848	0.6398	5
2	0.22454	0.26974	0.13947	0.23821	0.0753	0.15936	0.679	3
3	0.50115	0.50358	0.51367	0.47643	0.163	0.10323	0.3877	8
4	0.27986	0.49233	0.37532	0.20327	0.1376	0.09305	0.4034	7
5	0.20827	0.36124	0.13428	0.45737	0.0595	0.17761	**0.7489**	**1**
6	0.26034	0.21061	0.22467	0.20327	0.0856	0.14403	0.6273	6
7	0.32542	0.30411	0.15064	0.37161	0.0689	0.15613	0.6939	2
8	0.52719	0.19736	0.62407	0.18580	0.1786	0.08104	0.3122	9
9	0.31891	0.32677	0.29032	0.49548	0.0787	0.14982	0.6556	4

Further, from Figure 3.16, representing the main effect plot of C_i, it can be visualized that cutting parameters (cutting speed of 320 m/min, feed of 0.12 mm/rev, depth of cut of 0.3 mm and cutting time of 5 min) are attained as optimal turning cutting parameters to achieve minimum value of VB, Fz, Ra and maximum value of MRR.

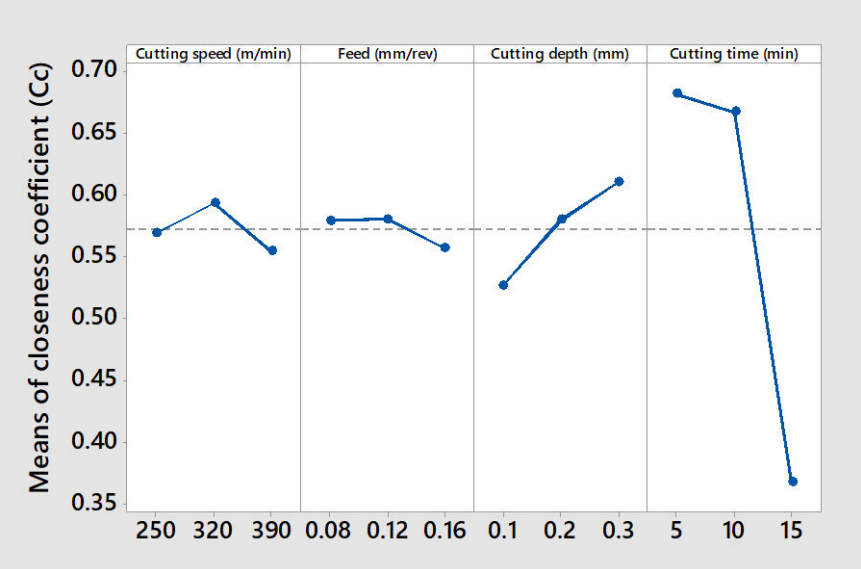

Figure 3.16. Main effect plot of Closeness coefficient.

According to ANOVA approach (Table 3.9), the cutting time indicates higher contribution (73.01%) among the selected process parameters. It is the most effective parameter influencing the performance characteristics of turning process of AISI 316L.

Table 3.9. ANOVA for TOPSIS.

Source	DF	SS	MS	F	Cont. (%)
Cutting speed (m/min)	1	0.000335	0.000335	0.03	0.17
Feed (mm/rev)	1	0.000737	0.000737	0.07	0.36
Cutting depth (mm)	1	0.010517	0.010517	0.98	5.20
Cutting time (min)	1	0.147580	0.147580	13.74	73.01
Error	4	0.042966	0.010741		21.36
total	8	0.202135			100

Figure 3.17 shows chip morphologies produced in trails number 2, 5 and 8. In test number 5, chip has helical segment geometry and it is broken at regular distances forming a discontinuous chip. According to Klocke [3.55], this kind of chip is classified as acceptable one. On the contrary, the flat helical chip and snarled chip were produced during cutting tests 2 and 8 which are specified as unacceptable chip forms.

Test 2

Test 5

Test 8

Figure 3.17. Chip morphologies produced during cutting tests 2,5 and 8.

3.4. Conclusion

This chapter deals with the machinability of AISI 316L ASS using the PVD cermet tool. The latter was cut under varying parameters including cutting speed, feed, cutting depth and cutting time. In the present research work, the concept of the machinability concerns the study of evolutions of flank wear, tangential cutting force, surface roughness and material removal rate. According to ANOVA approach, flank wear was affected mainly by the cutting time. Variations of tangential cutting force and surface roughness are impacted by the cutting depth and feed with a contribution of 50.84 % and 58.97 %, respectively. Also, the cutting depth was the most dominant parameter influencing material removal rate (MRR) followed, in order, by feed and cutting speed. To find optimal cutting parameters, the Taguchi method was used. Also, to ensure the minimizations of VB, Fz, Ra and maximization of MRR, a signal to noise ratio was exploited. It can be underlined that for VB, optimal cutting conditions are (Vc= 320 m/min, f= 0.08 mm/rev, ap= 0.2 mm and tc= 5 min). For Fz, optimal cutting condition are (Vc= 250 m/min, f= 0.12 mm/rev, ap= 0.1 mm and tc= of 5 min). For Ra, optimal cutting condition are (Vc= 250 m/min, f= 0.08 mm/rev, ap= 0.3 mm and tc= 5 min). Whereas, for MRR, optimal cutting conditions are (Vc= 390 m/min, f= 0.16 mm/rev, ap= 0.3 mm and tc= 5 min).

In addition, the TOPSIS approach for multi-criteria optimization was applied in this research. It is important to note that the test number 5 *(Vc= 320 m/min, f= 0.12 mm/rev, ap= 0.3 mm and tc= 5 min)* provides an optimal solution for achieving low value of flank wear (VB= 0.064 mm), tangential cutting force (Fz =103.12 N) and surface roughness (Ra = 0.67 µm) with high value of material removal rate (MRR = 11.52 cm^3/min), simultaneously.

Finally, the TOPSIS optimization approach is an effective and efficient approach and certainly understandable to convert the problems having multiple responses into a single response.

Chapter 4: Evaluation of MQL Performances using Various Nanofluids in Turning of AISI 304 Stainless Steel

4.1. Introduction

Machining of AISI 304 (ASS), which is extensively employed in various industrial applications, is well-known as very challenging due to its low thermal conductivity and work hardening tendency. High cutting forces, high temperature generation at the cutting zone and rapidly progress in tool wear are the common problems encountered during its machining. These difficulties can have a negative impact on the cost and surface integrity of the machined part. Therefore, delivering the cutting fluids into the cutting area while machining of such materials is one of the effective methods proven by researchers to figure out the above-mentioned issues, thereby increasing cutting performance [4.1]. The critical roles of these cutting fluids are to reduce the cutting forces and cutting temperatures, and also to transport out the chip from the cutting region as well as to increase the cutting tool's life [4.2]. Due to these roles, the cutting fluids have been frequently and excessively used. Even though this employment of cutting fluids by conventional wet lubricating strategy improved the overall machining productivity, it has adversely affected both the environment and the operator's health due to their petroleum-based nature, applying ample amount, being toxic etc. In addition, the lubricant can also be contaminated, not only causing environment and health concerns, but also decreasing machining efficiency by making fluids lose their characteristics [4.3].

Proceeding from that, dry cutting, MQL and nanofluids assisted MQL have been applied in the metal working industry as alternative techniques to replace wet lubricating applications. Consequently, mitigating environmental issues, health concerns, and production costs. Excluding the use of lubricant, the dry cutting concept, which has received attention from research community in the past, can be used. However, it has its own machining limitations such as excessive tool wear, heat dissipation and poor surface integrity, especially in the case of hard-to-cut materials [4.4]. These drawbacks led the researchers to explore another conscious strategy known as MQL in the recent past. The MQL strategy involves using a minimum quantity of lubricant (oil) in principle. In this process, an optimal amount of cutting fluid (usually at a flow rate that varies between 10-500 ml/h) associated with compressed air is pulverized as micro-droplets to the cutting

zone. Numerous published studies have shown that the MQL mode produces better *Fc*, *T*, *Ra* and *VB* results than wet and dry conditions [4.5-4.8]. In literature, Li and Lin [4.9] used the MQL approach in micro-grinding operation and they concluded that this approach provided an improvement in *Ra* and reduction in *Fc*. Similarly, an enhancement by 15% in the matter of *Ra* and *Fc* was reported by Singh et al. [4.10] in turning of hard-to-cut material under MQL technique. Bedi et al. [4.11] studied the impact of cutting speed on *Ra* and *Fc* when turning AISI 304 under dry and MQL conditions and they found that MQL provided better Ra and lower *Fc* than dry turning. Rajaguru and Arunachalam [4.12] have investigated the machining of super duplex stainless steel under different coolant environments to improve its machinability. Turning experiments were performed under dry, flood and MQL conditions to enhance the machinability in respect of *Fc* and *Ra*. Findings have indicated that the MQL method outperformed other conditions. Also, Uysal [4.13,4.14] investigated the milling of AISI 430 under MQL at flow rates of 20 ml/h and 40 ml/h from the perspective of cutting temperature and flank wear. The outcomes showed that MQL at a flow rate of 40 ml/h delivered acceptable results in comparison to MQL at a flow rate of 20 ml/h.

The application of the MQL approach in machining operations exhibited various benefits such as limited harmful effects on the environment caused by the abundant use of the conventional cutting fluid, less production cost, increased workers' safety [4.15]. Nevertheless, it has its own restrictions related to the mediocre cooling function because of the incapability of the lesser oil flow rate to fully limit heat generation at both primary and secondary machining regions in the cutting of hard-to-machine materials [4.16]. Therefore, there appears to be a need to improve the cutting performance of the MQL process. In this way, the applications of nanofluids assisted MQL [4.17,4.18] and hybrid nanofluids assisted MQL [4.19] have recently become important research trends in order to enhance MQL efficiency. Researchers have tried various nano particles with lubricating properties such as Al_2O_3 (Aluminum Oxide), MoS_2 (Molybdenum Disulphide), CuO (Copper oxide), Fe_2O_3 (Iron oxide) and MWCNT (Multi-walled Carbon Nanotube) [4.20-4.22]. Das et al. [4.21] carried out the hard turning experiments of HSLA steel using three different nanofluids (AL_2O_3, CuO, and Fe_2O_3) and compared the results with regard to the *Fc* and *Ra*. Based on the experimental results, it was concluded that CuO reinforced

nanofluid performed better than other nanofluids. Öndin et al. [4.22] evaluated the performance of MWCNT particles enriched vegetable cutting fluid in straight turning of PH 13-8 Mo stainless steel and obtained that MQL and MWCNT assisted nanofluid MQL reduced the surface roughness by 5% and 12%, respectively, in comparison with dry cutting. Uysal et al. [4.23] added 1% nano MoS_2 particles to the vegetable cutting fluid in milling of AISI 304 steel. The authors noticed an amelioration in surface roughness compared to MQL and dry environments. Patole and Kulkarni [4.24] analyzed the machinability characteristics including cutting force and surface roughness of AISI 4340 under MWCNT assisted nanofluid MQL. They observed that the nanofluid assisted MQL method yielded an improved surface roughness than conventional cooling. Singh et al. [4.25] used nano graphene reinforced vegetable oil in nanofluid assisted MQL machining in order to ameliorate the machinability regarding tool life, cutting forces and cutting temperature. Findings have underlined a maximum of a 190% improvement in tool life, 40% reduction in cutting forces and 42% reduction in cutting temperature when compared to dry cutting. However, the use of hybrid nanofluids is still a relatively new research trend, with only a small number of studies conducted to investigate their performance. For instance, Sharma et al. [4.26] studied the influence of nano Al_2O_3 particles reinforced nanofluid and nano Al_2O_3/MWCNT reinforced hybrid nanofluid on *Fc* and *Ra* during straight turning of AISI 304. The research showed that the potential of hybrid nanofluid was notably better than nanofluid. Jamil et al. [4.19] have claimed that the application of hybrid nanofluid (Al_2O_3/MWCNT) underscored an 8.72% reduction in *Ra*, 11.8% reduction in *Fc* and 23% enhancement in tool life. Gugulothu and Pasam [4.27] reported the reduction in *T*, *Ra*, *Fc* and *VB* in turning of AISI 1045 steel using 2 wt.% concentration of MWCNT/MoS_2 reinforced hybrid nanofluid assisted MQL condition compared to 0.5, 1, 1.5, 2.5 and 3 wt.% concentrations.

Based on previous studies, the usage of nanofluids in the MQL method improved its machining performance. However, the preformed researches especially on machining of AISI 304 (ASS) under hybrid nanofluid assisted MQL are relatively seldom. Actually, no published research has been found in literature that assessed and compared the effects of dispersed nano graphene, nano MoS_2 and MWCNT particles and their hybrids such as nano graphene/MoS_2 and MWCNT/MoS_2 enriched MQL into the vegetable cutting fluid

on different machining responses. Therefore, with this objective, an attempt was made in this study to improve the machining characteristics performance with respective of surface roughness (*Ra*), main cutting force (*Fc*), cutting temperature (*T*) and flank wear (*VB*) by adding MWCNT, nano MoS_2, nano graphene particles and their hybrids (MWCNT/MoS_2 and nano graphene/MoS_2) to the vegetable cutting fluid in straight turning of AISI 304 (ASS). Ultimately, to explicate the experimental findings from different aspects, statistical analysis, regression modeling and multi-criteria optimization were performed.

4.2. Experimentation and Methodology

This section outlines a brief description of the nanofluids' preparation, workpiece material, cutting tool, CNC machine tool and lubricating environments used in this experimental work as well as machining characteristics measurements.

4.2.1. Minimum Quantity Lubrication (MQL)

4.2.1.1. MQL strategy

Minimum quantity of lubricant (MQL) (also known as near/dry machining (NDM)) has recently been an option as compared to conventional wet cooling strategies that use bulk amounts of fluids. The MQL system contains a compressor, fluid reservoir, the fluid supplying pump, air-oil mixing chamber, nozzle, and external pipes for air and oil supply. The MQL strategy involves using minimum quantity of lubricant (oil) in principle. In this process, an optimal amount of cutting fluid, usually at a flow rate vary between 10-500 ml/h instead of the 50-1000 l/h in the case of flood cooling strategy, associated with compressed air, as pure MQL (without the addition of nanoparticles), that is directly pulverized as micro-droplets to the cutting zone.

The pulverizing of aerosol (mixture of highly compressed air with the typical pressure of 4-6 bar and cutting fluid) to the cutting zone can be done in two ways:

- External: the aerosol is penetrated in this case through external nozzle into the cutting area.
- Internal or through the tool: the aerosol is transported via tunnels inside the cutting tool.

4.2.1.2. Advantage of MQL method

Minimum quantity lubrication method is emerging as viable alternative to conventional wet cooling due to its several advantage, which can be summarized as below:

- It consumes quite lower amount of cutting fluid, thereby making the process almost clean and dry and also resulting in a significant cost reduction.
- As per minimal amount of cutting fluid (mostly vegetable oil), less vaporization takes place, which is more environmentally friendly and less harmful for employee health sensitivity.
- As the process involves precisely controlled flow of compressed air, it helps small droplets of aerosol to penetrate into the cutting zone easily.
- The mixture of highly pressurized air and cutting fluid easily transports out the forming chip effectively, thereby making the chip handling task much easier.
- The machining processes which concerns with MQL is more productive with increased tool life and better surface finish of workpiece.

4.2.1.3. Nanofluid based MQL

Applying the nanofluid assisted MQL has newly become the center of interest for many researchers in order to enhance the MQL performance.

A nanofluid (alternatively nano-lubricant) is a new fluid formed by the dispersion of ultrafine nanoparticles (non-metallic/metallic) with a size of between 1-100 nm into the base fluid. This formed fluid is atomized in the MQL device with the use of compressed air. By this action, a fine cool mist is created which is able to successfully penetrate into the tool-workpiece interface region, forming a tribofilm (Figure 4.1). This tribofilm provides a vital role in diminishing the produced machining heat, as well as reducing the coefficient of friction at the contact area.

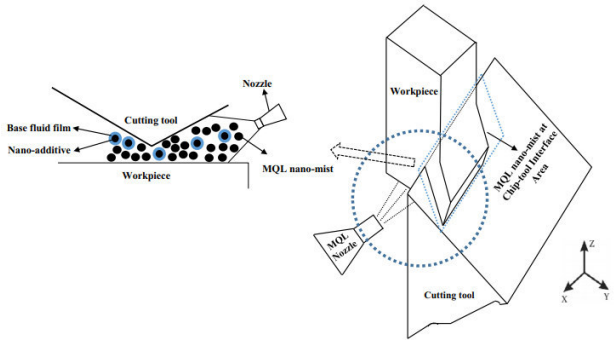

Figure 4.1. The MQL-nanofluid mechanism schematic [4.20].

Some typical types of nanofluids which have wide application nowadays are MoS_2 based nanofluid, MWCNT based nanofluid, graphene based nanofluid, Al_2O_3 based nanofluid, etc.

This recently introduced category of cooling/lubricating strategy has shown fascinating behavior during experiments in terms of increased thermal conductivity and augmented heat transfer coefficient compared to a pure liquid, as demonstrated visually in Figure 4.2

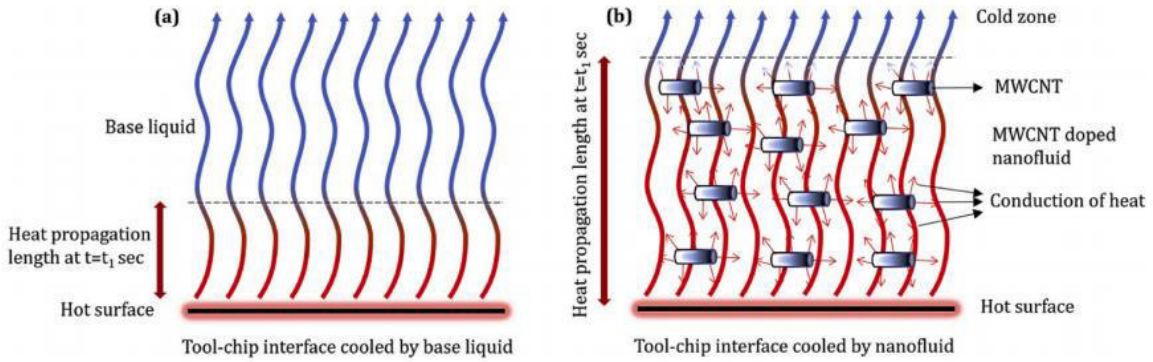

Figure 4.2. Heat dissipation mechanism through a) base liquid b) MWCNTs based nanofluid [4.22]

In addition, hybrid nanofluids are a relatively recent class of cooling/lubricating strategy which have been prepared by combining more than one kind of nano-lubricant into the main liquid in equal or varying proportions.

Moreover, compared to conventional coolants, nanofluids possess the following advantages [4.28-4.30]:

- High specific surface area and therefore more heat transfer surface between particles and fluids.
- High dispersion stability with predominant Brownian motion of particles.
- More advanced lubrication mechanisms viz., mending effect that fills and repairs the grooves (Fig 4.3 (a)), protective film effect forming a protective layer on the surface (Fig 4.3. (b)), third-body effect exhibiting load bearing (Fig 4.3 (c)), rolling-sliding effect reducing friction and wear (Fig 4.3 (d)) and polishing effect removing debris on the machined surface (Fig 4.3 (e)),
- Ability to significantly reduce the friction and wear, thus improving the tribological characteristics of the lubricants.

- Adjustable properties, including thermal conductivity and surface wettability, by varying particle concentrations to suit different applications.

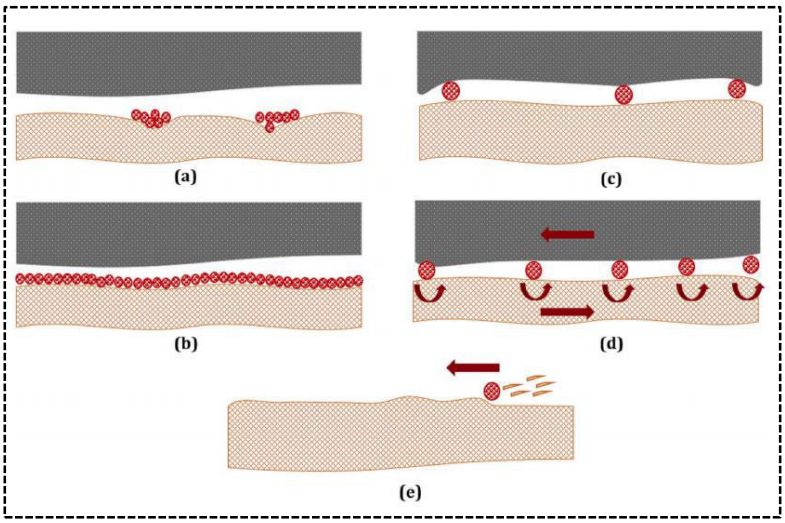

Figure 4.3. Functions on nanoparticles between contacting surfaces a) mending effect b) protective film effect c) third body effect d) rolling/ sliding effect e) polishing effect [4.22].

4.2.1.4. Summary of Nanofluid-MQL's Mechanism

Understanding the nano-fluid MQL mechanism is highly critical for gaining more improvements in cutting performance. The MQL nano-fluid mechanism can be summarized as follows (Figure 4.1):

- Using a compressed air stream, the aerosol is atomized through the MQL nozzle, resulting in a very fine cool mist.
- Thus, the droplets of the nano-cutting fluid are produced on the workpiece and cutting tool surfaces, as well as a tribofilm, which greatly improves the tribological properties and decreases the induced friction.
- As the concentration of nano-lubricants increases, so does the number of nano-lubricants at the tool-workpiece interface, these nano-lubricants serve as spacers, limiting the contact between the tool and workpiece.
- As the concentration of nano-lubricants increases with high compression, the nano-lubricants shape changes and shearing becomes more extreme.

- As a result of the high pressure in the fluid-MQL and the existence of a void at tool-workpiece interface, nano-lubricants offer high contact resistance assisting in the formation of a chemical reaction film on the workpiece surface. The thickness of this thin protective film on the manufactured surface increases as the concentration of nano-lubricants increases.

4.2.2. Preparation nanofluids

In order to formulate a nanofluid, there are at least two key ingredients that should be incorporated. These ingredients are cutting fluid and nano additive (s). Indeed, this present work involved the use of a commercial vegetable based oil as the cutting fluid and three types of commercially available nano particles. These particles are nano Molybdenum disulfide (MoS_2), Multi-walled Carbon Nanotubes (MWCNT) and nano graphene. The technical properties of the nano particles are listed in Table 1. The nano particles were dried in a drying oven at 120°C for 2 hours and then the 0.1 wt.% of these particles were blended into the vegetable cutting fluid. For proper blending of nano particles with vegetable cutting fluid, Daihan WiseTis HG-15D digital homogenizer was employed at 5000 rpm for 1 hour. Similarly, the hybrid nanofluids were also produced by mixing both nano MoS_2 and MWCNT particles at 0.05 wt.% for each and nano MoS_2 and nano graphene particles at 0.05 wt.% for each with the vegetable cutting fluid. For producing a stable mixture, Sodium Dodecyl Sulfate was added for carbon based nano particles and lecithin was added for nano MoS_2 particles in the preparation process. In the end, the five sets of prepared nanofluids were pulverized through the MQL system.

Table 4.1: Technical properties and specifications of nano particles

Properties	**Nano MoS_2**	**MWCNT**	**Nano Graphene**
Color	Grey	Black	Grey
Purity (%)	99.9	99	99
Thermal conductivity (W/mK)	35	~ 3000-5000	~ 3000-5000
Surface area (m^2/g)	120	275	120-150
Density (g/cm^3)	4.8	2.1	2
Thermal expansion (4-6 m/m/dg-K)	/	106	106
Young's modulus (GPa)	/	910	1000
Tensile Strength (GPa)	/	10-60	10-20
Thickness	/	/	5-8 nanometers
Diameter	/	9.5 nanometers	5-10 micrometers
Length	/	1.5 micrometers	/
Dimensions	10-20 nanometers	/	/

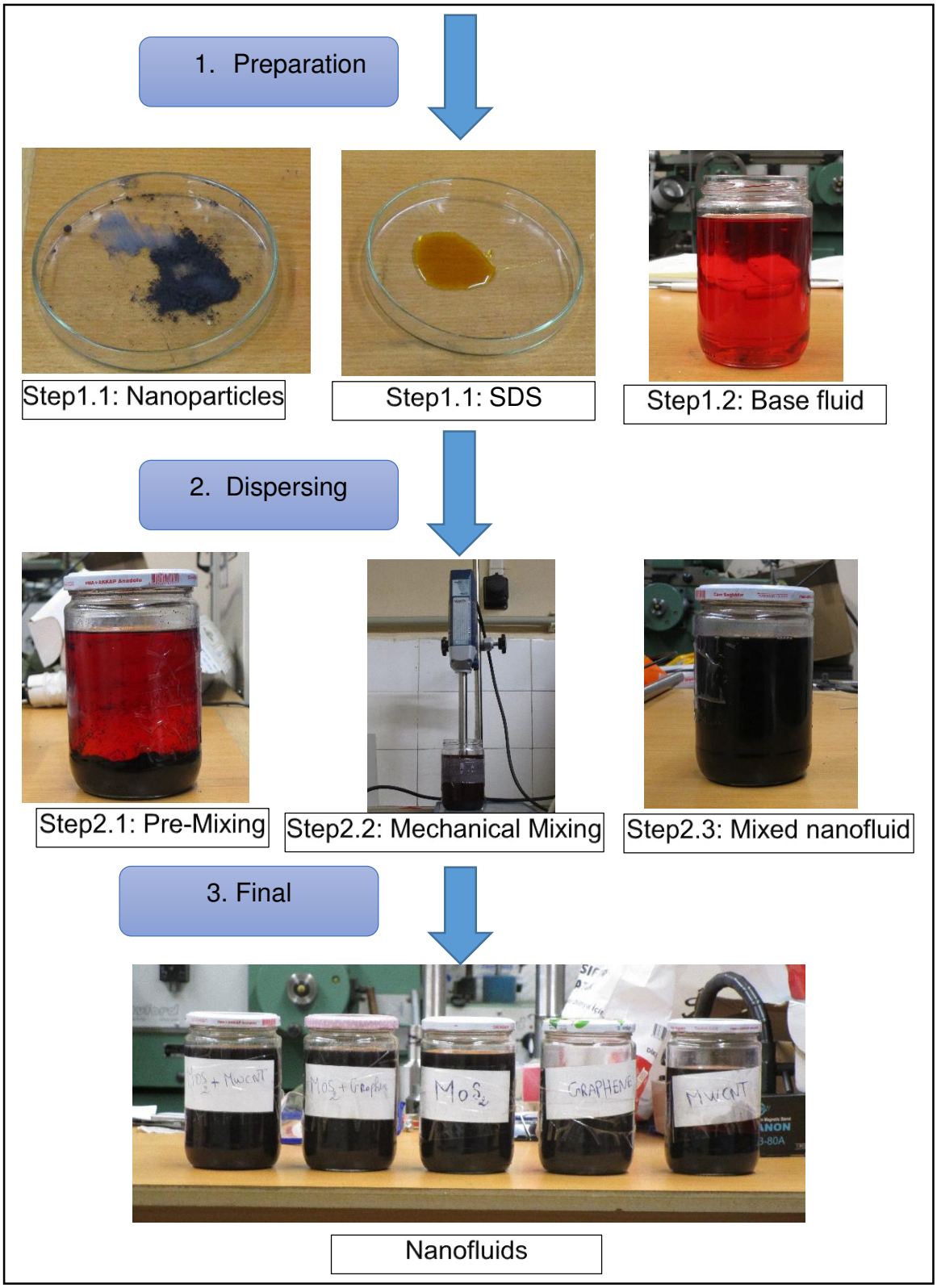

Figure 4.4. A double-step method for nanofluids preparing.

4.2.3. Workpiece material, cutting tool and CNC machine tool

AISI 304 austenitic stainless steels having a diameter of 70 mm and a length of 300 mm were selected as workpiece material to ascertain the machinability indices in turning trials. Its corresponding chemical composition and mechanical properties are presented in Table 2. Turning tests were carried out by using a CNC lathe having a maximum spindle speed of 4200 rpm. In the experimental studies, Sandvik brand Ti (C, N)/Al_2O_3/TiN coated TNMG 160408-MM 2025 Tungsten Carbide (WC) cutting tools and MTJNL 2525M 16M1 tool holder were used. The experimental set-up is shown in Figure 1.

Table 4.2: Chemical composition and mechanical properties of AISI 304

<table>
<tr><td colspan="7">Chemical composition of AISI 304</td></tr>
<tr><td>C (%)</td><td>Si (%)</td><td>Mn (%)</td><td>P (%)</td><td>S (%)</td><td>Ni (%)</td><td>Cr (%)</td></tr>
<tr><td>0.071</td><td>0.39</td><td>1.31</td><td>0.036</td><td>0.022</td><td>8.02</td><td>18.16</td></tr>
<tr><td colspan="7">Mechanical properties of AISI 304</td></tr>
<tr><td colspan="3">Ultimate Tensile Strength (N/mm^2)</td><td>636</td><td colspan="2">Elongation (%)</td><td>68</td></tr>
<tr><td colspan="3">Yield Strength (N/mm^2)</td><td>456</td><td colspan="2" rowspan="2">Reduction of area (%)</td><td rowspan="2">75</td></tr>
<tr><td colspan="3">Hardness (HB)</td><td>175</td></tr>
</table>

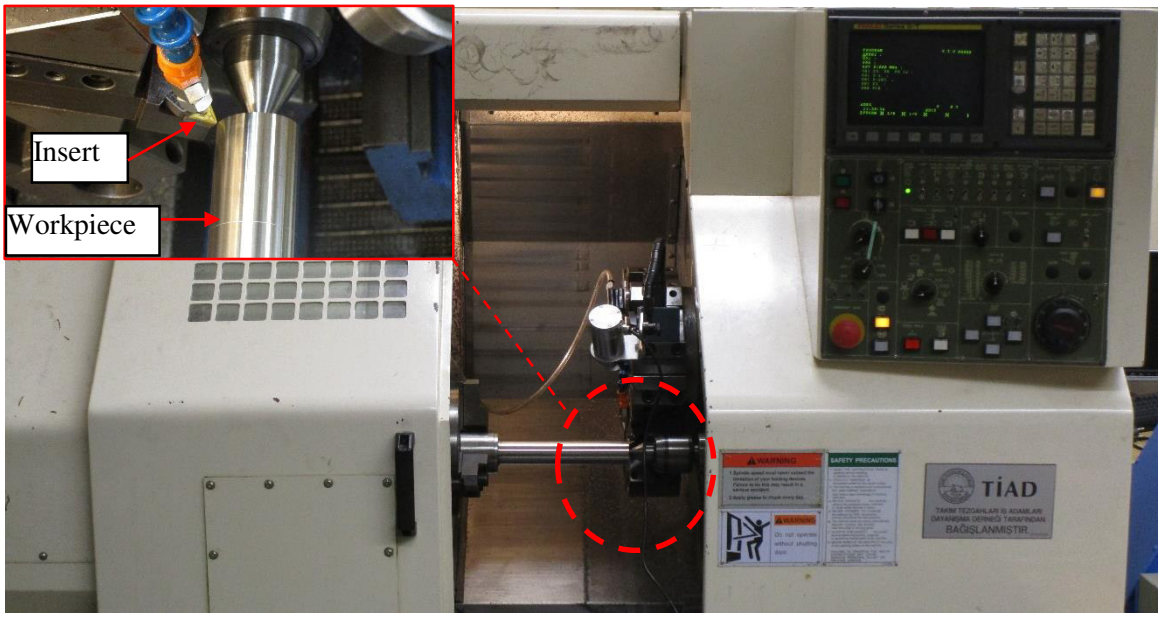

Figure. 4.5. Illustration of CNC machine, workpiece and insert used in this work.

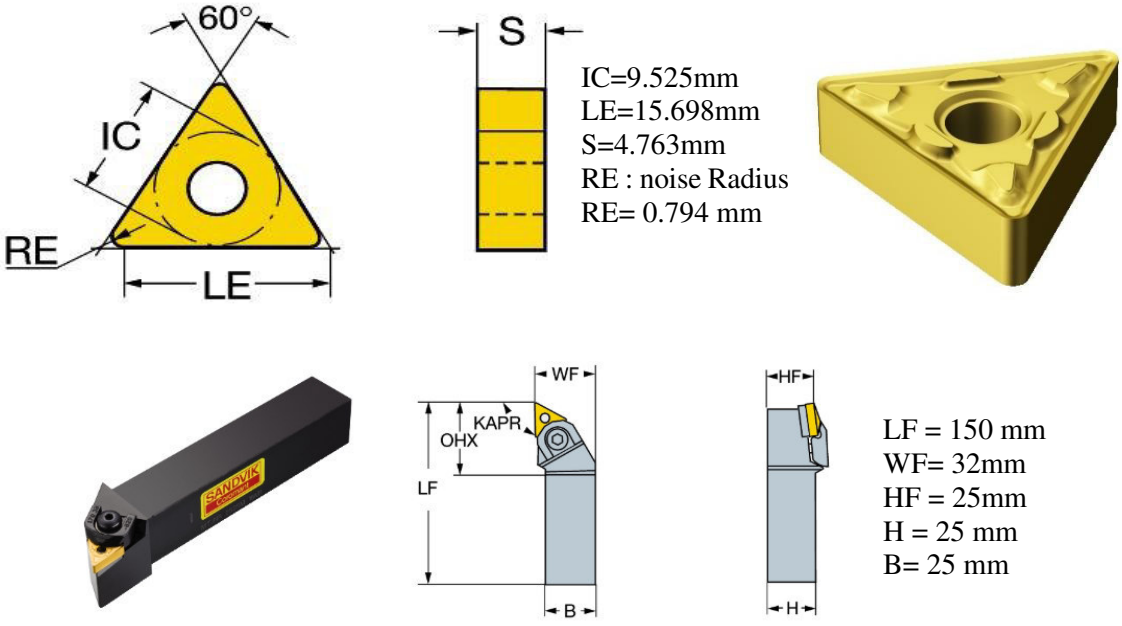

Figure 4.6. Cutting insert and its holder geometries

4.2.4. Cutting parameters and conditions

Cutting speed and feed with three different levels were chosen as variable cutting parameters and depth of cut was kept constant. It should be emphasized that the cutting parameters were selected purely based on the cutting tools' manufacturer recommendations as well as the details available in literature. For each set of turning experiments, the machining time was settled at 20 seconds. In the same context, dry, pure MQL, nanofluid assisted MQL and hybrid nanofluids were implemented as the cutting conditions. The complete details of cutting parameters and conditions are given in Table 4.3. A total of 63 cutting experiments were performed, taking into account that the cutting parameters (*Vc* and *f*) were defined as continuous variables and different lubricating conditions were termed as categorical variables.

4.2.5. Measurements of turning characteristics

In this study, four prominent turning criteria, namely surface roughness (*Ra*), main cutting forces (*Fc*), cutting temperature (*T*) and flank wear (*VB*) were analyzed under different cutting conditions. The main cutting force and cutting temperature were recorded using online mode and surface roughness as well as flank wear measured using offline mode. The surface roughness measurements were performed at three different points along the workpiece by utilizing a Mitutoyo surftest-210 device having a cutoff length of 0.8 mm. Ten measurements were made at each point and arithmetic averages were determined. The cutting forces and the cutting temperatures were measured by Kistler piezoelectric dynamometer (type 9257B) and Optris® CTlaser 3MH1 two-wire infrared thermometer with a measuring interval of 150°C–1000°C, respectively. Flank wear experiments were repeated twice, and the reported value represents the average of flank wear value obtained by at least five measurements using SOIF XJP-6A trinocular microscope device.

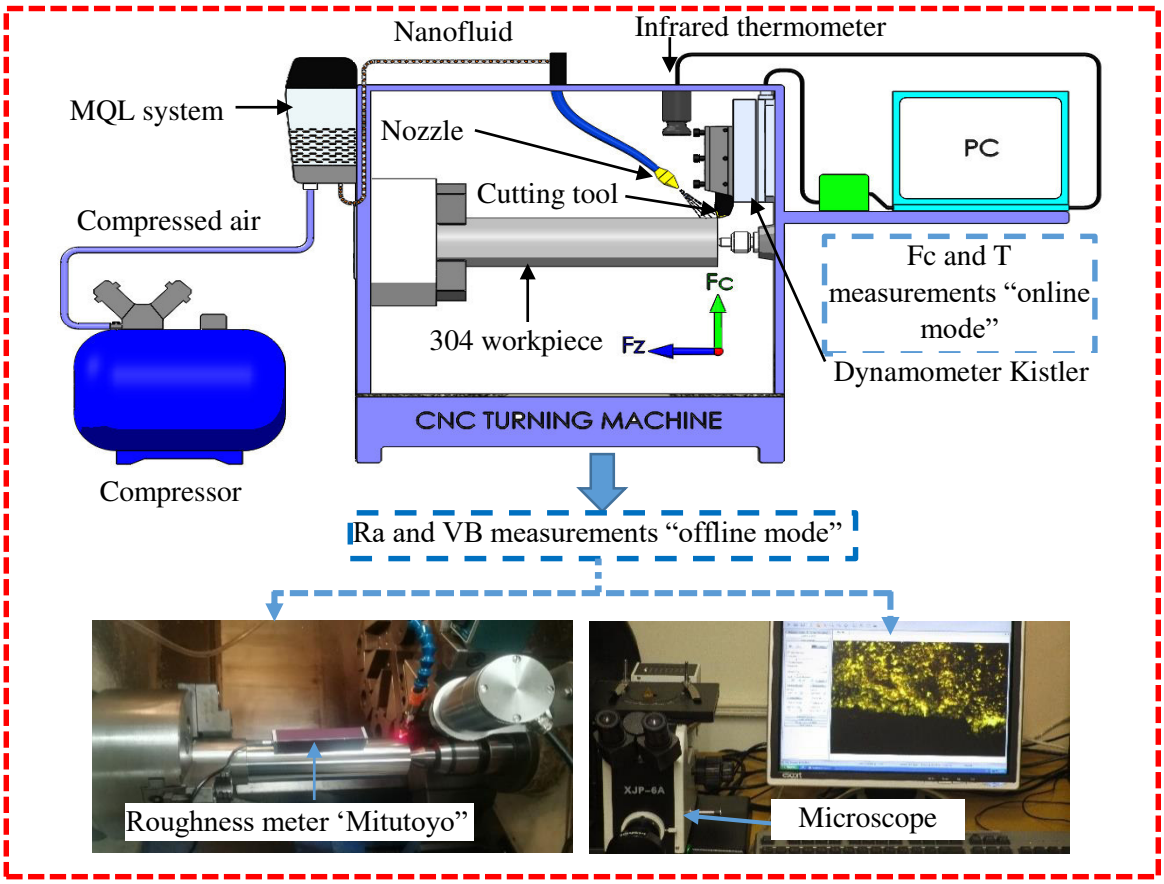

Figure 4.7. Experimental set-up

Table 4.3. Turning parameters and cutting conditions

Parameters	**Explanations**
Cutting conditions	Dry MQL nano MoS_2 reinforced nanofluid assisted MQL **(MoS_2-MQL)** MWCNT reinforced nanofluid assisted MQL **(MWCNT-MQL)** nano graphene reinforced nanofluid assisted MQL **(Graphene-MQL)** MWCNT/MoS_2 reinforced hybrid nanofluid assisted MQL **(Hybrid-1-MQL)** graphene/MoS_2 reinforced hybrid nanofluid assisted MQL **(Hybrid-2-MQL)**
MQL flow rate	30 ml/h
MQL pressure	5 bar
Nozzle angle	30 degree
Nozzle distance	30 mm
Nozzle tip diameter	1 mm
Cutting speed	160, 190, and 220 m/min
Feed	0.12, 0.16 and 0.2 mm/rev
Depth of cut	1 mm

4.3. Results and Discussion

In this section, the responses were evaluated based on the various conditions and cutting parameters. Table 4.4. presents the results of the considered outputs obtained during the experimental work.

Table 4.4. Experimental results of measured outputs.

Exp.no	Cutting speed, m/min	Feed, mm/rev	Cutting depth, mm	Cooling conditions	Ra (µm)	F (N)	T (°C)
1	160	0.12	1	Dry	1	305.56	190
2	190	0.12	1		0.76	302.27	195.36
3	220	0.12	1		0.79	300.97	199.7
4	160	0.16	1		1.34	385.38	195.7
5	190	0.16	1		1.3	352.67	210.51
6	220	0.16	1		1.26	344.9	217.09
7	160	0.2	1		1.96	459.8	212.433
8	190	0.2	1		1.82	453.17	218.01
9	220	0.2	1		1.75	448.73	223.548
10	160	0.12	1	MQL	0.89	290.55	184.23
11	190	0.12	1		0.72	286.35	190.42
12	220	0.12	1		0.69	283.49	194.71
13	160	0.16	1		1.28	370.24	187.8
14	190	0.16	1		1.23	340.04	200.94
15	220	0.16	1		1.17	334.07	207.31
16	160	0.2	1		1.9	444.19	203.02
17	190	0.2	1		1.8	437.39	208.95
18	220	0.2	1		1.71	431.65	213.85
19	160	0.12	1	MoS_2 nanofluid-based MQL	0.78	289.29	180.63
20	190	0.12	1		0.67	285.35	186.76
21	220	0.12	1		0.66	281.64	191.32
22	160	0.16	1		1.23	367.37	182.91
23	190	0.16	1		1.12	338.05	192.81
24	220	0.16	1		1.11	332.67	200.54
25	160	0.2	1		1.75	439.32	199.13
26	190	0.2	1		1.75	433.61	204.64
27	220	0.2	1		1.66	425.03	210.43
28	160	0.12	1	MWCNT nanofluid-based MQL	0.72	287.7	177.22
29	190	0.12	1		0.61	283.61	183.06
30	220	0.12	1		0.58	279.11	187.32
31	160	0.16	1		1.15	363.75	180.17
32	190	0.16	1		1.08	336.91	187.86
33	220	0.16	1		1.08	331.56	195.86

34	160	0.2	1		1.7	435.96	194.98
35	190	0.2	1		1.68	431.95	200.16
36	220	0.2	1		1.6	420.87	205.5
37	160	0.12	1	Graphene nanofluid-based MQL	0.65	275.41	165.07
38	190	0.12	1		0.49	272.5	172.02
39	220	0.12	1		0.43	265.28	175.3
40	160	0.16	1		0.97	354.56	168.61
41	190	0.16	1		0.92	328.49	173.84
42	220	0.16	1		0.91	322.18	182.39
43	160	0.2	1		1.55	422.06	182.9
44	190	0.2	1		1.49	415.13	186.75
45	220	0.2	1		1.42	404.86	190.67
46	160	0.12	1	MWCNT-MoS_2 hybrid nanofluid-based MQL	0.7	285.97	173.77
47	190	0.12	1		0.59	281.59	179.62
48	220	0.12	1		0.55	276.78	183.05
49	160	0.16	1		1.1	361.67	176.6
50	190	0.16	1		1.05	334.5	182.97
51	220	0.16	1		0.99	330.38	191.34
52	160	0.2	1		1.65	429.8	190.11
53	190	0.2	1		1.6	425.99	194.58
54	220	0.2	1		1.55	417.21	200.64
55	160	0.12	1	Graphene-MoS_2 hybrid nanofluid-based MQL	0.68	278.46	169.39
56	190	0.12	1		0.57	275.95	175.04
57	220	0.12	1		0.53	272.37	179.35
58	160	0.16	1		1.02	358.67	172.59
59	190	0.16	1		0.99	331.66	178.1
60	220	0.16	1		0.93	324.59	187.14
61	160	0.2	1		1.6	428.47	186.25
62	190	0.2	1		1.55	420.14	190.08
63	220	0.2	1		1.48	410.01	195.49

4.3.1. Surface roughness

In order to evaluate the quality of the machined parts, arithmetic surface roughness (*Ra*) is often considered as the main valuable criterion. Figure 4.8 shows the variation of *Ra* as a function of cutting speed, feed and lubricating conditions. It is clear that the *Ra* increased as the feed increased and decreased as the cutting speed increased. Probably, with increasing the feed, the increment in *Ra* is thought to be due to the generation of thick feed marks produced by the relative motion between the workpiece and the cutting tool [4.31]. In the turning process, thicker feed marks cause more improper surface finish. Whereas an increment in cutting speed caused a decrease in *Ra*. This is due to the fact

that increased cutting speed contributes to generating high heat in the cutting zone. As a result, the possibility of formatting the build-up edges (BUE) could be reduced, thereby *Ra* decreased [4.19]. Regardless of cutting parameters, the alteration in *Ra* was also dependent on the lubricating conditions. Arithmetic means of *Ra* under dry, MQL, MoS_2-MQL, MWCNT-MQL, graphene-MQL, hybrid-1-MQL and hybrid-2-MQL conditions were determined as 1.33 µm, 1.27 µm, 1.19 µm, 1.13 µm, 0.98 µm, 1.09 µm and 1.04 µm, respectively. It is clearly to be observed that there are improvements in *Ra* by approximately 4.9%, 10.43%, 14.86%, 26.29%, 18.36% and 21.95% under MQL, MoS_2-MQL, MWCNT-MQL, graphene-MQL, hybrid-1-MQL and hybrid-2-MQL conditions, respectively as compared to dry cutting. This can be explained due to the absent of any lubricant. Similarly, the addition of nanoparticles to the vegetable cutting fluid in the MQL system induced the surface to be smoother and hence lower surface roughness values were obtained as compared to pure MQL condition. This is because of the ability of nanoparticles to reduce coefficient of friction [4.16] thanks to their structures at nano level that help to format a thin layer at the rubbing zone, leading to separating the asperities of sliding surfaces effectively [4.32]. Interestingly, it can be seen that MWCNT/MoS_2 and nano graphene/MoS_2 reinforced hybrid nanofluids assisted MQL provided enhanced *Ra* compared to MWCNT and nano MoS_2 reinforced nanofluids. The primary reason is that combining between the nanoparticles (MWCNT/MoS_2 and nano graphene/MoS_2) and increasing their Brownian motion in liquid resulted in an increase in thermal conductivity of the formulated nanofluid, which resulted in a reduction in heat generated in cutting area due to its heat dissipation capability [4.27]. As a result, the turning operation could be completed smoothly, lowering *Ra* [4.22,4.33]. However, only nano graphene reinforced nanofluid produced better improvement in terms of *Ra* than other nanofluids and hybrid nanofluids. This is believed due to the nano graphene particles' nanoscale structure (platelets), which helps to excellent penetration into the tool-workpiece interface, and its well lubrication properties [4.34,35].

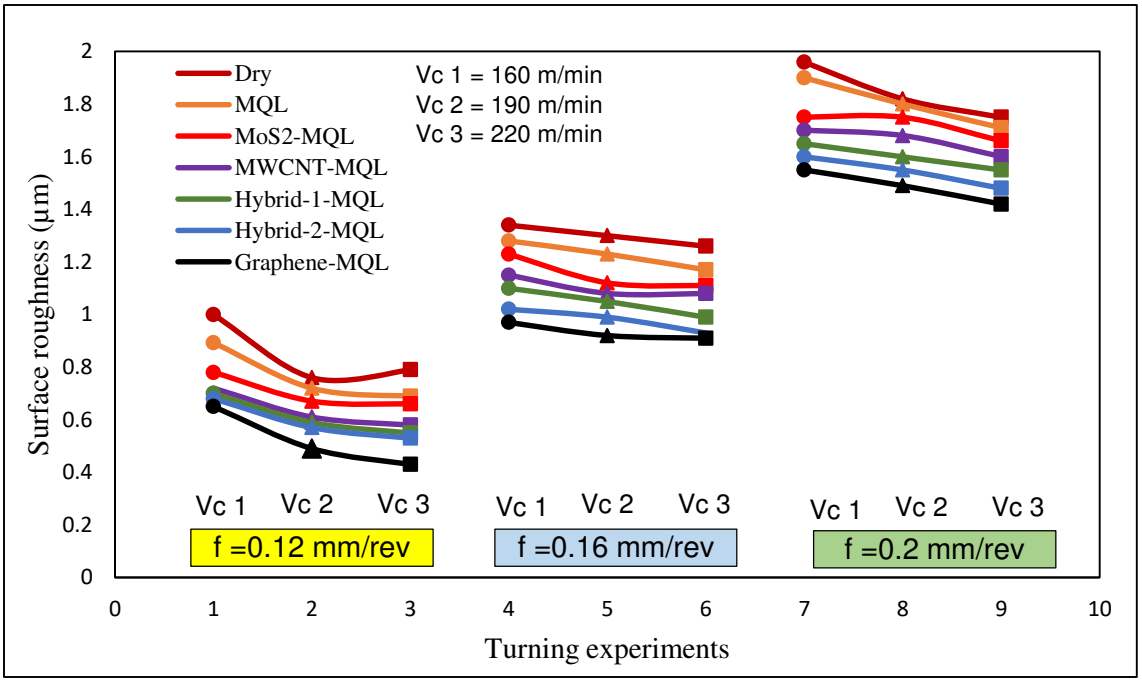

Figure 4.8. The variation of *Ra* under different cutting conditions

4.3.2. Cutting force

Cutting force (*Fc*) is considered as one of the main machining responses that assesses the power and energy consumption during the machining operations. However, many important variables such as the cutting parameters, the machine tool dynamics, characteristics of tool and workpiece material and tribological properties of cutting fluid influence the cutting forces [4.21,4.16]. Figure 4.9 presents the variation of *Fc* according to cutting speed, feed and different lubricating conditions. Based on the results, it was clear that increasing the feed increased the main cutting force significantly. The major belief of the increase in cutting force is due to an increase in the chip cross-section causing an increment in friction force at the tool-chip interface [4.36]. Further, the cutting speed had substantially less effect on the *Fc* than the feed. At lower cutting speeds, higher cutting forces values were recorded. This can be interpreted by increasing in the chip-tool contact length caused by the remaining chip in the rake face of the tool over a long period of time [4.37]. Decreased cutting force was observed at high cutting speed (*Vc*=220 m/min). In general, with an increase in cutting speed, the temperature rises at the cutting region. Therefore, thermal softening occurs, thereby cutting forces reduced [4.38]. In addition, as shown in Figure 4.9, it is obvious that the lubricating conditions also affected

the cutting force. Cutting forces under dry, MQL, MoS_2-MQL, MWCNT-MQL, graphene-MQL, hybrid-1-MQL and hybrid-2-MQL conditions were measured as 372.61 N, 357.55 N, 354.7 N, 352.38 N, 340.05 N, 349.32 N and 344.48 N, respectively. There was a visible reduction in *Fc* by approximately 4.04%, 4.80%, 5.42%, 8.73%, 6.24% and 7.54% under MQL, MoS_2-MQL, MWCNT-MQL, graphene-MQL, hybrid-1-MQL and hybrid-2-MQL conditions, respectively as compared to dry cutting. Low cutting forces were obtained with the application of MWCNT and nano MoS_2 reinforced nanofluids assisted MQL method as compared to dry and pure MQL cutting environments. A good reason for this fact is attributed to the dispersion of MWCNT and nano MoS_2 particles into the cutting fluid, which enhanced the viscosity and thermal conductivity of the cutting fluid [4.16]. In addition, MWCNT particles reinforced nanofluid caused lower cutting forces than nano MoS_2 particles reinforced nanofluid. Similar observation is reported in literature [4.27] for superior performance of MWCNT than nano MoS_2. Moreover, lower cutting forces were obtained with the application of hybrid nanofluids assisted MQL method. This can be due to the fact that the interaction of the combined nanoparticles helps to form adhesive film, thus more lubrication that leads to reduced friction between sliding surfaces, resulting in a declining magnitude of *Fc* [4.27]. Furthermore, the lowest cutting forces were measured while using nano graphene reinforced nanofluid assisted MQL method. As previously stated, this is due to the effective interaction of nano graphene particles with the cutting tool and the workpiece due to its superior lubricating and super thin nanoscale structure, resulting in reduced friction, minimizing cutting force and improving dimensional accuracy of the machined part.

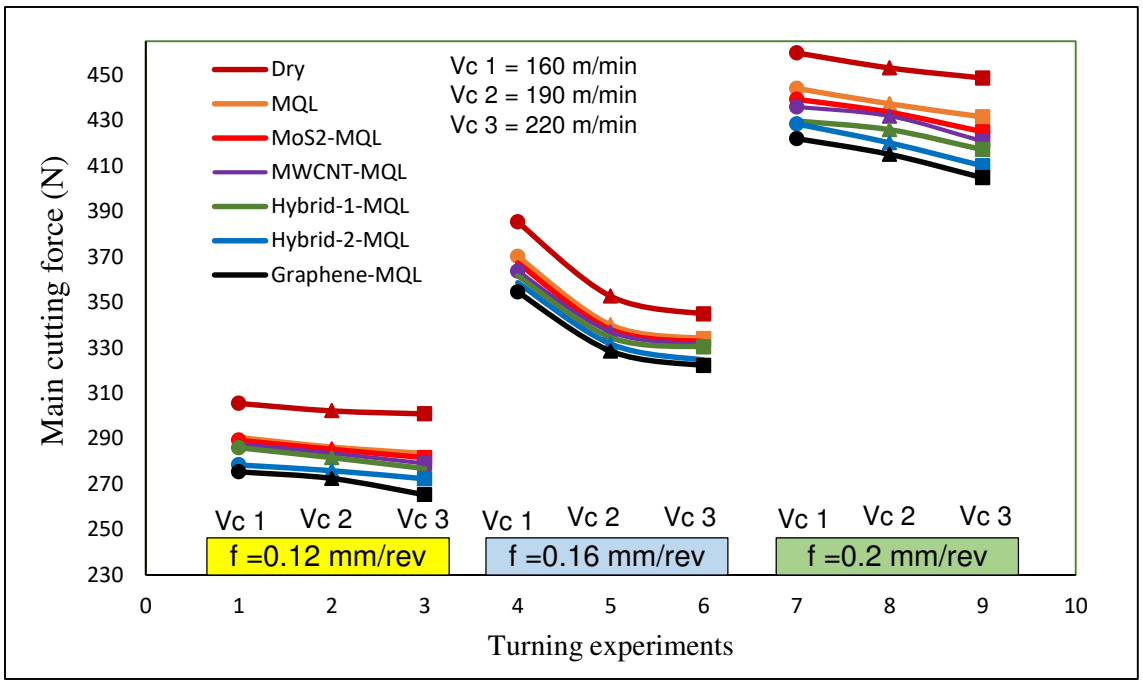

Figure 4.9. The variation of *Fc* under different cutting conditions and parameters

4.3.3. Cutting temperature

Cutting temperature (*T*) is an important index that helps to determine the quality of machining performance in terms of production efficiency. The main factor that directly affects the cutting temperature is the amount of heat produced at the cutting tool-chip interface. Figure 4.10 displays graphically the effects of dry, MQL, MoS_2-MQL, MWCNT-MQL, graphene-MQL, hybrid-1-MQL and hybrid-2-MQL conditions and cutting parameters on the *T* in the cutting zone. Accordingly, it is highly visible that there is a significant growth trend in *T* with feed raising. This is justified due to the fact that increased feed is responsible for the rise of chip thickness, which impacts friction, and hence leads to an increment in the heat generation and cutting temperatures [4.22]. Despite not having the same effect on *T* as the feed, increasing the cutting speed resulted in an increase in the *T* in the cutting area. It is well-known that increased cutting speed causes an increase in the plastic deformation speed. However, the effect of cutting speed on *T* can be explained by the inclusion of cutting fluid, which resulted in less heat being distributed into workpiece-tool-chip interfaces [4.11]. Irrespective of cutting parameters, the variation in cutting temperature was also found to depend on the cutting environment, as shown in Figure 4.10. The highest cutting temperature was measured under dry conditions. The

reason for this was primarily due to the lack of any lubrication [4.15]. Including the cutting fluid in the turning process, the cutting temperature was diminished by about 3.82%, 6.08%, 8.06%, 12.22%, 10.18% and 12.29%, respectively under MQL, MoS_2-MQL, MWCNT-MQL, graphene-MQL, hybrid-1-MQL and hybrid-2-MQL conditions as compared to dry cutting. However, there was a slight decrease in *T* with the pure MQL method due to deficient in cooling effects, particularly when machining of hard-to-cut materials [4.33]. Further, the addition of nanoparticles and their hybrids to the vegetable cutting fluid resulted in a better reduction in *T* in the cutting zone. A significant reduction of 14.21% in *T* with the use of nano graphene reinforced nanofluid may be imputed to the superior thermal conductivity properties of the nano graphene particles than nano MoS_2 and MWCNT reinforced nanofluids and their hybrids. It was suggested that higher thermal conductivity presents better heat extraction ability [4.39]. The obtained results are in good concordance with previous published work [4.40].

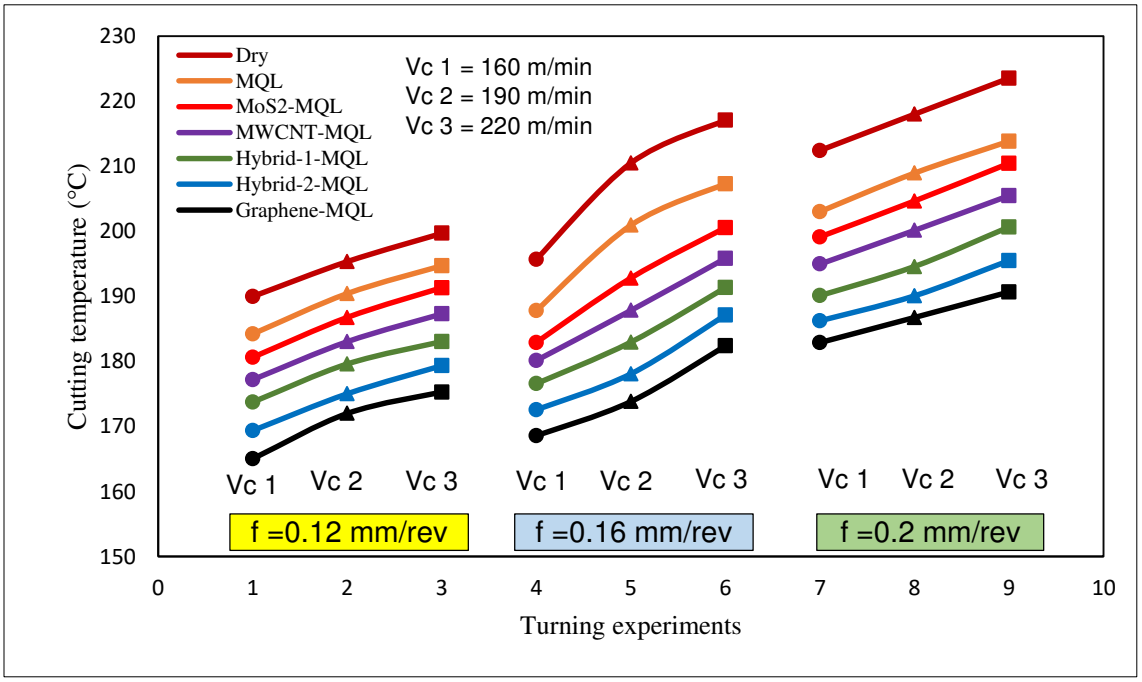

Figure 4.10. The variation of *T* under different cutting conditions and parameters

4.3.4. Comparison of performance outputs

In this section, a direct comparison of the effects of the cutting conditions on performance measures was made. To fulfill this purpose, the cutting parameters were kept constant as the cutting speed of 220 m/min and the feed of 0.12 mm/rev (Experiment number 3). All performance indices (*Ra*, *Fc* and *T*) were found to be better in the nano graphene reinforced nanofluid assisted MQL method as compared to other lubricating environments as shown in Figure 4.11. Based on the experimental results, *Ra* values were reduced by 45.56%, 37.68%, 34.84%, 25.86%, 21.81% and 18.86%, *Fc* values were reduced by 11.85%, 6.42%, 5.80%, 4.95%, 4.15%, and 2.60% and *T* values were also reduced by 12.22%, 9.97%, 8.37%, 6.42%, 4.23% and 2.26% under nano graphene reinforced nanofluid assisted MQL method as compared to dry, MQL, MoS_2-MQL, MWCNT-MQL, hybrid-1-MQL and hybrid-2-MQL conditions. The main reason for this improvement of *Ra* and reduction of *Fc* and *T* is thought to be due to the better physical synergetic effect of nano graphene reinforced nanofluid. Similar observation was documented in literature [4.34]. However, as not expected, it can be seen that nano graphene reinforced nanofluid assisted MQL outperformed its hybrid (graphene/MoS_2) reinforced nanofluid assisted MQL. This result can be attributed to the higher weight percentage of graphene (0.1%), which improves the wettability of the nanofluid, allowing nano graphene platelets to successfully penetrate into the cutting tool-workpiece interface, reducing friction and heat generation, and thus contributing to improved machining performance (*Ra*, *Fc* and *T*). This is in accordance with justification reported in literature [4.35,4.40,4.41].

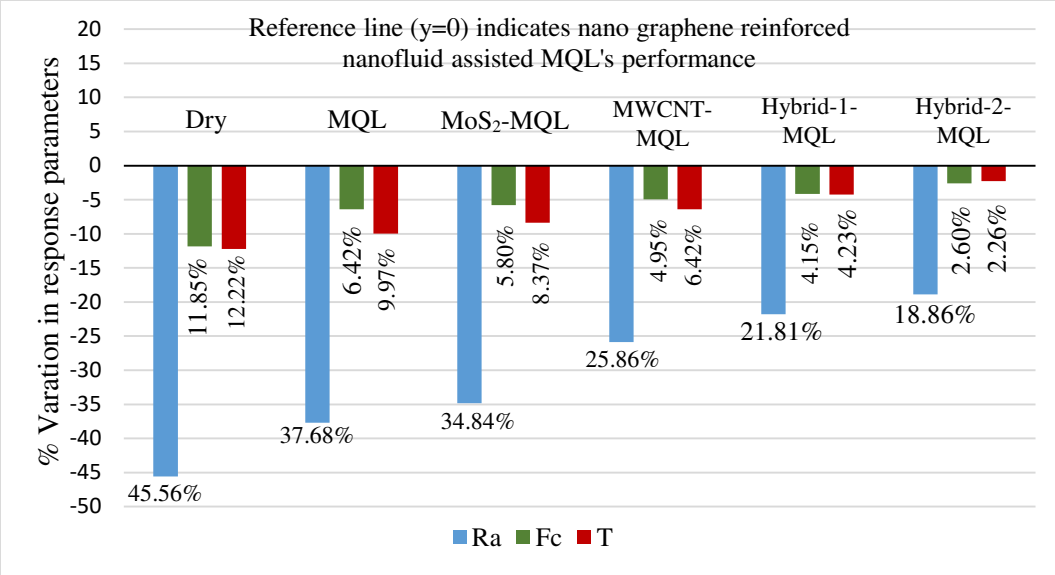

Figure 4.11. Effect of nano graphene reinforced nanofluid assisted MQL on performance outputs against other lubricating conditions.

4.3.5. Flank wear

In the current work, a set of turning experiment tests were conducted at constant cutting parameters (Vc=190 m/min and f=0.12 mm/rev) to assess the positive and negative impacts of the investigated lubricating conditions, especially nano MoS_2, MWCNT and nano graphene nanofluids and their hybrid nanofluids assisted MQL method on *VB* in straight turning of AISI 304. The behaviors of flank wear are given in Figure 4.12 in accordance with machining time. Based on the measurement results, significant reductions of 6.67%, 11.11%, 17.78%, 48.89%, 24.44%, 33.33% in *VB* were observed by utilizing MQL, MoS_2-MQL, MWCNT-MQL, graphene-MQL, hybrid-1-MQL and hybrid-2-MQL conditions, respectively as compared to dry cutting. The main reason for dry cutting's poor performance can be attributed to the fact that the lack of lubricant exposes the cutting tool to extreme high heat generation, resulting in increased friction between cutting tool-chip-workpiece interfaces. As a result, adhesion or welding of the chips on the rake face occurs and this leads to deteriorating the sharpness of the cutting edge. Similar explanations were stated in literature [4.31,4.42]. Likewise, noticeable reductions of 4.76%, 11.90%, 45.24%, 20% and 28.57% in flank wear were also noticed under MoS_2-MQL, MWCNT-MQL, graphene-MQL, hybrid-1-MQL and hybrid-2-MQL conditions, respectively as compared to pure MQL environment. It is thought that insufficient cooling

of the pure MQL method is due to its inability to effectively penetrate into the cutting zone. And this may be the main reason for its moderate performance. Overall, the addition of nanoadditives to the vegetable cutting fluid ameliorates its thermal-physical properties, thereby resulting in less *VB*. It is clearly obvious from Figure 4.12 that the best machining performance in terms of lower *VB* was observed under the nano graphene reinforced nanofluid assisted MQL method. Its hybrid performance (nano graphene/MoS_2 reinforced hybrid nanofluid) was ranked second, followed by MWCNT/MoS_2 reinforced hybrid nanofluid assisted MQL, MWCNT reinforced nanofluid assisted MQL and nano MoS_2 reinforced nanofluid assisted MQL. This fact is because of the higher thermal conductivity, low viscosity, spreadability and improved wettability properties of nano graphene reinforced nanofluid [4.42] and so forth. Hence, it can conclude that nano graphene platelets are better for using as a cooling/lubricating agent to improve the thermal-physical properties of the vegetable cutting fluid. Doing so has the potential to contribute positively to the turning process. This research highlighted similar outcomes to research performed by Singh et al. [4.25] for the potential of nano graphene particles to act as lubricant/coolant agent in turning operations.

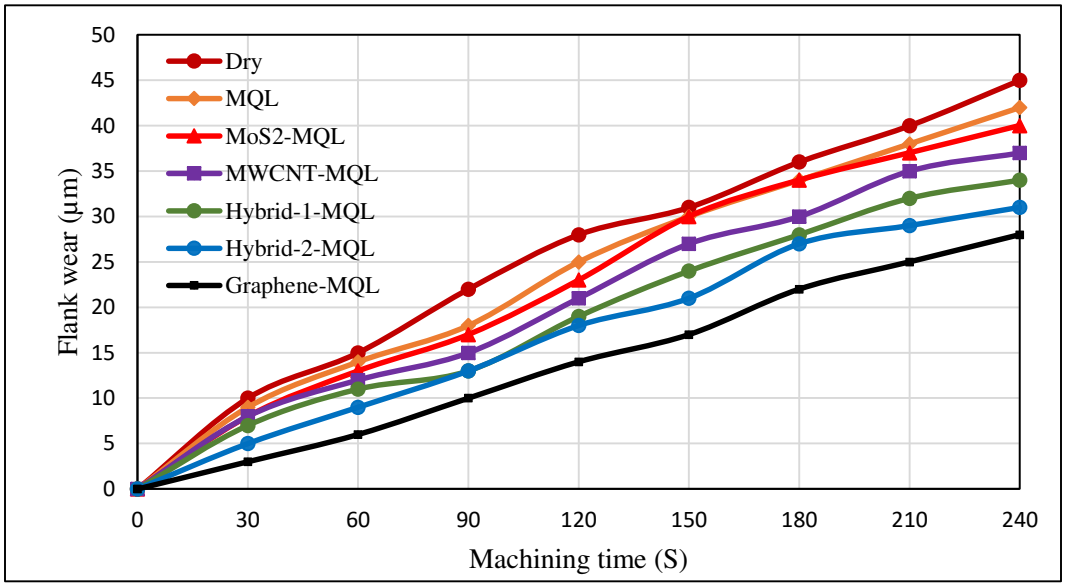

Figure 4.12. The evolution of *VB* with respect of machining time under different cutting conditions and parameters.

4.3.6. Statistical analysis

In order to examine the degree of statistical significance of process parameters on machinability characteristics, analyses of variance (ANOVA) was introduced as provided in Table 4.5. Table 4.5 contains a statistical indictor known as the F-ratio, which is used to determine which control factors have a significant effect on the characteristic being evaluated (in this case, *Ra*, *Fc* and *T)*. Also, the degree of influence was explained with the percentage contribution (PC), which is the product of division of each parameter's sum of squares (SS) onto their total. The higher the PC, the higher the effect a variable has on a measured response [4.43]. The analyses were carried out at confidence levels of 95% [4.44]. As a result of assessment of surface roughness results, it was obtained that the feed is the most significant cutting parameter affecting *Ra* with the F value of 4865.32 and percentage contribution of 90.20% followed by lubricating condition (F = 368.09 and PC = 7.55%) and cutting speed (F = 85.59 and PC = 1.56%). When the cutting force results were analyzed, the F values and the PC of cutting speed, feed and lubricating condition were found to be: (46.65 and 1.56%), (2815.38 and 94.14%) and (65.94 and 2.6%), respectively. In this case, feed has the greatest statistical signification for cutting force. As far as the cutting temperature results in the cutting zone were concerned, the effects of process parameters were ranked as follows: 1) lubricating condition with F = 875.58 and PC = 51.37%; 2) feed with F = 539.89 and PC = 31.02%; 3) cutting speed with F = 252.49 and PC = 14.51%. Therefore, the process parameter with the dominate influence on *Ra* and *Fc* was the feed, while the effective cutting parameter affecting *T* in the cutting zone was the lubricating condition. This is in agreement with findings reported in literature [4.22]. Figure 4.13 depicts the ANOVA results in terms of percentage contributions of all process parameters to each measured outputs.

Table 4.5. ANOVA for a) *Ra*, b) *Fc* and c) *T*

Factors	**Degree of freedom**	**Sum of Squares**	**Mean of squares**	**F-ratio**	**PC (%)**
a) Surface Roughness					
Cutting speed	1	0.18	0.18	85.59	1.56
Feed	1	10.41	10.41	4865.32	90.20
Lubricating conditions	6	0.84	0.14	368.09	7.55
Error	54	0.12	2.14E-003		1.03
Total	62	11.54			
b) Cutting Force					
Cutting speed	1	3730.51	3730.51	46.65	1.56
Feed	1	225154	225154	2815.38	94.14
Lubricating conditions	6	5959.39	993.23	65.94	2.6
Error	54	4318.54	79.97		1.8
Total	62	239163			
c) Cutting Temperature					
Cutting speed	1	1597.60	1597.60	252.49	14.51
Feed	1	3416.07	3416.07	539.89	31.02
Lubricating conditions	6	5656.90	942.82	875.58	51.37
Error	54	341.68	6.33		3.1
Total	62	11012.25			

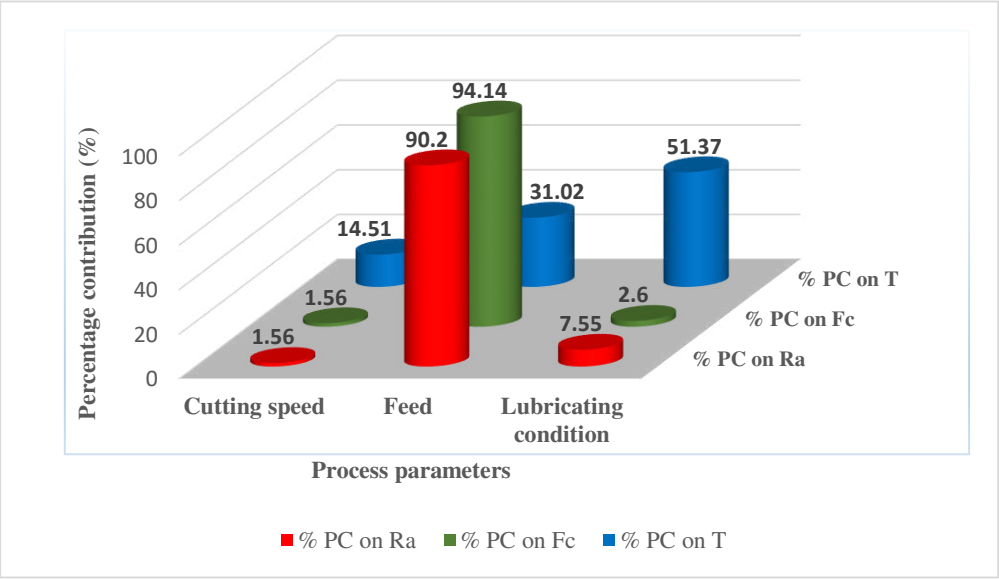

Figure 4.13. Percentage contributions of the process parameters on measured outputs

In order to perform the multi-criteria optimization task, adequate models should be established to describe the output indices in terms of the pre-defined design factors. A multi-regression analysis approach was employed to conduct the modeling task. This approach is extensively reported in establishing a relationship between the measured outputs and included process parameters [4.45]. Through this approach, it is possible to derive a second order model. Note that LC indicates the lubricating conditions that are coded as 1, 2, 3, 4, 5, 6 and 7 for dry, MQL, MoS_2-MQL, MWCNT-MQL, Graphene-MQL, Hybrid-1-MQL and Hybrid-2-MQL, respectively. The proposed regression models for *Ra*, *Fc* and *T* are expressed in Equations (4.1) to (4.3), respectively. The accuracy of all yielded models (R^2) was higher than 0.98. The residual plot, which is defined as the difference among the measured values of *Ra*, *Fc* and *T* and their predicted one, was used to assess the goodness fit of the simulated models.

$$Ra = 1.915 - 0.0188 * Vc - 0.74 * f - 0.1310\, LC + 0.00753 * Vc * f + 0.000124 * Vc * LC - 0.126 * f * LC + 0.000024 * Vc^2 + 38.29 * f^2 + 0.00948 * LC^2 \quad (4.1)$$

$$Fc = 408.0 - 1.468 * Vc - 238 * f - 9.70\, LC - 1.43 * Vc * f - 0.0010 * Vc * LC - 18.5 * f * LC + 0.00365 * Vc^2 + 7543 * f^2 + 1.091 * LC^2 \quad (4.2)$$

$$T = 146.3 + 0.428 * Vc - 201 * f - 6.76\,LC + 0.026 * Vc * f - 0.0091 * Vc * LC - 12.70 * f * LC - 0.00050 * Vc^2 + 1478 * f^2 + 0.781 * LC^2 \quad (4.3)$$

Figure 4.14 presents the normal probability plots of models for *Ra*, *Fc* and *T*. It was noticeable that most of the data points had fallen over the straight line pattern. Therefore, it can be indicated that the normality assumptions were verified [4.46], proving the precision of the regression models given. Moreover, it can be concluded that the yielded models were suitable and hence could be used to accomplish the optimization objective.

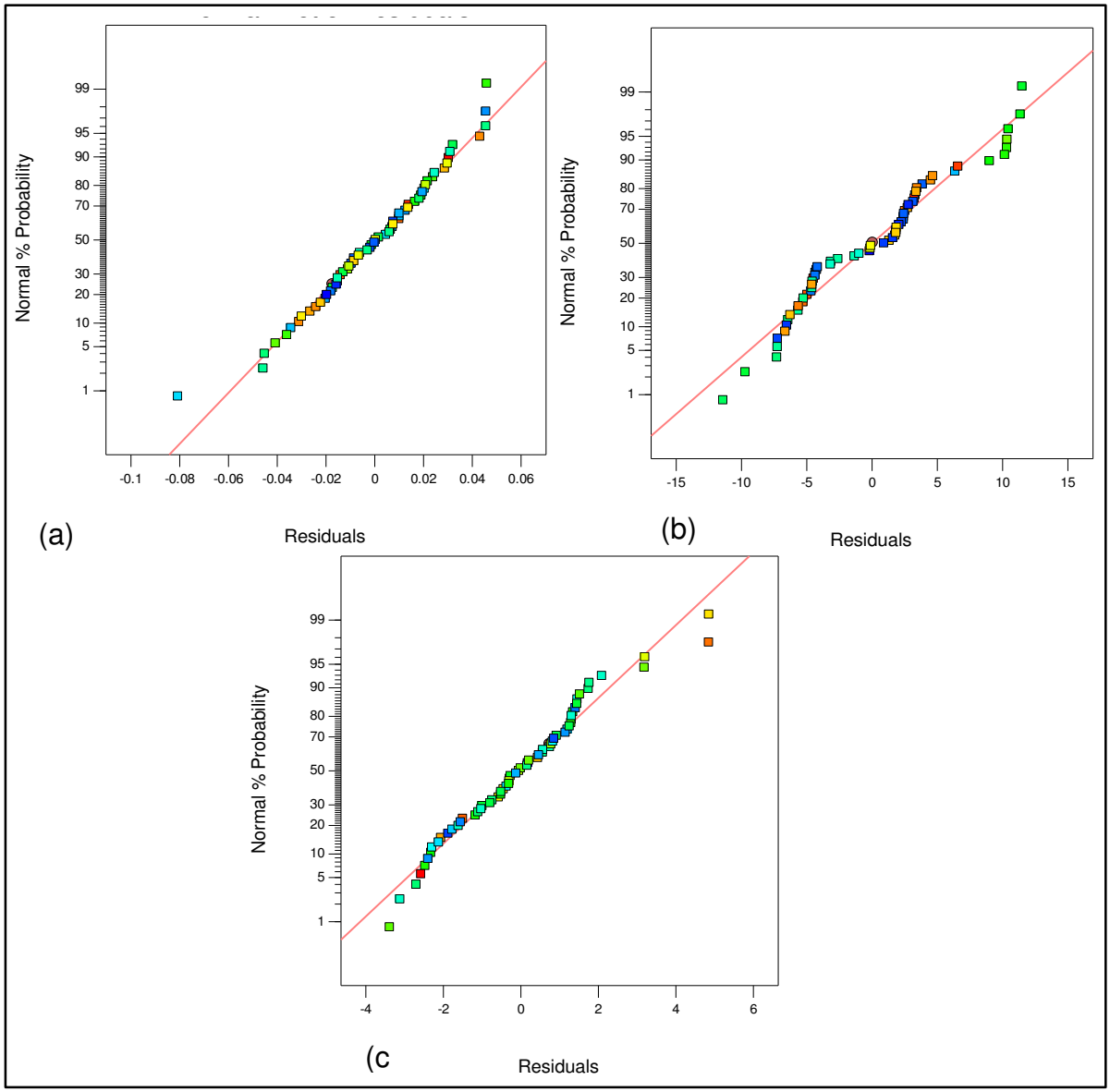

Figure 4.14. Residuals plots for normal probability of a) *Ra*, b) *Fc* and c) *T*

4.3.7. Composite Desirability Approach

Due to its simplicity and efficiency, the composite desirability approach (CDA) has been extensively used in machining industry to determine the best cutting parameters settings for multi-responses [4.25]. In CDA approach, each estimated response (y_i) is converted to an individual value, called a desirability (d_i). Its range is between 0 and 1, according to Eq (4.4) [4.47].

$$d_i = \begin{cases} 1 & if\ \ q_i \leq S \\ \left(\frac{L-q_i}{L-S}\right)^{\alpha} & if\ S < q_i < L \\ 0 & if\ q_i \geq L \end{cases} \tag{4.4}$$

where S and L present the smallest and the largest acceptable values of q_i , respectively, α is the weight parameter and q_i presents the output to be optimized.

After converting each estimated response variable q_i to its corresponding desirability value d_i, the optimal setting for response (s) is achieved through maximizing the overall desirability *D*, which is also varied from 0 to 1 and known as geometric mean of all the individual desirability functions. The total multi-objective function identifying desirability *D* is expressed by Eq (4.5) [4.48].

$$D = (d_1 \times d_2 \times \ldots\ldots d_m)^{\frac{1}{m}} = (\prod_{i=1}^{m} d_i)^{\frac{1}{m}} \tag{4.5}$$

Through CDA approach, the operating condition with the highest desirability value is considered as the optimal solution [4.49].

Furthermore, it is worth mentioning that for multi-criteria optimizations, each response must take whether low or high value assigned to the desired goal. Meaning, the “Goal” for investigated responses has to be one of the five choices including “none”, “maximum”, “minimum”, “target”, or “in range”. Generally, three optimization purposes could be considered, namely the quality optimization, productivity optimization and quality-productivity optimization, which is the combination between the two previous ones. Therefore, The CDA was implemented in this research work to carry out the multi-criteria optimization to achieve quality optimization goal.

Herein, the process parameters were maintained within experimental range, while the investigated outputs were considered to be minimized, as shown in Table 4.6.

Table 4.7 lists the optimum eight possible solutions derived by employing the DF technique. The feasible solution, that led to minimize simultaneously the measured outputs *(Ra*, *Fc* and *T*), was chosen as the one possessing the higher desirability value. Figure 4.15 presents the contour plots underscored for *Ra*, *Fc* and *T* at the higher desirability value (0.943). The ideal solution after multi-criteria optimization was found with the following parameters: the cutting speed of 188 m/min, feed of 0.12 mm/rev and nano graphene reinforced nanofluid assisted MQL condition. Through this combination, the estimated values were found to be 0.51µm, 270 N and 170°C for Ra, *Fc* and *T,* respectively. The desirability bar graphs for each optimum solution were given in Figure 4.16. The parameter settings were presented in the first 3 bars and the target and optimal anticipated response values were illustrated in the remaining bars.

In addition, the optimum results delivered by DF approach were compared with experimental run (experiment number of 2 according to Figures 4.5, 4.6 and 4.7), as provided in Table 4.8. According to Table 4.8, the obtained percentage deviations are within the acceptable range, i.e., within < 5%, confirming the validity of the suggested optimal results achieved in this investigation.

Table 4.6. Conditions and goals for optimization of cutting parameters and responses

Conditions						
Parameters and responses	**Unit**	**Goal**	**Lower limit**	**Upper limit**	**Lower weight**	**Upper weight**
Vc	m/min	In range	160	220	1	1
f	mm/rev	In range	0.12	0.2	1	1
ap	mm	In range	1	1	1	1
Cooling conditions		In range	LC-1	LC-7	1	1
Ra	µm	Minimize	0.43	1.96	1	1
Fz	N	Minimize	265.28	459.8	1	1
T	°C	Minimize	165.07	223.54	1	1

Table 4.7. Optimum findings derived by composite desirability approach (C*DA*) for multi-criteria *Ra*, *Fc* and *T*

Process parameters			Outputs			Desirability
Vc, m/min	f, mm/rev	Lubricating conditions	*Ra,* µm	*Fc,* N	*T,* °C	
188.86	0.12	Graphene-MQL	0.51	270.77	170.37	0.943
182.48	0.12	Graphene-MQL	0.526	272.67	169.25	0.942
202	0.12	Graphene-MQL	0.478	267.62	172.65	0.941
214	0.12	Graphene-MQL	0.457	265.89	174.57	0.936
180.85	0.12	Hybrid-2-MQL	0.59	277.21	172.77	0.899
171.68	0.12	Hybrid-2-MQL	0.62	280	170.99	0.899
194.50	0.12	Hybrid-2-MQL	0.560	273.20	175.40	0.897
199.77	0.12	Hybrid-2-MQL	0.55	272.06	176.34	0.895

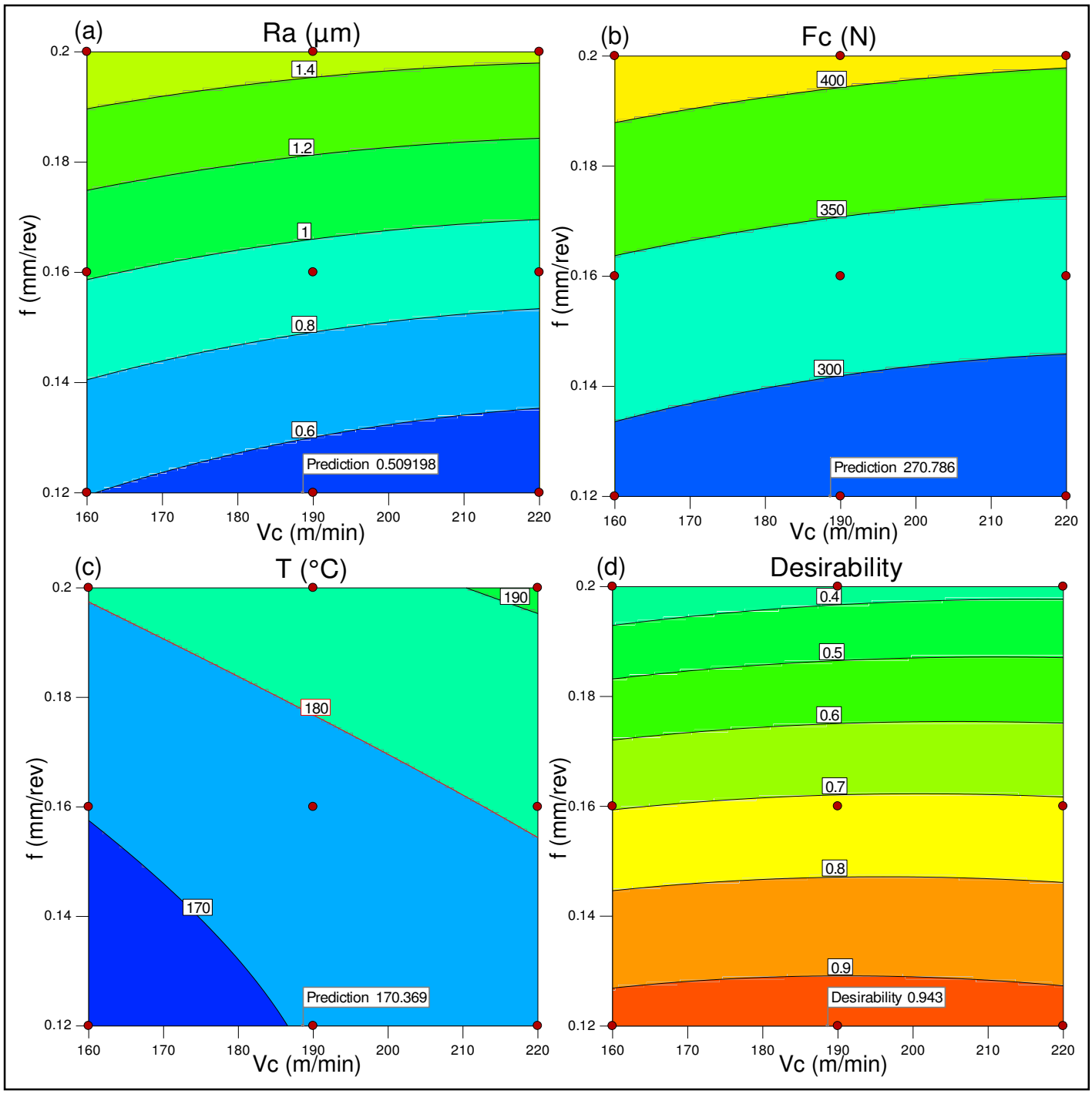

Figure 4.15. Contour plots for a) *Ra*, b) *Fc*, c) *T* and d) overall desirability.

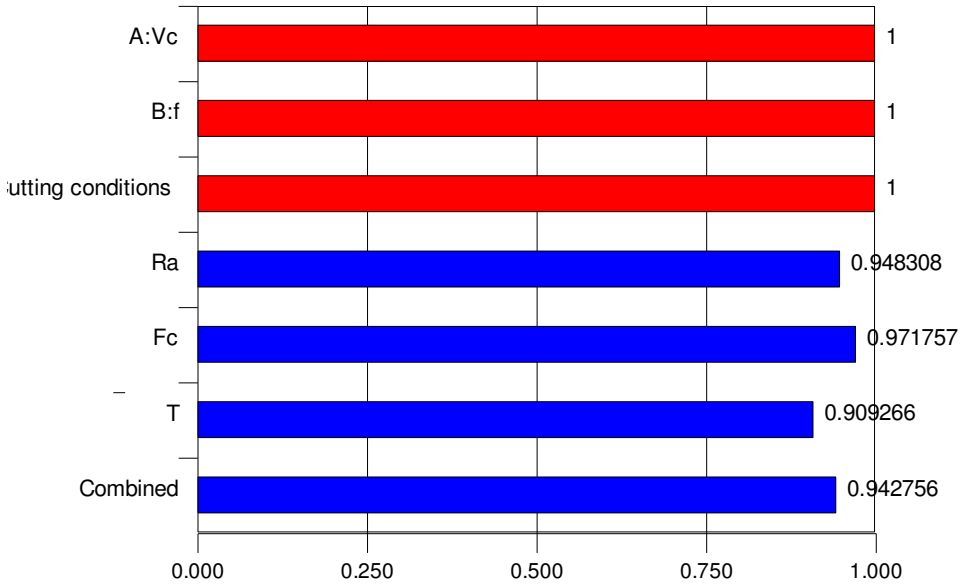

Figure 4.16: Desirability bar-graph for the optimization

Table 4.8. Comparison between optimal solutions delivered by DF and experimental run

Run	Process parameters			Outputs		
	Vc, m/min	*f*, mm/rev	Lubricating condition	*Ra*, *µm*	*Fc*, N	*T*, °C
DF	188	0.12	Graphene-MQL	0.51	270.77	170.37
Experimental run	190	0.12	Graphene-MQL	0.49	272.05	172.02
Deviation (%)				3.92	0.47	0.95

4.4. Conclusion

This research focuses on the analysis of surface roughness, cutting force, cutting temperature and flank wear in the turning of AISI 304 austenitic stainless steel under various cutting parameters and conditions, such as dry, MQL, nano MoS_2 reinforced nanofluid assisted MQL, MWCNT reinforced nanofluid assisted MQL, nano graphene reinforced nanofluid assisted MQL, MWCNT/MoS_2 reinforced hybrid nanofluid assisted MQL and nano graphene/MoS_2 reinforced hybrid nanofluid assisted MQL. The following conclusions were drawn after evaluating the data collected throughout the current work:

- Average surface roughness (*Ra*) was obtained to be 1.33 µm, 1.27 µm, 1.19 µm, 1.13 µm, 0.98 µm, 1.09 µm and 1.04 µm under dry, MQL, MoS_2-MQL, MWCNT-MQL, graphene-MQL, hybrid-1-MQL and hybrid-2-MQL conditions, respectively. Surface roughness was reduced by about 4.9%, 10.43%, 14.86%, 26.29%, 18.36% and 21.95% when MQL, MoS_2-MQL, MWCNT-MQL, graphene-MQL, hybrid-1-MQL and hybrid-2-MQL conditions were used, respectively, when compared to dry cutting.
- The cutting force (*Fc*) values were measured as 372.61 N, 357.55 N, 354.7 N, 352.38 N, 340.05 N, 349.32 N and 344.48 N under dry, MQL, MoS_2-MQL, MWCNT-MQL, graphene-MQL, hybrid-1-MQL and hybrid-2-MQL conditions, respectively. There was visible reduction in *Fc* by about 4.04%, 4.80%, 5.42%, 8.73%, 6.24% and 7.54% under MQL, MoS_2-MQL, MWCNT-MQL, graphene-MQL, hybrid-1-MQL and hybrid-2-MQL conditions, respectively, over dry cutting.
- The cutting temperature at the cutting zone was reduced by incorporating the vegetable cutting fluid into the turning process. In comparison with dry cutting, MQL, MoS_2-MQL, MWCNT-MQL, graphene-MQL, hybrid-1-MQL and hybrid-2-MQL conditions, respectively, showed approximately 3.82%, 6.08%, 8.06%, 14.21%, 10.18% and 12.29% lower cutting temperatures.
- Significant reductions of 6.67%, 11.11%, 17.78%, 48.89%, 24.44% and 33.33% in flank wear were obtained by using MQL, MoS_2-MQL, MWCNT-MQL, graphene-MQL, hybrid-1-MQL and hybrid-2-MQL conditions, respectively over dry cutting.

- The addition of nanoparticles (nano MoS_2, MWCNT, nano graphene and their hybrids) to the vegetable cutting fluid increases the solid-liquid interfacial contact zone, providing improved thermal-physical properties of the cutting fluid, thereby resulting in less *Ra*, *Fc*, *T* and *VB*.
- When all nanoparticles added to the vegetable cutting fluid were compared, the nano graphene reinforced nanofluid assisted MQL performed better in terms of improving machining measures. It is mostly owing to its better thermal conductivity, superior lubricating qualities, and greater wettability, which allows the vegetable cutting fluid to enhance its cooling/lubricating capabilities.
- The ANOVA analysis revealed that the feed had the most effective influence on *Ra* and *Fc,* with contribution ratios of 90.20% and 94.14%, respectively, while the lubricating conditions had the most influence on T*,* with a contribution ratio of 51.37%.
- The simulated models obtained using multi-regression analysis were statistically significant in terms of R^2, and their precision was verified using residual plots. As a result, the established models are useful for predicting *Ra*, *Fc* and *T* in straight turning of AISI 304 (ASS) material.
- Based on multi-criteria optimization findings, it was suggested that a cutting speed of 188 m/min, feed of 0.12 mm/rev and lubricating condition of nano graphene reinforced nanofluid assisted MQL method is a practical solution for dependently approaching the lower *Ra*, *Fc* and *T* values.

Even though the results of this investigation were highly beneficial for industrial practice as technical guidelines for using nano MoS_2, MWCNT and nano graphene reinforced nanofluids and their hybrids in the MQL method to improve turning process efficiency, some additional research is still needed to optimize the MQL flow rate and also to determine the effects of percentage weight and size of nano particles on the machining process performance.

General Conclusion

Machining of austenitic stainless steels, which are extensively employed in various industrial applications, is well-known as very demanding due to their low thermal conductivity and work hardening tendency. High cutting forces, high temperature generation at the cutting zone and rapidly progress in tool wear are the common problems encountered during their machining. These difficulties can have a negative impact on the machined part's cost and surface integrity, thereby reducing the productivity in machining of this kind of hard to cut materials.

This thesis focuses on addressing the afro-mentioned serious difficulties, aiming to improve the machinability of austenitic stainless steels (e.g. AISI 316L, AISI 304). The noteworthy general conclusions are summarized below:

- The comparison between Cermet and coated carbide inserts' performance enhances the engineers awareness about the machining issues before selecting the Cermet insert as a replacement for the coated carbide inserts.
- Cermet insert can be recommended to support the work of coated carbide for finish turning of stainless steel AISI 316L at cutting parameters ranging from cutting speed of (125-390) m/min, feed rate of (0.08-0.16) mm/rev and depth of cut of (0.1-0.3) mm.
- Taguchi method, Simulated Annealing and Simple Genetic Algorithm may be more effective in the case of a single response optimization. On the other hand, TOPSIS, Genetic Algorithm and Desirability function may be the best for multi-objective optimization.
- Comparison between different nanofluids revealed that Graphene nanofluid provided the best performance.

Current research contributions

The current research covers the research gap in the literature by focusing on:

- Preforming turning experiments on AISI 316L and AISI 304 under sustainable environments such as dry, MQL and nanofluid-MQL.
- Investigating of cermet insert performance to support the usage of coated carbide when turning austenitic stainless steel alloys.

- Applying a recent optimization approach called TOPSIS, which is an effective and efficient approach and certainly understandable, to convert the problems having multiple responses into a single response.
- Embracing Simulated Annealing (SA) and Genetic Algorithm (GA) appeared to be encouraging computational approaches for single and multi-objective optimization in order to obtain optimum cutting parameter sets.
- Adding nanoparticles (i.e., graphene, MoS2, MWCNT and their hybrids) into the vegetable oil cutting fluid, which was identified as critical for improving MQL efficiency.

Gaining knowledge regarding turning operations, cutting inserts performance, tool wear behavior and surface quality can contribute to improving the machinability of austenitic stainless steels under environmentally friendly environments (e.g. dry, MQL and nanofluid-MQL).

Future Perspective

Finally, the present study may be extended in the future work by taking the following points into account:

- Including more process parameters (i.e., radius nose, cutting tool geometry, MQL flow rate, percentage weight and size of nano particles) to study their effects on more measured responses (i.e., vibration, residual stresses).
- Analyzing the chip morphology in terms of chip thickness and color in order to give more details about the effects of cutting conditions on the chip-tool interface temperature.
- Application of other modelling methods such as (Artificial neural networks (ANN), Genetic programming (GP) and Fizzy logic flow) and other optimization methods (PSO and NSGAII)
- Developing an integrated finite element model (2D and 3D) to analyze the plasticity and thermomechanical reaction of the assessed cutting process of AISI 304 and AISI 316L alloys using DEFORM or ABAQUS software. The validation process of the constructed FEA model with experimental results should be performed.

- Comparing the technological characteristics results when turning austenitic stainless steel alloys using graphene, MWCNT, MoS2 nanofluids and their hybrids with other types of nanoparticles (i.e., Al_2o_3, CuO, and Fe_2O_3), and then exploring their tribological and heat transfer properties in turning performance.
- Creating a general evaluation model for turning process that incorporates five major sustainable metrics (i.e., energy consumption, machining costs, waste management, personal health and operational safety, environmental impact) in order to articulate the overall sustainability assessment index.

References

Chapter 1

[1.1] W. Grzesik, Advanced Machining processes of metallic materials: theory, modelling and applications, Elsevier, 2008.

[1.2] Kalpakjain S, Manufacturing Process for Engineering Materials, Addison-Wesley, New York, 2006.

[1.3] H A. Youssef, 'Types and classifications of stainless steels' in Machining of stainless steels and super alloys, John Wiley & Sons, Ltd, pp:11-26, 2016.

[1.4] Y. Seid Ahmed, Machinability enhancement of stainless steels through control of built-up edge formation, doctoral thesis, McMaster University, 2020.

[1.5] S. Kalpakjain, S.R Schmid, Manufacturing engineering and technology. Seventh edition, Prentice Hall: Upper Saddle River, NJ Pearson, 2014.

[1.6] S Wang, et al. Plastic deformation and fracture behaviors of nitrogen alloyed austenitic stainless steels. Materials science and engineering: A, 490 (1): p.95-104, 2008.

[1.7] M. Kaladhar, K.V. Subbaiah, C.H.S. Rao, Machining of austenitic stainless steels- a review, Int J Mach Mater, 12, 178, 2012.

[1.8] M. Anthony Xavior, M. Adithan, Determining the influence of cutting fluids on tool wear and surface roughness during turning of AISI 304 austenitic stainless steel, Journal of Materials Processing Technology, 209, pp.900-909, 2009.

[1.9] A.T. Abbas, S. Anwar, E. Abdelnasser, M. Luqman, J.E. A. Qudeiri, A. Elkaseer, Effect of different cooling strategies on surface quality and power consumption in finishing end milling of stainless steel 316, Materials 14, 903, 2021.

[1.10] F. Klocke, Manufacturing Processes 1: Cutting. Berlin, Heidelberg: Springer Berlin Heidelberg, 2011.

[1.11] M. Mia, P.R. Dey, M.S. Hossain, T. Arafat, M.D. Asaduzzaman, S. Ullah, Z.S.M. Tareq, Taguchi S/N based optimization of machining parameters for surface roughness, tool wear and material removal rate in hard turning under MQL cutting condition. Measurement. 122, 380-391 (2018).

[1.12] C. Y. H. Lim, P.P.T. Lau, S. C. Lim, The effects of work material on tool wear. Wear, 250, 344-348, 2001.

[1.13] R. M'Saoubi, H. Chandrasekaran, Investigation of the effects of tool micro-geometry and coating on tool temperature during orthogonal turning of quenched and tempered steel. International Journal of Machine Tools and Manufacturing, 44: 213-224, 2004.

[1.14] C.E.H. Ventura, J. Köhler, B. Denkena, Influence of cutting edge geometry on tool wear performance in interrupted hard turning, Journal of Manufacturing Process, 19, pp.129-134, 2015.

[1.15] T. Özel, T.K. Hsu, E. Zeren, Effects of cutting edge geometry, workpiece hardness, feed rate and cutting speed on surface roughness and forces in finish turning of hardened AISI H13 steel, International Journal of Advanced Manufacturing Technology, 25, pp.262-269, 2005.

[1.16] T. Zhao, J.M. Zhou, V. Bushlya, J.E. Stahl, Effect of cutting edge radius on surface roughness and tool wear in hard turning of AISI 52100 steel, International Journal of Advanced Manufacturing Technology, 91, 3611-3618, 2017.

[1.17] M. Lotfi, A.A. Farid, H. Soleimanimelhr, The effect of chip breaker geometry on chip shape, bending moment, and cutting force: FE analysis and experimental study, International Journal of Advanced Manufacturing Technology 78, pp.917-925, 2015.

[1.18] CIRP, Dictionary of production engineering, vol 2, Springer, Berlin, 2004.

[1.19] D. Jianxin, Z. Hui, Y. Pei, Wear mechanisms of cemented carbide tools in dry cutting of precipitation hardening semi-austenitic stainless steels. Wear, 270, 520-527, 2011.

[1.20] D. A. Stephenson, "Machinability of Materials," p. 42, 2016.

[1.21] G. List, Étude des mécanismes d'endommagement des outils carbure WC-CO par la caractérisation de l'interface outil-copeau-application à l'usinage à sec de l'alliage d'aluminium aéronautique AA2024 T351. Thèse de doctorat de l'école nationale supérieur d'arts et métiers de Bordeaux, 2004.

[1.22] Y. Touggui, S. Belhadi, S. Mechraoui, A. Uysal, M. Temmar, M.A. Yallese, Multi-objective optimization for turning parameters for targeting surface roughness and maximizing material removal rate in dry turning of AISI 316 L with PVD-coated cermet insert, SN Applied Sciences 2: 1360, (2020).

[1.23] B. Zou, H. Zhou, Ch. Huang, K. Xu, J. Wang, Tool damage and machined surface quality using hot-pressed sintering Ti(C7N3)/WC/TaC cermet cutting inserts for high-speed turing stainless steels, Inter J Adv Manuf Technol, 79, pp.197-210, 2015.

[1.24] D. Moskowitz, L.L. Terner, Cemented titanium carbonitrides: Effects of temperature and carbon-to-nitrogen ration, Mater Sci Eng, 265-268, 1988.

[1.25] Y. Kang, S. Kang, The surface microstructure of TiC-(Ti,W)C-WC-Ni cermets sintered in nitrogen atmosphere, Mater Sci Eng, 7241-7246, 2010.

[1.26] D.A. Stephenson, J.S. Agapiou, Metal cutting theory and practice, Mercel Dekker, Inc., New York, 2016.

[1.27] C. Subramanian and K.N. Strafford, Review of multicomponent and multilayer coatings for tribological applications, Wear 165, 85-95, 1993.

[1.28] S. Paldey and S.C. Deevi, Single layer and multilayer wear resistant coatings of (Ti, Al)N: A review, Mater Sci Eng, 342, 58-79, 2003.

[1.29] Documentation Sandvik Coromant. Main catalogue, the official website of the sandvik coromant, (2006): http://www.coromant.sandvik.com (accessed July, 15, 2020).

[1.30] I. Ciftci, Machining of austenitic stainless steels using CVD multi-layer coated cemented carbide tools,Tribology International, 39, pp. 565-569, 2006.

[1.31] P. Marimuthu, K. Chandrasekaran, Machinability study on stainless steel and optimum setting of cutting parameters in turning process using Taguchi design of experiments. Int.J. Materials and Product Technology 43(1-4),pp.122–133, 2012.

[1.32] M. Kaladhar, Evolution of hard coating materilas performance on machinability issues and material removal rate during turning operations, Mesurement, 135(1), pp.493-502, 2019.

[1.33] M. Kaladhar, K. Venkata Subbaiah, Ch. Srinivasa Rao, Performance evaluation of coating materials and process parameters optimization for surface quality during turning of AISI 304 austenitic stainless steel, International Journal of Engineering, Science and Technology, 3, pp.89-102, 2011.

[1.34] F.C. Victor Sousa and J.G. Francisco Silva, Recent advances in turning processes using coated tools-A Comprehensive Review. Metals, 2020.

[1.35] L. Bouzid, M.A. Yallese, S. Belhadi, L. Boulanouar, Tool life evaluation of cutting materials in turning of X20Cr13 stainless steel, Springer International Publishing Switzerland, 447-452, 2017.

[1.36] S. Gariani, Development and evaluation of a novel supply to reduce cutting fluid consumption and improve machining performance. Doctoral thesis, Northumbria University, 2019.

[1.37] V. Astakhov, Cutting fluids and their application in deep-hole machining, Available: http://viktorastakhov.tripod.com/DH/coolant-pd

[1.38] J. Vieira, À. Machado, E. Ezugwu, Performance of cutting fluids during face milling of steels, Journal of Materials Processing Technology, 166, pp.244-251, 2001.

[1.39] E. Kuram, B. Ozcelik, E. Demirbas, E. Sik, Effects of the cutting fluid types and cutting parameters on surface roughness and thrust force, in Proceedings of the World congress on Engineering, 2010.

[1.40] El Baradie M, Cutting fluids: Part I. Characterization, Journal of Materials Processing Technology, 56, 786-797, 1996.

[1.41] Debnath S, Reddy M, Yi Q, Environmental friendly cutting fluids and cooling techniques in machining: a review, Journal of Cleaner Production, 83, 33-47, 2014.

[1.42] S. El Wakil, Processes and design for manufacturing: Prentice-Hall, 1989.

[1.43] M. Sarikaya, M.K. Gupta, I. Tomaz, M. Danish, M. Mia, S. Rubaiee, M. Jamil, D.Y. Pimenov, N. Khanna, Cooling techniques to improve the machinability and sustainability of light-weight alloys: A state-of-the-art review, Journal of Manufacturing Processes, 62, pp.179-201, 2021.

[1.44] E.M. Trent, P.K. Wright, Metal cutting, Butterworth-Heinemann, Boston, 2000.

[1.45] K. Karino, Trouble shooting for cutting, Mitsubishi Materials, Japan, 1998.

[1.46] H. Youssef, H. El-Hofy, Principle of traditional and nontraditional machining, Dar Elfath Press, Alexandria, 2012.

[1.47] A. Mohanad, Machinability analysis of super austenitic stainless steel. PhD thesis, School of engineering Deakin university, Australia, 2017.

[1.48] E. M. Trent, Metal cutting, Butterworth's, London, U.K., pp.139-180, 1977.

[1.49] T. Kosa and R. P. Ney Sr., Machining of stainless steels, Metals Handbook, 16: Machining, 9th edn., ASM, Materials Park, OH, pp.681-707, 1989.

[1.50] R.A. Laghari, J. Li, M. Mia, Effects of turning parameters and parametric optimization of the cutting forces in machining SiCp/Al wt% composite, Metals,10, 840, 2020.

[1.51]: H. Ay, Heat transfer and life of metal cutting tools in turning, International Journal of Heat and Mass Transfer 41, pp. 613-623, 1998.

[1.52] A, Sebhi, Etude tribologique des outils de coupe et aciers, Thèse de doctorat, Université Ferhat Abbès-Sétif, Algérie 2013.

[1.53] J.M. Longbottom, J.D. Lanham, Cutting temperature measurement while machining-a review, Aircraft Engineering and Aerospace Technology, 77(2) pp.122-130, 2005.

[1.54] W.F. Sales, G. Guimaraes, A.R. Machado, E.O. Ezugwu, cooling ability of cutting fluids and the measurement of the chip-tool interface temperatures, Industrial Lubrication and Tribology, 54, pp.57-68, 2002.

[1.55] R.K. Kountanya, W.J. Endres, A high-Magbification experimental study of orthogonal cutting with edge-honed tools, ASME International Mechanical Engineering Congress and Exposition, New York, pp. 1-8, 2001.

[1.56] G. Boothroyed, Temperature in orthogonal metal cutting, Proceedings of the Institute Mechanical Engineers, 177(29), pp.789-810, 1963.

[1.57] M.B. da Silva, J. Wallbank, Cutting temperature: prediction and measurement methods- a review, Journal of Materials Processing Technology, 88, pp:195-202, 1999.

[1.58] L. Tu, F. Xu, W. Xue, J. Gao. S. Tian, M. Yuen. D. Zuo, Temperature distribution of cubic boron nitride-coated cutting tools by finite element analysis, International Journal of Advanced Manufacturing Technology, 105, pp.3197-3207, 2019.

[1.59] J.P. Davim, Machining of hard materials, Springer, London, 2011.

[1.60] H.J. Hu, W.J Huang, Tool life models of nano ceramic tool for turning hard steel based on FEM simulation and experiments, Ceramic International, 40(7), pp.8987-8996, 2014.

[1.61] K. Weinert, I. Inasaki, J.W. Sutherland, T. Wakabayashi, Dry machining and minimum quantity lubrication. CIRP Annals- Manufacturing Technology, 52(2), pp.511-537, 2004.

[1.62] M.J. Hadad, B. Sadeghi, Minimum quantity lubrication-MQL turning of AISI 4140 steel alloy. Journal of Cleaner Production, 54, pp.332-343, 2013.

[1.63] G. Boothroyed, Fundamentals of Machining and Machine Tools, 2nd ed., Marcel Dekker, 1989.

[1.64] E. Ezugwu, W. Sales, J. Landre, Machining dynamics in turning processes, in Machining dynamics, K. Cheng, Editor, pp:151-166, 2009.

[1.65] I. Rosenthal, E Tiferet, M Ganor, and A Stern, Post-processing of AM-SLM AlSi10Mg specimens: Mechanical properties and fracture behaviour' Ann. 'Dunarea Jos' Univ. Galati, Fascicle XII, Weld. Equip. Technol., Vol. 26, pp.33-38, 2015.

[1.66] Groover M.P. Fundamentals of modern manufacturing: materials processes, and systems. 2nd ed., New York: Johan Wiley & Sons, 2007.

[1.67] H. Aouici, M.A. Yallese, B. Fnides, K. Chaoui, T. Mabrouki, Modeling and optimization of hard turning of X38CrMoV5-1 steel with CBN tool: machining parameters effects on flank wear and surface roughness, J Mech Sci Technol 25(11): 2843-2851, 2011.

[1.68] R. Mahdavinejad and S. Saeedy, Investigation of the influential parameters of machining of AISI 304 stainless steel, Sadhana, 36(6), pp: 963-970, 2011.

[1.69] A. Sandvik, Modern Metal cutting-a practical handbook. Idereklam, Sandviken: Tofters Tryckeri AB, 1994.

[1.70] C. A. De. Oliveira Junior, A. E. Diniz, R. Bertazzolit, Correlationg tool wear, surface roughness and corrosion resistance in the turning process of super duplex stainless steel. J. Brazilian Soc. Mech. Sci. Mech. Sci. Eng, vol 36(4) pp.775-785, 2014.

[1.71] M. C. Shaw, The theory of metal cutting, in Proceedings of the Twenty-Fifth International Machine Tool Design and Research Conference, S. A. Tobias, Ed. London: Macmillan Education UK, pp.33-36, 1985.

[1.72] P. Benardos and G.C. Vosniakos, Predicting surface roughness in machining: a review, International Journal of Machine Tools and Manufacture, pp: 833-844, 2003.

[1.73] M. Davies, Y. Chou, C. Evans, On chip morphology, tool wear and cutting mechanics in finish hard turning. CIRP Annals-Manufacturing Technology, 45, pp: 77-82, 1996.

[1.74] G. Poulachon, A. Moisan, I. Jawahir, Tool-wear mechanisms in hard turning with polycrystalline cubic boron nitride tools. Wear, 250, pp: 576-586, 2001.

[1.75] I.S. Jawahir, C.A. van Luttervelt, Recent developments in chip control research and applications, CIRP Annals-Manufacturing Technology, 42(2), pp.659-693, 1993.

[1.76] G. Boothroyed and W.A. Knight, Fundamentals of machining and machine tools, CRC Press, Boca Raton, 2006.

Chapter 2

[2.1] A. Uysal, F. Demiren, E. Altan, Investigation of surface roughness and chips forms in milling of stainless steel by MQL Method, Acta Physica Polonica A 129(4): 439-441, 2016.

[2.2] M. Kaladhar, K.V. Subbaiah, C.H.S. Rao, Machining of austenitic stainless steels- a rview, Int. J. Machining and machinabilty of Meterilas 12(1/2):178-192, 2012.

[2.3] M. Kaladhar, Evolution of hard coating materilas performance on machinability issues and material removal rate during turning operations. Mesurement 135(1),493-502, 2019.

[2.4] U.S. Patel, S.K. Rawal, A.F.M. Arif, S.C. Veldhuis, Influence of secondary carbides on microstructure, wear mechanism, and tool performance for different cermet grades during high-speed dry finish turning of AISI 304 stainless steel. Wear 452-453, 2020.

[2.5] M. Nouioua, M. Yallese, R. Khettabi, S. Belhadi, M. Bouhalais, F. Girardin, Investigation of the performance of the MQL, dry and wet turning by response surface methodology (RSM) and artificial neural network (ANN), Int J Adv Manuf Technol 93(5-8):2485-2504, 2017.

[2.6] A. Laouissi, M. Yallese, A. Belbah, S. Belhadi, A. Haddad, Investigation, modeling, and optimization of cutting parameters in turning of gray iron using coated and uncoated silicon nitride ceramic tools. Based on ANN, RSM, and GA optimization. Int J Adv Manuf Technol 101:523-548,2019.

[2.7] H. Tebassi, M.A. Yallese, I. Meddour, F. Girardin, T. Mabrouki, On the modeling of surface roughness and cutting force when turning of Incol 718 using artificial neural network and response surface methodology: accuracy and benefit, Period Polytech Mech Engrg 61 (1):1-11, 2017.

[2.8] A.K. Gupta, Predicive modelling of turning operations using response surface methodolgy, artificial neural networks and support vector regression, Int J Adv Manuf Technol 48:763-778, 2010.

[2.9] M. Mia, M.D.A.Khan, N.R. Dhar, Study of surface roughness and cutting forces using ANN, RSM and ANOVA in turning of Ti-6Al-4V under cryogenic jets applied at flank and rake feces of coated WC tool, Int J Adv Manuf Technol, 93:975-991, 2017.

[2.10] A. Bouziane, L. Boulanouar, M.W. Azizi, O. Keblouti, S. Belhadi, Analysis of cutting forces and roughness during hard turning of bearing steel, Structural Engineering and Mechanics 66.3: 285-294, 2018.

[2.11] M. Kaladhar, K. Venkata Subbaiah, R.C. Srinivasa, Determination of optimum Process Parameters during turning of AISI 304 Austenitic stainless steels using Taguchi method and ANOVA. *International Journal of lean thinking*; 1: 1-19, 2012.

[2.12] B. Lakhder, S. Boutabba, M.A. Yallese et al, Simultaneous optimization of surface roughness and material removal rate for turning of X20Cr13 stainless steel. International Journal of Advanced Manufacturing Technology, 74: 879-891, 2014.

[2.13] Y. Seid Ahmed, H. Youssef, H. El-Hofy, Prediction and Optimization of Drilling Parameters in Drilling of AISI 304 and AISI 2205 Steels with PVD Monolayer and Multilayer Coated Drills, Journal of Manufacturing and Materials Processing 2(1): 1-16, 2018.

[2.14] M. Sarikaya and V. Yilmaz, Optimization and predictive modeling using S/N, RSM, RA and ANNs for micro-electrial disharge drilling of AISI 304 stainless steel. Neural comput &Applic 30, 1503-1517, 2018.

[2.15] A. Selaimia, M.A. Yallese, H. Bensouilah, I.K. Meddour, R. Khattabi, T. Mabrouki, Modeling and optimization in dry face milling of X2CrNi18-9 austenitic stainless steel using RMS and Desirability approach. Measurement. 107(1), 53-67, 2017.

[2.16] M. Mia, M.A. Bashir, M.A. Khan, N.R. Dhar, optimization of MQL flow rate for minimum cutting force and surface roughness in end milling of hardened steel (HRC40). Int J Adv Manu Technol 89:675-690, 2017.

[2.17] A.M. Zain, H. Haron, S. Sharif, Genetic algorithm and simulated annealing to estimate optiman process parameters of the abrasive waterjet machining, Engineering with Computers, 27:251-259, 2011.

[2.18] M. Mia, N.R. Dhar, Modeling of Surface Roughness using RSM, FL and SA in dry hard turning, Arab J Sci Eng (43), 1125-1136, 2018.

[2.19] M. Mia, N.R. Dhar, Prediction and optimization by using SVR, RSM and GA in hard turning of temperated AISI 1060 steel under effective cooling condition. Neural Comput & Applic 31:2349-2370, 2019.

[2.20] S.A. Bagaber and A.R. Yousof, Multi objective optimization of cutting parameters to minimize power consumption in dry turning of stainless steel 316, Journal of cleaner Production 157: 30-46, 2017.

[2.21] S. Berkani, M.A. Yallese, L. Boulanouar, T. Mabrouki, Statistcal analysis of AISI 304 austenitic stainless steel machining using Ti(C,N)/ Al_2O_3/IiN CVD coated carbide tool, International Journal od Industrial Engineering Computations 6:539-522, 2015.

[2.22] A. Zerti, M.A. Yallese, I. Meddour, S. Belhadi, A. Haddad, T. Mabrouki, Modeling and multi-objective optimization for minimizing surface roughness, cutting force, and power, and maximizing productivity for tempered stainless steel AISI 420 in turning operations, Int. J. Adv. Manuf. Technol 102:135-157, 2019.

[2.23] N. Metropolis, A. Rosenbluth, M. Rosenbluth, A. Teller, Equation of state calculations by fast computing machines, J. Chem. Phys, 21, 1087-1092, 1953.

[2.24] S. Kirkpatrick, C.D. Gelatt, M.P. Vecchi, Optimization by simulated annealing, Science, 220, 671-680.

[2.25] S.P. Brooks and B.J.T. Morgan, Optimization using simulated annealing, Journal of the Royal Statistical Society, Series D, 44(2), pp: 241-257, 1995.

[2.26] M.A. Sofuoğlu, F.H. Çakir, M.C. Kuşhan, S. Orak, Optimization of different non-traditional turning processes using soft computing methods, Soft computing 23: 5213-5231, 2019.

[2.27] J.H. Holland, Adaptation in natural and artificial systems. Volume 31, MI: University of Michigan Press, 1975.

[2.28] M. Srinivas and L.M. Patnaik, Genetic algorithms: a survey, Computer, 27(6), pp:17-26, 1994.

[2.29] J.C. Spall, Introduction to stochastic search and optimization: Estimation, Simulation, and Control, Chapter9, Wiley INTERSCIENCE, 2003.

[2.30] A. Caggioano, Tool wear prediction in Ti-6Al-4V machining through multiple sensor monitoring and PCA features pattern ercongnition, Sensors (Switzerland) 18, 823, 2018.

[2.31] V. Meruane, Damage assessment algorithms for structural health monitoring, EBook 'Chapter 7', Taylor & Francis Group, 2016. https://doi.org/10.1201/9781315373492

[2.32] J.H. Holland, Adaptation in natural and artificial systems, University of Michigan Press Ann Arbor, 1975.

[2.33] J.A. Joines and C.R. Houck, On the use of non-stationary penalty functions to solve nonlinear constrained optimization problems with GA's, In IEEE International Symposium Evolutionary Computation, pp: 579-584, Orlando, USA, 1994.

[2.34] B.L. Miller and D.E. Goldberg, Genetic algorithms, tournament selection, and the effect of noise, Technical report 95006, Department of General Engineering, University of Illinois at Urbana-Champaign, 1995.

[2.35] H.M. Elkamchouchi and M.M. Wagih, Genetic algorithm operators effect in optimizing the antenna array pattern synthesis, In Proceeding of the 20th National Radio Science Conference, Cairo, Egypt, 2003.

[2.36] T.D. Gwiazda, Genetic algorithms reference Volume I Crossover for single-objective numerical optimization problems, Tomaszgwiazda e-Books, 2006.

[2.37] Z. Michalewicz, Genetic Algorithms+ Data Structures= Evolution Programs, Springer, 1996.

[2.38] M.M.A. Hashem, M. Watanabe, K. Izumi, Evolution strategy: a new time-variant mutation for fine localtuning, in Proceedings of the 36th SICE Annual Conference, pp:1099-1104. 1997.

[2.39] K. Deep and M. Thakur, A new mutation operator for real coded genetic algorithms, Applied Mathematics and Computation, 193(1), pp:211-230, 2007.

[2.40] T.D. Gwiazda, Genetic algorithms reference Volume II Mutation for numerical optimization problems, Tomaszgwiazda e-Books, 2007.

[2.41] D. Wu, C. Jennings, J. Terpenny, R. Gao, S. Kumara, A comparative study on machine learning algorithms for smart manufacturing: tool wear prediction using random forests, Journal of Manufacturing Science and Engineering, 139 (7):071018, 2017.

[2.42] O. Zerti, M.A. Yallese, R. Khettabi, K. Chaoui, T. Mabrouki, Design optimization for minimum technological parameters when dry turning of AISI D3 steel using Taguchi method. Int J Adv Manuf Technol 89: 1915-1934, 2016.

[2.43] D.A. Stephension and J.S. Agaipou, Metal cutting theaory and Practice, third ed., third ed., CRC Press, Taylor & Francis Group, https://doi.org/10.1201/b19559, 2016.

[2.44] M. Mia, N.R. Dhar, Prediction of surface roughness in hard turning under high pressure coolant using artificial neural network, Measurment 92:464-474, 2016.

[2.45] A.J. Oliveria, A.E. Diniz, D.J. Ursolino, Hard turning in continuous and interrupted cut with PCBN and whisker reinforced cutting tools, J Master Process Technol 209(12): 5262-5270, 2009.

[2.46] R. Saidi, B. Ben Fathallah, T. Mabrouki, S. Belhadi, M.A. Yallese, Modeling and optimization of the turning parameters of cobalt alloy (Stellite 6) based on RSM and desirabilty function. Int J Adv Manuf Technol 100: 2945-2968, 2019.

[2.47] R.M.D. Karim, F. Dilwar, R.A. Siddique, Predicitve Modeling of surface roughness in MQL assisted turning of SiC-Al alloy composites using Artificial neural network and adaptive Neuro fuzzy interface system, Journal of advanced research in Manufactring Material Science& Metallurgical Engineering, 5(3): 12-28, 2018.

[2.48] K. Bouacha, M.A. Yallese, K. Chaoui, S. Belhadi, Analysis and optimization of hard turning operation using cubic boron nitride tool, Int J Refract Metal Hard Mater 45: 160-178, 2014.

[2.49] B. Rajeswari and K.S. Amirthagadeswaran, Study of machinability and parametric optimization of end milling on aluminim hybrid composites using multi-objective genetic algorithm. Journal of thr Brazilian Society of Mechanical Science and Engineering, 40:377, 2018.

[2.50] H. Aouici, M.A. Yallese, B. Findes, K. Chaoui, T. Mabrouki, Modeling and optimization of hard turning of X38CrMoV5-1 steel with CBN tool:machining parameters effects on flank wear and surface roughnes, J ;ech Sci Technol 25 (11): 2843-2851, 2011.

[2.51] M.A. Yallese, L. Boulanour, K. Chaoui, Machining of hardened 100Cr steel using a cubic boron nitride tool. Mecanique & industries, 5:355-368, 2004.

[2.52] M.A. Yallese, K. Chaoui, N. Zeghib, L. Boulanour, J.F. Rigal, Hard machining of hardened bearing steel using cubic boron nitride tool. J Mater Process Technol 209(2): 1092-1104, 2009.

[2.53] H. Bouchelaghem, M.A. Yallese, T. Mabrouki, A. Amirat, J.F. Rigal, Experimental investigation and performance anatyses of CBN insert in hard turning of cold work tool steel (D3), Mach Sci Technol 14(14):471-501, 2010.

[2.54] R. Nur, M.Y. Noordin, S. Izman, D. Kurniawn, Machining parameters effect in dry turning of AISI 316L stainless steel using coated carbide tools, J Process Mechanical Engineering 231(1): 676-683, 2017.

[2.55] R. Singh, J.S. Dureja, M. Dogra, J.S. Randdhawa, Optimization of machining parameters under MQL turning of Ti-6Al-4V alloy with textured tool using multi-attribute decision-making methods. World Journal of Engieering, 16 (5), 648-659, 2019.

[2.56] G.M. Krolczyk, R.W. Maruda, P. Nieslony, M. Wieczornwski, Surface morphology analysis of Dublex stainless steel (DSS) in clean production using the power spectral density. 94: 654-470, 2016.

Chapter 3

[3.1] L. Bouzid, S. Berkani, M.A. Yallese et al, Estimation and optimization of flank wear and tool lifespan in finish turning of AISI 304 stainless steel using desirability function approach, *International Journal of Industrial Engineering Computations*; 9 (3): 349-368, 2018.

[3.2] R. Nur, M.Y. Noordin, S. Izman et al, Machining parameters effect in dry turning of AISI 316L stainless steel using coated carbide tools. *Journal of Process Mechanical Engineering*; 231(1): 676-683, 2017.

[3.3] M. Kaladhar, K. Venkata Subbaiah, R.C. Srinivasa, Determination of optimum Process Parameters during turning of AISI 304 Austenitic stainless steels using Taguchi method and ANOVA. *International Journal of lean thinking*; 1: 1-19, 2012.

[3.4] P. Marimuthu, and K. Chandrasekaran, Machinability study on stainless steel and optimum setting of cutting parameters in turning process using Taguchi design of experiments. *Int J Materials and Product Technology*; 43(1-4): 122–133, 2012.

[3.6] Y. Seid Ahmed , H, Youssef, H. El-Hofy et al, Prediction and Optimization of Drilling Parameters in Drilling of AISI 304 and AISI 2205 Steels with PVD Monolayer and Multilayer Coated Drills. *Journal of Manufacturing and Materials Processing*; 2(1): 1-16, 2018.

[3.7] I. Nomani, A. Pramanik, T. Hilditch et al, Machinability study of first generation duplex (2205), second generation duplex (2507) and austenite stainless steel during drilling process. *Wear* , 304: 20-28, 2013.

[3.8] K. Ananthakumar, D. Rajamaani, E. Balasubramanian et al, Measurement and optimization of multi-response characteristics in plasme arc cutting of Monel 400™ using RSM and TOPSIS. Measurement 135(1): 725-737, 2019.

[3.9] S.A. Bagaber and A.R. Yousof, Multi objective optimisation of cutting parameters to minimise power consumption in dry turning of stainless steel 316. *Journal of cleaner Production*, 157(1): 30-46, 2017.

[3.10] D.P. Selvaraj and P. Chandramohan, Optimization of surface roughness of AISI 304 Austenitic Stainless steel in dry turning operation using Taguchi design method. Eng Sci Technol; 5: 293-301, 2010.

[3.11] A. Selaimia, M.A. Yallese, H. Bensouilah et al, Modeling and optimization in dry face milling of X2CrNi18-9 austenitic stainless steel using RMS and Desirability approach. Measurement, 107(1): 53-67, 2017.

[3.12] L. Bouzid, S. Boutabba, M.A. Yallese et al, Simultaneous optimization of surface roughness and material removal rate for turning of X20Cr13 stainless steel. International Journal of Advanced Manufacturing Technology, 74: 879-891, 2014.

[3.13] O. Zerti, M.A. Yallese, R. Khettabi et al, Design optimization for minimum technological parameters when dry turning of AISI D3 steel using Taguchi method. International Journal of Advanced Manufacturing Technology; 89(5-8): 1915-1934, 2017.

[3.14] S. Sudhagar, M. Sakthivel, P.J. Mathew et al, A multi criteria descision making approach for process improvement in friction stir welding of Aluminium Alloy. Measurement; 108: 1-8, 2017.

[3.15] A. Khan and K. Maity, Application potential of combined fuzzy-TOPSIS approach in minimization of surface roughness, cutting force and tool wear during machining of CP-Ti grade II. Soft Computing, 15: 6667-6678, 2018.

[3.16] K. Anand Babu, P. Venkataramaiah, P. Dileep, AHP-Deng's similarity based optimization of WEDM process parameters of Al/SiCp composite. American Journal of Materials Science and Technology , 6 (1): 1-14, 2017.

[3.17] S. Chakraborty, P. Chatterjee, P.P. Das, A DoE- TOPSIS method based meta-model for parametric optimization of non traditional machining processes. Journal of Modelling in Management, 14 (2): 430-455, 2019.

[3.18] T. Sugihara, P. Singh, T. Enomoto, Development of novel cutting tools with dimple textured surfaces for dry machining of aluminum alloys. Procedia Manufacturing, 14: 111-117, 2017.

[3.19] F.A.E.G. Klocke, G. Eisenblatter, Dry cutting, CIRP Annals 46, 519-526, 1997.

[3-20] D.P. Adler, S. Hii WW, D.J. Michalek, J.W. Sutherland, Examining the role of cutting fluids in machining and efforts to address associated environmental/health concerns. Mach Sci Technol, 10, 23-58, 2006.

[3.21] J. Deng, S. Wenlong, Z. Hui, Design, fabrication and properties of a self-lubricated tool in dry cutting. Int J Mach Tools Manuf 49, 66-72, 2009.

[3.22] H. Abdelrazek Ali, I.A. Choudhury, Y. Nukman, S.N. Kazi, Metal cutting lubricants and cutting tools: a review on the performance improvement and sustainability assessment, International Journal of Advanced Manufacturing Technology, 106: 4221-4245, 2020.

[3.23] S. Kalpakjain, S.R Schmid, Manufacturing engineering and technology. Seventh edition, Prentice Hall: Upper Saddle River, NJ Pearson, 2014.

[3.24] G. E. D'Errico, E. Guglielmi, G. Rutelli, A study of coatings for ends mills in high speed metal cutting, Journal of Materials Processing Technology, 92-93, pp:251-256, 1999.

[3.25] C.G. Guleryuz, J.E. Krzanowski, S.C. Veldhuis, G.S. Fox-Rabinovich, Machining performance of TiN coatings incorporating indium as solid lubricant, Surface and Coatings Technology, 203, pp. 3370-3376, 2009.

[3.26] H. Hanyu, Y Murakami, S. Kamiya, M. Saka, New diamond coating with finely crystallized smooth surface for the tools to achieve fine surface finish of non-ferrous metals, Proceedings of Frontiers of Surface Engineering, 169-170, pp: 258-261, 2003.

[3.27] G.R. Dos Santos, D.D. Da Costa, F.L. Amorim, R.D. Torres, Characterization of DLC thin film and evaluation of machining forces using coated inserts in turning of AL-Si alloys, Surface & Coating Technology, 202, pp: 1029-1033, 2007.

[3.28] A. Shokrani, V. Dhokia, S.T. Newman, Environmentally conscious machining of difficult-to-machine materials with regard to cutting fluids, Inter J Mach Tools Manuf, 57, pp:83-1010, 2012.

[3.29] S. Debnath, M.M Reddy, Yi Qs, Environmental friendly cutting fluids and cooling techniques in machining: a review, J Clean Prod, 83, pp:33-47, 2014.

[3.30] M. Sarikaya, M.K. Gupta, I. Tomaz, M. Danish, M. Mia, S. Rubaiee, M. Jamil, D.Y. Pimenov, N. Khanna, Cooling techniques to improve the machinability and sustainability of light-weight alloys: A state-of-the-art review, Journal of Manufacturing Processes, 62, pp.179-201, 2021.

[3.31] I.H. Mulyadi, Improving the performance of minimum quantity lubrication in high speed milling and environmental performance analysis, PhD thesis, University of Manchester, 2013.

[3.32] P.S. Sreejith, B.K.A. Ngoi, Dry machining: Machining of the future, Journal of Materials Processing Technology, 101, pp: 287-291, 2000.

[3.33] K. Weinert, I. Inasaki, J.W. Sutherland, T. Wakabayashi, Dry machining and minimum quantity lubrication. CIRP Ann, 53:511-37, 2004.

[3.34] B. Sorana and J. Lorentz, Design of experiments: Useful orthogonal arrays for number of experiments from 4 to 16, Entropy, 9, pp: 198-232, 2007.

[3.35] H. Chibane, Contribution à l'optimisation multi-objectif des paramètres de coupe en usinage et apport de l'analyse vibratoire : Application aux matériaux métallique et composites, Thèse doctorat, Université François-Rabelais de Tours, 2013.

[3.36] S. Gariani, Development and evaluation of a novel supply to reduce cutting fluid consumption and improve machining performance. Doctoral thesis, Northumbria University, 2019.

[3.37] M. Ramana, G. Rao, D. Rao, Experimental investigation, optimization of process parameters and mathematical modelling in turning of titanium alloy under different lubricant conditions, Journal of Engineering (IOSRJEN),2, pp:86-101, 2012.

[3.38] M. Cavazzuti, Design of experiments; in optimization methods, Springer, pp. 13-42, 2013.

[3.39] I. Mukherjee and P. Ray, A review of optimization techniques in metal cutting processes, Computers & Industrial Engineering, 50, pp. 15-34, 2006.

[3.40] E. Dean, Design of experiments, ed, 2000.

[3.41] V. Balakumaran, C. Parthasarathy, J. Chandradass, Optimization of drilling parameters on EN31 steel with Chromium coated drill bit by using Taguchi method. *Asian Rev Mech Eng* 4, pp:18-22, 2015.

[3.42] H.R. Myers, A.I. Khuri, G. Vining, Response surface alternatives to the Taguchi robust parameter design approach, The American statistician, 46, pp: 131-139, 1992.

[3.43] W.T. Foster, Basic Taguchi design of experiments, National association of industrial technology conference, Pittsburgh, PA, 2000.

[3.44] G. Taguchi, System of experimental design, Quality resources, 1987.

[3.45] Montgomery DC. Design and Analysis of Experiments. *8nd edition, John Wiley & Sons, New York* 2013.

[3.46] Norme International ISO 3534-3. Statistics Vocabulary and Symbols Part 3: Design of experiments, 1999.

[3.47] B. Soulier, Sur la modélisation expérimentale en mécanique : précision, optimisationet applications industrielles, Thèse doctorat E.N.S. de Cachan, 1994.

[3.48] J.H.W. Nicolodi, L.A. Consalter, O. Duràn et al, Effect of wear progression in an 'S'-type mixed ceramic tool on machining forces and surface roughness in the turning of hardened AISI 4140 steel. Int J Machining and Machinabilty of Materials 21 (3): 228-243, 2019.

[3.49] Y. Seid Ahmed, J.M. Paiva, B. Bose et al, New observation on built-up edge structures for improving machining performance during the cutting of superduplex stainless steel. Tribology International 137: 212-227, 2019.

[3.50] A. Hamdan, A.D. Ahmed, M. Hamdi, An optimisation method of the machining parameters in high-speed machining of stainless steel using coated carbide tool for best surface finish, The International Journal of Advanced Manufacturing Technology; 58: 81-91, 2012.

[3.51] A. Khan A and N.R. Dhar, Performance evaluation of minimum quantity lubrication by vegetable oil in term of cutting force, cutting zone temperature, tool wear, job dimension and surface finish in turning AISI-1060 steel. J Zhejiang University *7*, 1790-1799, 2006.

[3.52] I. Ciftci, Machining of austenitic stainless steels using CVD multi-layer coated cemented carbide tools. Tribology International, 39: 565-569, 2006.

[3.53] F.R. Lima Junior, L. Osiro, L. Carpinetti, A comparison between fuzzy AHP and fuzzy TOPSIS methods to supplier selection. Applied soft compution, 21: 194-209, 2014.

[3.54] M. Yurdakul and Y.Y. İç, Develpment of a performance measurment model for manufacturing companies using AHP and TOPSIS approaches. International Journal of Production Resarch, 43 (21): 4609-4641, 2005.

[3.55] F. Klocke, Manufacturing processes 1 cutting. *Springer Heidelberg Dordrecht London New York* 2011.

Chapter 4

[4.1] M. Mia, M.K. Gupta, G. Singh, G. Krolczyk, D.Y. Pimenov, An approach to cleaner production for machining hardened steel using different cooling-lubrication conditions, J Clean Prod 187: 1069-1081, 2018.

[4.2] M.A.M. Ali, A.L. Azmi, M.N. Murad, M.Z.M. Zain, A.N.M. Khalil, N.A. Shuaib, Roles of new bio-based nanolubricants towards eco-friendly and improved machinability of Inconal 718 alloy, Tribology International 144: 106106, 2020.

[4.3] C.V. Yildirim, T. Kivak, M. Sarikaya, F. Erzincanli, Determination of MQL parameters contributing to sustainable machining in the milling of nickel-base superalloy waspaloy, Arabian J Sci Eng; 42: 4667-4681, 2017.

[4.4] B. Sen, S.A.I. Hussain, M. Mia, U.K. Mandal, S.P. Mondal, Selection of an ideal MQL-assisted milling condition: an NSGA-II-coupled TOPSIS approach for improving machinability of Inconel 690, Int J Adv Manuf Technol 103: 1811-1829, 2019.

[4.5] M. Nouioua, M.A. Yallese, R. Khettabi, S. Belhadi, T. Mabrouki, Comparative assessment of cooling conditions, including MQL technology on machining factors in an environmentally friendly approach. Int J Manuf Technol 91:3079-3094, 2017.

[4.6] C.V. Yildirim, T. Kivak, F. Erzincanli, Tool wear and surface roughness analysis in milling with ceramic tools of Waspaloy: A comparison of machining performance with different cooling methods. J Brazilian Soc. Mech. Sci. Eng 41, 83, 2019.

[4.7] M. Sarikaya and A. Güllü, Multi-response optimization of minimum quantity lubrication parameters using Taguchi-based grey relational analysis in turning of difficult-to-cut alloy Haynes 25, J Clean Prod 91: 347-357, 2015.

[4.8] M. Elbah, H. Laouici, S. Benlahmidi, M. Nouioua, M.A. Yallese, Comparative assessment of machining environments (dry, wet and MQL) in hard turning of AISI 4140 steel with CC6050 tools, Inter J Manuf Technol 105, 2581-2597, 2019.

[4.9] K.M. Li and C.P. Lin, Study on minimum quantity lubrication in micro-grinding. Inter. J. Adv. Manuf. Technol 62, 99-105, 2012.

[4.10] G. Singh, C.I. Pruncu, M.K. Gupta, M. Mia, A.M. Khan, M. Jamil, D.Y. Pimenov, B. Sen, V.S. Sharma, Investigations of machining characteristics in the upgraded MQL-assisted turning of pure titanium alloys using evolutionary algorithms, Materials 19, 999, 2019.

[4.11] S.S. Bedi, G.C. Behera, S. Datta, Effects of cutting speed on MQL machining performance of AISI 304 stainless steel using uncoated carbide insert: application potential of coconut oil and rice bran oil as cutting fluids. Arabian Journal for Science and Engineering 45: 8877-8893, 2020.

[4.12] J. Rajaguru and N. Arunachalam, A comprehensive investigation on the effect of flood and MQL coolant on the machinability and stress corrosion cracking of super duplex stainless steel. Journal of Materials Processing Tech 276, 116417, 2020.

[4.13] A. Uysal, Investigation of flank wear in MQL milling of ferritic stainless steel by using nano graphene reinforced vegetable cutting fluid. Industrial Lubrication and Tribology 68/4: 446-451, 2016.

[4.14] A. Uysal, An experimental study on cutting temperature and burr in milling of ferritic stainless steel under MQL using nano graphene reinforced cutting fluid. Advanced Materials Proceedings 2 (9): 560-563, 2017.

[4.15] G.M. Krolczyk, R.W. Maruda, J.B. Krolczyk, S. Wojciechowski, M. Mia, P. Nieslony, G. Budzik, Ecological trends in machining as a key factor in sustainable production- A review, J Clean Prod 218: 601-615, 2019.

[4.16] M.K. Gupta, M. Jamil, X. Wang, Q. Song, Z. Liu, M. Mia, H. Hegab, A.M. Khan, A.G. Collado, C.I. Pruncu, G.M. Shah Imran, Performance evaluation of vegetable oil-based nano-cutting fluids in environmentally friendly machining of Inconel-800 Alloy. Materials 12, 2792, 2019.

[4.17] A.K. Sharma, A.K. Tiwari, A.R. Dixit, Effects of minimum quantity lubrication (MQL) in machining processes using conventional and nanofluid based cutting fluids: A review, J. Clean. Prod 127: 1-18, 2016.

[4.18] A.K Sharma, R.K. Singh, A.R. Dixit, A.K. Tiwari, Characterization and experimental investigation of Al_2O_3 nanoparticle based cutting fluid in turning of AISI 1040 steel under minimum quantity lubrication (MQL), Mater. Today Proc 3: 1899-1906, 2016.

[4.19] M. Jamil, A.M. Khan, H. Hegab, L. Gong, M. Mia, M.K. Gupta, N. He, Effects of hybrid Al_2O_3-CNT nanofluids and cryogenic cooling on machining of Ti-6Al-4V, Int. J. Adv. Manuf. Techno 102: 3895-3909, 2019.

[4.20] H. Hegab, U. Umer, M. Soliman, H.A. Kishawy, Effects on nano-cutting fluids on tool performance and chip morphology during machining Inconel 718. Inter J Adv Maunf Technol 96: 3449-3458, 2018.

[4.21] A. Das, S. Kumar Patel, S.R. Das, Performance comparison of vegetable oil based nanofluids towards machinability improvement in hard turning of HSLA steel using minimum quantity lubrication, Mechanics & Industry 20, 506, 2019.

[4.22] O. Öndin, T. Kıvak, M. Sarıkaya, Ç.V. Yıldırım, Investigation of the influence of MWCNTs mixed nanofluid on the machinability characteristics of PH 13-8 Mo stainless steel, Tribology International 148:106323, 2020.

[4.23] A. Uysal, F. Demiren, E. Altan, Applying minimum quantity lubrication (MQL) method on milling of martensitic stainless steel by using nano MoS_2 reinforced vegetable cutting fluid. Procedia- Social and Behavioral Sciences 195, 2742-2747, 2015.

[4.24] P.B. Patole and V.V. Kulkarni, Optimization of process parameters based on surface roughness and cutting force in MQL turning of AISI 4340 using nano fluid. Mater. Today Proc 5 :104-112, 2018.

[4.25] R. Singh, J.S. Dureja, M. Dogra, M.K. Gupta, M. Mia, Influence of graphene-enriched nanofluids and textured tool on machining behavior of Ti-6Al-AV alloy, Inter J Adv Manuf Techno 105: 1685-1697, 2019.

[4.26] A.K. Sharma, A.K. Tiwari, A.R. Dixit, R.K. Singh, Measurement of machining force and surface roughness in turning of AISI 304 steel using alumina-MWCNT hybrid nanoparticles enriched cutting fluid, Measurement 150, 107078, 2020.

[4.27] S. Gugulothu and V.K. Pasam, Experimental investigation to study the performance of CNT/MoS_2 hybrid nanofluid in turning of AISI 1040 steel. Australian Journal of Mechanical Engineering, 2020 https://doi.org/10.1080/14484846.2020.1756067.

[4.28] Z. Said, M. Gupta, H. Hegab, N. Arora, A.M. Khan, M. Jamil, E. Bellos, A comprehensive review on minimum quantity lubrication (MQL) in machining processes using nano-cutting fluids, Inter J Adv Manuf Technol, 105, pp:2057-2086.

[4.29] R. Saidur, K.Y. Leong, H.A. Mohammad, A review on applications and challenges of nanofluids, Renewable and Sustainable Energy Reviews, 15, pp: 1646-1668.

[4.30] M. Sarikaya, M.K. Gupta, I. Tomaz, M. Danish, M. Mia, S. Rubaiee, M. Jamil, D.Y. Pimenov, N. Khanna, Cooling techniques to improve the machinability and sustainability of light-weight alloys: A state-of-the-art review, Journal of Manufacturing Processes, 62, pp.179-201, 2021.

[4.31] Y. Touggui, S. Belhadi, A. Uysal, M. Temmar, M.A. Yallese, A comparative study on performance of cermet and coated carbide inserts in straight tuning AISI 316L austenitic stainless steel. Inter J Adv Manuf Techno 112: 241-260, 2021.

[4.32] R.K. Singh, A.R. Dixit, A. Mandal, A.K. Sharma, Emerging application of nanoparticle-enriched cutting fluid in metal removal processes: a review, J. Braz. Soc. Mech. Sci. Eng 39, 4677-4717, 2017.

[4.33] Ç.V. Yıldırım, T. Kıvak, M. Sarıkaya, Ş. Şirin, Evaluation of tool wear, surface roughness/topography and chip morphology when machining of Ni-based alloy 625 under MQL, cryogenic cooling and cryoMQL. J Mater Res Technol, 2020 http://doi-org/10.1016/J.JMRT.201912.069.

[4.34] Y. Xu, Y. Peng, K.D. Dearn, X. Zheng, L. Yao, X. Hu, Synergistic lubricating behaviors of graphene and MoS_2 dispersed in esterified bio-oil for steel/steel contact, Wear (342-343):297-309, 2015.

[4.35] A. Uysal, Effects of nano graphene particles on surface roughness and cutting temperature during MQL milling of AISI 430 stainless steel, Materials Testing 60(5): 533-537, 2018.

[4.36] O. Gunichenko, V. Bushlya, J. Zhou, J.E. Stahl, Tool wear and machining dynamics when turning high chromium white cast iron with pcBN tools. Wear 309, 253-269, 2017.

[4.37] A.P. Kulkarni, G.G. Joshi, V.G. Sargade, Dry turning of AISI 304 austenitic stainless steel using AlTiCrN coated insert produced by HPPMS technique. Procedia Engineering 64: 737-746, 2013.

[4.38] A. Pramanik, M.N. Islam, A. Basak, G. Littlefair, Machining and tool wear mechanisms during machining titanium alloys, Adv. Mater. Res 651: 338-343, 2013.

[4.39] A.K. Sharma, J.K. Katiyar, S. Bhaumik, S. Roy, Influence of alumina/MWCNT hybrid nanoparticle additive on tribological properties of lubricants in turning operations. Friction 7(2): 153-168, 2019.

[4.40] J. Samuel, J. Rafiee, P. Dhiman, Z. Yu, N. Korartkar, Graphene colloidal suspensions as high performance semi-synthetic metal-working fluids. J Phys Chem C 115(8): 3410-3415, 2011.

[4.41] A.K. Sharma, A.K. Tiwari, A.R. Dixit, R.K. Singh, M. Singh, Novel use of alumina/graphene hybrid nanoparticle additives for improved tribological properties of lubricant in turning operation, Tribology International 119: 99-111, 2018.

[4.42] R. Singh, J.S. Dureja, M. Dogra, M.K. Gupta, M. Mia, Q. Song, Wear behavior of textured tools under graphene-assisted minimum quantity lubrication system in machining Ti-6Al-4V alloy, Tribology 145, 106183, 2020.

[4.43] Y. Seid Ahmed, H. Youssef, H. El-Hofy et al, Prediction and Optimization of Drilling Parameters in Drilling of AISI 304 and AISI 2205 Steels with PVD Monolayer and Multilayer Coated Drills. Journal of Manufacturing and Materials Processing 2(1): 1-16, 2018.

[4.44] M. Mia and N.R. Dhar, Modeling of Surface Roughness using RSM, FL and SA in dry hard turning, Arab J Sci Eng (43), 1125-1136, 2018.

[4.45] M. Mia, M.A. Bashir, M.A. Khan, N.R. Dhar, Optimization of MQL flow rate for minimum cutting force and surface roughness in end milling of hardened steel (HRC40), Int J Adv Manu Technol 2016:1-16, 2016.

[4.46] M. Mia, M. Al Bashir, N.R. Dhar, Effects of cutting parameters and machining environment on surface roughness in hard turning using desgin of experiment. In AIP conference proceedings; AIP Publishng LLC: Melville, NY, USA 1754, p.60012, 2016.

[4.47] R. Saidi, B. Ben Fathallah, T. Mabrouki, S. Belhadi, M.A. Yallese, Modeling and optimization of the turning parameters of cobalt alloy (Stellite 6) based on RSM and desirabilty function, Int J Adv Manuf Technol 100: 2945-2968, 2018.

[4.48] K. Bouacha, M.A. Yallese, K. Choui, S. Belhadi, Analysis and optimization of hard turning operation using cubic boron nitride tool. Int J Refract Metal Hard Mater 45: 160-178, 2014.

[4.49] S. Gopalakannan, T. Senthilvelan, Application of response surface method on machining of Al-SiC nano-composites, Measurement 46(8), pp: 2705-2715, 2013.